Report of Research and Development between 2001 and 2006 by Mutsu Institute for Oceanography

Japan Agency for Marine-Earth Science and Technology

Mutsu Institute for Oceanography

Contents

1. Introduction 1

2. Overview of MIO activity for respective fiscal year 4

3. Highlights of research

3.1 Time-series observation with mooring system 11

(1) Scheme of increase of primary productivity in autumn season 15

(2) Time-series observation of phytoplankton biomass and primary productivity by Submersible Incubation Devise (SID) and Bio-optical Long-term Optical Ocean Measuring System (BLOOMS) 19

(3) Quick transport of primary produced organic carbon to the ocean interior 26

(4) Seasonal variability in nutrients observed by Remotely Access Sampler (RAS) 28

(5) Vertical transport of materials in the mesopelagic layer or twilight zone 32

3.2 Time-series observation with research vessels

(1) Export flux and export ratio in the northwestern North Pacific 35

(2) Seasonal changes in dissolved inorganic carbon and annual new production suspected with annual amplitude of nutrients and dissolved carbon 40

(3) Interannual increase in dissolved inorganic carbon (DIC) at station K2 43

(4) Comparative study on biogeochemistry between the western and eastern North Pacific 45

(5) High resolution time-series observation for biogeochemistry in the Blooming season. 49

(6) Repeat hydrographic observation along 155°E line 52

(7) Role of marginal seas in controlling biogeochemistry in the North Pacific 54

(8) Development of drifting buoy system with in situ sea surface pCO_2 sensor for long term observation 56

4. Summary 58

5. For future observation 58

Appendix

Honda, M. C. (2003) Biological pump in the northwestern North Pacific, J. Oceanogr. 59, 671-684.

Honda, M. C., H. Kawakami, K. Sasaoka, S. Watanabe and T. Dickey (2006) Quick transport of primary produced organic carbon to the ocean interior. Geophys. Res. Let., 33, L16603, doi:10.1029/2006GL026466.

Honda, M. C. and S. Watanabe (2007) Utility of an automatic water sampler to observe seasonal variability in nutrients and DIC in the northwestern North Pacific, accepted to J. Oceanogr.

Idai, T., M. Honda, S. Honjo and J. Kemp (2005) Mooring systems for time-series observation for biogeochemistry in the northwestern North Pacific: design, preparation and mooring work. JAMSTEC Rep. Res. Dev., 1, 73-91.

Kawakami, H., Y-L. Tang, M. C. Honda, and M. Kusakabe (2004) Particulate organic carbon fluxes estimated from ^{234}Th deficiency in winters and springs in the northwestern North Pacific, Geochemical Journal, 38. 581-592.

Wakita, M., S. Watanabe, Y. W. Watanabe, T. Ono, N. Tsurushima and S. Tsunogai (2005) Temporal change of dissolved inorganic carbon in the subsurface water at station KNOT (44° N, 155° E) in the Western North Pacific subpolar region. J. Oceanogr. 61, 129-139.

1. Introduction

In 2001, Mutsu office where is the mother port of research vessel MIRAI, Japan Agency for Marine-Earth Science and Technology (JAMSTEC: former Japan Marine Science and Technology Center) was converted to Mutsu Institute for Oceanography (MIO). Dr. Susumu Honjo (Senior Scientist emeritus of Woods Hole Oceanographic Institution) was welcome to JAMSTEC as an executive director and launched time-series observational study for biogeochemistry in the northwestern North Pacific, named HiLATS. Principle goals and questions are as follows:

Overarching goal

To expand our understanding of the delicate balance between the Earth's planetary environment and life through study of carbon cycle in the North Pacific by decadal long-term time-series observation

Immediate Goals and Questions

Goal 1: Document the interactions between plankton biodiversity, chemical composition of seawater and physical processes that create the unique biological pump operating in the high-latitude N. W. Pacific.

Questions:

- Why is primary production in the NW Pacific so large?
- Is it related to the high nutrient pool in the mesopelagic zone?
- Why are seawater nutrient concentrations in the Subarctic Zone so high?
- Is the Thermohaline Circulation controlling or affecting the biological pump in northwestern Pacific?
- How does variability in atmospheric forcing (winds, buoyancy loss) affect interannual/decadal variability in the halocline depth, T/S/nutrient structure and thus biological processes?

Goal 2: Contrast the scale and rates of the biological pump in the opal-dominated subarctic with that of the carbonated-dominated zoned further south.

Questions:

- Is the NW Pacific a more efficient CO_2 sink than the regions further south?
- Is it a globally significant sink for anthropogenic CO_2?
- What is the origin and the fate of the large pool of regenerated CO_2 present in the Northwestern Pacific Ocean Intermediate Waters?

Goal 3: Explain the persistence of the "Silica Oceans" in the Northwestern Pacific Ocean and compare it to its biogeochemical sibling, the Southern Ocean.

Question:

- Why doesn't a Silica Ocean develop in the North Atlantic?
- Is the large nutracline under the N. Pacific Subarctic Zone responsible for the huge opal production and export? How?
- What was the process, rate, and distribution of the Silica Ocean in the Glacial Periods?

Goal 4: Confirm and explain to association between the boundaries of the Silica Ocean and the hydrographically defined N. Pacific Subarctic Front.

Questions:

- Does the position NP Silica/Carbonate Ocean boundary moves on seasonal, decadal, or Milankovitch time scales?
- Is this in response to a shift in the position of the Subarctic Front?

Strategy

(1) Deployment of MIO Mooring Array with physical oceanographic and biogeochemical instruments at several stations to correct high resolution time-series oceanographic data

(2) Full-water column analysis of chemical composition and hydrographic / 3-D current profiling to deepen the understanding of the North Pacific Intermediate Water and Deep/Bottom Currents

(3) The recurrent (more than biannual) transects observation between the mooring locations by research vessels for hopefully at least 10-years.

(4) International collaboration to compare time-series observation in other oceans and characterize oceanographic properties in the NP.

(Detail is available on line: http://jpac.whoi.edu/hilats/index.html)

Based on his experiences and knowledge, and suggestions from an international workshop (The 1st workshop on the Mutsu project: Long-term ocean environmental research plan to understand the North Pacific ocean and its global significance), mooring system with automatic samplers were designed and constructed as a principle observation gear and several stations in the northwestern North Pacific were set up for time-series observation.

Since 2001, mooring systems have been deployed and recovery repeatedly with grate assistance of scientists and research specialists from Woods Hole Oceanographic Institution (WHOI) and University of California, Santa Barbara (UCSB), and time-series data with high resolution have been obtained. Especially, time-series data collected in 2005 and 2006 enabled us to linkage seasonal variability of biological

activity in the surface sunlit layer with that of sinking particle in the “twilight zone” and deep sea. In addition, scientific cruise at our time-series station K2 by U.S. NSF supported VERTIGO project team made our time-series observation internationally collaborative study. During cruises with or without mooring work, ordinary observation such as hydrocasting, measurements of primary productivity, natural radionuclide and optical situation have been conducted in different seasons and year-round seasonal data have been also accumulated. This result has revealed general oceanographic properties in the Western North Pacific such as seasonal and interannual variability in nutrients, dissolved inorganic carbon and carbon export flux.

FY2006 is the last year of the first HiLATS project. We herewith wrap up MIO scientific activity during the last 5 years in order to evaluate our activity and propose the future plan for time-series observation for biogeochemistry in the Northwestern North Pacific.

2. Overview of MIO activity for respective fiscal years (FY)

Fig. 1 shows scientific cruises relating MIO project. The followings are summary of MIO activity for respective fiscal years.

(FY2001)

In March, an international workshop entitled "The 1st workshop on the Mutsu project: Long-term ocean environmental research plan to understand the North Pacific ocean and its global significance" was held in order to introduce MIO's overarching goal (to expend our understanding of the delicate balance between the Earth's planetary environment and life through the study of the carbon cycles in the North Pacific) and scientific plan (to acquire high resolution time-series biogeochemical and physical data from the euphotic layer of the open ocean by using automated time-series measurements system). Approximate 40 scientists from several countries (United States, Australia, China, Korea, Russia, Canada and Japan) joined and discussed appropriate scientific gears, observation plan and stations from physical, chemical, biological and geological points of view. In this workshop, the importance of interdisciplinary and international collaboration was emphasized for pursuing a principal objective (http://jpac.whoi.edu/archives/index.html).

Referring to ideas proposed in the workshop, MIO designed and constructed mooring system, and decided time-series stations. Before cruise, research spdecialists of MIO stayed at WHOI and learned construction of mooring system such as "pre-stretch technique" and operation of variable automated sampling or measurement systems. First cruise for HiLATS project was conducted in September 2001 by R/V MIRAI (MR01-K05). During this cruise, much time was spent for precise site-survey because the top buoy of mooring system should be deployed around at 30 m, which depth was critical for escaping winter waves with 20 m heights and ships with draft of 20 m and, chiefly, maintaining automated sampler such as water sampling system within the euphotic layer. Using a multi narrow beam echo sounding system and an altimeter of CTD / hydrocasting system, flat deep seafloors within a few miles radius were selected and its precise water depth were determined. After this site-survey, two mooring systems for biogeochemistry (BGC mooring) were successfully deployed at time-series stations: K2 (47°N, 160°N) and K1 (51°N, 165°E), and one mooring system for physical oceanography (PO mooring) were deployed at station K1 (Figs. 2, 3).

(FY2002)

In October 2002, BGC mooring systems and PO mooring system were recovered during MR02-K05 cruise and the first year-round, high resolution time-series data such as nutrients in seawaters, in situ optical situation and salinity, temperature and current velocity were successfully obtained. Time-series observation of nutrients by water sampling system (RAS) revealed that concentrations increased from late autumn to March and, after late spring, those decreased toward autumn season. It was notable that concentrations of nutrients largely varied in October, suggesting possibility that

temporal supply of nutrients from subsurface enhances primary productivity in autumn.

During this cruise, a set of BGC mooring and PO mooring were deployed at three time-series stations: K1, K2 and K3 (39°N, 160°E) (Fig. 3).

(FY2003)

In September 2003, we visited our time-series stations by R/V KAIREI. We recovered most of mooring systems deployed in 2002 (two BGC mooring systems and three PO mooring systems). However we lost one BGC mooring systems deployed at station K2. The cause was the partition of chain with breaking point of approximately 10 ton just above releaser. Although we planned to re-deploy all mooring systems, redeployment was suspended and remaining ship time was devoted to search for missing K2 BGC mooring. However we could not find that. After cruise, "investigative committee" was set up in JAMSTEC and this committee began to investigate the mechanism of this accident.

On the other hand, submersible incubation devise for measurement of primary productivity (SID), optical sensor (BLOOMS) and sediment trap at stations K1 and K2 fortunately collected high resolution, time-series samples and data. These data enabled us to link seasonal variability in sinking particles in the deep sea and seasonal variability in primary productivity and optical condition in the euphotic layer. In this fiscal year, beside R/V KAIREI cruise, we conducted two scientific cruises (in March by R/V MIRAI, in July by R/V NATSUSHIMA) and collected seasonal data of nutrients, carbon chemistry, primary productivity and natural radionuclide (^{234}Th) for study of the export carbon flux.

(FY2004)

Investigation of partition accident was continued. In the process of investigation, "weak noisy signals" transmitted from ARGOS compact mooring locator (CML) was found. These signals were transmitted only 10 days after deployment of missing mooring system. It meant that mooring system was partitioned and started to drift only 10 days after deployment. In the investigative committee, break test of partitioned chain and theoretical calculation about strength of chain-link were conducted. As a result of various investigations, the mechanism of partition on chain were suspected as follows:

(a) Partitioned chain was tangled when deployment.
(b) It ingenerated twisted link of chain, which should be weaker than normal (straight) link against tension.
(c) When normal tension of mooring system (usually 1.3 ton with maximum of, at most, 3 ton) was loaded on twisted link, this link was possibly broken.

In addition, problem in switching system (optical sensor) of ARGOS CML was pointed out. In this committee, usage of stronger chain and double ARGOS CMLs were proposed.

Although time-series observation with mooring systems was not able to restart, we conducted four cruises by R/V MIRAI and NATSUSHIMA in April, May,

August and October and could collect seasonal oceanographic data such as nutrients, carbon chemistry, primary productivity and radionuclide. These data became useful and helpful for validating time-series data obtained by automated sampler and sensor and enabled us to clarify seasonal variability in biogeochemistry in the northwestern North Pacific. During August cruise (MR04-04), we conducted "transect hydrographic observation" in the Russian Exclusive Economic Zone (along Kuril islands and the Kamchatka peninsula). These data will reveal mechanism of water and substances exchange between the northwestern North Pacific and Bering / Okhotsk seas.

(FY2005)

During R/V MIRAI MR05-03 cruise in March 2005, "stepped-up" BGC mooring system and PO mooring system were deployed on a trial basis for two weeks. After two weeks deployment, mooring systems were recovered and appearance of recovered mooring systems and variability in tension during deployment work and mooring period was checked. As there were not any problems, we redeployed a BGC mooring system at station K2.

In September 2006, we recovered this BGC mooring system without any problems during MR05-04 cruise. Time-series samples for nutrients and dissolved inorganic carbon by automated water sampler (RAS), and sinking particles at 4 layers (150 m, 540 m, 1000 m, and 4810 m) by sediment trap from March 2005 to September 2005 were successfully recovered with optical data. We left station K2 after deploying a BGC and a PO mooring systems. This cruise (MR05-04) was also "transect cruise" in the North Pacific. After time-series observation in the western North Pacific, we visited several stations north of 45°N including Ocean Station P in the Alaskan Gyre and conducted interdisciplinary observation such as measurements of nutrients, carbon species, pigment, radionuclide and primary productivity. These data will be useful to compare biological pumps between the west and east North Pacific and characterize the feature of the biological pump in the northwestern North Pacific.

Notable thing in this year was oceanographic observation held in July and August at station K2 by National Science Foundation (NSF) supported VERTIGO project team (cruise leader: Ken Buesseler from WHOI). Their data become very useful and helpful to validate our time-series data obtained by mooring system and vice versa.

(FY2006)

During MR06-03 cruise in June and July 2006, mooring systems were recovered. Time-series data from October 2005 to June 2006 were successfully obtained. In addition to the previous data, one year and half time-series data set such as nutrients and optical condition in the euphotic layer and settling particles from the bottom of winter mixing layer to deep sea were acquired. The MR06-03 cruise was approximate two months cruise in June and July when primary productivity usually begins to increase largely (spring bloom) and nutrients and dissolved inorganic carbon

begins to decrease. We deployed a BGC mooring system during approximately two months in order to collect high-resolution time-series water samples, optical data and settling particles. We also visited station K2 six times during two months and measured concentrations of nutrients, carbon species, primary productivity and radionuclide. This kind of concentrated observation in the pelagic ocean has been little and, therefore, precise change in biogeochemistry in the northwestern North Pacific will be verified.
To this cruise, JAMSTEC biologists participated and conducted biological research focusing on vertical distribution of meso-zooplankton and its grazing pressure. These data will enable us to study zooplanktons' role in ocean carbon cycle. After this cruise, all mooring systems and automatic samplers were brought back to MIO in order to be overhauled and repaired.

Beside cruise, the above-mentioned VERTIGO post-cruise meetings were held in February (at AGU Ocean Science Meeting in Hawaii) and in October (at WHOI). VERTIGO cruise data and time-series data by JAMSTEC mooring systems were compared and fruitful discussion about vertical change in carbon flux and sinking velocity were conducted. The results of data analysis would be published in near future. On the other hand, MIO hosted a symposium entitled "time-series observation for biogeochemistry in the western North Pacific" during Oceanographic Society of Japan 2006 fall meeting in September. Update and future plan were introduced and discussed by participants.

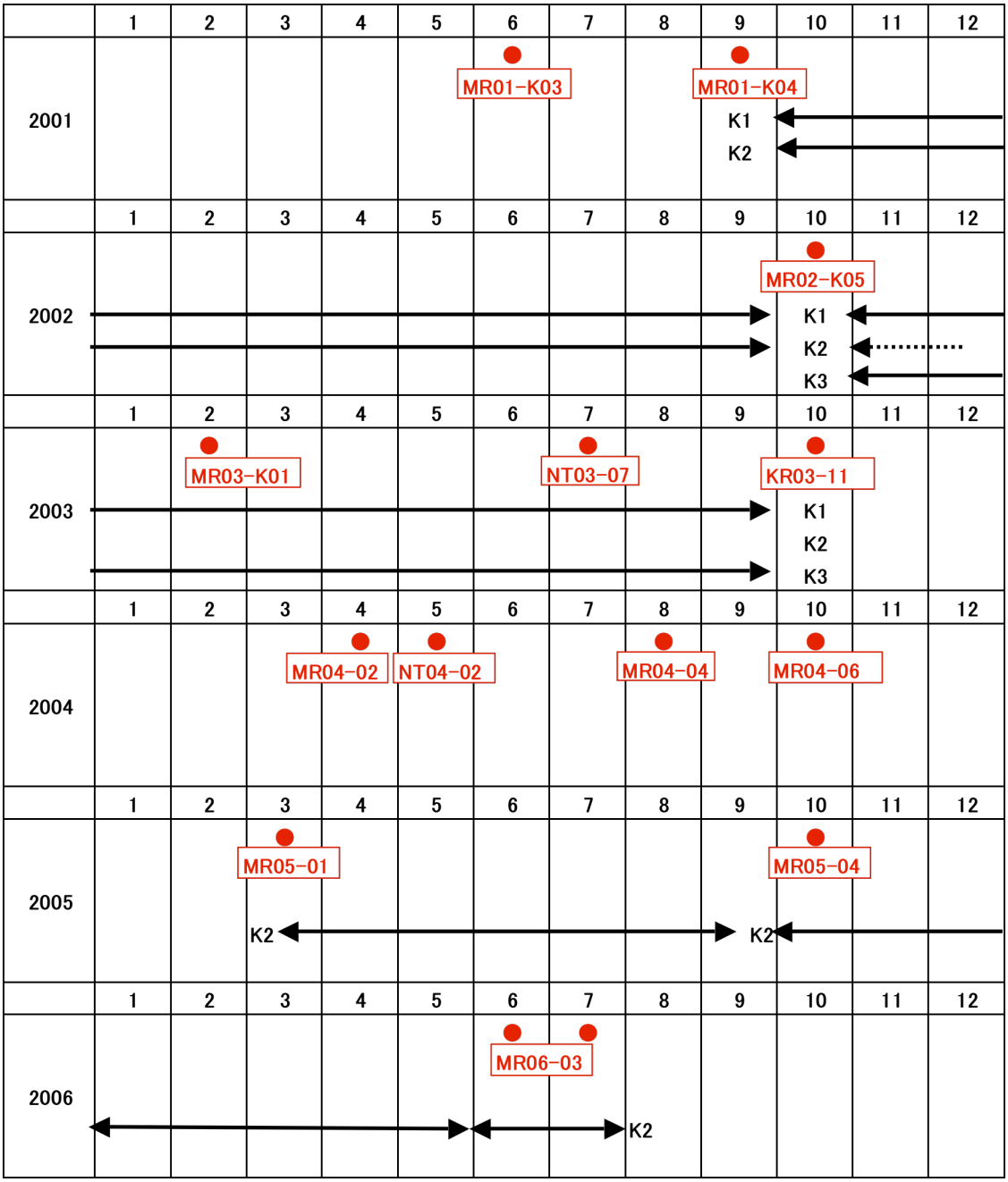

Fig. 1 Scientific cruises associating with HiLAST project. Red circles show cruises and arrows show mooring period for respective stations. MR: MIRAI, KR: KAIREI, NT: NATSUSHIMA

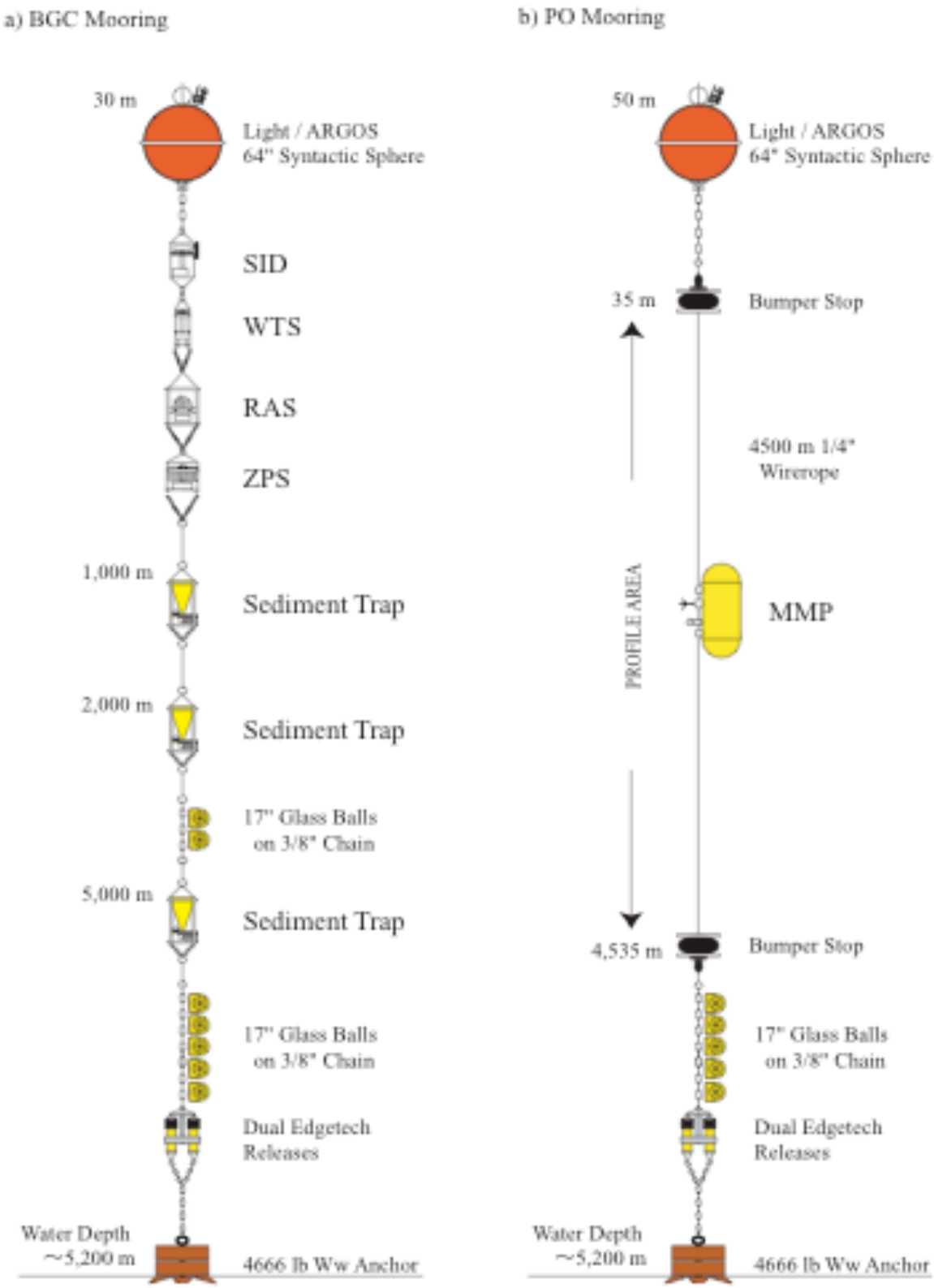

Fig. 2 Basic BGC and PO mooring systems (Idai *et al*., 2005)

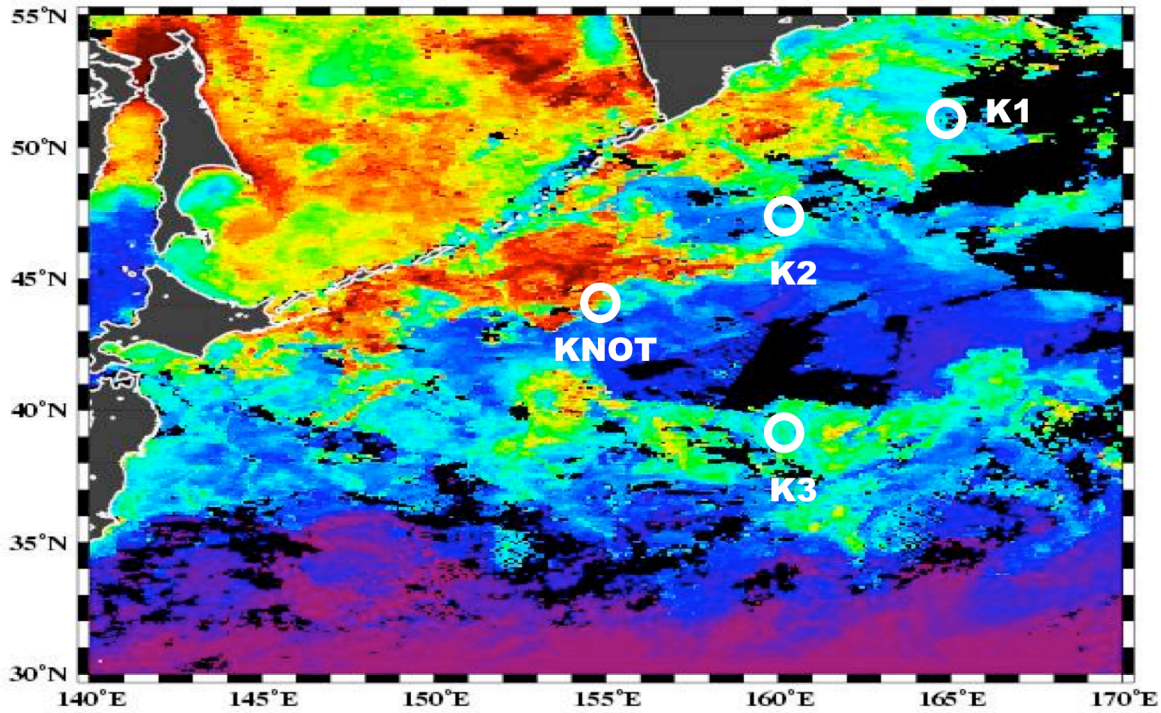

Fig. 3 Time-series observation stations by MIO: K1 (51°N / 165°N), K2 (47°N / 160°E), K3 (39°N / 160°E) and KNOT (44°N / 155°N). Background is the monthly composite of chlorophyll-a observed by SeaWiFS in May 2004 (courtesy of K. Sasaoka, JAMSTEC)

3. Highlights of research

3.1 Time-series observation with mooring system

HiLaTS mooring systems consist of following scientific gears:

a. Submersible Incubation Chamber for measurement of primary productivity (SID)

The SID is a mooring-compatible, automated instrument for performing multiple *in situ* ^{14}C-primary production experiments. Each incubation involves a cleaning cycle, procurement of a 420 ml sample at depth with simultaneous introduction of ^{14}C tracer, and the preservation of subsamples during incubations of user-determined length. For each incubation, 500 μl of the tracer solution was injected into the sample as it was being taken into the 420 ml incubation chamber. After each *in situ* incubation, the entire contents of the incubation chamber was filtered through a 47 mm Fixation Filter Unit (FFU) containing a Whatman GF/F glass-fiber filter. Each FFU contained a chemical fixative (0.36 N sulfuric acid) in a reservoir located behind the filter. When a given incubation was completed, the incubation chamber was flushed several times in preparation for the next incubation and the waste directed to an onboard waste container. Seawater was drawn into the incubation chamber, acidified by injection of the acid into the throat of the sample inlet and allowed to soak for 3 hr. Prior to the next incubation, the acidified water was removed and the chamber was flushed. Light-occluding particulate materials were continuously removed from the incubation chamber outer wall by an acid-containing external Biofouling Control Collar. During each deployment, background activities were measured.

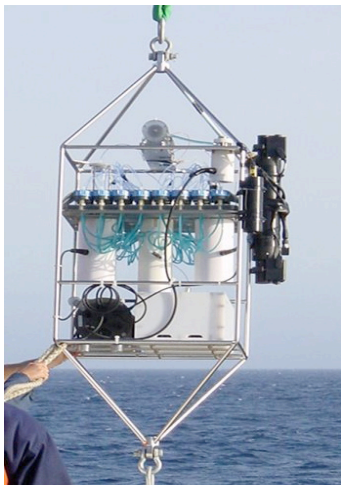

SID and BLOOMS

b.BLOOMS

The Bio-optical Long-term Optical Ocean Measuring System package (BLOOMS) developed by Dr. Tommy Dickey and his coworkers of UCSB consists of a WETLabs fluorometer and a Satlantic Inc. spectral radiometer (OCR-504-ICWS; Halifax, Canada) along with data acquisition / storage systems and a pressure housing. The BLOOMS was mounted on the frame of the SID for measurements of chlorophyll *a* (chl-*a*) concentrations as a proxy for phytoplankton biomass (fluorometer) and downwelling spectral irradiance at four wavelengths (412, 443, 490, and 555 nm). The optical system was kept free of biofouling by use of copper shutters. Data have been analyzed by UCSB and MIO.

c. Zooplankton sampler (ZPS)

Zooplankton Sampler (ZPS) filters large volume seawater (~ 100 L) and collects zooplankton samples in time-series. A sample is collected using a positive displacement pump that generates negative pressure. Zooplanktons are unaware of

being drawn towards the sampler until they are well inside and can not escape. Prefilter covers the mouth of the sample intake path to avoid invasion of large creatures. They are transported onto a 3.5 x 6 cm frame of a special roll of Nitex mesh (100 μm mesh). The zooplankton community retained on a frame is sandwiched by another piece of Nitex mesh for protection and immediately moved to the fixative bath for storage until recovery of the sampler. A new frame of mesh is positioned automatically to be ready for the next sampling cycle. This procedure can be repeated up to 50 times for each roll of Nitex mesh as instructed by the micro-controller. Before taking sample at programmed interval, seawater is flushed to opposite direction. This becomes clear out any particle and living things in the sampling way.

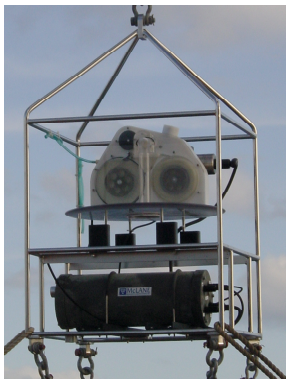

ZPS

d. Phytoplankton sampler (PPS)

The water transfer system – phytoplankton sampler (WTS-PPS) collects *in situ* suspended particulate matter especially phytoplankton in an aquatic environment by filtrating 10 L seawater. A dual multi-port valve directs the water through 24 x 47 mm GF/F filters for a time-series operation. The positive displacement pump is placed downstream from the filters to prevent sample contamination. Samples are preserved in an array of filter-preservation units that each contains a chemical fixative (seawater based 70 % Utermohl solution or seawater based buffered 5 % formalin). Before taking sample, seawater is flushed through the valve and tube. This becomes clear out any particle and living things in the sampling way. The flow rate is controlled in order to prevent the sample from being crushed onto the filter. The computer records the instantaneous flow rate and total volume at a constant interval of time for each filter.

PPS

e. Water sampler (RAS: Remotely Access Sampler)

There are four major components mounted within the RAS: (1) the controller housing, (2) the pump assembly, (3) the multi-port valve, and (4) the sample containers. The principle of water sampling is that the pump draws out water in the sample container in which the collapsed sample bag is mounted. This creates a pressure gradient that pushes ambient seawater through the intake and into the inflating sample bag.

The RAS instruments were loaded with acid-cleaned, 500 ml capacity bags made of the following 3 laminated layers; a thin exterior Mylar® film for protection, a vacuum

RAS

coated aluminum foil layer for blocking solar radiation and minimizing gas diffusion and an interior, Teflon® film for reinforcement and insulation of sample water from the Al layer. Each bag was pre-loaded with a preservative solution (2 ml $HgCl_2$ solution: 3.6 g $HgCl_2$ in 100 ml distilled water), connected to a distribution valve and placed within a sturdy 600 ml sample container (acrylic sheathe) within the instrument. The remaining spaces within sheathes were filled with seawater before deployment. There are 49 identical bag assemblages on a RAS. Of these, 48 were used to sample seawater on a scheduled sequence. The remaining bag was filled with 6 M HCl that was used to flush the intake path before each water sampling procedure in order to avoid biofouling. Five minutes before sampling, the multi-port valve aligns with the intake path and the cleansing acid bag and a 5 ml jet of 6 M HCl flushes the intake manifolds. After a one-minute pause, the same path was rinsed with 100 ml of *in situ* seawater. Then the multi-port valve aligns the intake valve to a designated sampling bag assemblage. As the seawater is removed from the acrylic sheathe by operating the pump in reverse to the previous flush stage, the resultant low pressure induces the *in situ* water to move into the sampling bag. To minimize cross contamination of water samples, the graphite-gear pump is not exposed to the sample water but only to the evacuated distilled water in the sheathes. Execution records documenting sample timing, estimated sample volume, flushing periods, and electricity consumption were logged by the RAS instruments and retrieved from the memory on recovery.

f. Sediment trap

In 2005-2006, a time-series sediment trap with 21 cups or 13 cups were installed at 150 m and three traps were installed at 500 m, 1000 m and 5000 m for collecting sinking particles in the mesopelagic and bathypelagic layer. Before deployment, collecting cups were filled up with seawater based 5 % buffered formalin.

g. Moored profiler for measurements of CTD and current (MMP)

The McLane Moored Profiler (MMP) is an autonomous, profiling, instrument platform. The purpose is to make moored profiler technology available to, operable by, and useful to a broad cross-section of the oceanographic community. The platform and software are designed for ease of access, operation, and maintenance. The instrument includes both a CTD and an acoustic current meter. There include the controller, the buoyancy elements, the drive motor and guide wheels, the instruments suite, the internal frame, and the hydrodynamically faired external shell. The platform is designed to profile between pressure limits (or physical stops), powered along a conventional, plastic jacketed mooring cable by a traction drive. While profiling it samples the water column with a suite of instruments and stores the measurements for later retrieval. The shape accommodates a cylindrical housing that has sufficient length for batteries and electronics and a 6,000 m depth rating. Two glass spheres are used for buoyancy only. The mooring cable threads through faired retainers at the top

and bottom of the vehicle. The retainers can be opened for launch and recovery and are strong enough to support the full weight, including trapped water, of the MMP on a horizontal cable, a normal situation during recovery.

These gears are installed on wire-based mooring system. In order to deploy mooring system at the exact position and locate some instruments within the surface sunlit layer, the length of wire used for mooring were measured on land (Idai et al., 2005).

MMP

(1) Scheme of increase of primary productivity in autumn season

Between October 2001 and September 2002, seawaters of approximately 450 ml were collected every eight days by automated water sampler (RAS) at stations K1 and K2 in the Western Subarctic Gyre (WSG). Samples were preserved with $HgCl_2$ solution. After recovery of RAS, concentrations of nutrients (NO_3, NO_2, $Si(OH)_4$) in seawater samples collected around 50 m were measured with continuous analytical system (BRAN+LUEBBE TRAACS 800) on board.

Concentrations of both nutrients at both stations began to increase at the late autumn in 2001 and increased by the end of April 2002 (Fig.4). These were suspected to be attributable to winter mixing. Sequentially, concentrations of nutrients at station K1 began to decrease toward September in 2002 while decrease in nutrients at station K2 were not large. Decrease in nutrients at station K1 were suspected to be attributable to increase of primary productivity in spring. For station K2, RAS was likely located below surface mixed layer (deeper than 50 m), resulting that decrease in nutrients was not observed.

Noteworthy observation was large variation in nutrients in October and November in 2001 at both stations. Annual maximum and minimum concentrations were observed during this period. Based on temperature, salinity and density observed by moored profiler (MMP) at station K1, water mass changed largely during this period. Change in concentrations of nutrients during this period correlated with change in physical oceanography: when concentrations of nutrients were lower, water temperature tended to be higher and salinity / density tended to be lower (Fig. 5). Water temperature was close to SST (~ 8°C) when nutrients were low. This is indicative of that vertical mixing temporally became active and near surface water invaded to the subsurface layer around RAS depth. Inversely, it was suspected that subsurface water with macronutrients and micronutrients such as Fe ascends to the surface layer. During this period, concentration of chlorophyll-a observed by satellite and organic carbon and inorganic carbon flux observed by time-series sediment trap increased (Fig.6). Increase in primary productivity in autumn has been sometimes reported in the WSG. In the northwestern North Pacific, autumn is one of season with high wind velocity (Fig. 4). Autumn increase in primary productivity might be attributed to temporal progress of surface mixing resulting supply of macro and micronutrients to the surface area.

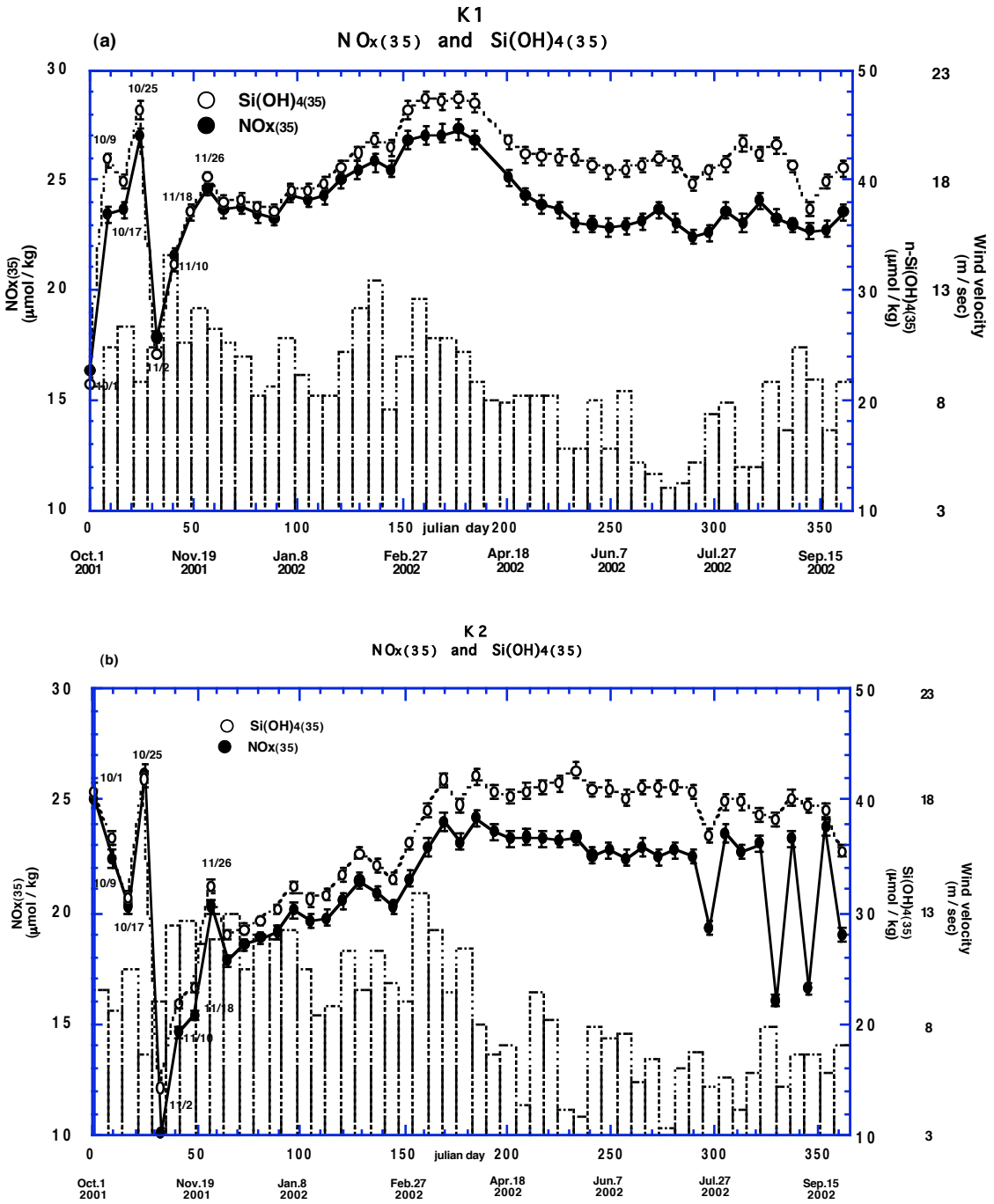

Fig.4 Seasonal variability in concentrations of nutrients (NOx and $Si(OH)_4$) normalized to salinity of 35 observed by RAS at station (a) K1 and (b) K2. Weekly composites of wind velocity (bar graphs: courtesy of Sasaoka of JAMSTEC) are also shown.

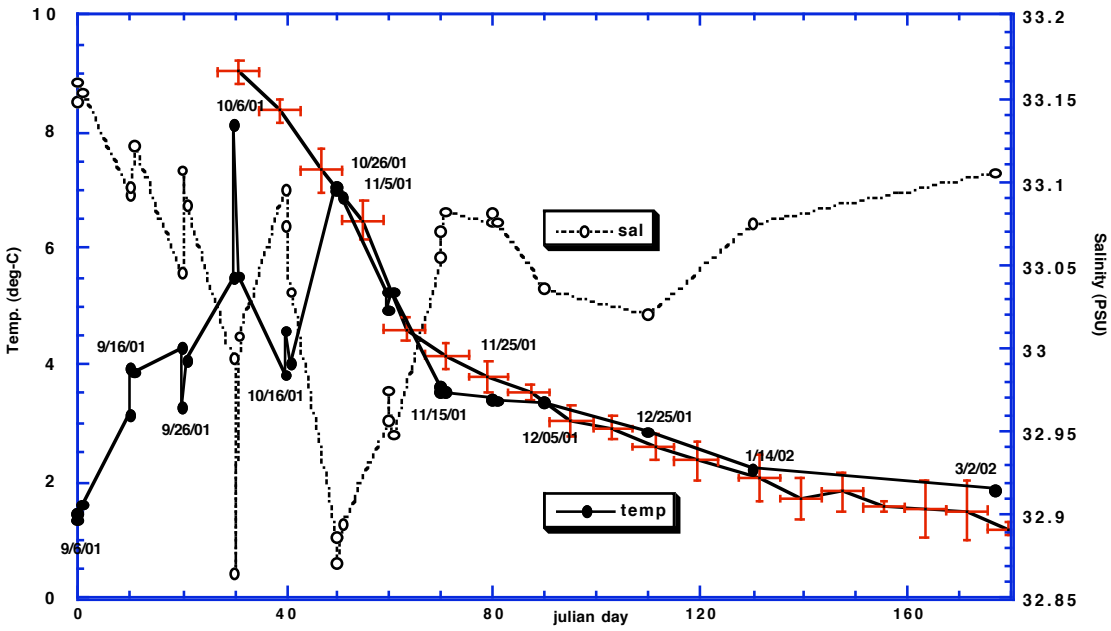

Fig. 5 Temporal variability in water temperature (closed circles with bold line), salinity (open circles with hatched line) at around 50 m depth at station K1. These data were observed by MMP between September 2001 and March 2002. Temporal variability in remotely sensed SST (courtesy of Sasaoka of JAMSTEC) is also shown.

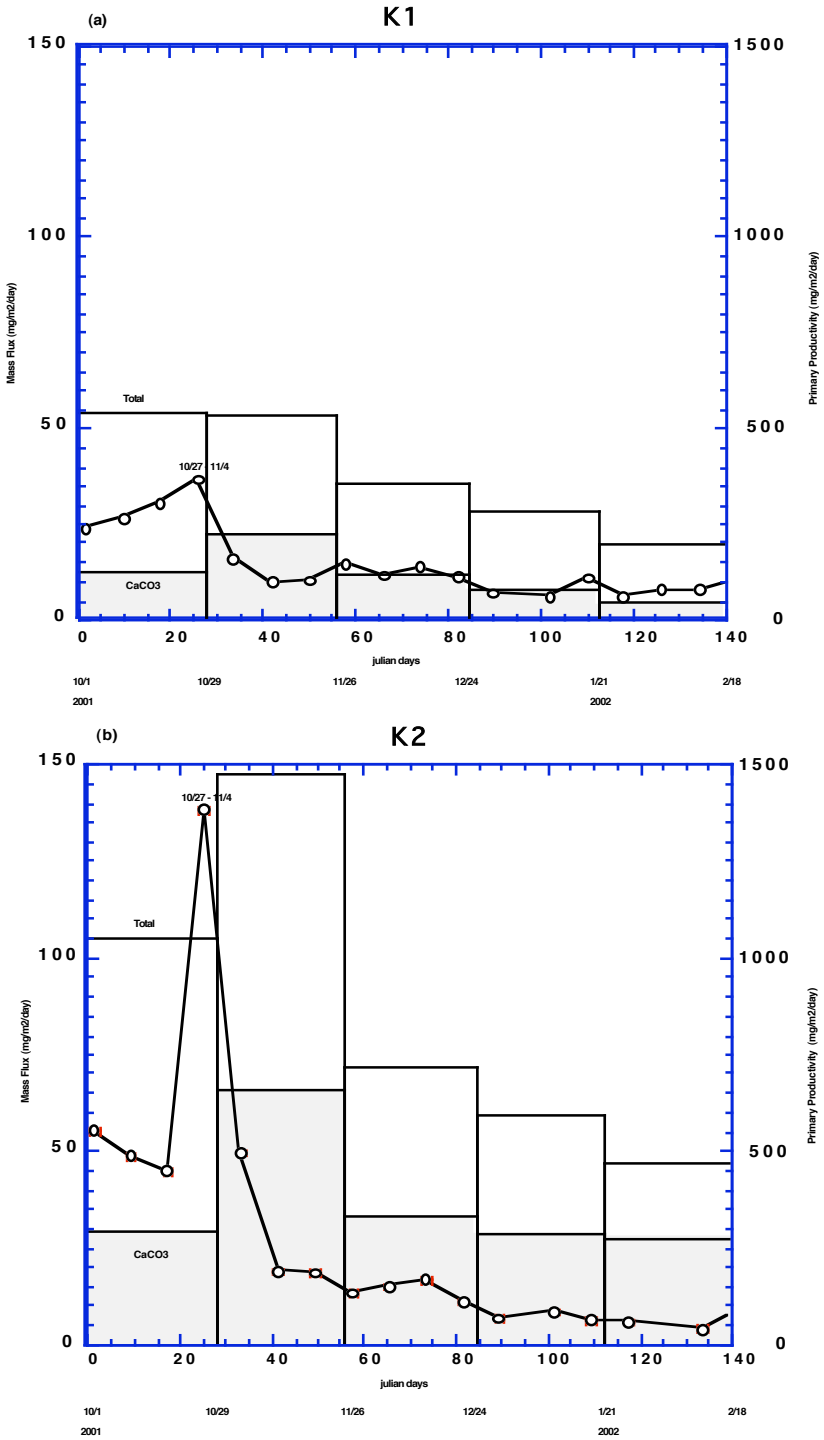

Fig. 6 Total mass flux (bar graphs) and $CaCO_3$ flux (gray bars) at station (a) K1 and (b) K2 during October 2001 and February 2002. Temporal variability in primary productivity estimated with remotely sensed data and empirical equation are also shown (line graph with opeen circles).

(2) Time-series observation of phytoplankton biomass and primary productivity by Submersible Incubation Device (SID) and Bio-optical Long-term Optical Ocean Measuring System (BLOOMS)

Between November 2002 and September 2003, time-series observations of phytoplankton biomass and primary productivity were conducted at station K1 and K3 in the northwestern North Pacific using a moored Time Series-Submersible Incubation Device (SID) and moored optical sensors (Bio-optical Long-term Optical Ocean Measuring System; BLOOMS). These instruments were planned to be located around 50 m within surface euphotic layer. Based on depth sensor, SID and BLOOMS at station K3 were deepened up to approximately 200 m while these instruments at station K1 were located around 50 m during mooring period (Fig. 7). Moored profiler (MMP) data revealed that current with high velocity > 40 cm/sec forced these instruments to be down to ocean interior (Fig.7). Data obtained below 70 m were, therefore eliminated from data analysis.

Primary productivity determined by 12 hr. daytime incubations by the SID (PP_{12}) at the approximate bottom of the euphotic zone varied seasonally with low values in winter and high values in summer (Fig. 8). The average of PP_{12} between November 2002 and July 2003 at station K3, which is located in the subarctic boundary, was approximately 2.6 mg m^{-3} $12hr.^{-1}$ and higher than that at station K1 (1.5 mg m^{-3} $12hr.^{-1}$), which is located at the northern edge of the Western Subarctic Gyre (WSG). Observed PP_{12} were converted to the daily net primary productivity (PP_{24}) based on PP_{12} and our shipboard experiments (Fig. 9). In contrast to station K1 results, PP_{24} at station K3 correlated well with daily spectral irradiance observed simultaneously with BLOOMS (Fig. 8). Higher PP_{24} values at station K3 were driven by higher light intensities and higher temperatures than was observed at station K1. *In situ* photosynthetically available radiation (PAR) based on the BLOOMS and satellite based surface PAR revealed that relative intensity of in situ PAR against surface PAR began to decrease in May with minimum in June and July. It was indicative of that phytoplankton increased between May and September. The ratio of downwelling irradiance measured at wave length 555 nm to that at 443 nm ($Ed_{(555)}$ / $Ed_{(443)}$) correlated with integrated chlorophyll-*a*. Seasonal variability in PP_{24} at both stations correlated with depth-integrated PP_{24} estimated with optical data obtained by BLOOMS and satellite, and an empirical equation proposed previously (Fig. 10).

This study demonstrates that autonomous instrumentation can be valuable for the study of seasonal variability of phytoplankton biomass and *in situ* primary productivity observations, and improve understanding of the biological carbon pump. Finally, estimated depth-integrated PP_{24} were compared with satellite based PP_{24}

estimated with general algorithm and organic carbon flux observed by sediment trap. General trend were comparable each other: PP and organic carbon flux was low in winter and high in spring and summer (Fig. 11). However there are many inconsistent points remaining. It was strongly requested to conduct interdisciplinary observation with variable automated sampler and sensor.

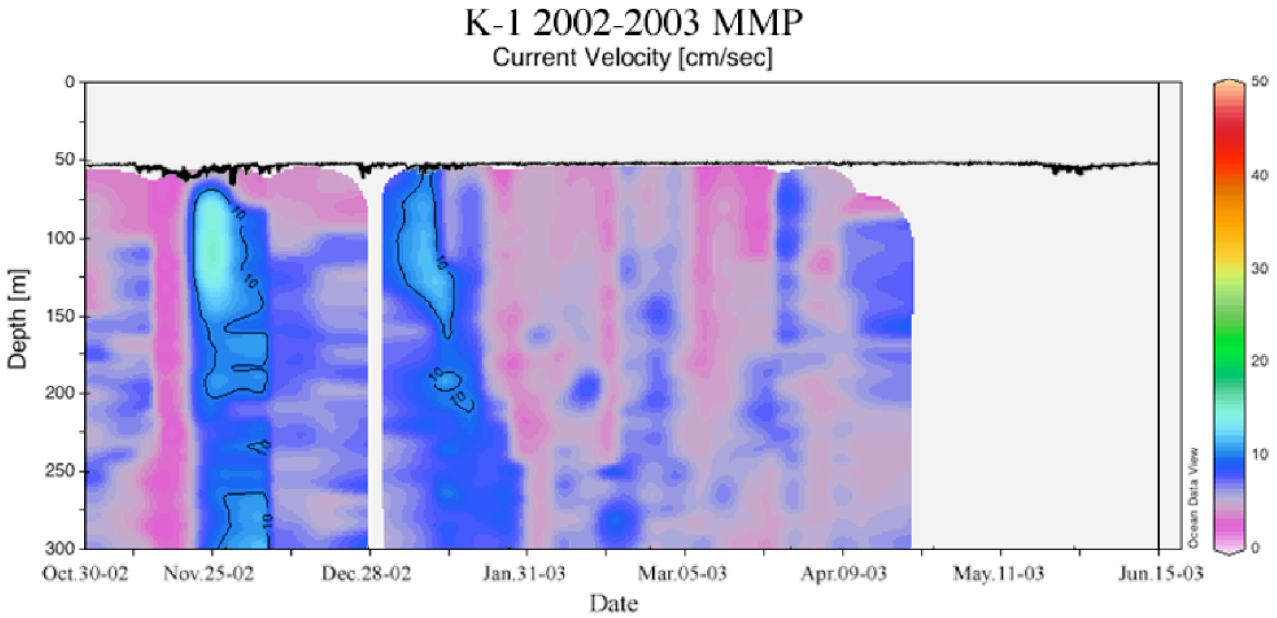

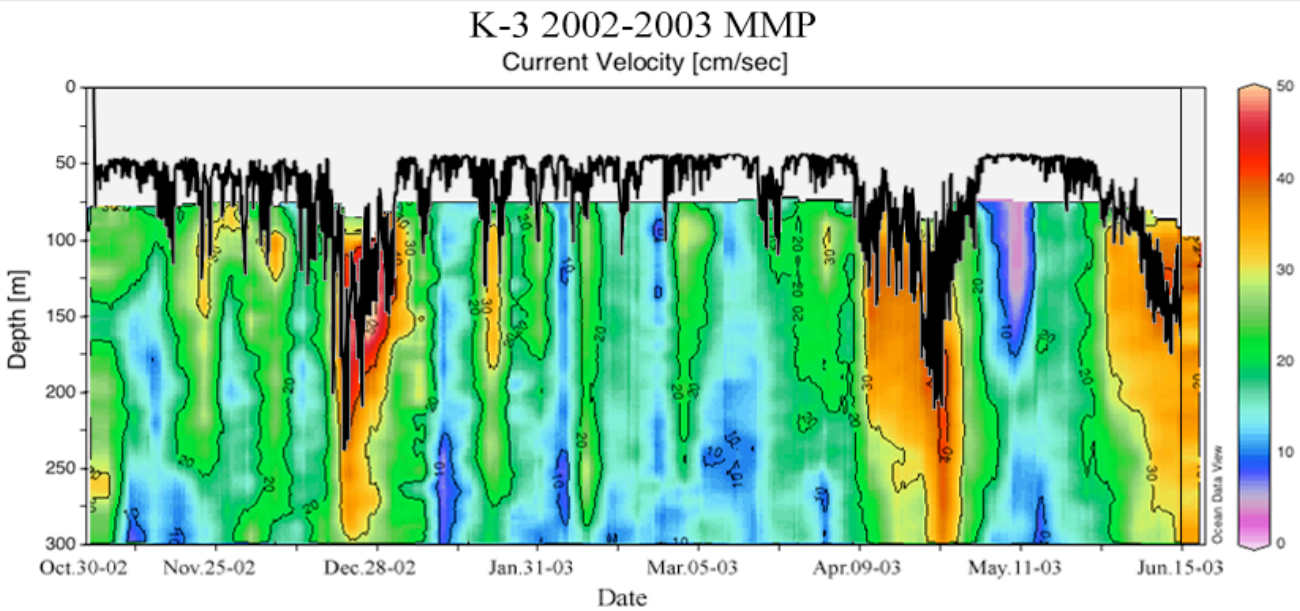

Fig. 7 Measured depths of the TS-SID throughout deployment at stations K-1 (a) and K-3 (b). Depth measurements were taken every 2 hours. Time-depth distribution of current velocity upper 300 m was observed by autonomous profiling acoustic current meter (ACM) / CTD system (MMP) are also shown (courtesy of T. Idai).

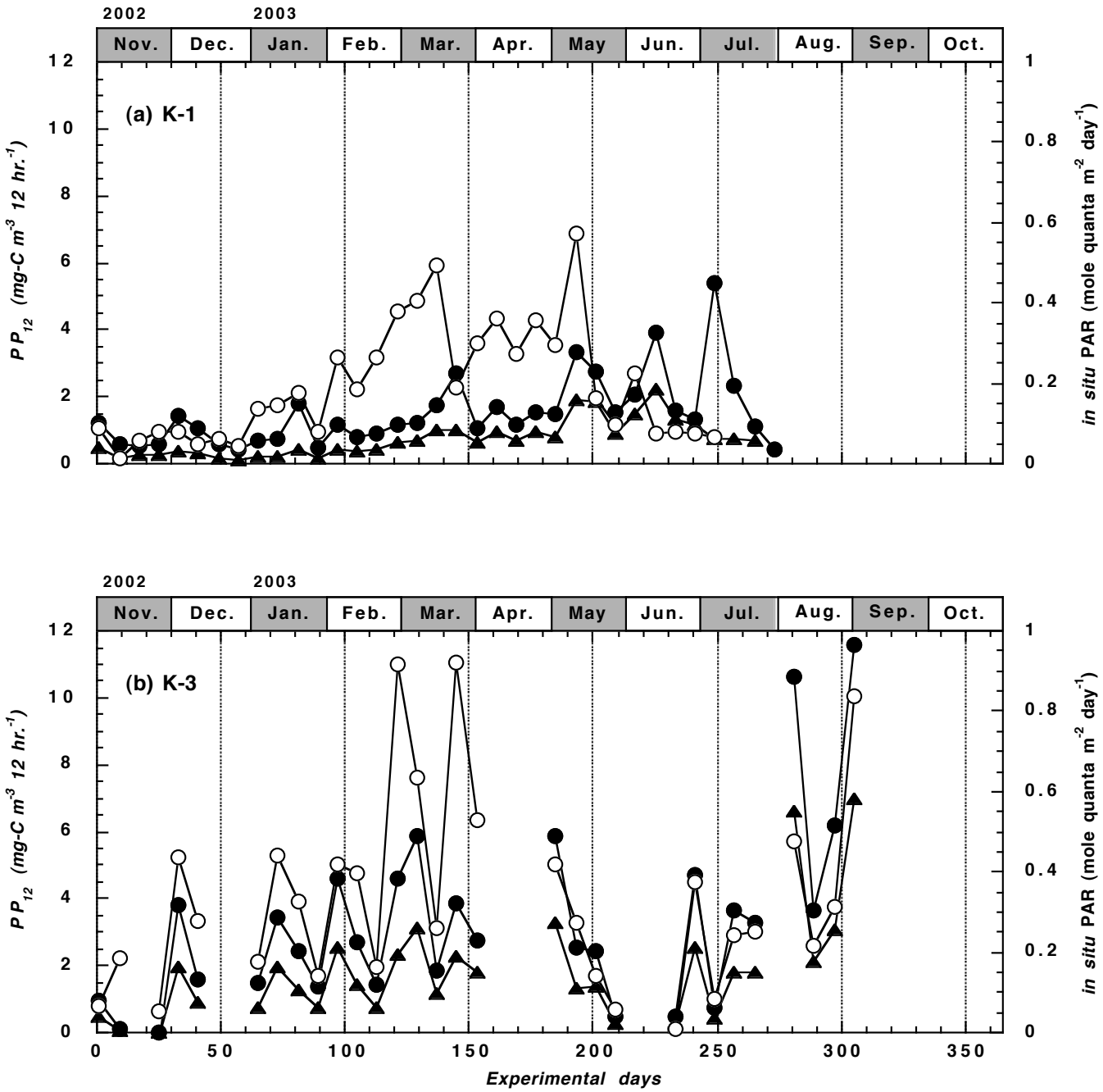

Fig. 8 Seasonal variability in primary productivity (PP_{12}) at stations K1(a) and K3(b). Closed circles and closed triangles are total PP($PP_{(t)}$) and PP of the acid precipitable organic carbon retained on Whatman GF/F filters ($PP_{(fit)}$), respectively. Seasonal variability of in situ PAR is also shown as open circles. Data obtained below 70 m are not included.

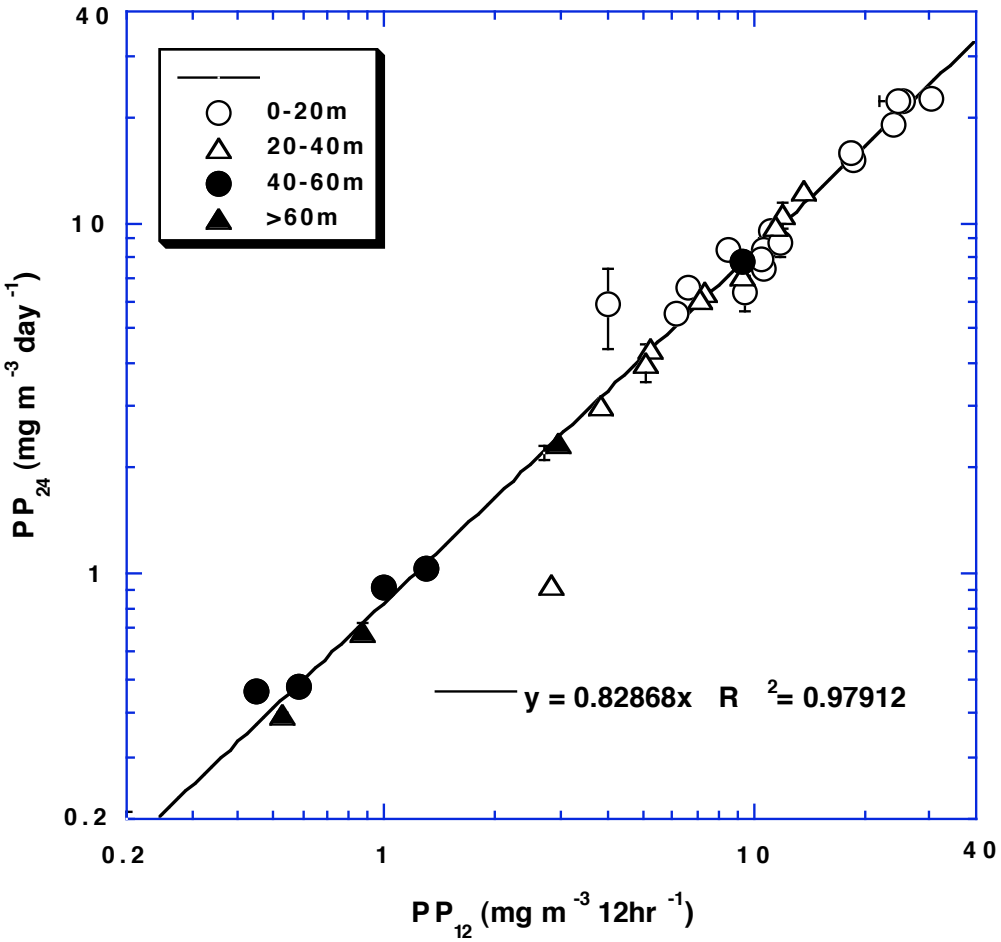

Fig. 9 The relationship between values of primary productivity obtained with 12 hr. ship-based incubations (PP_{12}) and 24 hr. ship-based incubations (PP_{24}) at the indicated depths. These data were obtained during R/V Mirai MR04-02. MR04-06 and MR05-01 cruises (Honda, unpublished data). Independent of the depth of incubation, the ratios of PP_{24} to PP_{12} were linearly correlated with a slope of 0.83

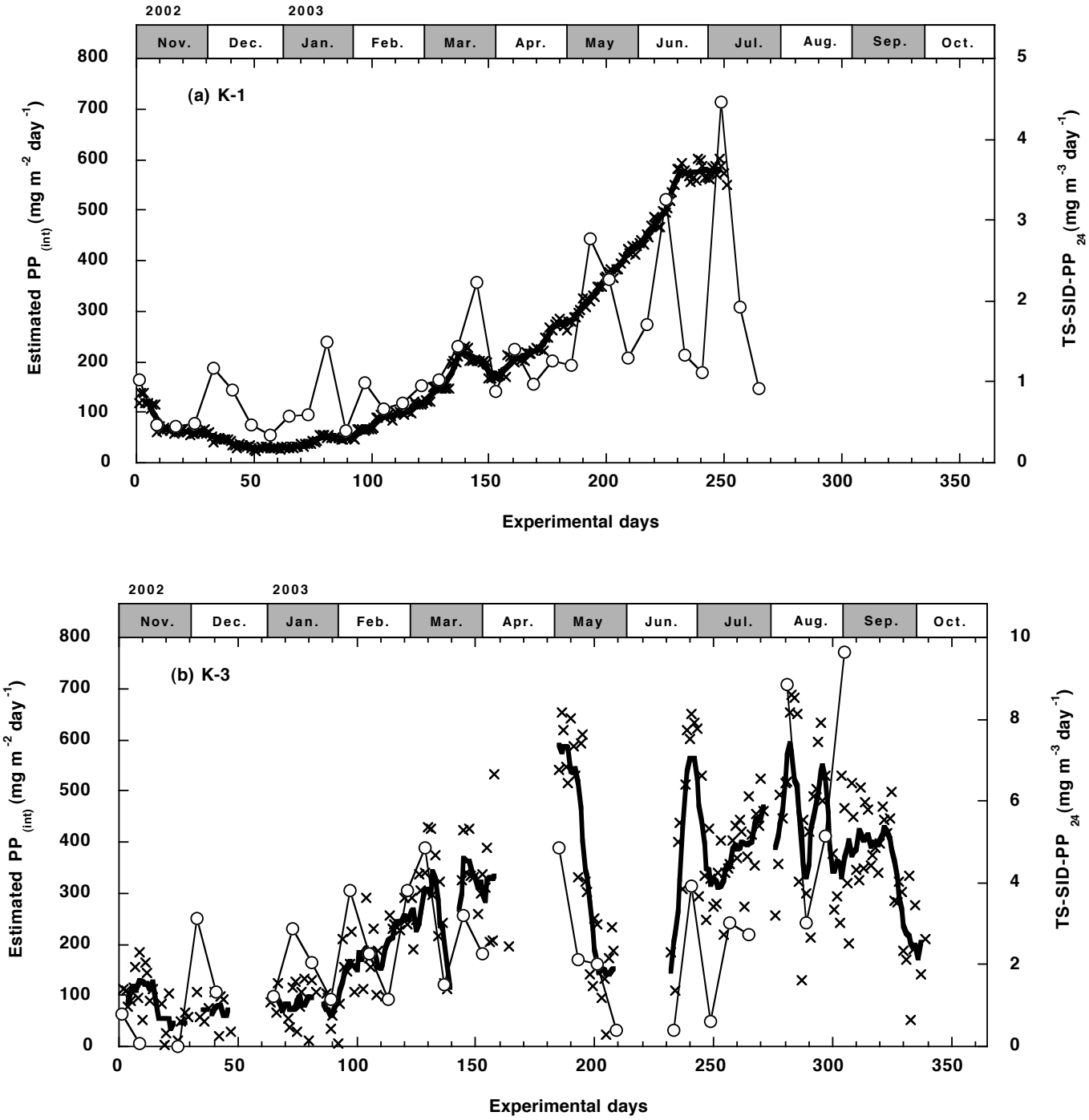

Fig. 10 Seasonal variability in TS-SID-PP_{24} at TS-SID depth (PP_{24}: open circles) and depth-integrated PP ($PP_{(int)}$: crosses) at stations K1 (a) and K3 (b). Thick solid line was a 7 day running mean of $PP_{(int)}$.

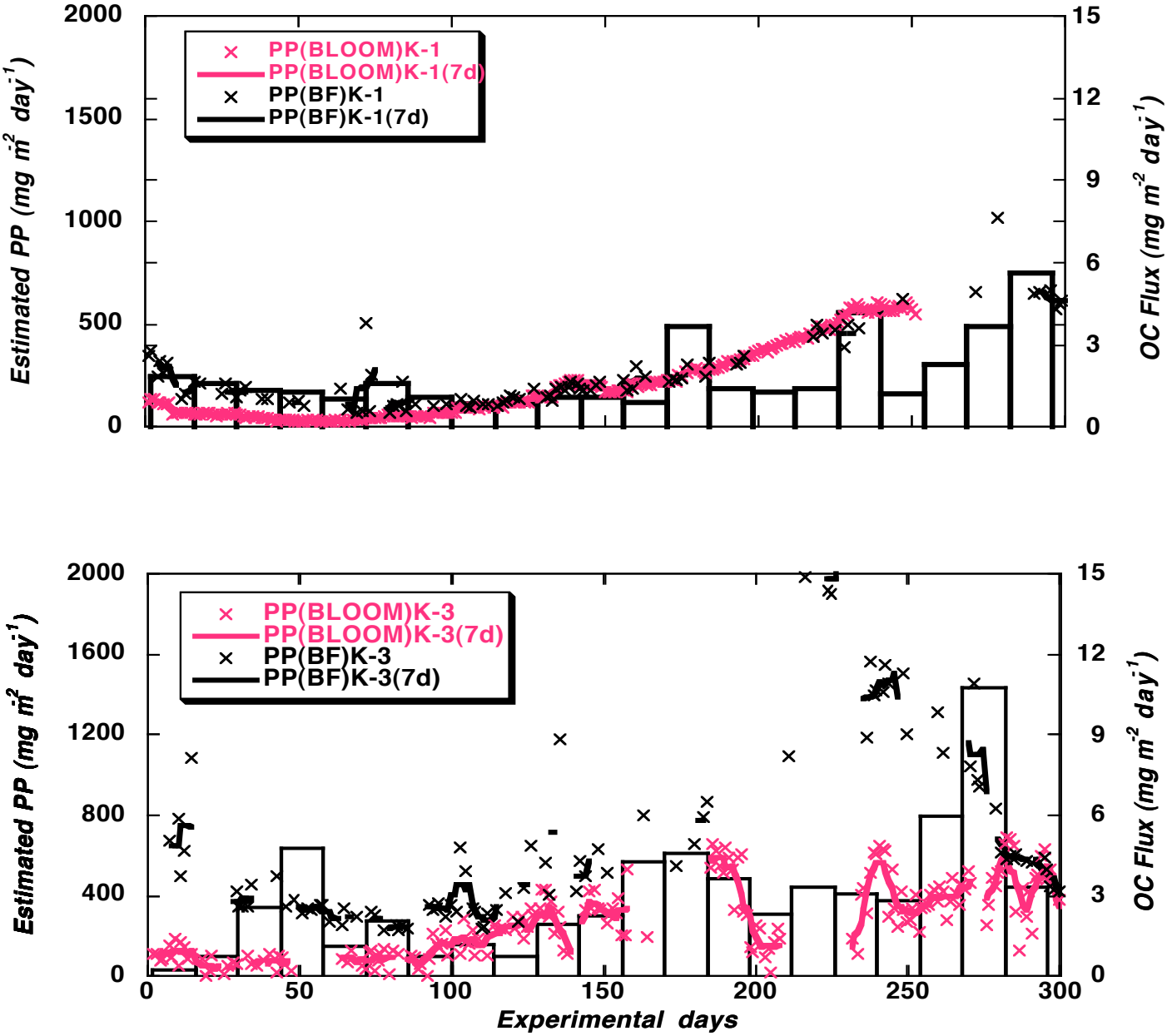

Fig. 11 Seasonal variability in estimated Primary productivity by BLOOMS data (red crosses) and satellite data with Behrenfeld and Falkowski's algorithm (black circles) with particulate organic carbon fluxes at 5000 m observed by sediment trap (bar graphs) at stations (a) K1 and (b) K3. Lines for estimated primary productivities are 7 days running mean

(3) Quick transport of primary produced organic carbon to the ocean interior

Time-series observations of optical fields in the euphotic layer and particle fluxes at 150 m were made at station K2 in the western North Pacific for half year of 2005 (March to September) by using BLOOMS and sediment trap at 150 m. The ratio of surface PAR to *in situ* quantum irradiance at approximately 40 m (*in situ* QI), as an index of turbidity, began to increase in the middle of April, peaking between the end of June and the middle of July (Fig. 12). Seasonal variability in the ratio of spectral irradiance at a wavelength of 555 nm to that at 443 nm ($Ed_{(555)}/Ed_{(443)}$) at 40 m, as an index of chlorophyll-*a* abundance, synchronized well with the surface PAR / *in situ* QI ratio (Fig. 13). Organic carbon flux also increased between the end of June and the middle of July and correlated well with optical variability. This result suggests that primary produced carbon in the euphotic layer was quickly transported to the ocean interior at least 150 m without significant time lag unlike the previous report that there is a time lag between increase in primary productivity and increase in organic carbon flux because of food web,

Good relation was found between the $Ed_{(555)}/Ed_{(443)}$ at 40 m observed by optical sensor and integrated chlorophyll-*a* abundance (Chl-$a_{(int)}$) upper 40 m observed with discrete seawater samples in the northern North Pacific (Fig. 13). Using proposed empirical equation and the following equation, seasonal variability in primary productivity was estimated:

$$PP = \text{Chl-}a_{(int)} \times \text{surface PAR} \times \Psi$$

Where Ψ is light utilization index and 0.3 ± 0.1 for the Western Subarctic Gyre.
Seasonal variability in estimated primary productivity coincided well with that in organic carbon flux (Fig. 14). Average primary productivity was estimated to be approximately 300 mgC m^{-2} day^{-1} and this value was comparable to primary productivity reported previously at station KNOT. Assuming that trapping efficiency was only 20% based on ^{230}Th measurement and organic carbon flux decreased drastically between 100 m and 150m following "Martin curve", the export ratio at 100 m was estimated to be *ca.* 30 ± 10%, which is significantly higher than that in other oceans reported previously.

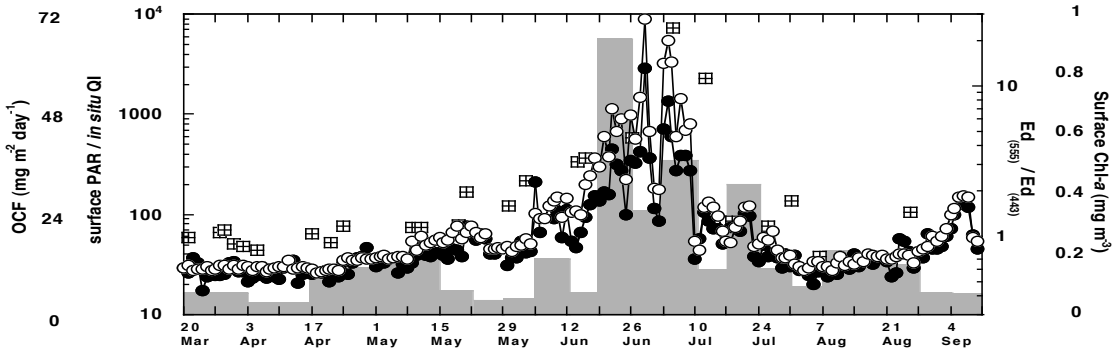

Fig. 12 The $Ed_{(555)}/Ed_{(443)}$ (open circles), surface PAR / *in situ* QI ratios (closed circles), and Organic Carbon Flux (OCF) at 150 m (bar graphs). Squares are SeaWiFS derived surface Chl-*a*.

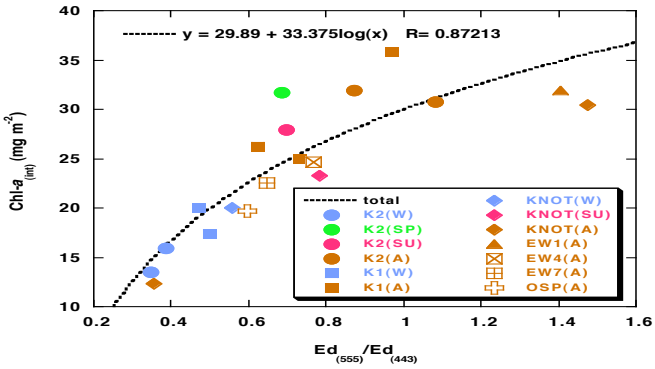

Fig. 13 Relation between $Ed_{(555)}/Ed_{(443)}$ at 40 m and integrated Chl-*a* abundances upper 40 m ($Chl\text{-}a_{(int)}$). The $Ed_{(555)}/Ed_{(443)}$ were measured at 40 m with underwater optical sensor (Satlantic SeaWiFS Multichannel Radiometer), and Chl-*a* of discrete seawater samples upper 40 m were measured using Turner designs fluorometer aboard ship at various stations and seasons in the northern North Pacific during previous *R/V MIRAI* cruises [*Honda*, unpublished data]. Stations K2, K1, KNOT, EW1, EW4, EW7 and OSP are located at 47°N/160°E, 51°N/165°E, 44°N/155°E, 47°N/169°E, 46°N/175°W, 49-30°N/160°W and 50°N/145°W, respectively. W, SP, SU, and A in parenthesis indicate observation seasons of winter, spring, summer and autumn, respectively. Despite data collected at different locations and seasons, good correlation between $Ed_{(555)}/Ed_{(444)}$ and Chl-$a_{(int)}$ can be seen.

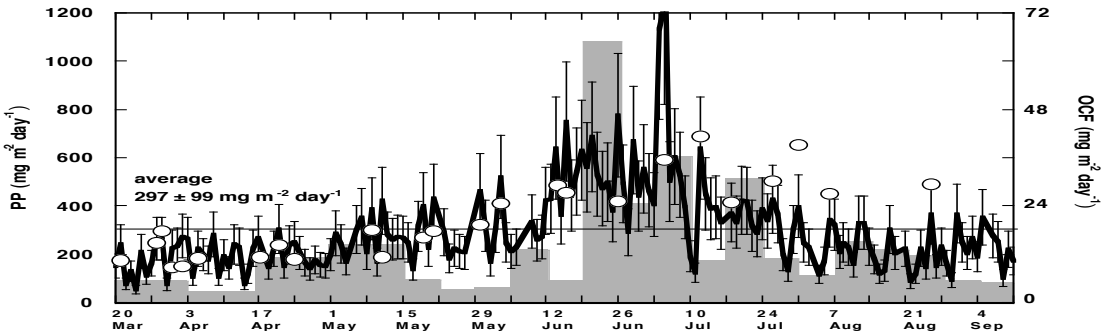

Fig. 14 Seasonal variability in primary productivity estimated with the $Ed_{(555)}$ / $Ed_{(443)}$ ratio and empirical equation (see text). Open circles are PP estimated with satellite data and algorithm [*Kameda and Ishizaka*, 2002]. Bar graphs are OCF at 150 m.

(4) Seasonal variability in nutrients observed by Remotely Access Sampler (RAS)

Concentrations of nutrients (NO_3, NO_2, $Si(OH)_4$, PO_4) and dissolved inorganic carbon (DIC) were measured in time-series seawater samples collected by automatic water sampler (Remote Access Sampler, RAS) at station K2 in the Northwestern North Pacific for approximately 15 months in 2005 and 2006. Collected seawater samples were preserved with $HgCl_2$ solution. Based on depth sensor, the RAS was located around 40 m (35 ± 1 m between March and September 2005 and 40 ± 5 m between October 2005 and May 2006) in the surface mixed layer during whole mooring period except period between Jun and September (Fig. 15 a). Corrected salinity values of RAS samples were comparable with climatological salinity data (Fig. 15 c). Although there were some problems in measurements of PO_4 (by effect of $HgCl_2$?) and DIC (by effect of degassing caused by HCl for anti-biofouling or mechanical problem ?), seasonal variability and concentrations of NO_3 + NO_2 (NO_x) and $Si(OH)_4$ were comparable to previous shipboard observations and observation by US NSF supported VERTIGO cruise (Fig. 16). Concentrations of these nutrients began to decrease in late April. After the end of June, NO_x and $Si(OH)_4$ decreased rapidly with large fluctuations. After October, these nutrients increased again until late spring 2006. The ratio of the decrease of $Si(OH)_4$ to that of NO_x suggested that numbers of biogenic opal-producing creatures such as diatoms increased after the end of June (Fig. 17). This conclusion was supported by a rapid increase in biogenic opal flux recorded in a sediment trap at 150 m (Fig. 18).

The relationship between NO_x concentrations at the RAS depth of 35 m and NO_x integrated over the upper 100 m was determined using previous shipboard hydrocast data. This relationship was used to estimate integrated mixed layer NO_x from RAS data. Estimated new production based on seasonal drawdown of integrated NO_x averaged approximately 156 mg-C m^{-2} day^{-1} annually and agreed with previous estimates. Thus, an automatic seawater sampler that documents annual maximum and minimum nutrient concentrations and episodic events such as storms and spring blooms, which might be missed by ordinary research vessel observation, will contribute to time-series observations of nutrients and biological pump activity.

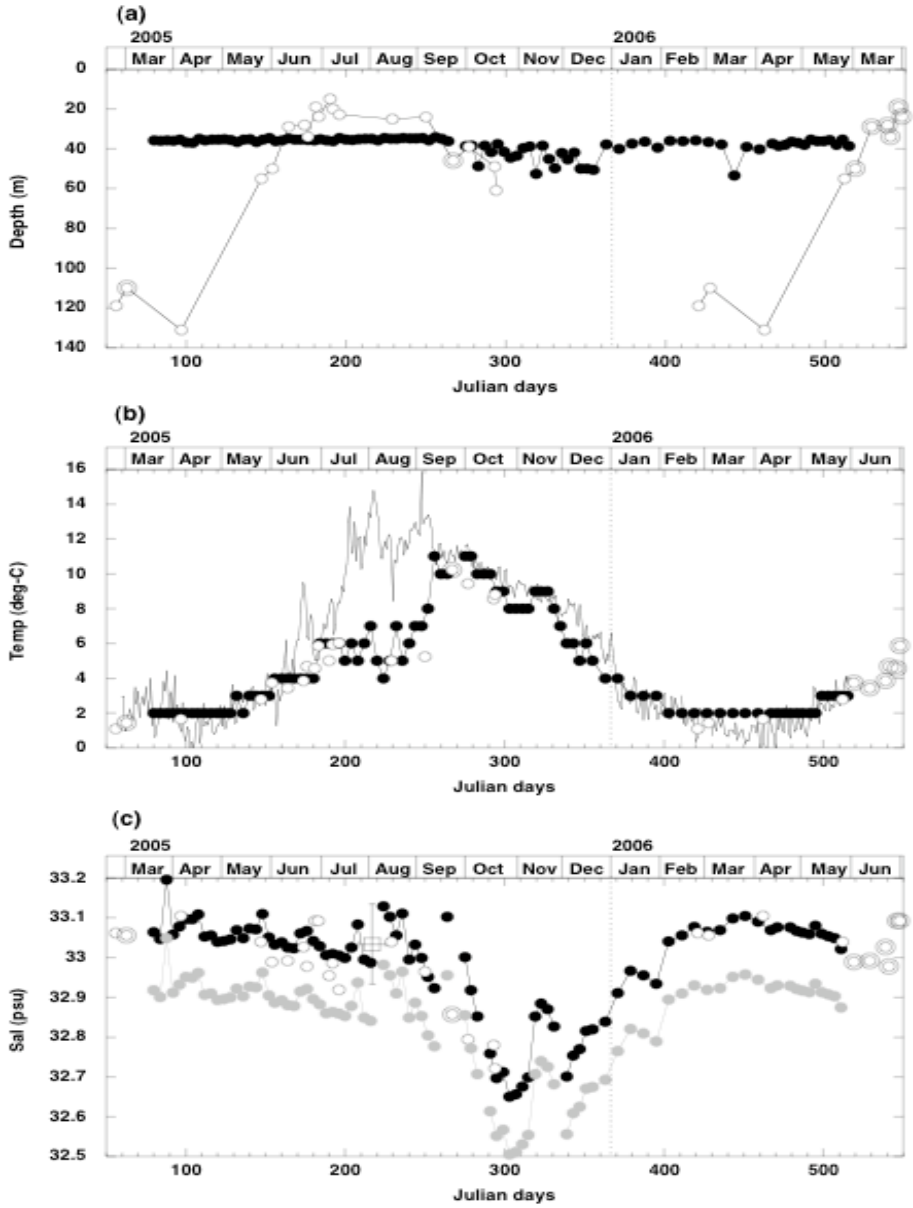

Fig. 15 (a) Seasonal variability in RAS depth (closed circles), and the mixed layer depth (MLD) based on hydrocast data (double circles) and climatological data (open circles) (see text). Horizontal axis is Julian days (JD). JD 1 and JD 367 are 1 January 2005 and 1 January 2006, respectively. (b) Seasonal variability in *in situ* temperature observed by RAS thermister (closed circles), and water temperature at 35 m based on hydrocast data (double circles) and climatological data (open circles). Solid line indicates Sea Surface Temperature (SST) obtained by satellite (courtesy of K. Sasaoka, JAMSTEC). (c) Seasonal variability in salinity of RAS samples. Gray circles are observed salinities and closed circles are salinities corrected for dilution of RAS sample by mainly preservative. Double circles and open circles show hydrocast and climatological data, respectively. A square with cross is a mean VERTIGO salinity data. Vertical error bar is standard deviation (1σ) of VERTIGO salinity data (n = 26) and horizontal error bar is period when VERTIGO data were obtained.

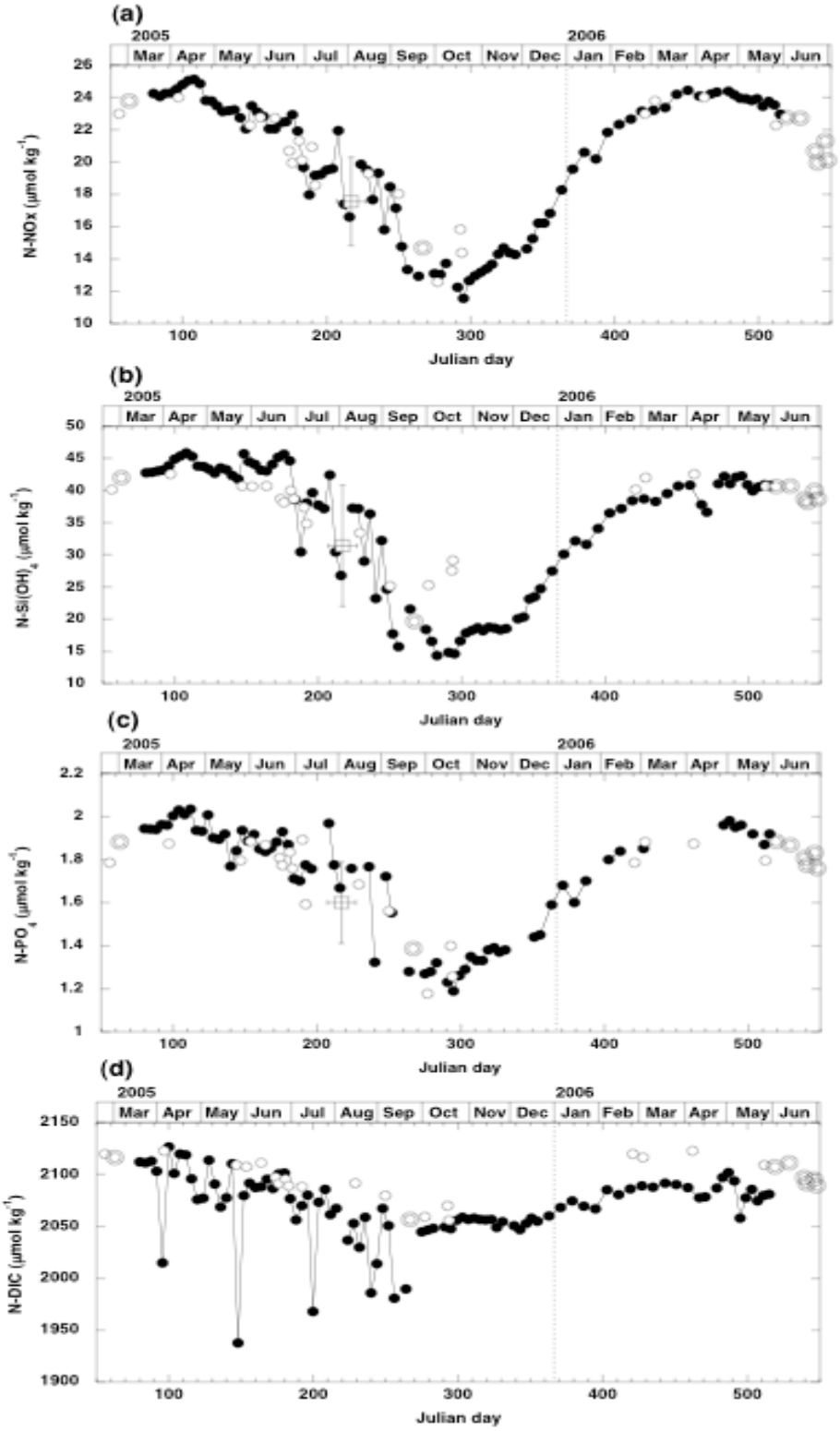

Fig. 16 Seasonal variability in (a) NO_x, (b) $Si(OH)_4$, (c) PO_4^{3-}, and (d) DIC. Closed circles, open circles and double circles show observed data from RAS, climatological data and hydrocast data, respectively. A square with cross is VERTIGO data with standard deviation. All data are normalized to a salinity of 33.

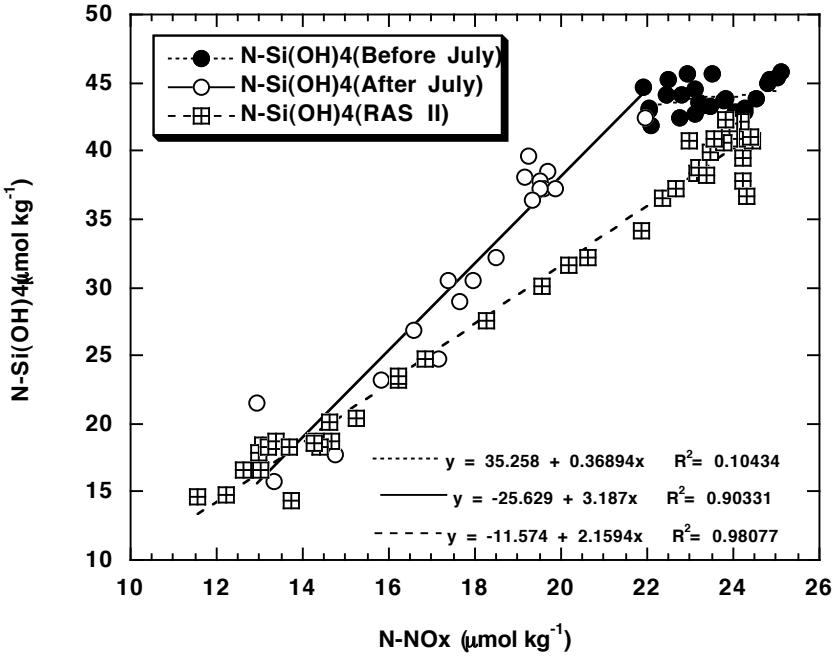

Fig.17 The relationship between normalized NO_x ($N\text{-}NO_x$) and $Si(OH)_4$ ($N\text{-}Si(OH)_4$). Data are divided into three groups: closed circles with dotted regression line, data from before the end of June 2005; open circles with solid regression line, from July through September 2005; squares with broken regression line, after October 2005 (phase II).

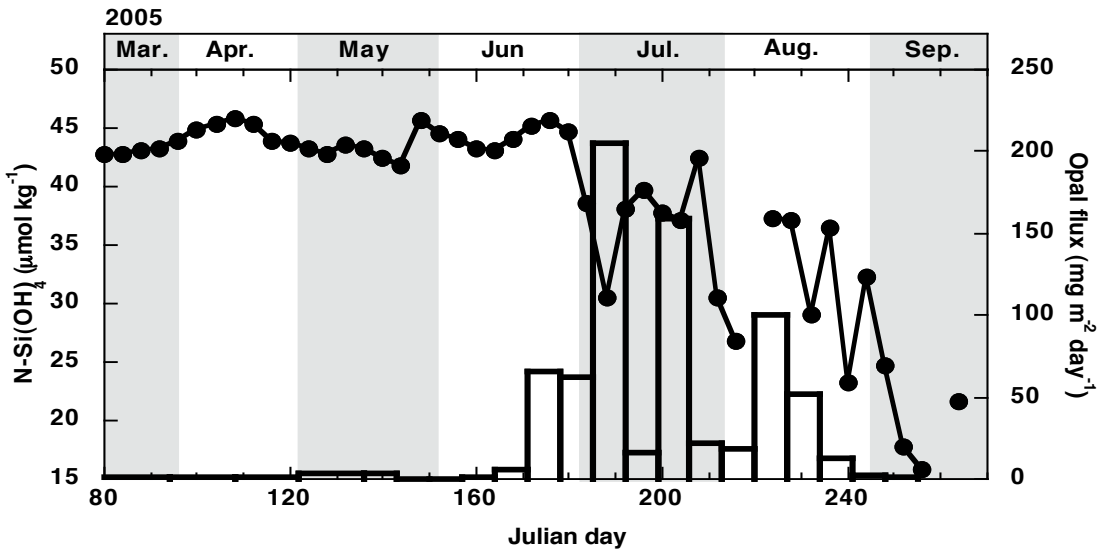

Fig. 18 $N\text{-}Si(OH)_4$ concentrations between 20 March 2005 and 20 September 2005 (line graph) and biogenic opal flux at 150 m observed by sediment trap (bar graph, Honda *et al.*, 2006).

(4) Vertical transport of materials in the mesopelagic layer or twilight zone

Based on good synchronization of change of optical condition, which is deeply associated with primary productivity, and nutrients with change in biogenic materials' fluxes collected by sediment trap at 150 m, it was certified that primary produced carbon and opal are quickly transported to the ocean interior at station K2. In order to verify destination of transported materials, time-series sediment trap were deployed at 540 m, 1000 m and 4810 m between March 2005 and May 2006 and settling particles were collected. Based on data during March 2005 and September 2005, which chemical analysis were completed, the following properties have been certified.

Flux peaks of total mass flux (TMF) were observed in middle March and in late June at 150 m (Fig. 19). The later TMF flux peaks were also observed at 540 m, 1000 m, and 4810 m with time lag. TMF averages were approximately 96, 24, 36 and 145 mg m-2 day-1 at 150 m, 540 m, 1000 m, and 4810 m, respectively. Assuming the steady state and no lateral transport, trapping efficiencies of sediment traps suspected by ^{230}Th flux were approximately 20, 1, 8 and 68 % at 150 m, 540 m, 1000 m, and 4810 m, respectively.

Fig. 20 shows chemical composition of settling particles at respective depths. At 150 m, concentration of $CaCO_3$ was higher than 50 % in March. Concentration of opal began to increase in middle June and was peaked in late July when concentration of $CaCO_3$ was little. Concentrations of organic materials were higher at 150 m than that at other depths. Although relative concentrations of respective components (organic materials, Opal, $CaCO_3$, lithogenic materials) are different, variability of chemical composition of settling particles at deeper depths showed similar pattern: $CaCO_3$ was predominate in March and opal was predominate in late July.

In general, organic carbon flux at 150 m was low at the beginning of experiment (March 2005) and gradually increased (Fig. 21). Organic carbon flux was largest in late June. Seasonal change in organic carbon flux at deeper depths synchronized well with that at 150 m with time lag. $CaCO_3$ flux was large in March at 150 m (Fig. 22). Based on observation by the naked eye", foraminiferas were predominate in this particles. This larger $CaCO_3$ flux was also observed in settling particles for same period at deeper layer. On the other hand, opal flux increased in late June at 150 m and in early August at 4810 m. Opal fluxes correlated well with organic carbon fluxes ($r > 0.9$).

Based on the preliminary analysis with above results, the following properties were summarized.

(1) Surface-derived particles were transported vertically without significant lateral transport.
(2) Sinking velocity increased with depth ranging from approximately 30 m day^{-1} (on average between 150 m and 540 m) to 130 m day^{-1} (on average between 1000 m and 4810 m)
(3) Opal flux played a role in ballast for transport of organic carbon at station K2.

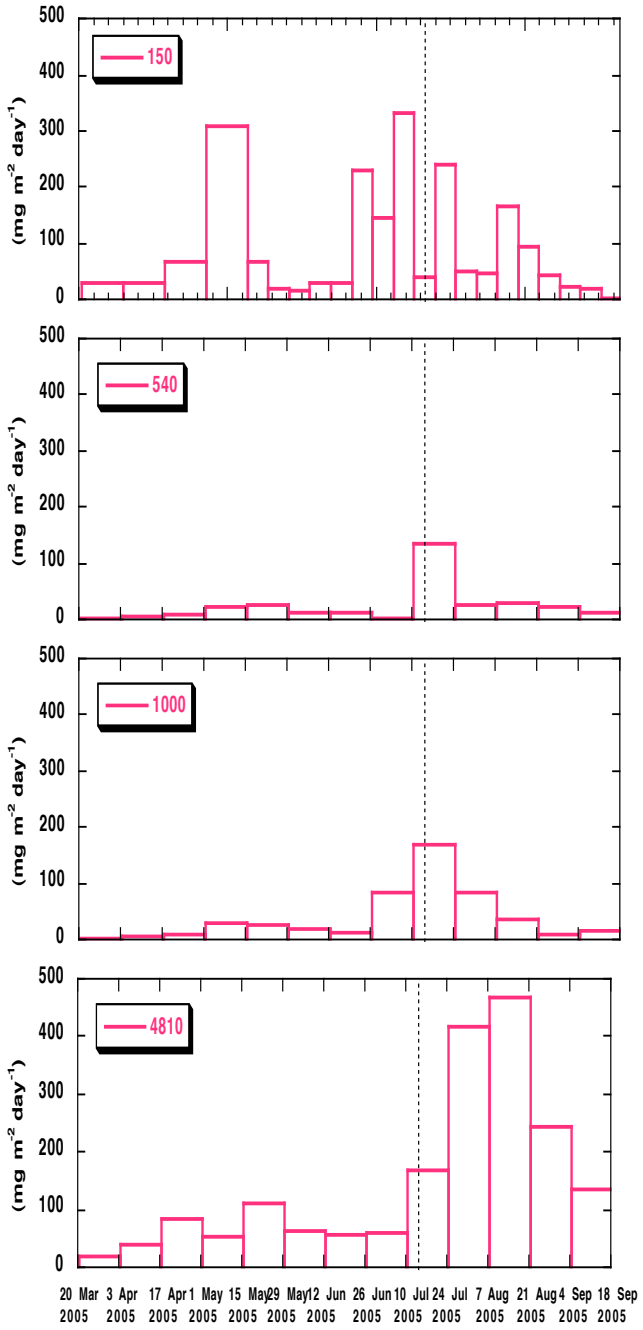

Fig. 19 Total mass fluxes at 150 m, 540 m, 1000 m and 4810 m between March 2005 and September 2005

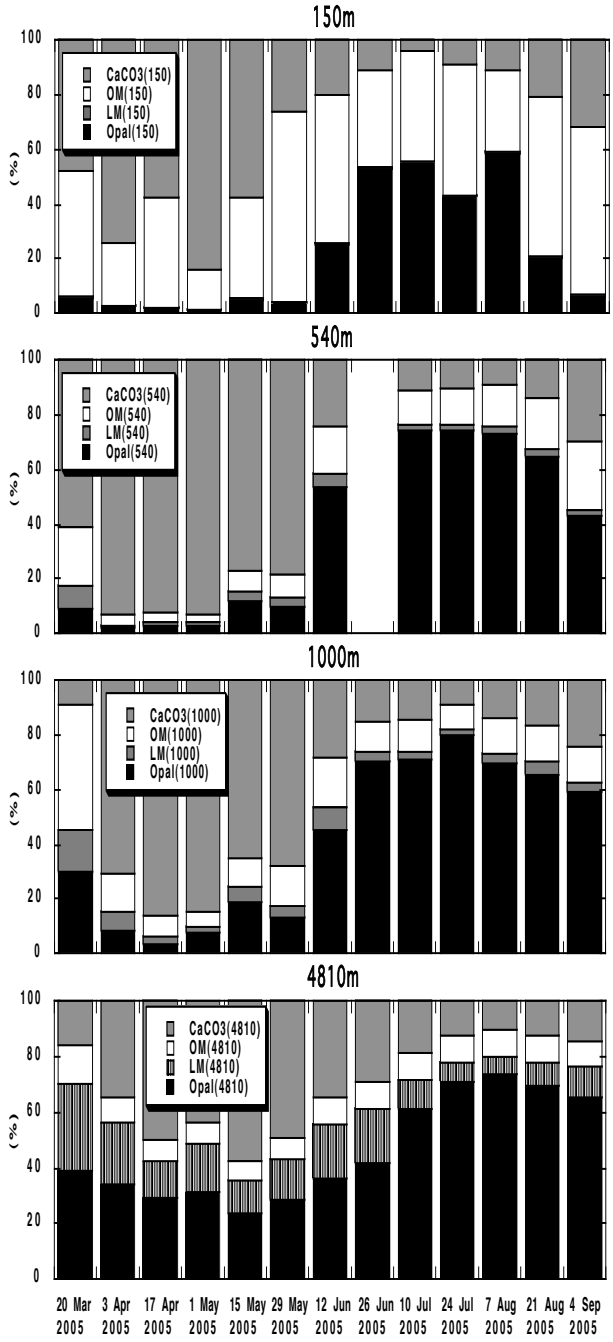

Fig. 20 Chemical composition of settling particles at respective depths. Gray, white, striped and black bars are proportions of $CaCO_3$, organic material (OM), lithogenic materials and opal, respectively.

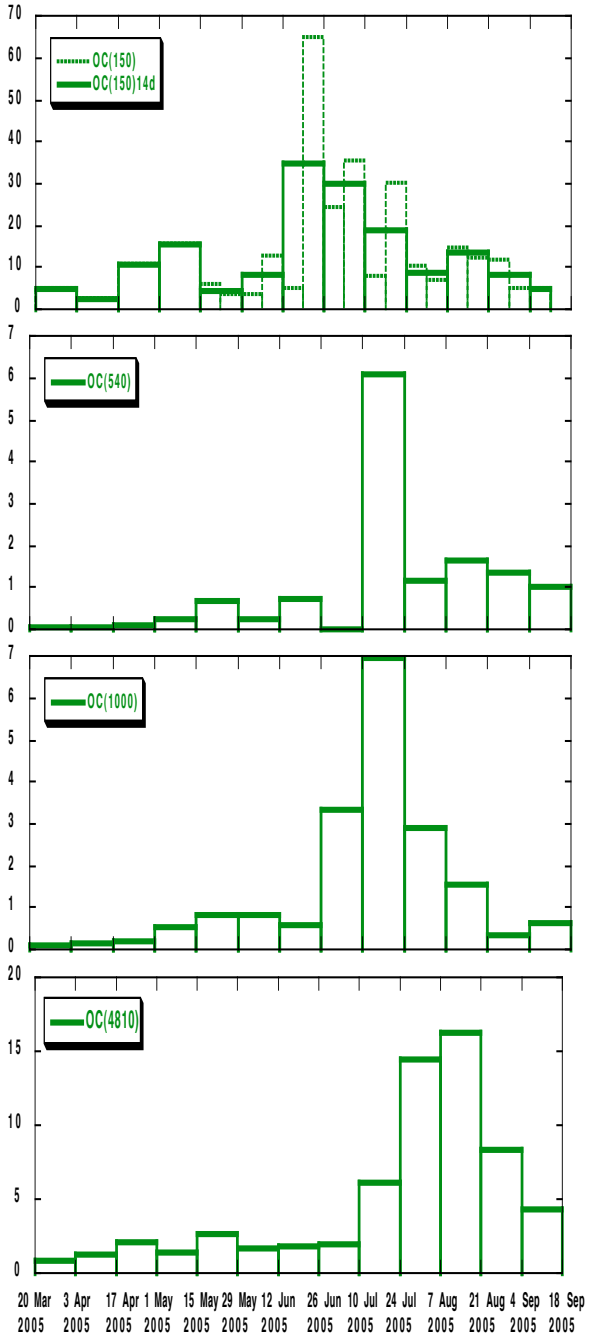

Fig. 21 Organic carbon fluxes at 150 m, 540 m, 1000 m and 4810 m between March 2005 and September 2005. It is noted that vertical scales of graphs are not same.

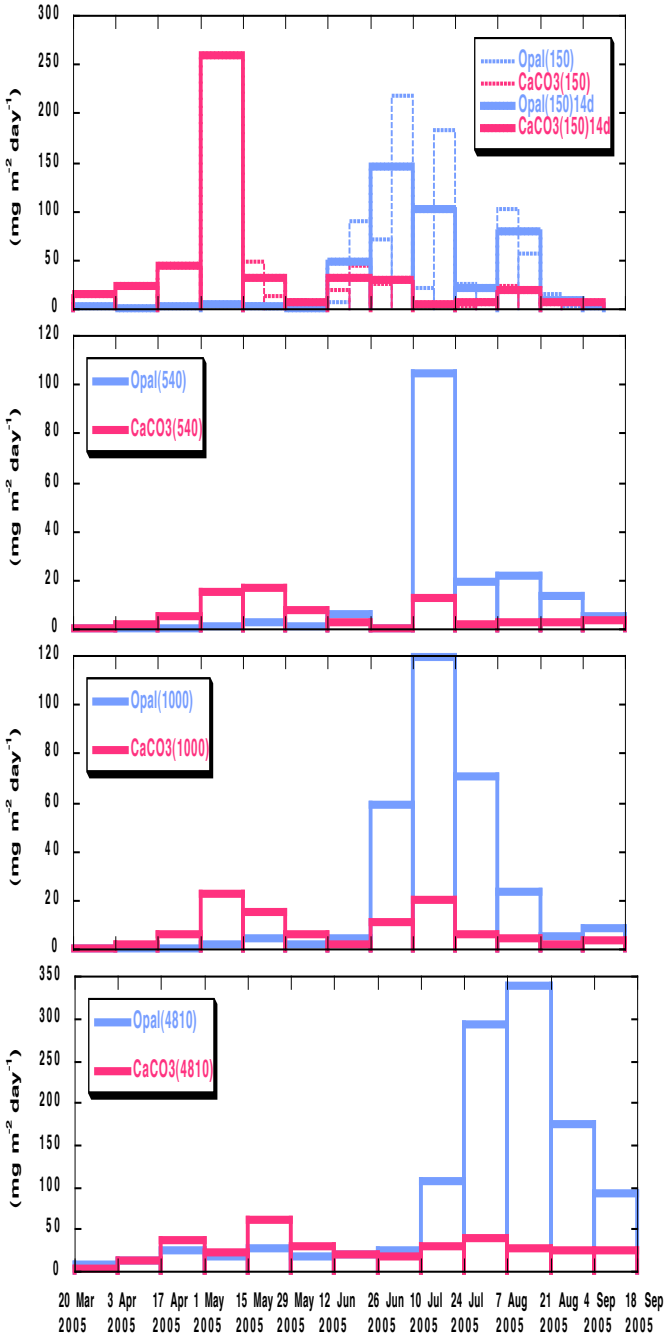

Fig. 22 $CaCO_3$ fluxes (red line) and Opal flux (blue line) at respective depths. It is noted that vertical scales of graphs are not same.

3.2 Time-series observation by research vessel

Since 2001, 13 scientific cruises have been devoted to our time-series observational study (Fig. 1). Though main mission was usually to turn around our mooring systems, we conducted interdisciplinary observation such as hydrocasting, measuring primary productivity and collecting suspended and sinking particles by in situ pumping system and drifting sediment trap so on. The following are highlights of these observations.

(1) Export flux and export ratio in the northwestern North Pacific

Time-series measurements of ^{234}Th activities and particulate organic carbon (POC) concentrations were conducted at several rime-series stations in the northwestern North Pacific from October 2002 to August 2004. Samples for measurement of dissolved ^{234}Th were collected with using Rosetta Multiple Sampler (RMS) or Carousel Multiple Sampler (CMS) systems with CTD from 10 m to 200 m. Particulate materials > 0.7 mm for measurements of particulate ^{234}Th and organic carbon were collected by in situ Large Volume Pumping system (LVP).

The total (dissolved + particulate) ^{234}Th generally showed depletion relative to ^{238}U throughout the above 100 m and increased with depth until 100 m. Between 100 and 200 m, the total ^{234}Th was close to the radioactive equilibrium value. The deficiencies of ^{234}Th were small from February to April and activities of ^{234}Th were nearly equivalent to those of ^{238}U (Figs. 23 a, b). The depletions of ^{234}Th relative to ^{238}U increased from May to July (Figs. 23 c, d) and slightly decreased from August to October (Figs. 23 e, f, g). This deficiency is likely attributed to ^{234}Th scavenging and subsequent downward export via settling particles.

The vertical profiles of concentrations of POC, in general, tended to be mirror image of the total ^{234}Th: POC decreased with depth until 100 m and was relatively constant below 100 m. The POC also shows seasonal variability: In general, POC above 100 m was larger from spring to summer (Figs. 5c, d, and e) and was smaller in winter (Figs. 5a and b). POC at station K3 was smaller than that at other stations.

The ratios of POC/^{234}Th ranged from approximately 10 to 400 μgC dpm^{-1} (Fig. 23). POC/^{234}Th ratios exponentially decreased with depth until 100 m and were relatively constant below 100 m. The ratios of POC/^{234}Th from spring to summer were larger than those in other season above 100 m. POC/^{234}Th at station K3 was generally smaller than those at other stations except early summer. Although POC/^{234}Th ratio above 100 m showed temporal and spatial variability, this ratio in winter and below 100 m, in general, did not vary largely.

Seasonal changes in POC sinking fluxes from surface layer (~100 m) were estimated from deficiency of ^{234}Th and calculated POC/^{234}Th ratio at 100 m (Fig. 24). POC fluxes varied seasonally from approximately 0 mgC m^{-2} d^{-1} to 180 mgC m^{-2} d^{-1} and values were higher in spring-summer than autumn-winter (Fig. 25). The export ratio (*e*-ratio), which is the ratio of export flux to primary productivity, ranged from 6–55%

and was also higher in spring-summer (Fig. 26). The annual POC fluxes were estimated to be 31 gC m^{-2} y^{-1} at station K2 and 23 gC m^{-2} y^{-1} at station K3. POC fluxes and *e*-ratios (approximately 30 % on annual average) in the northwestern North Pacific were much higher than those in much of the world's oceans. The annual POC flux based on ^{234}Th corresponded to 61–69% of annual new production estimated with the seasonal difference in the nutrients in the Western Subarctic Gyre (45–51 gC m^{-2} y^{-1}). It is indicative of that much of the organic carbon assimilated in the surface layer in the northwestern North Pacific is transferred as particulate form to the deep ocean. Our conclusion supports previous reports that diatom plays an important role in the biological pump.

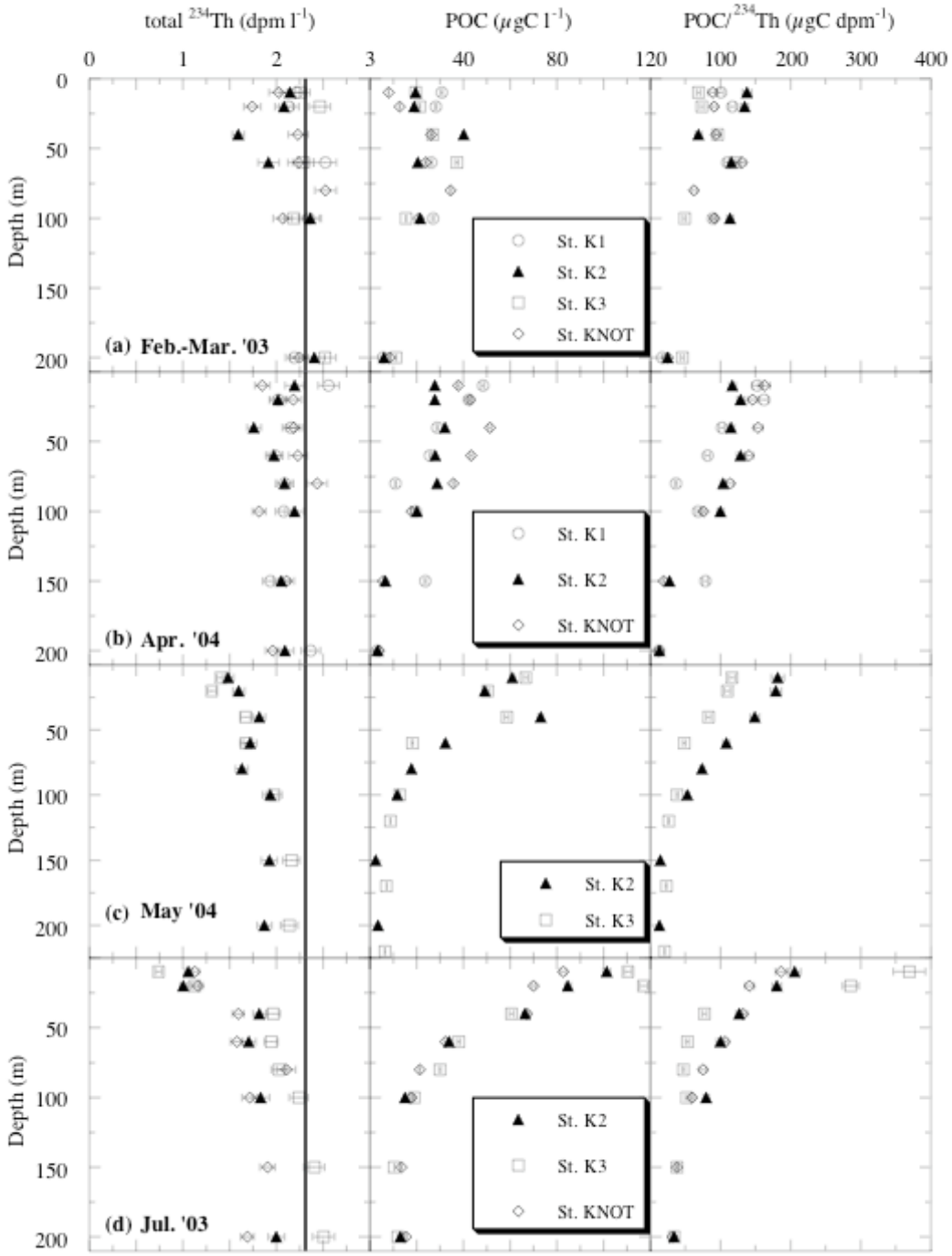

Fig. 23 Vertical profiles in concentrations of total ^{234}Th, POC and POC/^{234}Th ratios for respective cruises

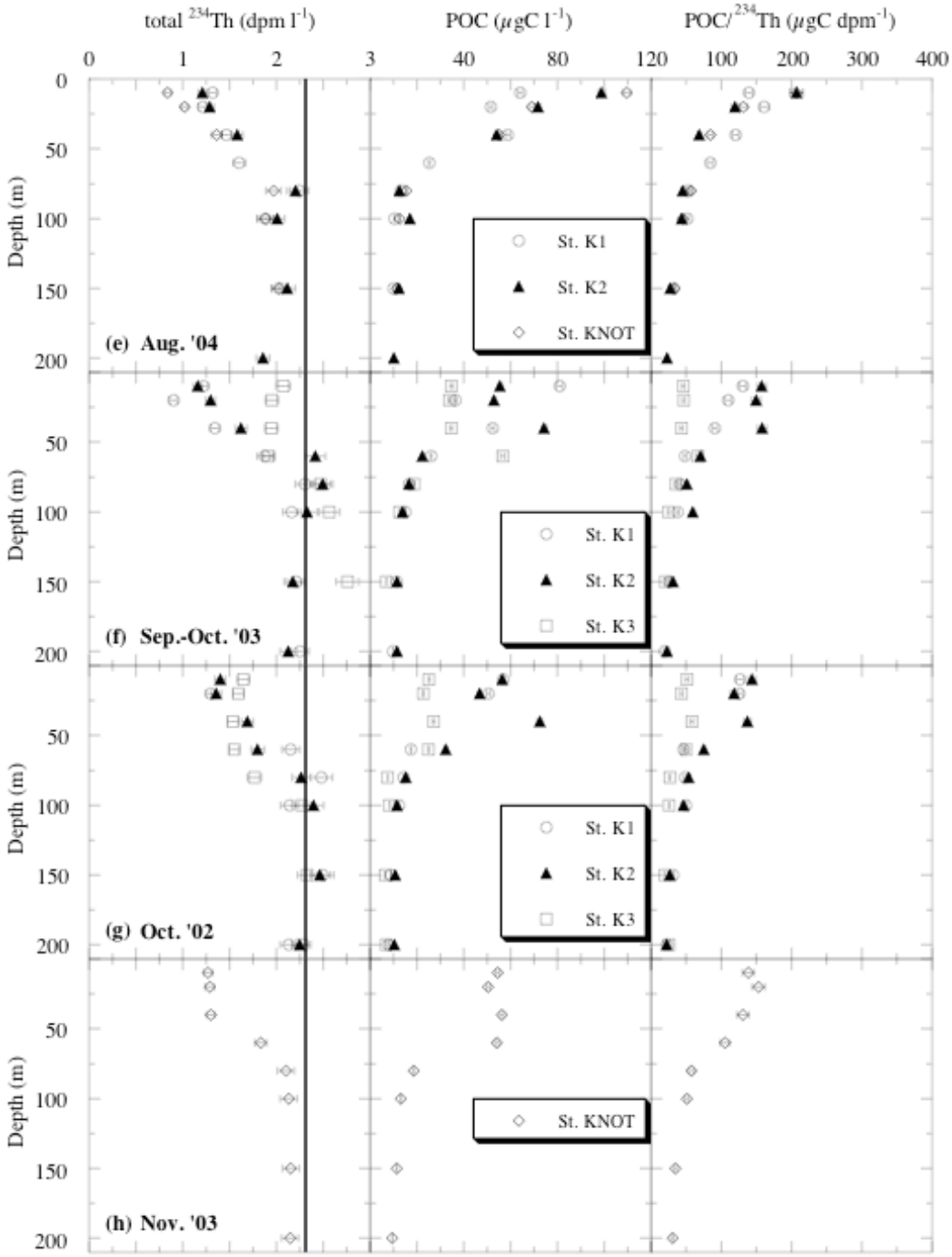

Fig. 23 continued

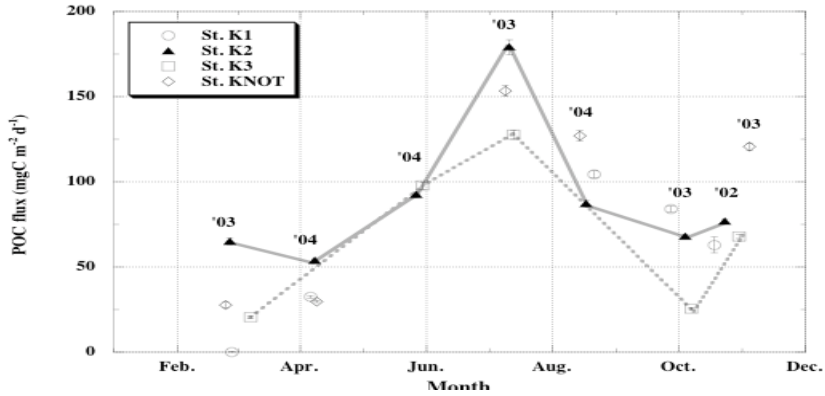

Fig. 24 Seasonal variability in POC export flux based on ^{234}Th measurement for respective stations. Data are arranged in order on Julian days in disregard for difference of years.

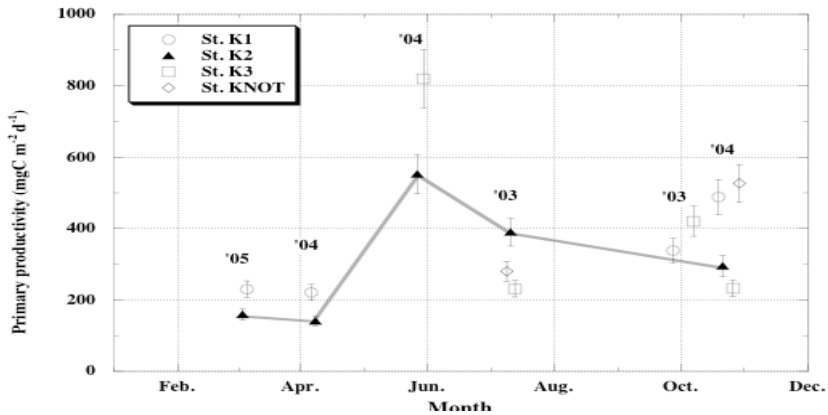

Fig. 25 Seasonal variability in primary productivity for respective stations.

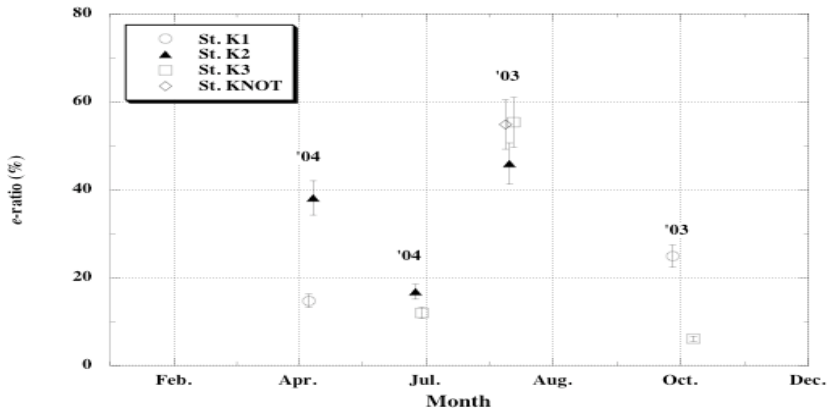

Fig. 26 Seasonal variability in export ratios (e ratios) for respective stations

(2) Seasonal changes in dissolved inorganic carbon and annual new production suspected with annual amplitude of nutrients and dissolved carbon

Time-series measurements of dissolved inorganic carbon (DIC) and nutrients concentrations have been made at time-series stations (K1, K2, K3 and KNOT) in the northwestern North Pacific from October 2002 to August 2004. Vertical distributions of DIC and nutrients showed large seasonal change in surface layer (~100 m) (Fig. 27). The seasonal variations of DIC and nitrate concentrations between maximum (in April) and minimum (in August) at the sea surface were 106–114 μmol kg^{-1} and 12.7–15.7 μmol kg^{-1} (Fig. 27). Assuming that respective data obtained in different years represent time-series seasonal data for a year, drawdowns of DIC and nutrients increased remarkably from May to July. The drawdown ratio of silicate to phosphate ($\Delta Si/\Delta P$) was higher at this period (26) than that at other periods (17–20), which is indicative of that large increase of diatom took place.

The column-integrated drawdown of DIC and nutrient in the surface mixed layer ($\sum A$ from 0 m to z m) can be expressed as following equation:

$$\sum A = \int_0^z (A_W - A_X)\, dz$$

Where A_W and A_X represent DIC and nutrients concentrations at each depth in winter (100 m) and other season, respectively. Both A_W and A_X were normalized to a constant salinity of 33 to remove the effect of evaporation and precipitation. Fig. 28 shows the seasonal changes in column-integrated drawdown of carbon ($\sum C$), nitrogen ($\sum N$), phosphorus ($\sum P$), and silicon ($\sum Si$) above 100 m at stations K1 and K2. The column-integrated drawdowns also show seasonal change; the minimum and maximum of the respective components were observed in April and October, respectively. Annual amplitudes (drawdowns from April to October) of DIC and nutrient at stations K1 and K2 can be estimated using the difference in minimum and maximum of the respective components, which were estimated with the sine curve fit on observed data. Using annual column-integrated drawdown of PO_4 (ΔP) and Redfield ratio (C/P = 106), annual drawdown of carbon upper 100 m (new production) at station K1 and K2 were estimated to be approximately 52 gC m^{-2} yr^{-1} or 142 mgC m^{-2} day^{-1}. This estimated new production was higher than those in the northeastern North Pacific and the equatorial Pacific reported previously. It is suggested that the efficiencies of biological pump in North Pacific are higher than those in other regions and these differences are attributed to differences in phytoplankton species and microbial loop.

The seasonal air-sea exchange of DIC (ΔC_{gas}) was estimated from column-integrated drawdowns of DIC (ΔC) and biological uptake of DIC (ΔC_{bio}), which was estimated from ΔP and Redfield ratio. Based on this calculation, it is verified that the northwestern North Pacific plays a role in source of CO_2 between winter and spring and sink of CO_2 between summer and autumn.

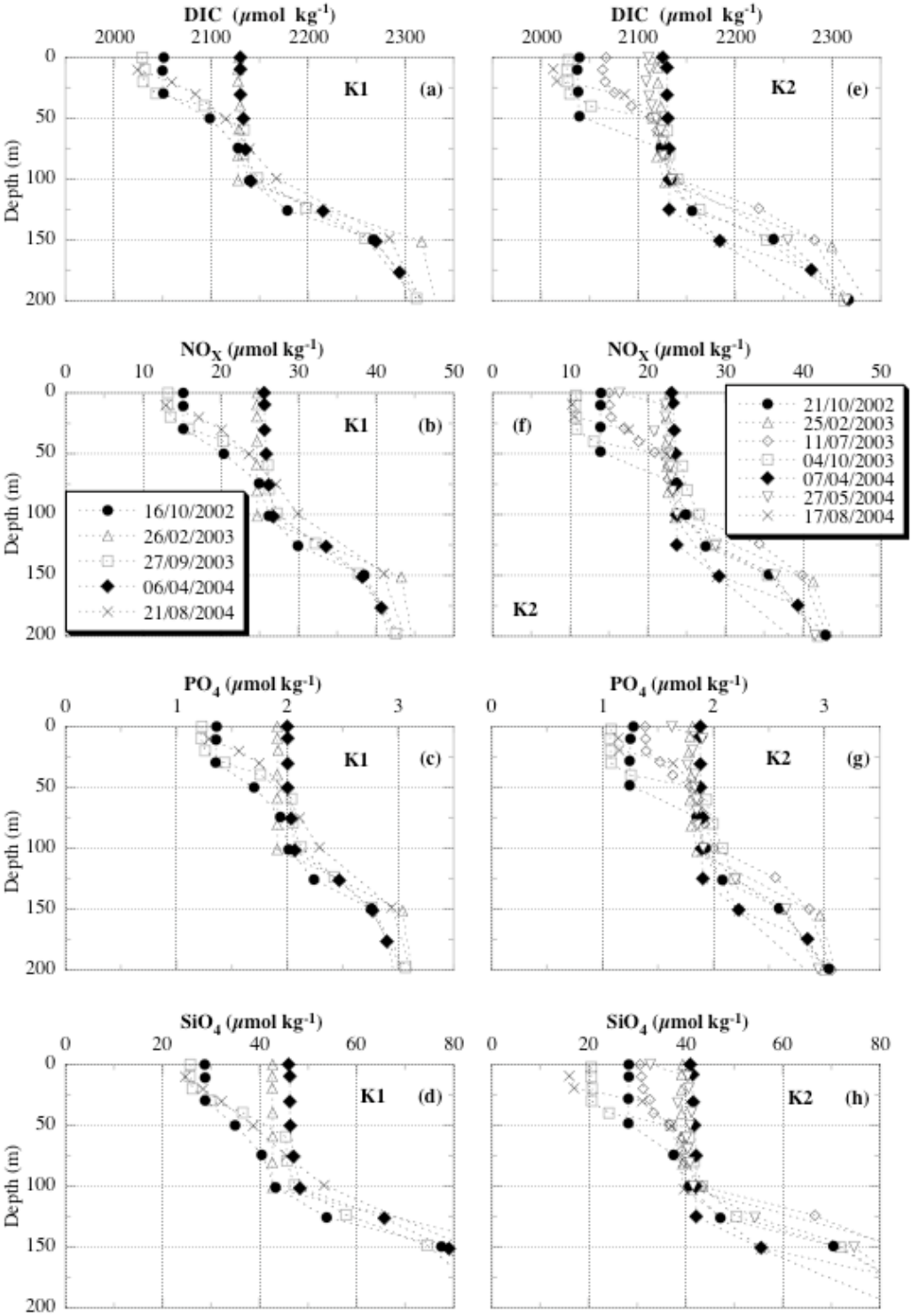

Fig.27 Vertical profiles in DIC and nutrients upper 200 m at stations K1 and K2

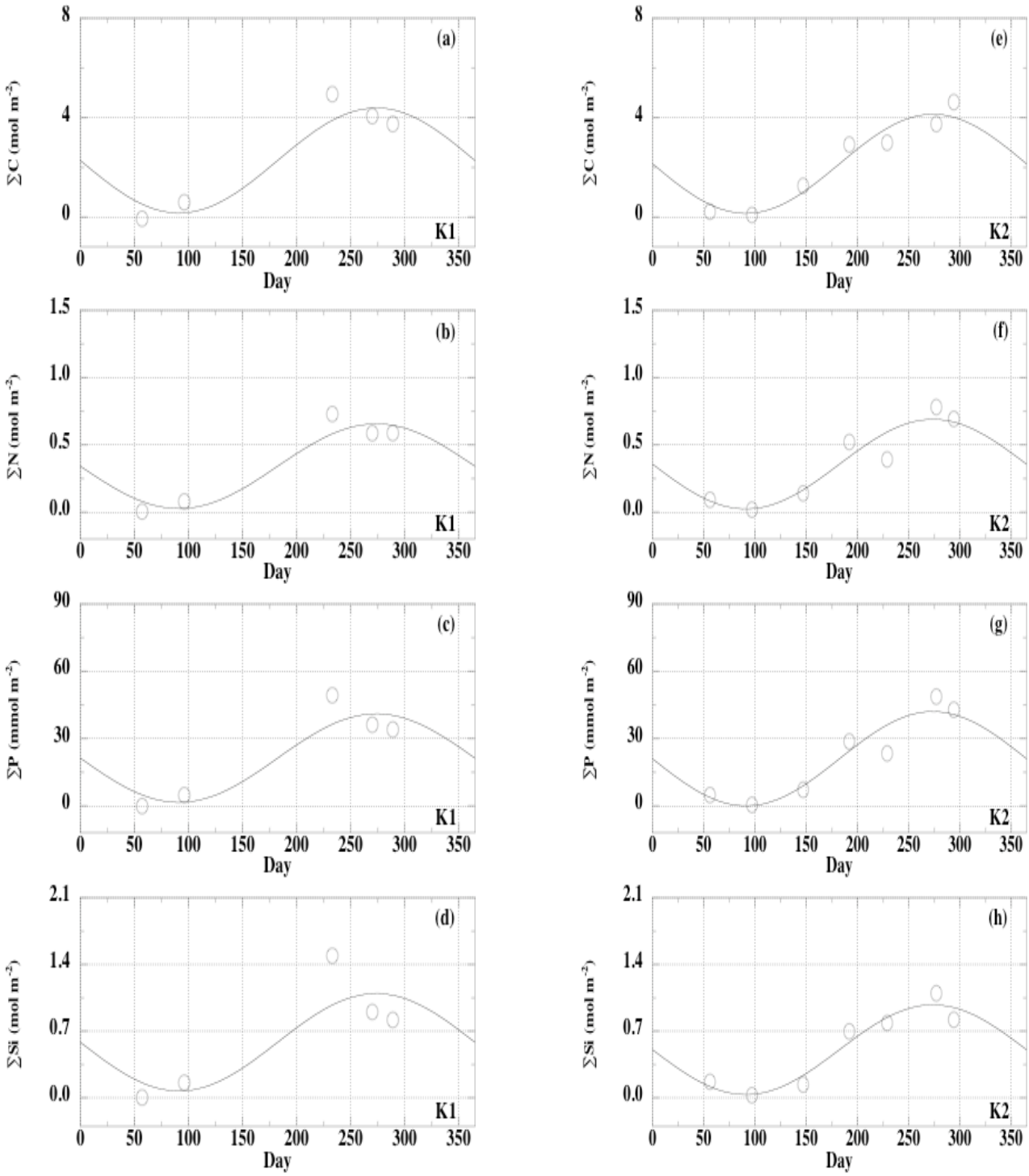

Fig. 28 Seasonal drawdown of integrated DIC and nutrients upper 100 m at station K1 and K2. Integrated DIC and nutrients for respective cruise are expressed as drawdown from annual maximum observed in April. Curves are sine curve fitting on observed data: $y = a*\sin(2\pi x/365) + b$.

(3) Interannual increase in dissolved inorganic carbon (DIC) at station K2

Among Hi-LATS stations, main station was station K2. Research vessels visited there the most frequently during the last 5 years (~ 15 times) and hydrocastings were conducted. As one of basic observation (routine work), the concentrations of dissolved inorganic carbon (DIC) and related chemical species (nutrients, total alkalinity: TALK, and dissolved oxygen) have been measured since 2001. The DIC and Apparent Oxygen Utilization (AOU) showed temporal variability along isopycnal layers 26.9 $\sigma\theta$ (~ 200 m) and 27.2 $\sigma\theta$ (~ 500 m), which corresponded the upper and lower boundary of the North Pacific Intermediate Water (NPIW). The concentration of DIC would be controlled by

1) Production and decomposition of organic matter
2) Production and dissolution of carbonate, mainly $CaCO_3$
3) Air-Sea CO_2 exchange at the region of NPIW formation.

Taking into account for 1) and 2), we estimated change of DIC by air-sea CO_2 exchange (Fig. 29). As a result, concentration of DIC at station K2 showed interannual increase along isopycnal layer of 26.9 $\sigma\theta$ (~ 200 m) while DIC did not show significant interannual increase along 27.2 $\sigma\theta$ (~ 500 m) Its increase rate was estimated to be approximately 2.0 μmol-C kg^{-1} yr^{-1} and coincided well with that at KNOT, which is the former Japanese time-series station located at the south-west edge of the Western Subarctic Gyre. DIC seemed to increase not monotonously but with fluctuation. However a limited data disable us to carry out statistical analysis.

In future, more accurate and longer time-series data will be required to confirm this data.

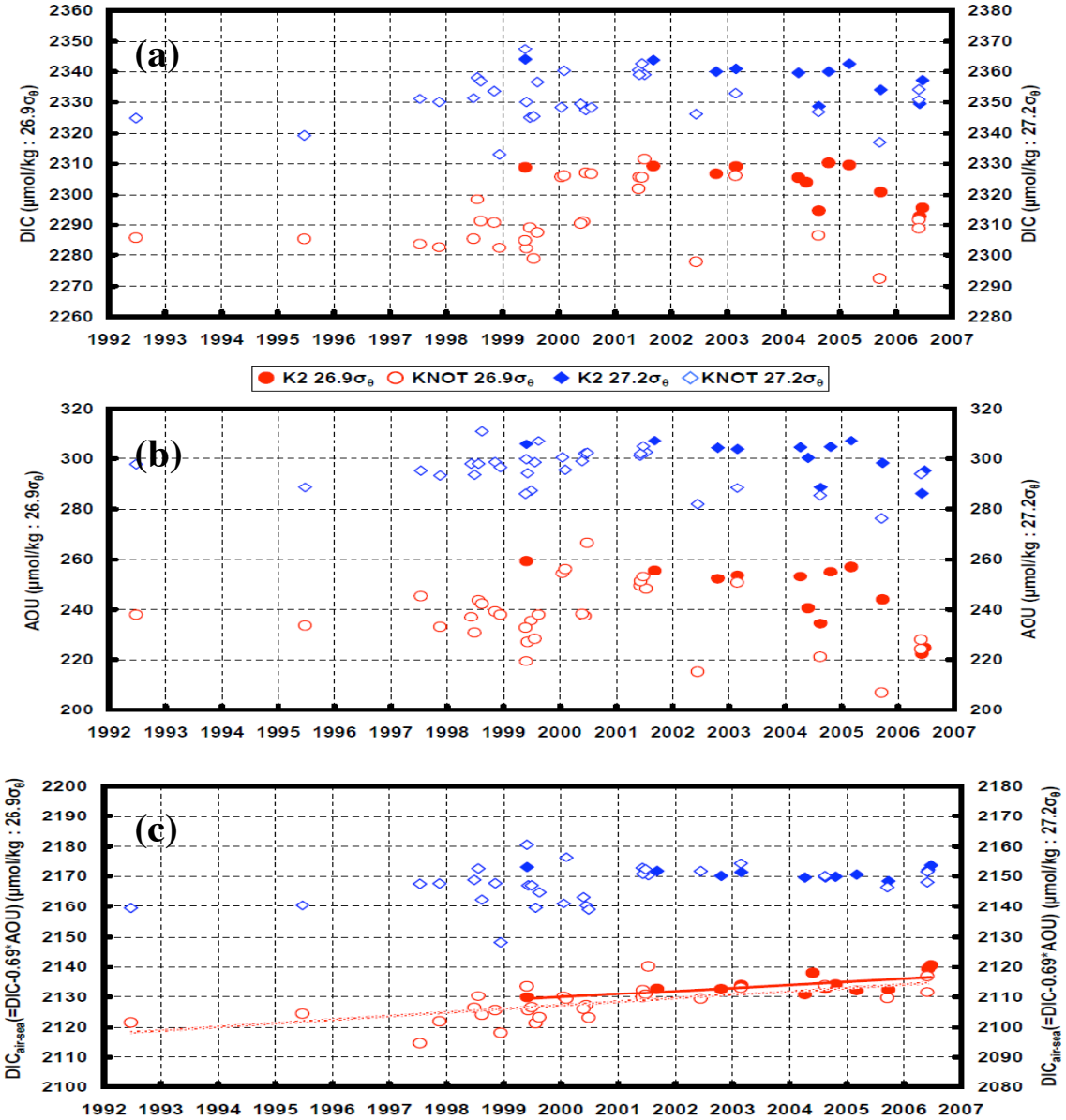

Fig. 29 Interannual variation in (a) measured DIC, (b) AOU and (c) estimated DIC originating from air-sea CO_2 exchange along two isophycnal layers (sigma-theta 26.9 and 27.2) at station K2 (closed symbols) and KNOT (open symbols)

(4) Comparative study on biogeochemistry between the western and eastern North Pacific

It has been reported that biogeochemistry such as species of phytoplankton, Fe supply and sinking particles are different between the Western Subarctic Gyre (WSG) and the Alaskan Gyre (AG). During MR05-04 cruise (September – October 2005), we crossed the northern North Pacific (north to 47°N) and conducted transect observation at several stations including station K1, K2 in the WSG and Ocean Station P (OSP) in the Alaskan Gyre (Fig. 30). We measured nutrients, carbon species, pigments, primary productivity and sinking particulate materials.

Horizontal distribution of phytoplankton pigments quantified with a HPLC system showed that diatoms, cyanobacteria, haptophytes and dinoflagellated were abundant in the western region while chlorophytes and haptophytes were abundant in the eastern region, especially haptophytes (coccolithophorids) occupied a great part of phytoplankton abundance at the OSP (Fig. 31). This result was consistent with previous reports and larger decrease of dissolved silicate in the western part.

Primary productivity at station K2 was approximately 450 mgC m^{-2} day^{-1} and larger than that at other stations during this period (Fig. 32). Primary productivity tended to decrease eastward. However it is noteworthy that light utilization index, which was production rate per chlorophyll per light intensity (PAR), were identical between respective stations and, therefore, there was not significant difference in "ability" of primary productivity between the western and eastern north Pacific during this period when difference in light intensity and temperature, which were generally lower in the eastern part and observed in October one month later than observation in the western part, were taken into account.

Particulate organic carbon fluxes at respective stations were measured by ^{234}Th-^{238}U methods and drifting sediment trap. Particulate organic carbon flux at 100 m (export flux) by ^{234}Th-^{238}U method ranged from approximately 21 mgC m^{-2} day^{-1} at station EW4 and 53 mgC m^{-2} day^{-1} and tended to decrease eastward (Fig. 33). Maximum export flux was observed at station EW1, which is located above the Emperor seamount. Export flux observed by drifting sediment trap (surface tethered PITS trap) ranged from approximately 23 mgC m^{-2} day^{-1} and 67 mgC m^{-2} day^{-1}. Maximum export flux was observed at station EW1 too. However export flux at station K2 was not high and the decrease eastward was not observed unlike export flux observed by ^{234}Th-^{238}U methods. Export ratios, which are ratios of export flux to primary productivity, ranged from approximately 8.5 to 16 % using ^{234}Th-^{238}U method-based export flux and ranged from 5 to 26 % using DST based export flux (Fig. 33). Although it has been reported that export ratio at station K2 or in the WSG are higher than 30 % on annual average and higher than other oceans, export ratios observed during this cruise in the WSG were at most 20 % and there was not significant difference between the western and eastern North Pacific. One of our hypotheses was that export flux and ratio in the WSG are higher than those in the AG because diatom is pre-dominant in the WSG and plays an important role in biological pump. However

results of observation did not support our hypothesis. Moreover chemical composition of sinking particles collected by DST showed that proportion of opal in sinking particles at station K2 was lower than that at station OSP (Fig. 34) and tended to increase eastward. This result seems to be inconsistent with horizontal distribution of phytoplankton pigments and previous report. Opal in sinking particles should be identified by microscopic analysis.

There are still uncertainties in determination of the ratio of organic carbon to ^{234}Th in sinking particle and trapping efficiency of DST. In addition, the above results were a "snap shot" of biogeochemistry in the northern North Pacific where has a large seasonal variability and, therefore, we can not describe difference in biogeochemistry between the western and eastern Pacific with only our data. For better understanding, simultaneous time-series observations for biogeochemistry at both gyres are requested in future.

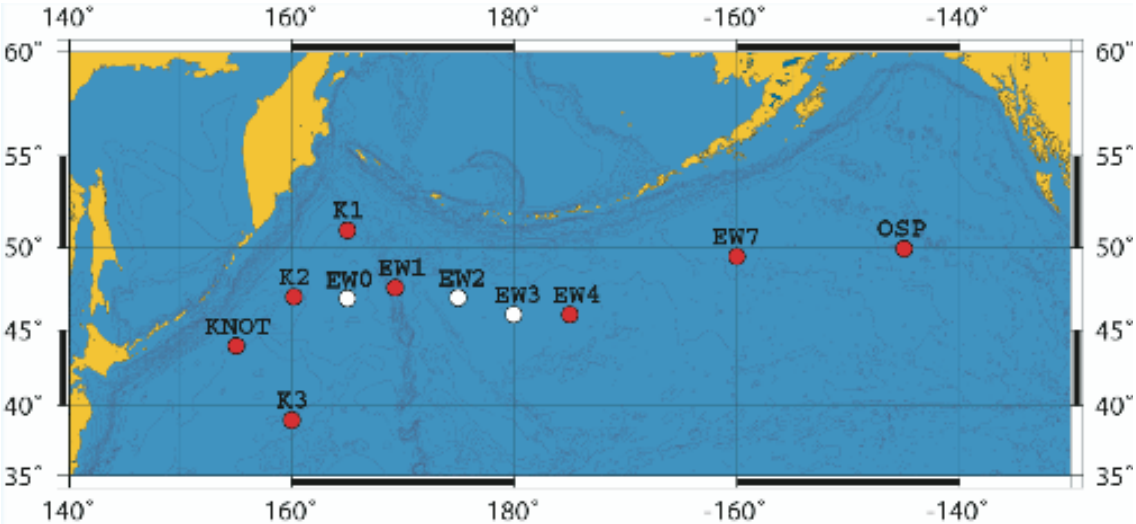

Fig. 30 MR05-04 Observation stations. Open circles are stations at where hydrocasting was conducted and red circles show stations at where measurements of pigments, primary productivity and sinking particles in addition to hydrocasting.

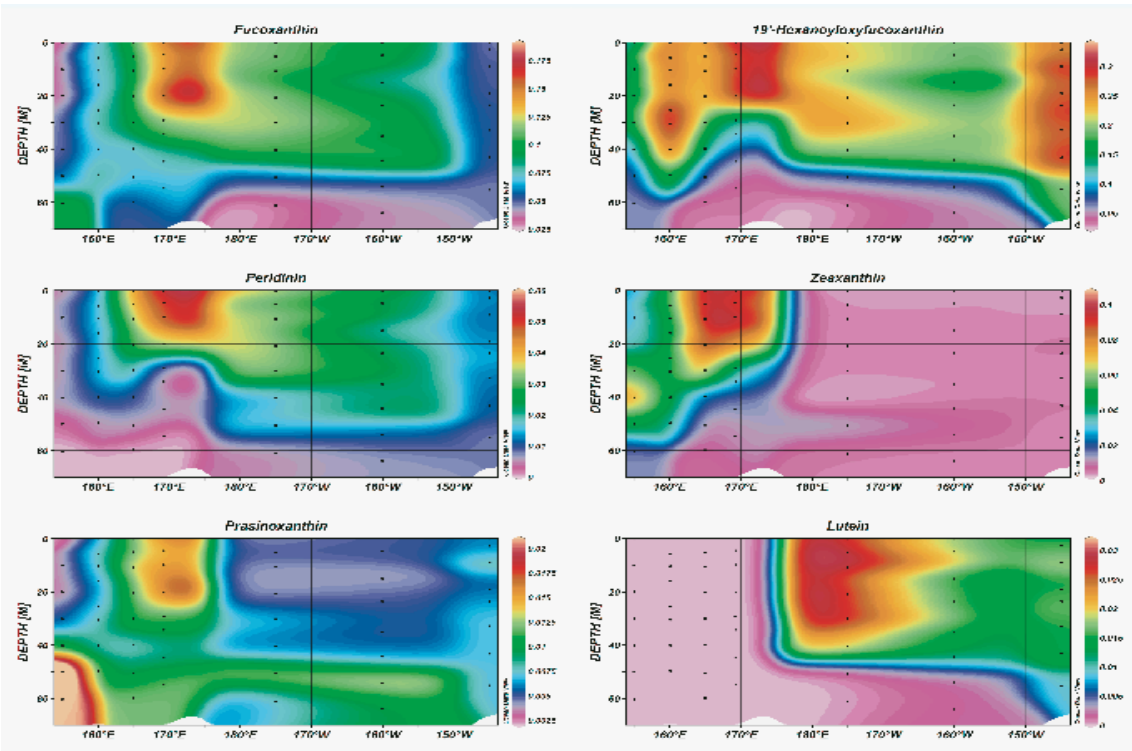

Fig. 31 The distributions of accessory pigments along an east-west transect. Fucoxanthin, Peridinin, Prasinoxanthin, 19'-Hexanoyloxyfucoxanthin, Zeaxanthin and Lutein are index of diatoms, dinoflagellates, prasinophytes, haptophytes, cyanobacteria and chlorophytes, respectively.

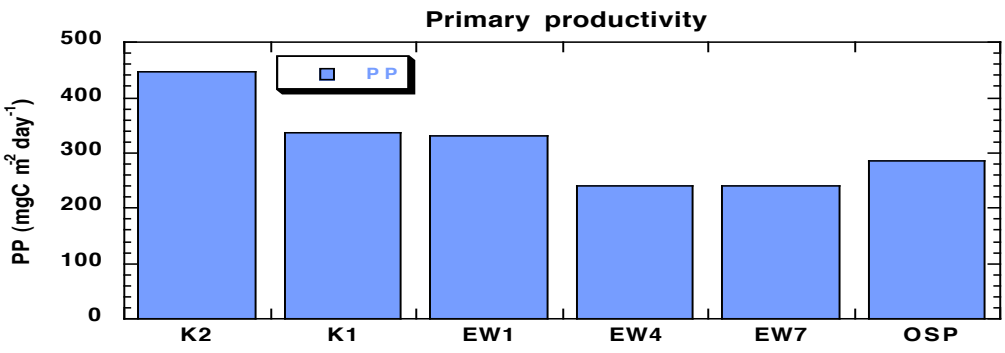

Fig. 32 Integrated primary productivity in the sunlit layer (> 0.5 % relative light intensity) at respective stations

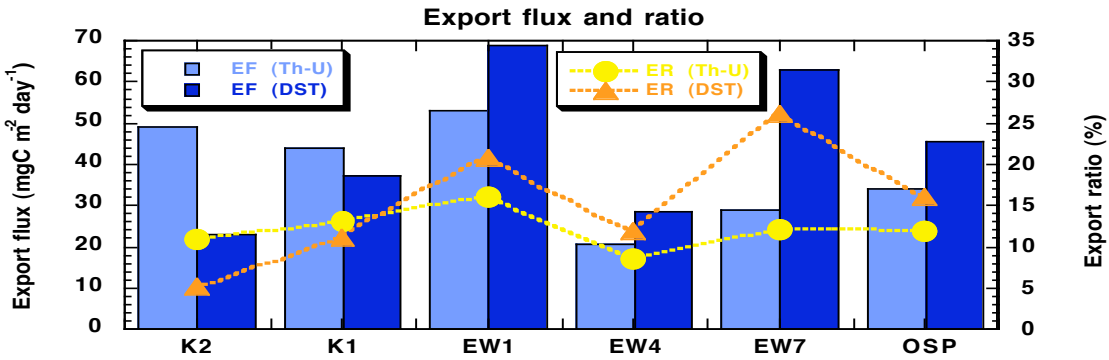

Fig. 33 Export flux (bar graphs) and ratio (line graphs) measured by ^{234}Th-^{238}U methods (Th-U) and drifting sediment trap (DST)

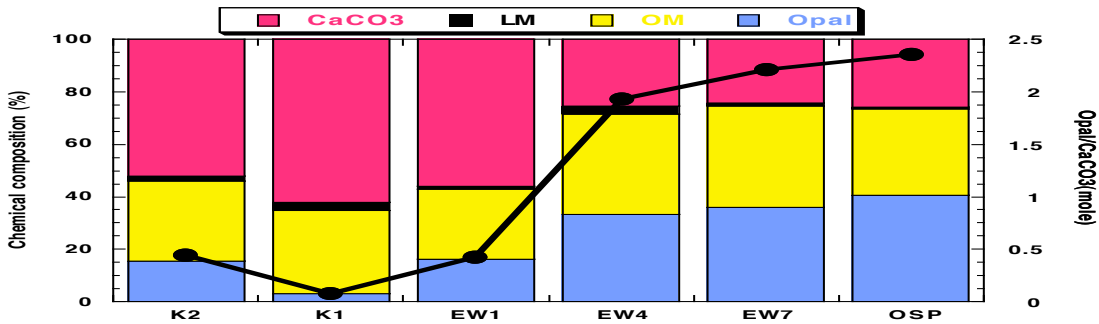

Fig. 34 Chemical composition of sinking particles collected by DST. Circles are mole ratio of opal to $CaCO_3$ fluxes.

(5) High resolution time-series observation for biogeochemistry in the Blooming season

Based on previous reports about nutrients, dissolved inorganic carbon, primary productivity and sinking particle flux, ocean productivity largely increases from late spring to early summer in the Western Subarctic Gyre. In order to study mechanism of increase of ocean productivity and associated materials' cycle focusing on carbon, we conducted approximately two months cruise in June and July 2006 (MR06-03). During this cruise, we visited station K2 six times and observed change in oceanography such as nutrients, primary productivity and sinking particle flux.

During two months, Surface Seawater Temperature (SST) increased from approximately 4°C to 9°C and water stratification was increased (Fig. 35). Concentrations of nutrients and dissolved inorganic carbon in the MLD were decreased (Fig. 35).

Concentration of chlorophyll was higher at the second visit and 5th visit, which was supported by increase of turbidity. During these visits, diatoms were pre-dominant in phytoplankton species followed by haptophytes based on HPLC analysis (Fig. 36).

Primary productivity (PP) ranged from approximately 260 to 730 mgC m^{-2} day^{-1} during cruise and PP at the 5th visit was maximum followed by that at the second visit (620 mgC m^{-2} day^{-1}) (Fig. 37), which coincided with higher chlorophyll concentration. Observed maximum PP was comparable to annual maximum PP reported previously. PP correlated well with surface photosynthetically available radiation (PAR) ($r = 0.91$). These results indicated that increase of primary productivity during bloom season is not monotonically and it depends on light condition chiefly.

One of scientific interests was export carbon flux and ratio at the bottom of winter mixed layer (~ 100m). We observed particulate organic carbon (POC) flux at 100 m by drifting sediment trap (DST) and also estimated POC flux by uranium-thorium (^{238}U-^{234}Th) method (Fig. 37). Assuming steady state and the ratio of POC to ^{234}Th of sinking particles, export flux were estimated to be from approximately 10 to 170 mg m^{-2} day^{-1}. Maximum export flux was observed at the 2nd visit followed by that at the 6th visit. Export ratio was at most 30 % and lower than previous estimates in productive season. However it is likely that assumption of steady state is not appropriate for this season. We will re-estimate export flux and ratio with non steady state model. In addition, high-resolution time-series sediment trap data during cruise will be useful and helpful for future precise discussion.

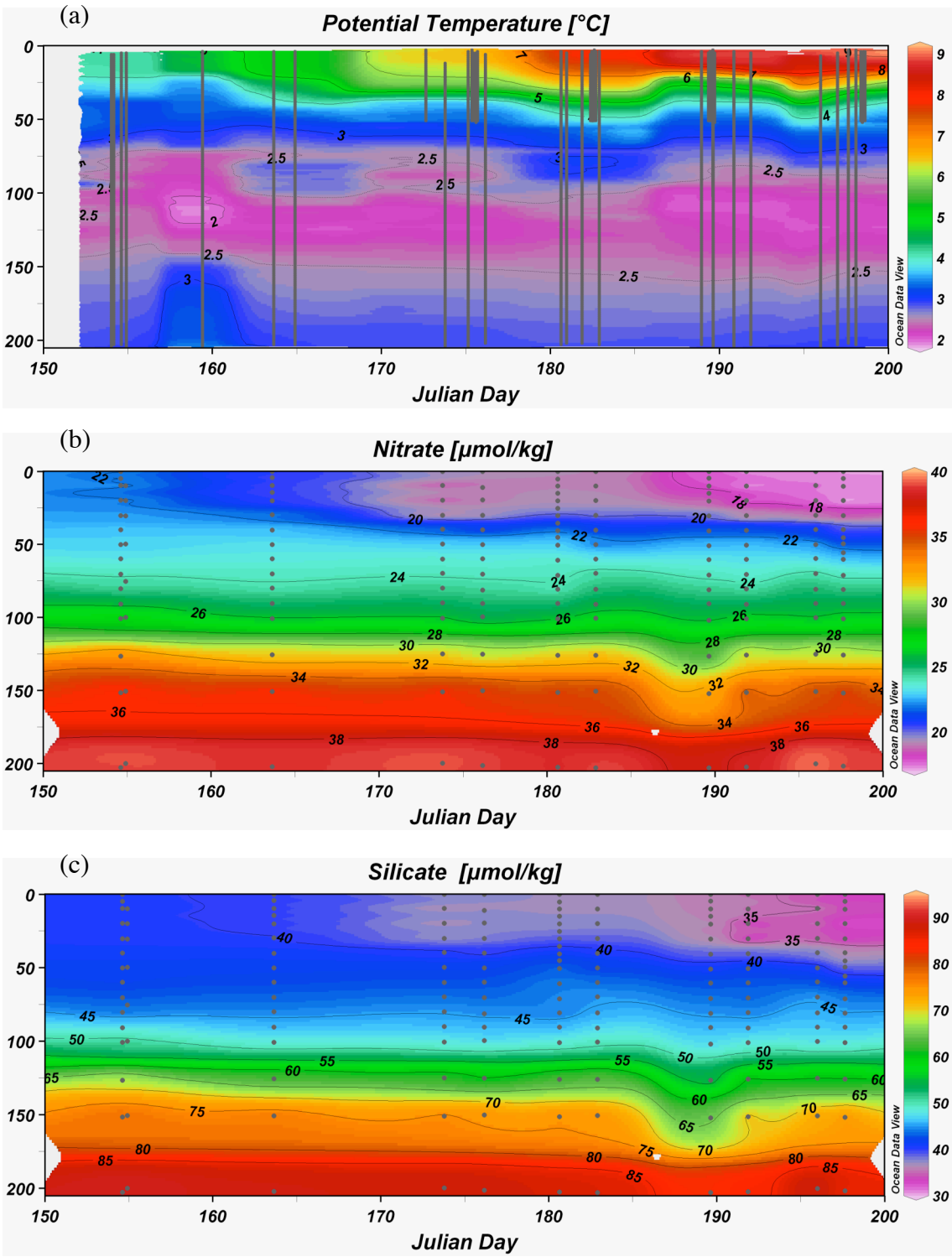

Fig. 35 Time-depth distribution of (a) potential temperature, (b) nitrate and (c) silicate during MR06-03.

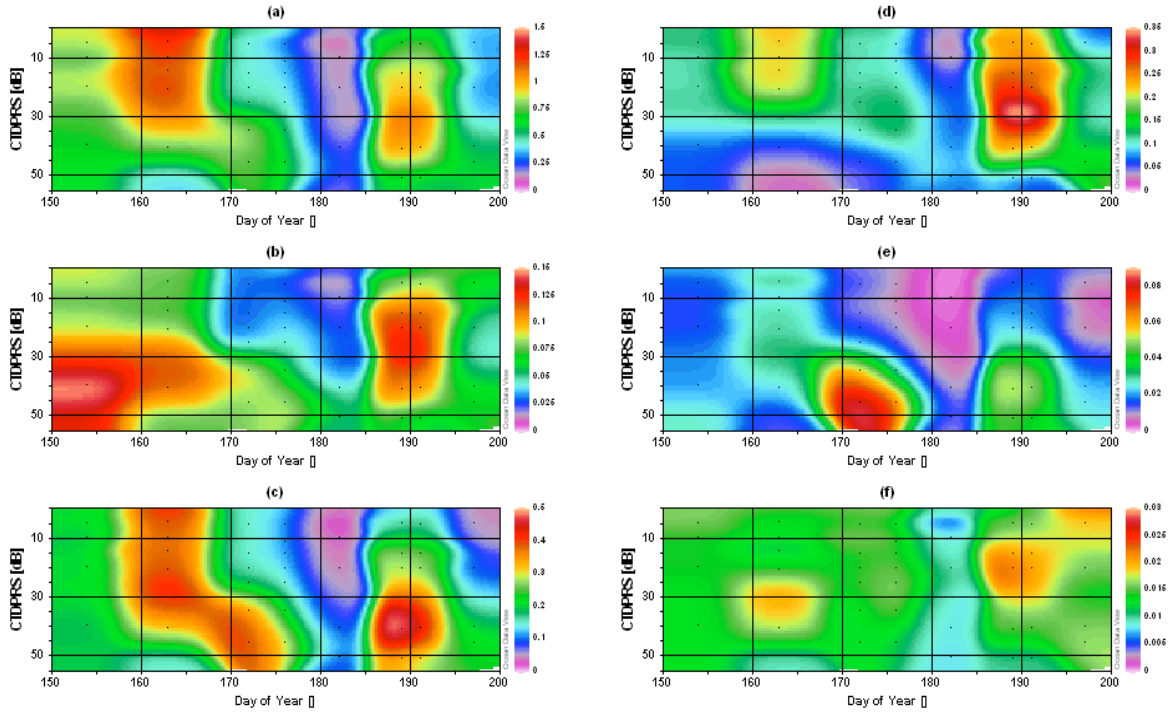

Fig. 36 Temporal variability of phytoplankton pigments concentrations (μg/L) at station K2. Chlorophyll *a* (a), Chlorophyll *b* (b), Fucoxanthin (c), 19'-Hexanoyloxyfucoxanthin (d), Peridinin (e) and Zeaxanthin (f) are roughly represented as the abundance of total phytoplankton, green algae, diatoms, haptophytes, dinoflagellates and cyanobacteria, respectively.

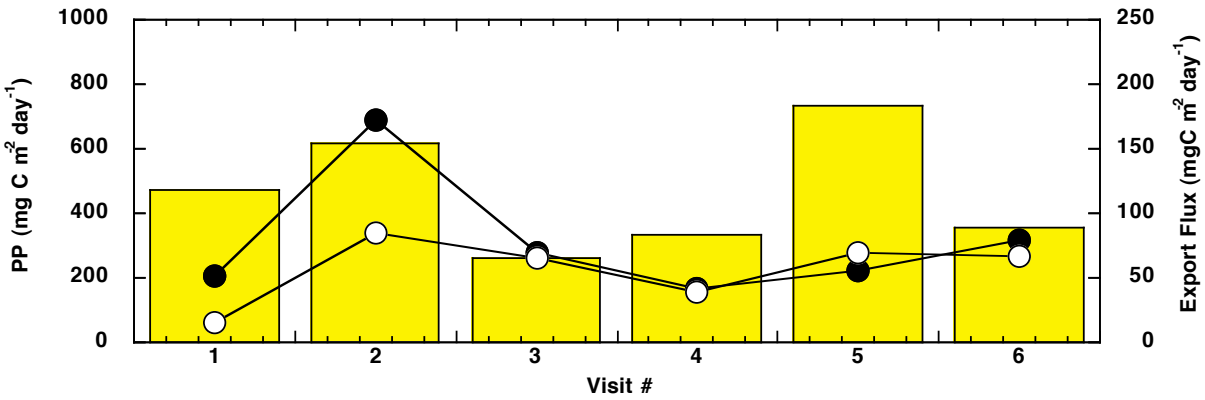

Fig. 37 Primary productivity (bar graphs) and export carbon flux estimated with DST (solid circles) and with ^{238}U-^{234}Th method (open circles)

(6) Repeat hydrographic observation along 155°E line

It has been reported that increase of atmospheric temperature and increase of atmospheric CO_2 has already began to affect marine physics, chemistry, and biology. In order to detect tiny, but significant ocean change precisely, predict the future aspect of ocean and its impact on the global environment, long-term accumulation of high quality oceanographic data is crucial. Repeat hydrographic observation along World Ocean Circulation Experiment (WOCE) lines conducted in 1980s is one of effective strategies.

JAMSTEC has also conducted repeat hydrographic observation along 155°E line since 2001 (Fig. 38). This line is time-series observation line set up by faculty of fishery, Hokkaido University. During cruise, basic physical and chemical components such as temperature, salinity, dissolved oxygen, nutrients, dissolved inorganic carbon, alkalinity and pH are measured on board following WOCE technique.

Fig. 39 shows vertical sections of dissolved oxygen. In future, compilation of data obtained by JAMSTEC and Hokkaido University will reveal interannual variability or decadal change of oceanography in the North Pacific Intermediate Water, North Pacific Mode Water, Subtropical Mode Water and Antarctic Bottom Water along this line.

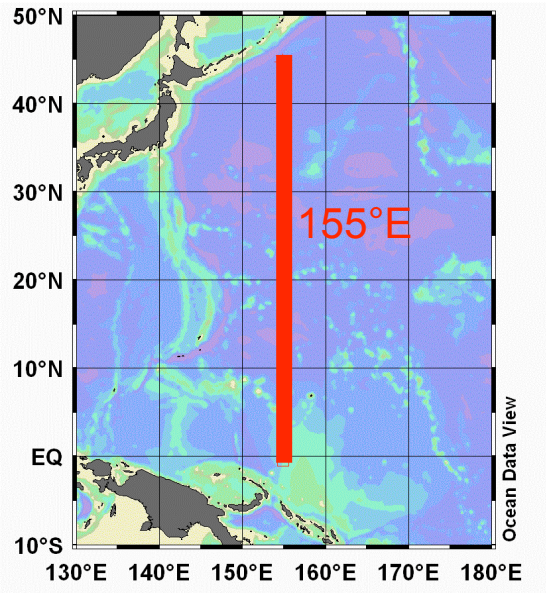

Fig. 38 Sampling locations in the 155 E section for repeat survey.

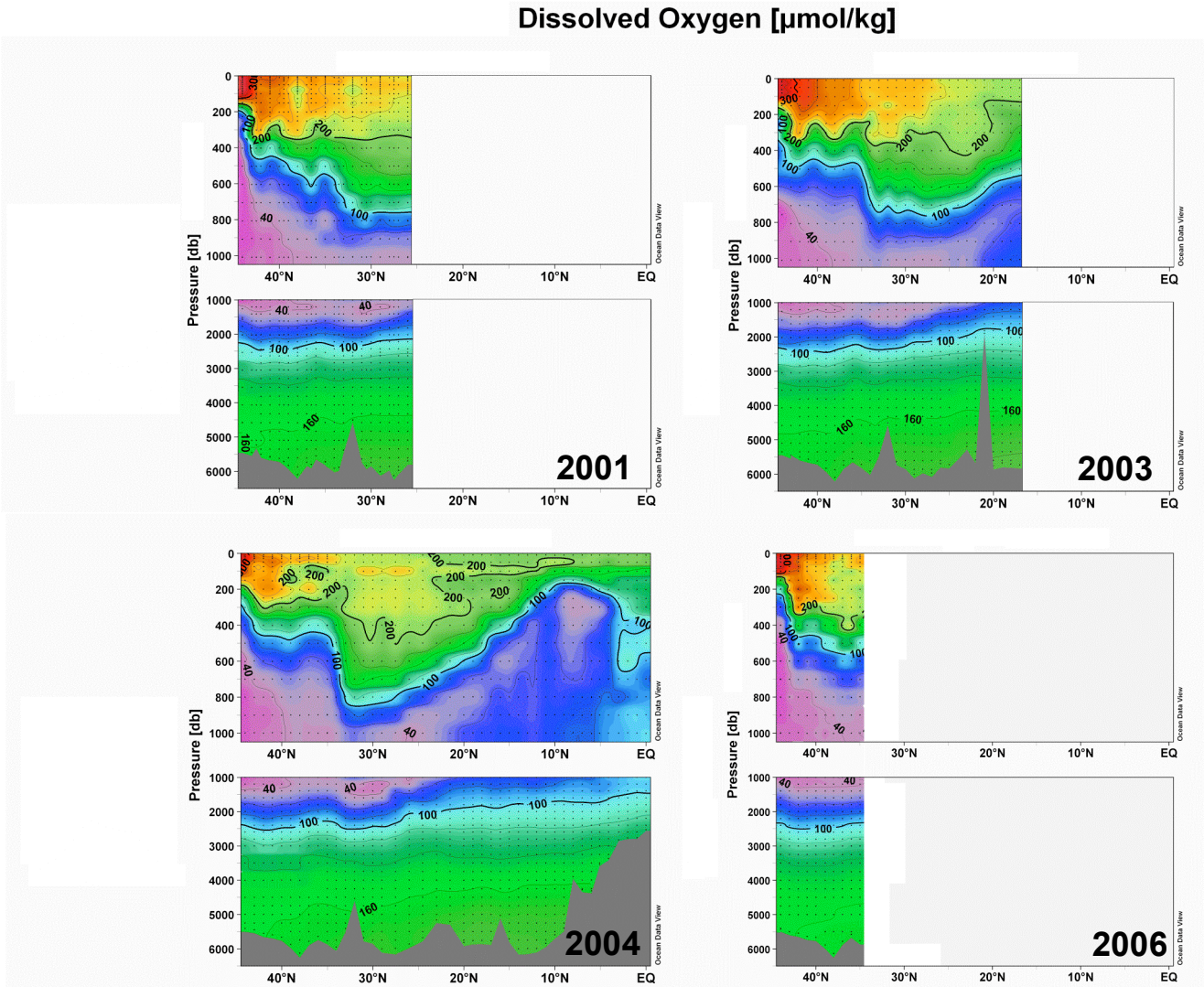

Fig.39 Vertical sections of dissolved oxygen along 155E from 2001 to 2006.

(7) Role of marginal seas in controlling biogeochemistry in the North Pacific

The northwestern North Pacific or Western Subarctic Gyre (WSG) lies adjacent to the Bering Sea and Sea of Okhotsk and it is suspected that the biogeochemistry in the WSG are affected by these marginal seas. Moreover coastal areas along Kamchatska peninsula, Kuril and Aleutian Islands have gigantic productivity based on satellite ocean color image. In order to verify exchange rate of water and materials between the WSG and marginal sea, occurrence of eddy along the Kuril islands and these effect on the biogeochemistry in the WSG, precise hydrographic observation along the Kuril islands and Kamchatka peninsula are strongly requested. However these areas are located in Russian Exclusive Economic Zone (EEZ) and observation cannot be conducted without permission.

In 2004, during MR04-03, JAMSTEC got permission for observation in these areas and conducted hydrographic observation along some transects successfully with cooperation of Russian scientists (Fig. 40). As a result, precise section of nutrients, dissolved oxygen, carbon species and CFSs were verified. Maximum concentration of dissolved silicate > 220 μmole kg^{-1} was observed in the deep sea of the Central Bering sea (Fig. 41). Fig. 42 shows relations between dissolved oxygen and silicate along isopycnal layer of 27.75 – 27.77 σθ. Highest concentrations of dissolved silicate and dissolved oxygen was observed in the Central Bering Sea. It is indicative of that deep sea water in the WSG, which is one of the oldest water in the world ocean, invades into the Bering Sea. CFCs concentrations in the North Pacific Intermediate Water (NPIW) were higher near the Bussol strait, which was indicative of that a part of NPIW is produced in the Sea of Okhotsk. For better understanding, future analysis and more data acquisition in the Russian EEZ are needed.

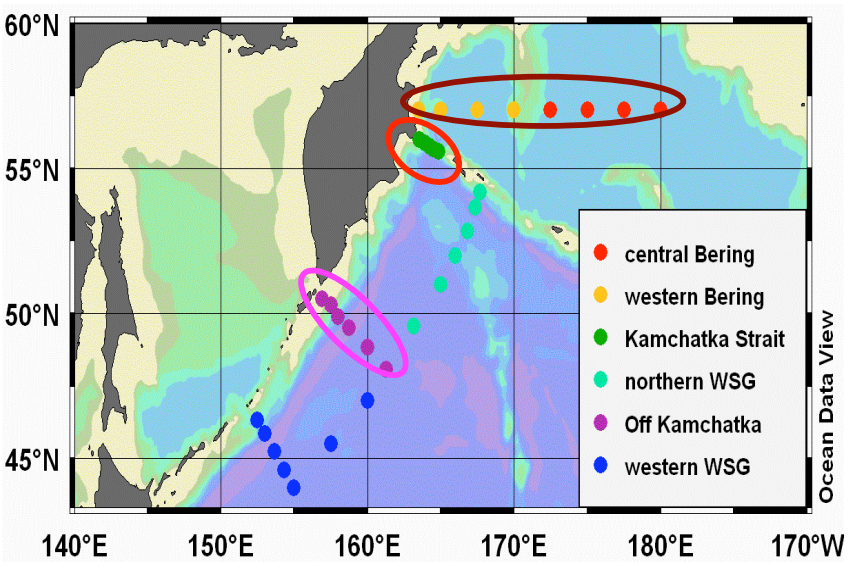

Fig. 40 Transects for hydrographic observation during MR04-03 cruise

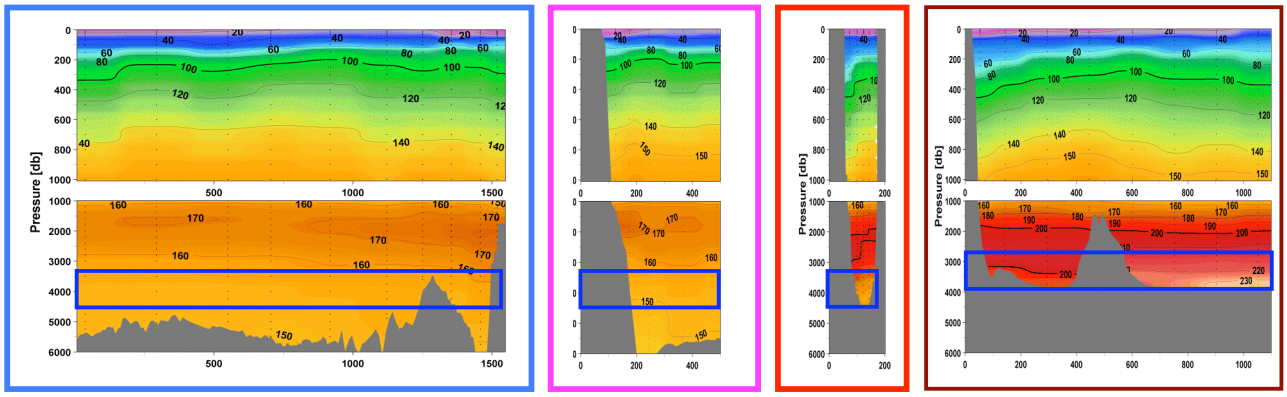

Fig. 41 Sections of dissolved silicate along respective transects (Fig. 40)

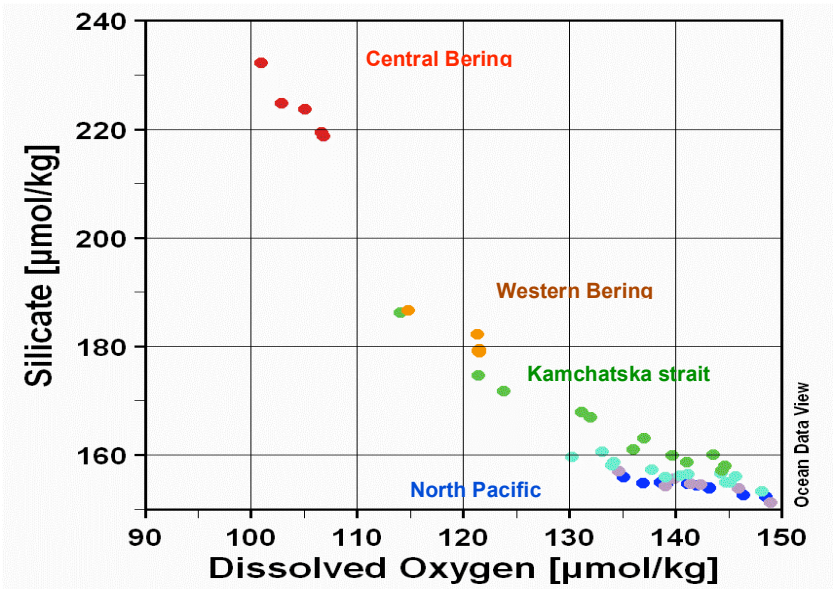

Fig. 42 Relation between DO and silicate along isopycnal layer of 27.75 – 27.77 σθ.

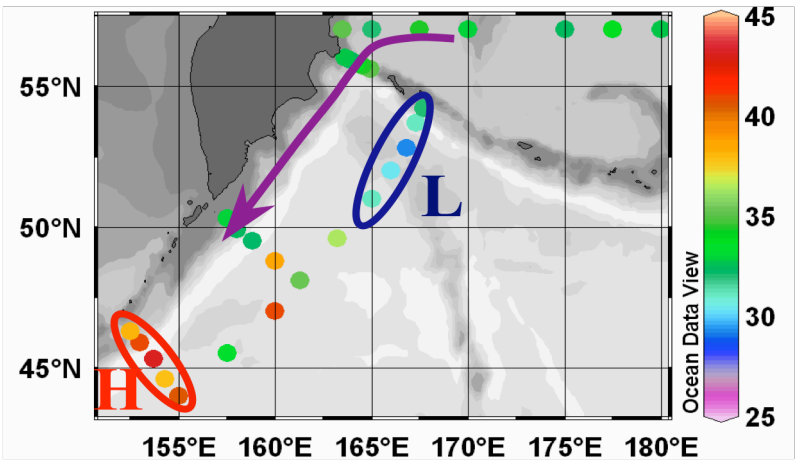

Fig. 43 Concentrations of CFCs along isophycnal layer of 27 σθ.

(8) Development of drifting buoy system with in situ sea surface pCO_2 sensor for long term observation

To predict future global climate changes, it is necessary to clarify the extent of the flux of CO_2 to each of the three reservoirs: the atmosphere, land biosphere and ocean. Above all, the ocean is huge carbon reservoir. In order to observe the temporal and spatial variations in oceanic CO_2, we have developed new systems for measuring *in situ* sea surface partial pressure of CO_2 using spectrophotometric technique (pCO_2 sensor). The pCO_2 sensor measures *in situ* pCO_2 by detecting the change of pH in a pH dye solution, equilibrated with the seawater through a gas permeable membrane. An amorphous fluoropolymer tubing form (AF-2400) with a high gas permeability coefficient is used as a gas permeable membrane.

The pCO_2 sensors can be mounted on drifting buoy with satellite communication systems. When the drifting buoy systems are deployed into world oceans, it is necessary to prepare as much as possible many systems to obtain the pCO_2 data from the world oceans. Therefore, the system is required cheap, small and light features. We adopt low cost and small parts for pCO_2 sensor (e.g. LED for light source, CCD for detector, micro pump and downsized PC). By using these parts, the size of drifting buoy made by aluminum housing is about 300 mm diameter, 500 mm length and the weight is within 30 kg and the mass-produced price is within $2000.

We also study about biofouling for buoy and sensor. When the buoy system is utilized for a long-term observation, the instruments are susceptible to biofouling in the form of microbial and algal films that can cover sensors and degrade data quality. In order to reduce the effects of biofouling on the sensors, we are conducting the antifouling tests with copper, titanium dioxide and paints.

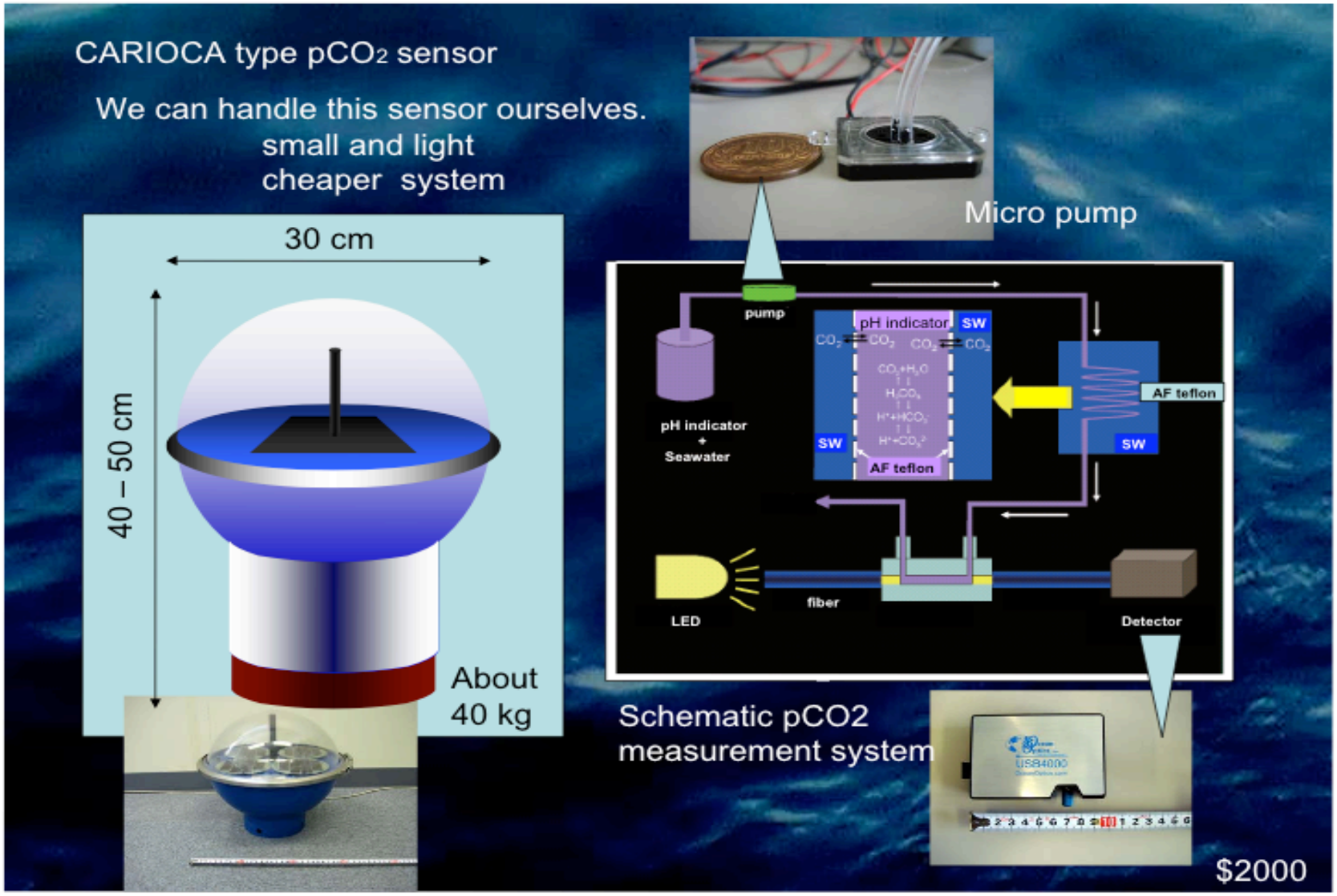

Fig. 44 Schematic diagram of pCO_2 drifting buoy

4. Summary

Since 2001, we conducted time-series observation in the northwestern North Pacific using mooring systems and research vessels. High resolution time-series observation with mooring systems revealed that assimilated carbon in the surface euphotic layer is quickly transported to the ocean interior without significant time lag and transported materials are vertically transported without significant lateral transportation. In addition, it is suggested that diatom plays an important role in transporting particulate carbon to the ocean interior.

Research vessels, mainly R/V MIRAI, have also observed seasonal variability in nutrients, carbon species, primary productivity and natural radionuclide. Based on measurements of radionuclide and primary productivity, it has been verified that export flux and ratio are higher in the northwestern North Pacific than other oceans. Measurements of seasonal nutrients' concentrations have enabled us to suspect annual new production. Moreover, 5 years observation has verified the significant increase in dissolved inorganic carbon in the upper layers.

However, high resolution time series observation in the surface layer upper 30 m have not been conducted explicitly though it is important for better understanding seasonal variability in the biological pump. Despite time-series sediment traps were deployed from subsurface to deep sea, problems of trapping efficiency and swimmer effect have been solved, especially for sediment traps < 1000 m.

5. For future observation

During the last 5 years, global warming issue has become more important social problem in the world. In 2003, the Earth Observation Summit was held and suggested importance of establishment of Global Environmental Observation System of Systems (GEOSS). Japan Council for Science and Technology Policy, Cabinet declared that the global warming issue is one of most important urgent problems and started to promote sciences and technology to clarify phenomena caused by, to predict the effect of, and adaptation of the earth to the global warming. Under this background, ocean observation is crucial and it is no doubt that ocean time-series observation in the world ocean is necessary.

As of this point (December 2006), concrete implementation plan has not been proposed for time-series observation (e.g. mooring design). However, the following research items and technology should be important in order to conduct effective ocean time-series observation in the Western North Pacific.

5.1 Research items

(1) Study of role of zooplankton and bacteria in oceanic carbon cycle

Recently marine biologists have reported the importance of zooplankton activity for oceanic carbon cycles. We should conduct scientific cruise with marine biologists and answer the following questions:

Does zooplankton's ontogenic migration really play an important role in transporting carbon to the ocean interior?
How is contribution of fecal pellet in carbon vertical transport?
How is microbial loop changed seasonally and vertically?

(2) Study of dissolved organic carbon (DOC)

We have conducted the study of biological pump focusing on particulate carbon assuming that dissolved organic carbon (DOC) does not play an important role in the high latitude area with low temperature. However it has been reported that abundance of bacteria is not low in the high latitude zone and DOC contribution to carbon cycle in the western North Pacific might be larger than that we expected. We should conducted time-series observation of DOC in the western North Pacific.

(3) Study of carbon cycle in the twilight zone

Time-series sediment trap experiment has revealed seasonal variability in sinking particles in deep sea > 1000 m. Satellite oceanography and our time-series observation in subsurface layer (0 – 100 m) have enabled us to study seasonal variability in surface biological activity. Though we can suspect oceanic carbon cycle such as vertical change in carbon flux with data from surface and deep sea, carbon cycle in the mesopelagic layer or twilight zone (100 – 1000 m) is still in the black box. Based on radiocarbon study and biological study, it has been reported that vertically transported carbon change not irreversibly but reversibly (mutual reaction with suspended particles, repackage by creatures, etc.). In order to know the precise carbon cycle in the ocean, the study of carbon cycle in the twilight zone should be conducted more frequently.

(4) Vertical and horizontal distribution of chemical components in the WSG including Russian EEZ

Increase of dissolved inorganic carbon has been observed at station K2 and other stations in the Western Subarctic Gyre (WSG). This has been accompanied by decreased of dissolved oxygen (or increase of AOU). It is interpreted that this decrease is attributed to decrease of ocean circulation. On the other hand, change in ocean biological change has not been observed yet despite it should change. By long-term observation of three-dimensional distribution of dissolved chemical components, this tiny but significantly influential change in future should be detected.

In addition, seasonal and decadal variability in water and substances' exchange between the WSG and the marginal seas (Bering sea and sea of Okhotsk) affects vertical and horizontal distribution of chemical components in the WSG. With Russian cooperation, hydrographic observation in the Russian EEZ is crucial in order to clarify carbon cycle in the WSG.

(5) Effect of meteorological event and eddy on biological activity and distribution of chemical components

It has been predicted that the global warming will change frequency and scale of temporal meteorological events such as low pressure and typhoon. In addition, frequency and scale of medium-scale eddies that appears along the Kuril Islands change seasonally and inter-annually in the WSG. It is well known that meteorological events and eddy affect ocean physical structure and primary productivity. The eddy study is one of important scientific issues in the WSG. However it is not easy to observe these events by ordinary research vessels. By using automated sensor and sampling system, we will be able to observe change in biogeochemistry by meteorological temporal events.

(6) Construction of biogeochemical model

For better understanding oceanic carbon cycle, we should sustain observation of the above research issues: carbon export flux, export ratio (the ratio of export flux to primary productivity), contribution of DOC, effect of micronutrients to carbon cycle, role of zooplankton and bacteria, and so on. In order to integrate a lot of observation and verify total system of biogeochemistry, mathematical simulation is crucial. Though biogeochemical model for the western North Pacific has been developed such as NEMRO (North pacific Ecosystem Model Used for Regional Oceanography: *e.g.* Kishi *et al.*, J. Oceanogr. 60, 63-73, 2004) model, this model does not always reproduce observation results. We will develop biogeochemical model for the WSG.

(7) Change in biogeochemistry by global warming and its feedback

As a result of the global warming, ocean change such as increase of seawater temperature, increase of stratification, and acidification of seawater has been predicted. Increase of temperature might increase microbial loop, resulting more degradation of carbon in the upper layer, while increase of water temperature potentially increase ocean primary productivity. Increase of stratification might reduce supply of macro nutrients, especially silicate in the WSG, and micro-nutrients such as iron from subsurface water while enhanced stability of surface water mass is preferable for phytoplankton activity. Acidification of seawater caused by increase of atmospheric CO_2 will be expected to reduce biological formation of $CaCO_3$ (calcification) in the pelagic ocean and sedimentation of $CaCO_3$ in coral reef and seafloor sediment. This will cause increase of ocean alkalinity, resulting decrease of CO_2 in the ocean and, by extension, increase of ocean uptake of atmospheric CO_2. On the other hand, it has been concerned that decrease of $CaCO_3$ might weaken the biological pump because it has been reported that $CaCO_3$ with larger density than opal and lithogenic materials effectively transport organic carbon to the ocean interior. Thus our knowledge is still too poor to suspect feedback of ocean change to the global climate (positive feedback or negative feedback). We should continue process study and collect essential data to answer this question.

5.2 New technology

In order to overcome the difficulty in observation for surface area and twilight

zone, following recent developed technology will be effective tactics.

(1) Underwater winch with sensor package

It remains difficult to deploy instruments near the sea surface (< 30 m) in the northwestern North Pacific because of rough seas, with waves exceeding 20 m in height, and the presence of ships with drafts greater than 10 m. Underwater winch has been developed and "an ocean observation buoy" (sensor package) that consist of CTD, DO sensor and optical sensor (FRRF: First Repetition Rate Fluorometer) supported by underwater winch has successfully conduct time-series observation in the euphotic zone (Saino et al., Final report of "Development of real time in situ measurement system of primary productivity for validation of satellite data", CREST, 2005; Fujiki et al., AGU Ocean Science Meeting 2006, OS45D-02, 2006) for several months. Underwater winch is usually located at subsurface layer (~100-200 m) and, thus, can avoid rough sea and ships. If additional sensors such as pCO_2 sensor and nutrients sensor can be installed on above sensor package and battery problem for long-term deployment (one year) can be overcome, combination of submersible winch and sensor package will become a counterpart to satellite and become great tool for time-series observation in the surface area.

(2) New sediment trap

1) NBST

Trapping efficiency of moored and surface-tethered sediment trap has been still principal problem although sediment trap can collect sinking particle directly. Recently Neutral Buoyancy Sediment Trap (NBST) has been developed. It has been reported that this sediment trap can reduce effects of hydrodynamics and swimmer (e.g. Valdes and Price, J. Atmos. Oceanogr. Tech. 17, 1, 62-68, 2000; Buesseler et al., Deep-Sea Res. I 47, 277-294, 2000). Although it is difficult to deploy this sediment trap all year round, several days-deployment during seasonal cruise might reveal more actual biological pump in the twilight zone.

2) Optical trap

Measurement of turbidity has been helpful and useful to suspect amount of suspended particles including sinking particle in the water column since old days. We have also certified utility of optical data for study of biological activity as long as optical sensor can be free from biofouling. Recently algorithm to convert amount of suspended and/or sinking particles to amount of carbon, and optical sensor has been attached on drifter like ARGO float. This new system have successfully observed increase of particle after artificial Fe supply, which has been difficult to observe by ship-time limited cruise (e.g. Bishop et al., Science 298, 817-821; Science 304, 417-420, 2004). In addition, it is reported that optical data can be also used to estimate $CaCO_3$ and sinking particle flux. This instrument, called Optical trap or Carbon Explorer, will be useful to certify change in particles in the water column.

5.3 Cruise plan

Scientific cruises for MIO project are planned in 2007 (MR07-05: 4 Sept.

2007 – 2 Oct. 2007) and in 2008 (approximately 30 days in summer). During these cruise, we will visit station K2 and Russian EEZ. We are planning concrete implementation plan taking into account for the above scientific issues and technology. We should also propose succeeding scientific cruise after 2008 for time-series observation.

5.4 International collaboration

We have been conducted ocean time-series observation in the WSG. However we have not always paid much attention to seasonal and interannual variability in the other areas in the Pacific. There should be "teleconnection" between various oceanic domains. In order to clarify the total ocean systems in the Pacific, we should conducted comparative study between other domains with different property from that of the WSG. Fortunately, ocean time-series stations have been established in the eastern North Pacific (station OSP) and in the subtropical gyre (station ALOHA). We would like to promote comparative study between K1 and OSP, and K2 and ALOHA by exchanging data, samples or conducting simultaneously scientific cruise with cooperation of scientists who has engaged in above time-series observation. Moreover, it is desired that this observation is conducted under international program such as CLIVAR (Climate Variability and Predictability Program), SOLAS (Surface Ocean Low Atmosphere Study) and IMBER (Integrated Marine Biogeochemistry and Ecosystem Research).

Publications

(Peer-reviewed)

=2001=

=2002=

Andreev, A. and S. Watanabe (2002) Temporal changes in dissolved oxygen of the intermediate water in the subarctic North Pacific. Geophys. Res. Letts. 29, 10.1029/2002GL015021.

Andreev, A., M. Kusakabe, M. C. Honda, A. Murata and C. Saito (2002) Vertical fluxes of nutrients and carbon through the halocline in the western subarctic Gyre calculated by mass balance, Deep-Sea Res. II, *49,* 5577-5593.

Aranami. K. S. Watanabe, S. Tsunogai, A. Ohki, K. Miura and H. Kojima (2002): Chemical assessment of oceanic and terrestrial sulfer in the marine boundary layer over the northern North Pacific during summer. J. Atmos. Chem. 41, 49-66,

Honda, M. C., K. Imai, Y. Nojiri, F. Hoshi, T. Sugawara, and M. Kusakabe (2002) The biological pump in the northwestern North Pacific based on fluxes and major components of particulate matter obtained by sediment trap experiments (1997-2000), Deep-Sea Res. II, 49, 5595-5625.

Kumamoto, Y., A. Murata, C. Saito, M. Honda and M. Kusakabe (2002) Bomb radiocarbon invasion into the northwestern North Pacific. Deep-Sea Res. II 49, 5339-5352.

Kuroyanagi, A., H. Kawahata, H. Nishi and M. C. Honda (2002) Seasonal change in planktonic foraminifera in the northwestern North Pacific Ocean: sediment trap experiments fromsubarctic and subtropical gyres, Deep-Sea Res. II, 49, 5627-5645.

Murata, A., Kumamoto, Y., Saito, C., Kawakami, H., Asanuma, I., Kusakabe, M., Inoue, H.Y., 2002. Impact of a spring phytoplankton bloom on the CO_2 system in the mixed layer of the northwestern North Pacific. Deep-Sea Res. II 49, 5531–5555.

Nakayama, N., S. Watanabe and S. Tsunogai (2002) Nitrogen, Oxygen and Argon dissolved in the northern North Pacific in early summer. J. Oceanogr., 58, 775-785.

Sasaoka, K., S. Saitoh, I. Asanuma, K. Imai, M. C. Honda, Y. Nojiri and T. Saino (2002) Temporal and spatial variability of chlorophyll-a in the western subarctic Pacific determined from satellite and ship observations from 1997 to 1999, Deep-Sea Res. II, 49, 5557-5576.

Tsurushima, N., Y. Nojiri, K. Imai and S. Watanabe (2002): Seasonal variations of carbon dioxide system and nutrients in the surface mixed layer at station KNOT (44°N, 155°E) in the subarctic western North Pacific. Deep-Sea Res. II 49, 5377-5394.

Yamamoto, M., S. Watanabe, S. Tsunogai, and M. Wakatsuchi (2002): Effects of sea ice formation and diapycnal mixing on the Okhotsk sea Intermediate water clarified with oxygen isotopes. Deep-Sea Res. I, 49, 1165-1174.

=2003=

Honda, M. C. (2003) Biological pump in the northwestern North Pacific, J. Oceanogr. 59, 671-684.

Okazaki, Y., K. Takahashi, T. Nakatsuka, and M. C. Honda (2003) The production scheme of *Cycladophora davisiana* (Radiolaria) in the Okhotsk Sea and the northwestern North Pacific: implication for the paleoceanographic conditions during the glacials in the high latitude oceans, Geophys. Res. Letts, 30(18), doi:10.1029/2003GL018070.

Otsuki, A. S. Watanabe, and S. Tsunogai (2003) Absorption of atmospheric CO2 and its transport to the intermediate layer in the Okhotsk sea. J. Oceanogr. 59, 709-717.

Tsunogai, S., K. Kawada, S. Watanabe, and T. Aramaki (2003) CFC indicating renewal of the Japan sea deep water in winter 2000-2001. J. Oceanogr. 59, 685-693.

Wakita, M., Y. W. Watanabe, S. Watanabe, S. Noriki and S. Wakatsuchi (2003) Oceanic uptake rate of anthropogenic CO_2 in the subpolar marginal sea: The sea of Okhotsk. Geophys. Res. Letts. 30(24), 2252, doi: 10.1029/2003GL018057.

Watanabe, Y. W., T. Ono, M. Wakita, N. Maeda and T. Gamo (2003) Synchronous bidecadal periodic changes of dissolved oxygen, phosphate and temperature between the Japan sea deep water and the North Pacific intermediate water. Geophys. Res. Letts. 30, 2273, doi:10.1029/2003GL018338.

=2004=

Kawakami, H., Y-L. Tang, M. C. Honda, and M. Kusakabe (2004) Particulate organic carbon fluxes estimated from ^{234}Th deficiency in winters and springs in the northwestern North Pacific, Geochem. Jour, 38. 581-592.

Otosaka, S., M. C. Honda and S. Norik (2004) La/Yb and Th/Sc in settling particles: Vertical and horizontal transport of lithogenic material in the western North Pacific, Geochem. Jour., 38, 515-525.

=2005=

Onodera, J., K. Takahashi and M. C. Honda (2005) Pelagic and coastal diatom fluxes and the environmental changes in the northwestern North Pacific during December 1997-May 2000, Deep-Sea Res. II, 52, 2218-2239.

Okazaki, Y., K. Takahashi, J. Onodera and M. C. Honda (2005) Temporal and spatial flux changes of radiolarians in the northwestern Pacific ocean during 1997-2000, Deep-Sea Res. II, 52, 2240-2274.

Wakita, M., S. Watanabe, Y. W. Watanabe, T. Ono, N. Tsurushima and S. Tsunogai (2005) Temporal change of dissolved inorganic carbon in the subsurface water at station KNOT (44° N, 155° E) in the Western North Pacific subpolar region. J. Oceanogr. 61, 129-139.

=2006=

Harada, N., M. Sato, A. Shiraishi and M. C. Honda (2006) Characteristics of alkenonedistributions in suspended and sinking particles in the northwestern North Pacific, Geochim. Cosmochim. Acta, 70, 2045-2062.

Honda, M. C., H. Kawakami, K. Sasaoka, S. Watanabe and T. Dickey (2006) Quick transport of primary produced organic carbon to the ocean interior. Geophys. Res. Let., 33, L16603, doi:10.1029/2006GL026466.

Nakano,Y., H. Kimoto, S. Watanabe, K. Harada and Y. W. Watanabe (2006) Simultaneous measurements of in situ pH and CO2 in the sea using spectrophotometric profilers. J. Oceanogr. 62, 71-81.

=2007=

Honda, M. C. and S. Watanabe (accepted) Utility of an automatic water sampler to observe seasonal variability in nutrients and DIC in the northwestern North Pacific, J. Oceanogr.

(non reviewed)

=2001=

=2002=

=2003=

Honda, M. (2003) Settling particle: Study of biological pump using sediment trap experiment. Kaiyo monthly 44, 85-91 (in Japanese)

Onodera J., K. Takahashi and M. C. Honda (2003) Diatom fluxes at station KNOT in the western subarctic Pacific, 1997-2000. Bull. Plankton Soc. Japan 50(1), 1-15. (in Japanese with English abstract)

=2004=

Y. Nakano, S. Watanabe, Y. W. Watanabe, and S. Noriki (2004): Research and development of in situ pH/fCO_2 profiler based on spectrophotometric technique. Kaiyo monthly, special issue for ocean observation system and research, 36, 99-104.

=2005=

Idai, T., M. Honda, S. Honjo and J. Kemp (2005) Mooring systems for time-series observation for biogeochemistry in the northwestern North Pacific: design, preparation and mooring work. JAMSTEC Rep. Res. Dev., 1, 73-91.

Kawakami, H., Yang, Y., Kusakabe, M., 2005. The distributions of ^{210}Po and ^{210}Pb in the intermediate layer of northwestern North Pacific. Proceedings of the sixth workshop on Environmental Radioactivity 2005-4, 68–76. (in Japanese).

Honda, M. C. (2005) The time-series observation of CO2 cycle in the North Pacific using the mooring system, Navigation 163、67-77. (in Japanese)

=2006=

Honda, M. C. (2006) Role of zooplankton in carbon cycle in the ocean, Bull. Plankton Soc. Japan 52(2), 103-106. (in Japanese with English abstract)

(Oral or poster presentation)

=2001=

Kawakami, H., Yang, Y., Kusakabe, M., 2001. POC flux estimated from ^{234}Th in the northwestern North Pacific. The fifth Mirai Symposium in Tokyo, 21 Dec. 2001. (in Japanese)

Honda, M. C., H. Sako, K. Hayashi, T. Idai, S. Honjo, S. Manganini, J. Kemp, J. Ryder, C. Taylor, and R. Francois（2001）Time-series observation in the North Pacific. 2001Advanced Marine Science and Technology Society fall meeting, Tokyo (in Japanese)

Honda, M. C., F. Hoshi, T. Sugawara and M. Kusakabe（2001）The study of biological pump suspected through sediment trap experiment. The fourth Mirai Symposium in Tokyo, Jan. 2001 (in Japanese)

Honda, M. C., H. Sako, K. Hayashi, T, Idai, S. Honjo, Steven Manganini, C. Taylor, R. Francois, J. Ryder and J. Kemp (2001) Time-series observation for biological pump in the North Pacific. The fifth Mirai Symposium in Tokyo, 21 Dec. 2001. (in Japanese)

Nakano, Y., S. Watanabe, S. Tsunogai, T. Kimoto, N. Tsurushima and K. Harada: Continuous measurements of pH, TA and fCO_2 based on spectrophotometric technique: 2. Application to an in situ pH/fCO2 profiler. International Workshop on Autonomous Measurements of Biogeochemical Parameters in the Ocean. Honolulu, Hawaii, Feb. 2001.

Watanabe, S., Y. Nakano and S. Tsunogai: Continuous measurements of pH, TA and fCO2 based on spectrophotometric technique: 1. A general idea. International Workshop on Autonomous

Measurements of Biogeochemical Parameters in the Ocean. Honolulu, Hawaii, Feb. 2001.

=2002=

Nakano, Y., T. Kimoto, H. Kimoto, W. Suh, S. Watanabe, K. Harada, N. Tsurushima, S. Sugito and S. Tsunogai: (2002) Development of an in situ CO2 profiler using spectrophotometric technique. TECHNO-OCEAN 2002. Kobe, Nov. 2002.

=2003=

Honda, M. C. (2003) The study of biological pump in the northwestern North Pacific. The sixth Mirai Symposium in Tokyo, Jan. 2003. (in Japanese)

Honda, M. C. (2003) JAMSTEC time-series observation for biogeochemistry. POGO 4 meeting, Hobart, Tasmania, Jan. 2003.

Honda, M. C. (2003) Biological pump in the northwestern North Pacific. JGOFS final open science conference: A sea of change-JGOFS accomplishments and the future of ocean biogeochemistry. Washington, D. C., May 2003.

=2004=

Kawakami, H., 2004. The estimation of POC flux used by ^{234}Th from surface layer in HiLaTS (High Latitude Time Series observatory). The seventh Mirai Symposium in Yokohama, 16 Jun. 2004.

Kawakami, H., 2004. Estimation of POC flux from the euphotic zone using Th-234 at the time-seriese station in the northwestern North Pacific. Oceanographic Society of Japan 2004 fall meeting in Matsuyama, 26 Sep. 2004.

Hayashi, K., M. C. Honda, T. Idai and S. Honjo (2004) High resolution time-series observation of nutrients and dissolved inorganic carbon at subsurface in the northwestern North Pacific. Oceanographic Society of Japan 2004 fall meeting Matsuyama, Japan (in Japanese)

Honda, M. C.（2004）Ballast for vertical transport of POC and vertical change in POC flux. Oceanographic Society of Japan 2004 fall meeting, Matsuyama, Japan (in Japanese)

Honda, M. C., K. Hayashi, T. Idai and S. Honjo (2004) Mechanism of autumn increase in ocean productivity. The seventh Mirai Symposium in Tokyo, Jan. 2004. (in Japanese)

Idai, T., M. Honda and S. Honjo (2004) Time-series observation of ocean dynamics by Moored Profiler (MMP) in the northwestern North Pacific. The seventh Mirai Symposium in Tokyo, Jan. 2004. (in Japanese)

Sako, H., C. D. Taylor, M. C. Honda, and S. Honjo (2004) Time-series observation of in situ primary productivity by Time-series submersible incubation device in the northwestern North Pacific. The seventh Mirai Symposium in Tokyo, Jan. 2004. (in Japanese)

Sako, H., M. C. Honda, C. D. Taylor, T. D. Dickey and S. Honjo (2004) Time-series observation of in situ productivity and optics in the northwestern North Pacific. Oceanographic Society of Japan 2004 fall meeting Matsuyama, Japan. (in Japanese)

=2005=

Kawakami, H., Yang, Y., Kusakabe, M., (2005). The distributions of ^{210}Po and ^{210}Pb in the intermediate layer of northwestern North Pacific. The sixth workshop on Environmental Radioactivity in Tsukuba, 9 Mar. 2005. (in Japanese)

Kawakami, H., Honda, M.C., (2005). Seasonal change of POC flux estimated from ^{234}Th in the northwestern North Pacific. The symposium of environmental science in Mutsu, 11 Nov.. (in

Japanese)

Kawakami, H., Kusakabe, M. (2005). The distributions of ^{228}Ra and ^{226}Ra at surface layer in northwestern North Pacific. The eighth Mirai Symposium, 14 Jun. 2005.

Kawakami, H., Kusakabe, M., (2005). The classification of the water mass in the surface layer using ^{228}Ra and ^{226}Ra in the northwestern North Pacific. The Oceanographic Society of Japan 2005 fall meeting in Sendai, 30 Sep. (in Japanese).

Honda, M., H. Kawakami and S. Watanabe (2005) Time-series observation for biological pump. The 11th JAPAN-US workshop on global change: Biodiversity, ecosystem function and dynamic human-nature interaction. In Tokohama, Oct-Nov. 2005.

Honda, M., H. Sako, K. Hayashi, T. Idai, S. Kimura, K. Yoshida, H. Kawakami, T. Dickey and S. Honjo (2005) Relation between primary productivity observed by mooring system and organic carbon flux. The eights Mirai Symposium in Tokyo, Jan. 2004. (in Japanese)

Honda, M. C. (2005) The time-series observation of CO2 cycle in the North Pacific using the mooring system, Japan Institute of Navigationspring meeting, Tokyo (in Japanese)

=2006=

Kawakami, H., Honda, M.C., Watanabe, S., 2006. Estimation of the biological pump in the northwestern North Pacific. The seventh Mirai Symposium in Yokohama, 24 Feb. 2006.

Kawakami, H., Honda, M.C., 2006. Time-series observation of POC fluxes estimated from ^{234}Th in the northwestern North Pacific. 2006 AGU Ocean Sciences Meeting in Honolulu, 21 Feb. 2006.

Kawakami, H., Honda, M.C., Watanabe, S., 2006. Seasonal change in the concentrations of dissolved inorganic carbon and nutrients in the northwestern North Pacific. The Oceanographic Society of Japan 2006 spring meeting in Yokohama, 28 Mar. 2006.

Kawakami, H., Honda, M.C., Watanabe, S., 2006. Secular change of the activity of the biological pump in the northwestern North Pacific. The Oceanographic Society of Japan 2006 fall meeting in Nagoya, 27 Sep. 2006.

Honda, M. C., H. Kawakami, S. Watanabe, H. Sako, K. Hayashi and T. Idai (2006) Seasonal variability in nutrient in the surface mixed layer, and that in settling particles in the meso- and bathy-pelagic ocean. The seventh Mirai Symposium in Yokohama, 24 Feb. (in Japanese)

Honda, M. H., Kawakami, and S. Watanabe (2006) Linkage between seasonal variability of nutrients in the epipelagic layer and that of biogenic particle fluxes in the mesopelagic and bathypelagic layers. 2006 AGU Ocean Science Meeting, Honolulu.

Honda, M. C., H. Kawakami, and S. Watanabe（2006）Seasonal variability in nutrient in the surface mixed layer, and that in settling particles in the meso- and bathy-pelagic ocean. Oceanographic Society of Japan 2006 spring meeting, Yokohama (in Japanese)

Honda, M. C. (2006) Study of biological pump using research vessels and mooring system. In special symposium “Time-series observation in the North Pacific: Current and Future”, Oceanographic Society of Japan 2006 fall meeting, Nagoya (in Japanese)

Matsumoto, K., M. C. Honda, H. Kawakami, and S. Watanabe (2006) Comparison of distribution of phytoplankton and primary productivity between the west-east Pacific. Oceanographic Society of Japan 2006 spring meeting, Yokohama (in Japanese)

Matsumoto, K., Honda, M., H. Kawakami, T. Fujiki and S. Watanabe (2006) Factors controlling

distribution of phytoplankton and primary productivity in autumn in the North Pacific. Oceanographic Society of Japan 2006 fall meeting, Nagoya (in Japanese)

Wakita, M., S. Watanabe, A. Murata, Y. Kumamoto and K. Sasaki (2006)Interannual variability in dissolved inorganic carbon in the western North Pacific. Oceanographic Society of Japan 2006 spring meeting, Yokohama (in Japanese)

（Others）

(1) Preliminary Cruise Reports: MR01-K04, MR02-K05, MR03-K01, MR04-04, MR04-06, MR05-01, MR06-03 (http://www.jamstec.go.jp/mirai/all_year/index.html)

(2) Routine data set of Station K2 (available on line in near future)

Journal of Oceanography, Vol. 59, pp. 671 to 684, 2003

Biological Pump in Northwestern North Pacific

MAKIO C. HONDA*

Mutsu Institute for Oceanography, Japan Marine Science and Technology Center, Natsushima, Yokosuka 237-0061, Japan

(Received 2 July 2002; in revised form 10 October 2002; accepted 31 October 2002)

The northwestern North Pacific is considered to be one of the most productive areas in the global ocean. Although the marginal zones along the Japanese and Kuril islands, Kamchatka Peninsula, and Aleutian Islands are certainly productive, recent studies do not always show high primary production values in the western subarctic gyre (WSG). In addition, a recent analysis of the biological pump in the WSG showed that, in contrast to what was previously reported, the vertical change of the particulate organic carbon flux with depth is large. Nevertheless, the biological pump in the northwestern North Pacific may function to draw down the partial pressure of CO_2 in the surface water because the ratio of the organic carbon flux to inorganic carbon flux (C_{org}/C_{inorg}), the export flux, and the export ratio from the surface water are higher than those in other oceans. This article also introduces recent research on changes to the biological pump that might have been caused by global warming.

Keywords:
· Western subarctic gyre,
· primary production,
· export flux,
· export ratio,
· vertical change,
· biogeochemical change.

1. Introduction

A better understanding of the ability of the ocean to control atmospheric CO_2 levels will only be gained from a quantitative investigation of the mechanism known as the biological pump. Mathematical simulations suggest that the pre-industrial atmospheric CO_2 concentration might have been as high as 460 ppm in the absence of a biological pump (Sarmiento and Toggweiler, 1984). In addition, the global annual average of the export carbon flux out of the surface layer (new production) has been estimated as approximately 10 Gt-C yr^{-1}, which is five times the estimated anthropogenic CO_2 input (2 Gt-C yr^{-1}) (IPCC, 1995).

The northwestern North Pacific, which is a terminal zone of deep-water circulation where nutrient-rich water is supplied to the surface layer, has high primary production (Koblents-Mishke *et al*., 1970; Berger *et al*., 1987). This upwelling and winter mixing results in increased biological activity in the euphotic layer in spring. As the water supplied is particularly rich in dissolved silicate, diatom species are predominant relative to coccolithophorids (e.g., Taniguchi, 1999). Because diatom species generally form large aggregates of settling particles, large particles containing organic carbon are thought to be transported vertically into the ocean interior without significant decomposition (Tsunogai and Noriki, 1987; Kemp *et al*., 2000; Smetacek, 2000). The great efficiency of this biological pump in the northwestern North Pacific can be also reflected by the large seasonal difference in the pCO_2 of the surface water (Takahashi *et al*., 1999, 2002). Many shipboard observations and sediment trap experiments have been carried out in this region, but our quantitative understanding of the biological pump is quite limited. A comprehensive study of the biogeochemistry at the KNOT time-series observational station has been carried out recently (Bychkov and Saino, 1998). Ships of opportunity have also collected data in the North Pacific (e.g., Wong *et al*., 2002). In addition, recent significant progress in satellite oceanography has yielded new insights into temporal and spatial changes in the oceanography of the northwestern North Pacific (e.g., Sasaoka *et al*., 2002).

This study reviews recent research on the biological pump in the global ocean and characterizes its functioning in the northwestern North Pacific. The biological pump has the following components (Fig. 1):

(1) Primary production

(2) Export carbon flux and export ratio from the surface mixed layer

(3) Vertical transport of particulate carbon in the water column or twilight zone (mesopelagic layer)

(4) Export carbon flux and export ratio in the deep sea

(5) Carbon sedimentation rate.

Sediment-trap experiments, in which settling particulate carbon is collected directly, have been the principal

* E-mail address: hondam@jamstec.go.jp

Copyright © The Oceanographic Society of Japan.

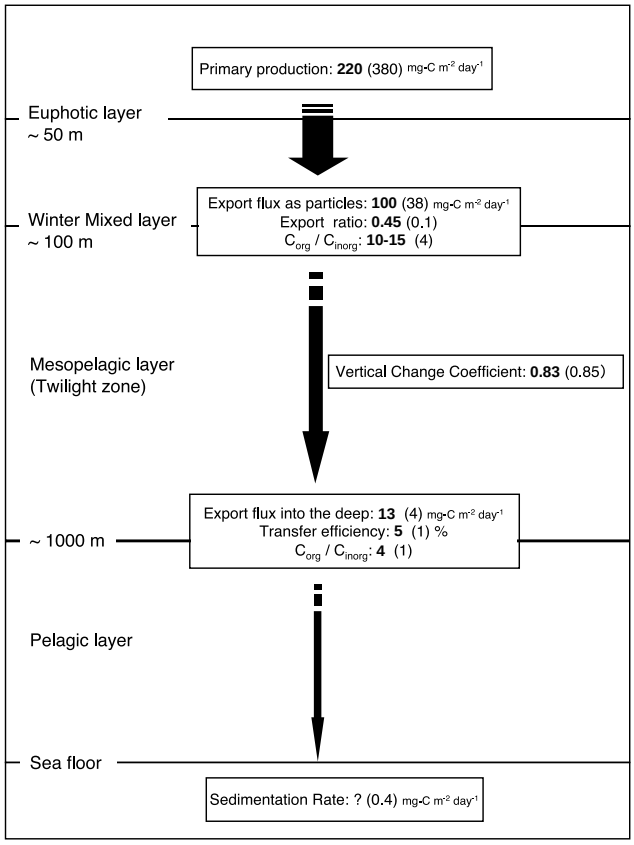

Fig. 1. Components of the biological pump. The depths of the euphotic layer and winter mixed layer are for the northwestern North Pacific. Bold numbers are annual averages estimated for the western subarctic gyre and numbers in parenthesis are those for the global ocean (see text). The sedimentation rate is not discussed in this review.

method used to study the biological pump (e.g., Honjo, 1996). This article begins by considering the export flux to the deep sea as revealed by sediment-trap experiments and then goes on to consider in sequence the other components of the biological pump, which have been studied by other, more indirect, methods. "Export flux" in this study is defined as the particulate organic carbon flux out of the euphotic zone or the winter mixed layer. Dissolved organic carbon (DOC) is not taken into account because the contribution of DOC to the export flux is considered to be low in high-latitude regions (e.g., Doval and Hansell, 2000). The "export ratio" is the ratio of the export flux to primary production. Some of the papers reviewed in this study use the terms "new production" and "f-ratio" rather than "export flux" and "export ratio," respectively. Total primary production consists of new production and regenerated production, where new production is production fueled by nitrate and N_2 and regenerated production is that fueled by urea-N, or amino acid-N, etc. The f-ratio is defined as the ratio of new production to total primary production (Dugdale and Goering, 1967; Eppley and Peterson, 1979). Thus, under steady state conditions and assuming that the DOC flux is negligible, the export flux and the export ratio are identical to new production and the f-ratio, respectively.

2. Carbon Flux to the Deep Sea

Since the late 1970s, sediment-trap experiments have been conducted in the global ocean. Although such experiments do not always clarify biological processes in the surface layer, they have been the principal method used to study the mechanism of the biological pump. On the basis of the compiled sediment-trap data, the annual mean organic carbon flux to the deep sea (2000 m depth) has been estimated as approximately 0.3 Gt-C yr^{-1} or 3 mg-C $m^{-2}day^{-1}$ (e.g., Lampitt and Antia, 1997). As diatom species are predominant in the western subarctic gyre (WSG), it has been supposed that the organic carbon flux collected by using sediment traps is higher there than that in other areas. Several sediment-trap experiments have been carried out in the WSG (e.g., Noriki and Tsunogai, 1986; Kawahata *et al.*, 1998; Honda, 2001). Honda (2001) compiled sediment-trap data from the global ocean (Table 1, Fig. 2), comparing the total carbon and organic carbon fluxes in the northwestern North Pacific with those obtained in other oceans. Using an empirical equation for the vertical change in the carbon flux, he estimated that the annual mean of the total carbon flux at 1000 m ranges from approximately 7 to 23 mg-C $m^{-2}day^{-1}$ (Table 1). The total carbon flux in the northwestern North Pacific, including the Sea of Okhotsk and the Bering Sea, is approximately 17 mg-C $m^{-2}day^{-1}$, which is the second largest in the global ocean, following that in the Arabian Sea (23 mg-C $m^{-2}day^{-1}$). However, the organic carbon flux at 1000 m (approximately 13 mg-C $m^{-2}day^{-1}$) is largest in the northwestern North Pacific, while the inorganic carbon flux is largest in the Arabian Sea, followed by that in the mid North Atlantic.

3. The Ratio of Organic Carbon to Inorganic Carbon

The ratio of organic carbon to inorganic carbon (C_{org}/C_{inorg}) is important for quantifying the efficiency of the biological pump in drawing down the pCO_2 in the surface water because photosynthesis (assimilation) decreases the pCO_2 of surface water, whereas calcite production (calcification) increases it. By drawing down the pCO_2 of the surface water, the biological pump enhances the potential uptake of atmospheric CO_2 by the ocean. Tsunogai and Noriki (1991) summarized sediment-trap data for the global ocean and, based on the fact that C_{org}/C_{inorg} ratios of sediment-trap samples collected in the mesopelagic and pelagic layers (deeper than 500 m) are

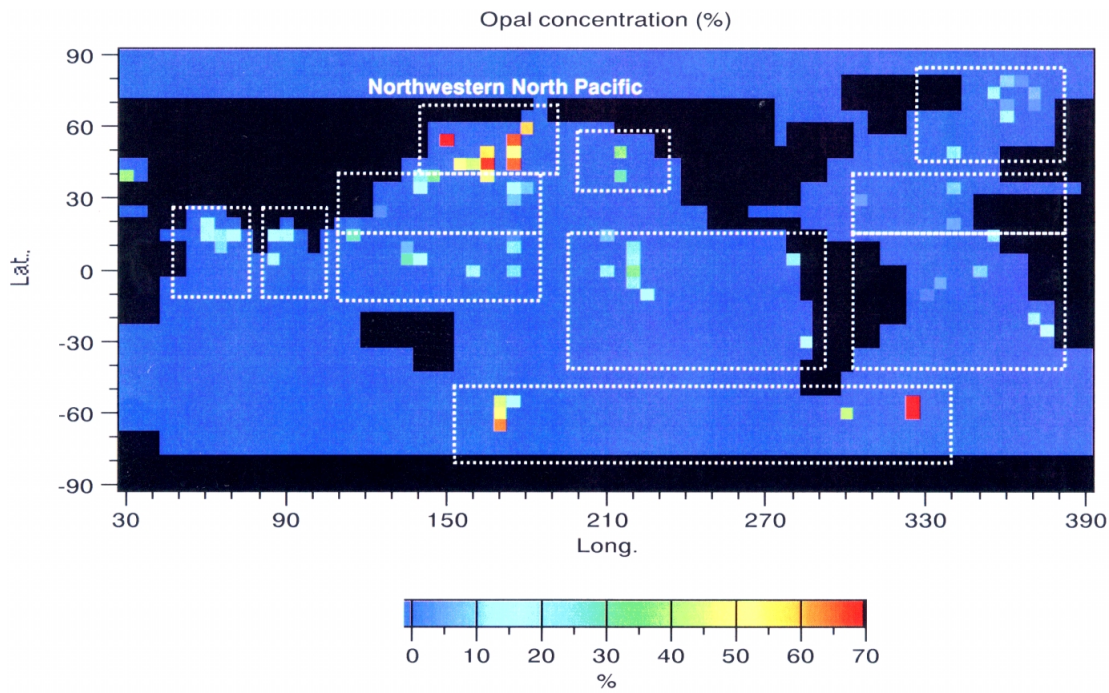

Fig. 2. The global distribution of opal concentration obtained by sediment trap experiments (Honda *et al*., 2002 and references therein). The regional averages in Table 1 are estimated for areas surrounded by hatched line on this figure.

greater than 1 on average, they concluded that the ocean's biological activity plays a role in the decrease of pCO_2 in the surface water. The C_{org}/C_{inorg} ratio of settling particles in the northwestern North Pacific has been estimated to be approximately 4, the second largest value recorded in the global ocean, after a value of about 7 recorded in the Southern Ocean (Table 1). The C_{org}/C_{inorg} ratio in the Arabian Sea is low (1.3) in spite of the large total carbon flux. If organic and inorganic carbon fluxes at the base of the winter mixed layer can be estimated by extrapolating carbon fluxes in the deep sea using empirical equations proposed by Martin *et al*. (1987) for the vertical change in the organic carbon flux, and by Yamanaka and Tajika (1996) for the vertical change in the inorganic carbon flux, the C_{org}/C_{inorg} ratio of settling particles at 100 m can be estimated as approximately 15 in the WSG. This ratio is consistent with the C_{org}/C_{inorg} ratio of approximately 10 estimated on the basis of carbonate solution chemistry (Andreev *et al*., 2002) and approximately 16 estimated by biogeochemical transport box model (Sarmiento *et al*., 2002), and it is approximately four times the global C_{org}/C_{inorg} average (4) estimated by biogeochemical models (Broecker and Peng, 1982; Knox and McElroy, 1984; Sarmiento and Toggweiler, 1984; Siegenthaler and Wenk, 1984). Furthermore, this ratio correlates positively with the ratio of opal flux to $CaCO_3$ flux (Si/Ca) and opal concentration (Fig. 2), which indicates that the efficiency of the biological pump in drawing down pCO_2 in the surface water is high in areas where diatoms are predominant relative to coccolithophorids.

Honda *et al*. (1997) and Honda (2001) estimated the ability of the biological pump to draw down pCO_2 in the surface water by using organic carbon and inorganic carbon flux data collected by sediment traps and an empirical equation to describe the vertical change in carbon fluxes. They concluded that the biological pump draws down the pCO_2 in the surface water more efficiently in the northwestern North Pacific and the Antarctic than in other oceans. Antia *et al*. (2001) suggested the following equation to quantify the efficiency of the biological pump for the uptake of atmospheric CO_2 (J_{eff});

$$J_{eff} = J_{POC(WML)} \times (RR_{(WML)} - 0.6)/(RR_{(WML)}) \quad (1)$$

where $J_{POC(WML)}$ is the organic carbon flux at the bottom of the winter mixed layer (WML) and $RR_{(WML)}$ is the "rain ratio," which is identical to the C_{org}/C_{inorg} ratio. On the basis of stoichiometry, Kano (1990) suggested that 0.6 is the boundary C_{org}/C_{inorg} ratio; in other words, the pCO_2 of seawater increases when the particulate carbon is biologically produced and its C_{org}/C_{inorg} ratio is less than approximately 0.6. The biological pump is more efficient in the northwestern North Pacific than in the Atlantic Ocean or the equatorial zone, not only because of the

Table 1. Summary of fluxes and ratios of biogenic materials obtained by sediment-trap experiments in the global ocean (modified from table 4.8 in Honda, 2001, and references therein).

Ocean	Maritime	TOC flux	Org-C flux	Inorg-C flux	Opal flux	C_{org}/C_{inorg} ratio	Si/Ca ratio	Note (including data from)
Atlantic	(Northern North Atlantic: $n = 8$)							
	average	10.15	5.99	4.16	7.34	1.76	0.41	Fram Strait
	stdev	5.85	4.42	2.44	5.86	1.31	0.26	US JGOFS NABE
	(Middle North Atlantic: $n = 5$)							
	average	15.33	7.03	8.30	7.37	1.03	0.16	Station S
	stdev	9.73	4.17	5.69	5.97	0.46	0.06	US JGOFS NABE
	(Equatorial Atlantic: $n = 8$)							
	average	13.05	6.86	6.19	10.16	1.14	0.28	Guinea
	stdev	10.92	6.98	4.89	9.87	0.53	0.12	Benguela
	(Southern Ocean: $n = 8$)							
	average	7.12	5.02	2.09	58.48	7.17	16.72	US JGOFS AESOPS
	stdev	4.94	4.08	1.74	56.11	9.12	18.81	Weddell Sea
Indian	(Bengal Bay: $n = 3$)							
	average	11.72	7.25	4.47	18.43	1.71	0.9	
	stdev	0.33	1.1	0.91	7.83	0.65	0.57	
	(Arabian Sea: $n = 11$)							
	average	22.82	11.27	9.17	21.43	1.29	0.51	US JGOFS Arabian Sea
	stdev	7.76	4.8	3.94	11.83	0.37	0.34	
Pacific	(Northeastern North Pacific: $n = 2$)							
	average	13.47	7.3	6.17	33.49	1.27	1.1	Station Papa
	stdev	1.95	0.06	2.01	13.7	0.39	0.13	off California
	(Northwestern North Pacific: $n = 16$)							
	average	16.56	12.94	4.45	91.47	3.73	4.78	Station KNOT
	stdev	8.46	7.07	1.7	48.68	2.3	2.9	Bering/Okhotsk
	(Middle Western North Pacific: $n = 10$)							
	average	11.03	6.3	4.73	13.31	1.41	0.53	
	stdev	3.03	2.32	1.36	13.59	0.65	0.52	
	(Equatorial Western Pacific: $n = 14$)							
	average	9.8	5.36	4.45	13.3	1.09	0.44	
	stdev	8.6	5.14	3.57	16.54	0.35	0.32	
	(Equatorial Eastern Pacific: $n = 12$)							
	average	13.17	6.41	6.76	17.35	0.99	0.53	US JGOFS EQPAC
	stdev	7.79	4.27	3.88	10.51	0.42	0.25	

Flux: mg $m^{-2}day^{-1}$.
Ratio: mole ratio.
n: numbers of sediment trap stations.

Table 2. Characteristics of the biological pump at the principal time-series stations.

		KNOT	OSP*[4]	HOT*[5]	BATS*[5]
a	Primary production (mg $m^{-2}day^{-1}$)	220*[1]	384	416 ± 178	480 ± 129
b	Export flux ($POC_{(100)}$: mg $m^{-2}day^{-1}$)	100*[2]	110	27 ± 13.9	28 ± 10
c	Export ratio (b/a)	0.45	0.29	0.07 ± 0.04	0.06 ± 0.03
d	POC flux into the deep ($POC_{(z)}$: mg $m^{-2}day^{-1}$)	6.0 (3000 m)*[3]	3.1 (3800 m)	3.1 (2800 m)*[6]	1.9 (3000 m)*[7]
e	Transfer efficiency (d/a) (%)	2.7	0.8	0.7	0.4
f	Vertical Change Coefficient (VCC)*[8]	0.83	0.98	0.65	0.79
	C_{org}/C_{inorg} (1000 m)*[9]	1.9	1.0	1.1	0.8
	Si/Ca (1000 m)*[9]	3.1	1.2	0.2	0.2

*[1]Imai *et al.* (2002); *[2]Andreev *et al.* (2002) and Midorikawa *et al.* (2002); *[3]Honda *et al.* (2002); *[4]Wong *et al.* (1999); *[5]Karl *et al.* (2001); *[6]Karl *et al.* (1996); *[7]Deuser *et al.* (1987); *[8]VCC = –log ($POC_{(z)}/POC_{(100)}$)/log(z/100): *z* is water depth (m); *[9]Honda (2001): Note that HOT sediment trap data are not available and, therefore, refered the other data in the subtropical area (references therein).

higher C_{org}/C_{inorg} ratio but also the shallower depth of the winter mixed layer (100–150 m in the North Pacific against 300 m in the Atlantic; Harrison, 2002).

4. Primary Production

The accurate determination of primary production is fundamental to an understanding of the biological pump. Based on previous estimations that used in situ observations (e.g., Sundquist, 1985), remotely sensed data (e.g., Longhurst *et al.*, 1995; Antoine *et al.*, 1996; Falkowski *et al.*, 1998; Field *et al.*, 1998), and mathematical modeling (e.g., Six and Maier-Reimer, 1996), the global annual mean primary production has been estimated to be 50 ± 10 Gt-C yr^{-1}. This can be converted to 379 ± 76 mg-C $m^{-2}day^{-1}$ by using 361 × 10^6 km^2 as the surface area of the global ocean. In general, the northwestern North Pacific is characterized as one of the highly productive regions (Koblents-Mishke *et al.*, 1970; Berger *et al.*, 1987). During the spring bloom, especially, a high primary production of 1000–2000 mg-C $m^{-2}day^{-1}$ has been measured (Taniguchi and Kawamura, 1972; Hama *et al.*, 1983; Maita and Odate, 1988; Shiomoto, 2000a, b). Data from the sea-viewing wide field of view sensor (SeaWiFs) also show a high concentration of chlorophyll *a* (chl *a*) of more than 5 mg m^{-3} in the coastal region during the late spring and early summer, which agrees with shipboard observations (e.g., Shiomoto *et al.*, 1998). Remotely sensed data to describe parameters such as chl *a*, photosynthetically available radiation (PAR) and SST have been used in developing algorithms to estimate ocean primary production (Platt *et al.*, 1991; Morel, 1991; Behrenfeld and Falkowski, 1997); global primary production synoptic maps have also been published (Platt *et al.*, 1991; Longhurst *et al.*, 1995; Antoine *et al.*, 1996; Behrenfeld and Falkowski, 1997). Longhurst *et al.* (1995), Antoine *et al.* (1996), Behrenfeld and Falkowski (1997), and Balkanski *et al.* (1999), estimated the annual mean primary production in the WSG as 264 (723), 50–150 (137–411), 150–250 (411–685), and 120–180 (329–493) g-C $m^{-2}yr^{-1}$ (mg-C $m^{-2}day^{-1}$), respectively. These data also show that primary production is high in the northwestern North Pacific.

However, some recent measurements of the primary production do not show such a high primary production in the WSG. According to Shiomoto (2000a, b), primary production varies seasonally variable in the WSG: primary production in spring was 318 ± 55; summer, 247 ± 177; autumn, 191 ± 57; and winter, 40 ± 36 mg-C $m^{-2}day^{-1}$, for an annual average of 199 mg-C $m^{-2}day^{-1}$. Imai *et al.* (2002) measured the seasonal variability in primary production at station KNOT for three years, during which primary production ranged from less than 100 mg-C $m^{-2}day^{-1}$ in winter to more than 500 mg-C $m^{-2}day^{-1}$ in spring. Although at one highly productive location primary production was more than 1000 mg-C $m^{-2}day^{-1}$, the annual average was estimated as approximately 220 mg-C $m^{-2}day^{-1}$, which is definitely lower than the global average (379 ± 76 mg-C $m^{-2}day^{-1}$). Moreover, it is also lower than the annual averages determined at the subtropical time-series stations HOT (ALOHA) and BATS (Karl *et al.*, 2001; see Table 2). The discrepancy between these recent measurements of primary productivity in the WSG and those previously reported might be attributed to the earlier reported values having been based on measurements in the coastal and hemipelagic zones or to a failure to include sufficient data collected in winter. In addition, primary production based on remotely sensed data might be overestimated because of problems with the algorithm proposed by Behrenfeld and Falkowski (1997) (Kameda and Ishizaka, 1999, 2000). It has also been pointed out that the WSG is a high-nutrient low-chlorophyll (HNLC) area (e.g., Tsuda and Takeda, 2002).

Primary production in the coastal regions of the northwestern North Pacific and during the spring bloom must be higher than the global average. However, in general, the primary production in the WSG might not be so high.

5. Export Flux

Another important component of the biological pump is the export flux, that is, the organic carbon flux out of the euphotic layer or the winter mixed layer. The global mean export flux has been estimated as about 5 (Berger *et al*., 1987), 7.4 (Martin *et al*., 1987), 12–15 (Najjar *et al*., 1992), 11.1 (Six and Maier-Reimer, 1996), 8 (Yamanaka and Tajika, 1996), 7 (Hansell and Carlson, 2001), 9.4 Gt-C yr^{-1} (Palmer and Totterdell, 2001), or 9.5 ± 1 Gt-C yr^{-1} (Schlitzer, 2002). Some estimates considered the contribution of DOC to the export flux to be negligible, but some researchers, such as Yamanaka and Tajika (1996) and Hansell and Carlson (2001), consider DOC to account for approximately 35% and 17%, respectively, of the export flux. The Intergovernmental Panel on Climate Change (IPCC; 1995) summarized the global carbon balance and reported that the export flux due to settling particles is approximately 40% of the global export flux (10 Gt-C yr^{-1}) or 4 Gt-C yr^{-1}.

Although the use of sediment traps is a direct method by which to measure the organic carbon flux, there remain some problems with the method, such as the swimmer, solubilization of collected materials, trapping efficiency, and difficulty mooring the traps at shallow depths (U.S. GOFS Working Group, 1989). The use of radiochemistry, such as the thorium–uranium method, is a powerful approach to the study of the export flux (e.g., Buesselar, 1998), although there is some controversy regarding the ratio of particulate organic carbon (POC) fluxes to ^{234}Th and assumption of a steady state/non steady state. In the western North Pacific, Harada *et al*. (2001) used this radiochemical method at station KNOT to estimate the export flux and reported export fluxes of 6 mmol-C $m^{-2}day^{-1}$ in the spring and 9 mmol-C $m^{-2}day^{-1}$ in the winter at 200 m depth. By averaging these two values, the annual average flux at station KNOT was estimated to be approximately 7.5 mmol-C $m^{-2}day^{-1}$ or 90 mg-C $m^{-2}day^{-1}$. Kawakami *et al*. (unpublished data) also used the radiochemical method to estimate the POC flux in the northwestern North Pacific and found that the POC fluxes at the depth at which chl *a* disappears (75–150 m) to be 20–190 mg-C $m^{-2}day^{-1}$ in winter and 20–900 mg-C $m^{-2}day^{-1}$ in spring. They also observed that the export flux and export ratios decreased eastward with distance from the Asian continent.

Another method for estimating the export flux is based on the difference in total dissolved carbon or nutrients between winter and summer in the mixed layer. The export flux estimated by this method is referred to as "net community production" (NCP) or "new production" (Codispoti *et al*., 1986; Minas *et al*., 1986). Goes *et al*. (2000) developed an algorithm to estimate the concentrations of nitrate with remotely sensed sea surface temperature (SST) data. Using this method, they estimated the new production to a depth of 25 m, which is the nitracline depth, as 40 ± 10 g-C $m^{-2}yr^{-1}$ or 110 ± 27 mg-C $m^{-2}day^{-1}$. Wong *et al*. (2002) compiled data on nutrients in the North Pacific obtained by the ships-of-opportunity program conducted in the North Pacific during 1995–2000. They estimated that new production to a depth of 50 m, which is the annual average depth of the base of the euphotic zone in the North Pacific, to be 67.2 g-C $m^{-2}yr^{-1}$ or 184 mg-C $m^{-2}day^{-1}$. Their results suggest that the export flux in the WSG is lower than that off Hokkaido (78.3 g-C $m^{-2}yr^{-1}$) and slightly larger than that in the Alaskan Gyre (49.7 g-C $m^{-2}yr^{-1}$). Tsuda *et al*. (2002) estimated new production to a depth of 50 m along their time-series observation line (A-line), which is located in a productive area off Kushiro, and found a value of 174 mg-C $m^{-2}day^{-1}$. Using the difference in the integrated nutrients in the mixed layer between late winter and late summer or between the surface mixed layer and the intermediate water, Midorikawa *et al*. (2002) and Andreev *et al*. (2002) estimated the annual average of new production to a depth of 100 m, which is the depth of the base of the winter mixed layer in the WSG (50°N, 165°E) and at station KNOT (44°N, 155°E), finding values of 95 ± 7 and 105 ± 20 mg-C $m^{-2}day^{-1}$, respectively. As described above, the new production and the export flux values depend on the boundary depth, in other words, the depth of the base of the euphotic layer or winter mixed layer. We should therefore pay close attention when we compare new production data and export fluxes reported by different researchers. However, the depth of the winter mixed layer is more important than that of the euphotic layer or the seasonal mixed layer when we consider how much carbon is eliminated from the surface layer and not easily returned. Therefore, the export flux at 100 m depth in the WSG, approximately 100 mg-C $m^{-2}day^{-1}$ or 36.5 g-C $m^{-2}yr^{-1}$ (at least, at station KNOT), is the appropriate value to use. Karl *et al*. (2001) summarized the export fluxes measured at stations HOT and BATS, which are U.S. Joint Global Ocean Flux Study (JGOFS) time-series stations located in the subtropical zones of the Pacific and Atlantic oceans, respectively. The export flux, which was measured seasonally with drifting sediment traps experiment, was approximately 30 mg-C $m^{-2}day^{-1}$ at each site (Table 2). Thus, the export flux in the WSG is approximately three times the values measured at the subtropical stations and comparable to or slightly less than that measured at station OSP in the Alaskan Gyre (110 mg-C $m^{-2}day^{-1}$; Sambrott and Lorenzen, 1987; Parsons and Lalli, 1988; Welschmeyer *et al*., 1993). Therefore, a

Table 3. Transfer efficiency (TE) in the global ocean (modified from table 6 in Honda *et al.*, 2002).

	Depth (m)	Primary Prod. (mg $m^{-2}day^{-1}$)	Org-C flux (mg $m^{-2}day^{-1}$)	TE (%)	Note	Reference
Western North Pacific	924	220	11.3	5.1	May~December, 1998–1999	Honda *et al.* (2002)
(Stn. KNOT)	2957	220	7.5	3.4	May~December, 1998–1999	Honda *et al.* (2002)
	4989	220	4.6	2.1	May~December, 1998–1999	Honda *et al.* (2002)
Bering Sea	3200			~2	53.5°N, 177°W (Takahashi *et al.*, 2000)	Lampitt and Antia (1997)
Eastern North Pacific (Stn. P)	3800	384	3.5	0.9		Wong *et al.* (1999)
Western Equatorial Pacific	1357	100	1.9	1.9	September	Kawahata *et al.* (2000)
	4363	100	1.3	1.3	September	Kawahata *et al.* (2000)
Eastern Equatorial Pacific	~3500	~580	~1.8	~0.3	9°N~12°S, El Niño period	Honjo *et al.* (1995)
(JGOFS EqPac)	~3500	~900	~3.5	~0.4	9°N~12°S, Post El Niño period	Honjo *et al.* (1995)
Arabian Sea	809~999	1386	11.5~11.8	0.8~0.9	stn. M1	Lee *et al.* (1998)
(JGOFS Arabian Sea)	839~3150	1378	13.3~17.4	1.0~1.3	stn. M2	Lee *et al.* (1998)
	778~2979	1131	13.1~18.2	1.2~1.6	stn. M3	Lee *et al.* (1998)
	814~3484	1405	8.9~12.6	0.6~0.9	stn. M4	Lee *et al.* (1998)
	800~3915	762	3.3~5.7	0.4~0.7	stn. M5	Lee *et al.* (1998)
North Atlantic	2000			1.7	48°N, 21°W (JGOFS NABE: Spring bloom)	Honjo and Manganini (1993)
	500~1000	302	5.9~13.4	2.0~4.4	60°N-80°N	Schluter *et al.* (2000)
	4000	230	2.0	0.9	24°N, 23°W	Jickells *et al.* (1996)
	4000	230	1.5	0.7	28°N, 2°W	Jickells *et al.* (1996)
	4000	267	4.2	1.6	48°N, 20°W	Jickells *et al.* (1996)
Middle and equatorial Atlantic	1000	~712	~20	~2.8	Site M (Mesotrophic: 18.5°N, 21°W)	Bory *et al.* (2001)
	1000	~301	~2	~0.6	Site O (Oligotrophic: 21°N, 31°W)	Bory *et al.* (2001)
	950	1349	30	2.2	Cariaco Basin (10.5°N, 64.4°W) Nov. 1995–Apr. 1996	Thunell *et al.* (2000)
	1225	1349	19	1.4	Cariaco Basin (10.5°N, 64.4°W) Nov. 1995–Apr. 1996	Thunell *et al.* (2000)
Global mean	2000	270~1400	1~16	1	trap data normalized to 2000 m by Martin equation and PP estimated by satellite data	Lampitt and Antia (1997)
	>1500			1.1		Lutz *et al.* (2002)

high export flux is one of the prominent characteristics of the biological pump in the WSG.

6. Export Ratio

Honda *et al*. (2002) estimated the "transfer efficiency," which is the ratio of the particulate organic carbon flux into the deep sea to primary production (i.e., the export ratio in the deep sea), at station KNOT. Using an annual mean primary production value of 220 mg-C $m^{-2}day^{-1}$ (Imai *et al*., 2002) and the organic carbon flux values obtained from a moored sediment-trap experiment, the transfer efficiency at 1000, 3000, and 5000 m depth was estimated to be approximately 5%, 3%, and 2%, respectively. These values are higher than those reported previously for other oceans (Table 3). It might be suspected that the export ratio at the bottom of the winter mixed layer is also higher in the WSG than other oceans.

Table 2 compares the export ratios at the bottom of the winter mixed layer at the principal ocean time-series stations. The annual average export ratio at station KNOT was estimated as approximately 0.45 (45%), which is larger than at other stations. On a global scale, Pace *et al*. (1987) estimated the export ratio or f-ratio to be 0.13–0.17 from a statistical analysis of sediment-trap experiments data. The global mean f-ratio estimated by mathematical simulation was approximately 0.2 (IPCC, 1995), 0.25 (Six and Maier-Reimer, 1996), 0.21 (Laws *et al*., 2000), or 0.15 (Palmer and Totterdell, 2001). Taking into account that these export ratios include the DOC flux fraction, the export ratio for settling particles is remarkably higher than the global mean at station KNOT. Using thorium–uranium methods, Buesselar (1998) determined the export ratio for the global ocean and concluded that the export ratio due to settling particles in most of the world's oceans is less than 10%, except in the high latitude zones, where diatom species are predominant and the export ratio is larger than 20%. This result supports the high export ratio determined at station KNOT. Therefore, the export ratio in the WSG is high and the organic carbon assimilated by biological activity is transported to the ocean interior more efficiently there than in other oceans.

On the other hand, the relation between the export ratio and primary production is still controversial. In general, the export flux increases with primary production and it was thought that the export ratio did, too (e.g., Betzer *et al*., 1984). A high export ratio, as well as a high transfer efficiency or f-ratio, can be seen in high-latitude oceans and other productive regions (Buesselar, 1998; Launchi and Najjar, 2000; Bory *et al*., 2001; Honda *et al*., 2002). On the basis of sediment-trap experiments, Pace *et al*. (1987) and Antia *et al*. (2001) reported that the export ratio increased as primary production increased. Others (Suess, 1980; Thunell *et al*., 2000; Muller-Karger *et al*., 2001) have found the export ratio to be independent of primary production. On the other hand, a hyperbolic relation between the export ratio and primary production has also been reported: for annual primary production less than 200 (Eppley and Peterson, 1979), 250 (Lampitt and Antia, 1997), or 50 g-C $m^{-2}yr^{-1}$ (Palmer and Totterdell, 2001), the export ratio was found to increase linearly with primary production, but when primary production was larger, the ratio decreased slowly or was constant. Moreover, on the basis of long-term time-series observations at stations BATS (Lohrenz *et al*., 1992; Michaels *et al*., 1994) and HOT (Karl *et al*., 1996), a decrease in the export ratio was observed as primary production increased. Thunell (1998) reported a similar trend in the Santa Barbara Basin. This negative correlation between the export ratio and primary production has been interpreted to result from increased grazing pressure (Michaels *et al*., 1994; Pilskaln *et al*., 1996; Thunell, 1998) and/or horizontal transport (Lohrenz *et al*., 1987; Pilskaln *et al*., 1996; Thunell, 1998). In addition, an increase in DOC with primary production (Fasham *et al*., 1993; Williams, 1995; Thingstad *et al*., 1997) may lower the apparent export ratio by settling particles (Michaels *et al*., 1994; Pilskaln *et al*., 1996). Laws *et al*. (2000) simulated the export flux and ratio in the global ocean. They assumed that the export flux and ratio depend primarily on the grazing pressure and constructed a food web model to estimate the "ef-ratio." This model led them to conclud that the "ef-ratio" has no relation or else a negative relation with primary production in oligotrophic or tropical areas.

Recently Japanese radiochemists also reported smaller export ratios under eutrophic (high production) conditions (Harada *et al*., 2001; Taguchi *et al*., 2002; Aono *et al*., 2002) than under oligotrophic conditions. Honda (2001) studied the relation between primary production estimated by satellite data and organic carbon flux data collected by sediment-trap experiments and found it to be negative, although there is controversy regarding the estimation of primary production from satellite data and the time lag between the primary production and carbon flux data. To understand this relation better, one needs observation and quantification of seasonal variability in grazing pressure and the formation of DOC.

7. Vertical Change Coefficient

To study the biological pump in more detail and contribute to the construction of a global biogeochemical model, the mechanism of vertical change in the organic carbon flux with depth or of the carbon cycle in the twilight zone must also be understood. Since Suess (1980) first presented an empirical equation for the vertical change in the carbon flux with depth, several additional equations have been proposed based on the results of sediment-trap experiments or mathematical simulations. Most

of the equations belong to one of the following two types (Honda *et al*., 1997):

$$POC_{(z)} = POC_{(100)} \times (Z/100)^{-b} \quad (2)$$

$$POC_{(z)} = a \times PP^{c} \times Z^{-b} \quad (3)$$

where $POC_{(z)}$ and $POC_{(100)}$ are the particulate organic carbon fluxes at Z m and 100 m, respectively, PP is primary production, and a, b and c are constants. When c (exponent of PP) is larger (or smaller) than 1, the export ratio increases (or decreases) with primary production. The exponent b is referred to as the vertical change coefficient (VCC) in this article. As VCC increases, vertical change in the particulate organic carbon flux also increases with depth. The VCC ranges from approximately 1.0 (Suess, 1980) to 0.57 (Pace *et al*., 1987). Among various equations reported previously, the equation suggested by Martin *et al*. (1987) has been used most frequently, and this gives a VCC of approximately 0.86. On the other hand, Tsunogai and Noriki (1987, 1991) and Tsunogai *et al*. (1990) suggested that the VCC (which they call the vertical change index) in high-latitude areas where diatom species are predominant should be small because diatoms produce large aggregate particles that are transported vertically without large decomposition. Using sediment-trap data from the Sea of Okhotsk and station KNOT, Honda *et al*. (1997, 2002) suggested that the VCC in the northwestern North Pacific is approximately 0.6 ± 0.1, which is a lower value than that proposed by Martin *et al*. (1987).

However, the estimation of VCC from multilayer sediment-trap data may potentially be problematic because it depends greatly on the trapping efficiency. If the trapping efficiency of the shallower trap is low, the estimated VCC would be low, with the result that the organic carbon would apparently be transported vertically without significant decomposition. Furthermore, a VCC estimated using data from sediment traps moored below 1000 m may be low because the labile organic carbon would have already decomposed in the twilight zone so that a large part of the organic carbon collected by deep-sediment traps is then refractory and barely changes with increasing depth. Recently, Berelson (2001) compiled biological pump data obtained by U.S. JGOFS Projects (NABE, EqPac, Arabian Sea, AESOPS) and found that the VCC tended to increase with the export flux. Francois *et al*. (2002a, b) compiled sediment-trap data for the global ocean and calculated the ratio of the export flux to the carbon flux in the deep sea by using a primary production value estimated from remote sensing data and an export flux value obtained by using an empirical equation for primary production (Behrenfeld and Falkowski, 1997) and for the "ef-ratio" (Laws *et al*., 2000). They concluded that the VCC is high in areas where primary production, the export flux, and the export ratio are high. Thus, a large amount of the organic carbon exported from the surface layer is decomposed in the water column in productive regions such as the WSG. Treguer and Anderson (2002) also reported that the organic carbon flux at depths greater than 2000 m in the Southern Ocean is almost comparable to values obtained in the rest of the world ocean, even though the export flux is high, which is indicative of high VCC in the productive Southern Ocean. These results all contradict the traditional hypothesis that the vertical change in carbon flux with depth is small in areas with high productivity or where diatoms are predominant (Tsunogai and Noriki, 1987, 1991). The export flux and organic carbon flux at 3000 m at station KNOT are 100 and 6 mg-C $m^{-2}day^{-1}$, respectively (Table 3). Using these values and Eq. (2), the VCC at station KNOT can be estimated as approximately 0.83, which is close to that proposed by Martin *et al*. (1987) and larger than that reported by Tsunogai *et al*. (1990) or Honda *et al*. (1997, 2002). A further study of vertical changes in the carbon flux and the mechanism which controls such change in the twilight zone is recommended.

8. Changes in the Biogeochemistry of the Ocean Caused by Global Warming

Although it is urgent that we clarify the basic mechanism of the biological pump, the ocean and the mechanism of the biological pump may gradually change in response to human activity. If this is the case, our understanding of the carbon cycle in the ocean and the ability of the ocean to regulate atmospheric CO_2 must be updated. Signs of change in the biogeochemistry in the ocean have been reported recently.

The longest time-series sediment-trap experiment has been conducted since 1978 in the Sargasso Sea. Deuser *et al*. (1995) reported a decadal decrease in the ratio of opal to $CaCO_3$. A similar trend and a decrease in the C_{org}/C_{inorg} ratio were also reported near the U.S. JGOFS NABE stations (34°N and 48°N) (Antia *et al*., 2001). In addition, a remarkable coccolith (*Coccolithus pelagicus*) bloom was observed in 1999 from sediment-trap experiments and SeaWiFS satellite imagery in the Iceland Sea (Ostermann, 2001). Diatoms are usually predominant in this area. In Ostermann's interpretation, this unusual condition was attributed to the strong stratification caused by freshwater input associated with Arctic sea-ice thinning and/or Greenland glacial wasting.

Although the biological pump works more efficiently in the northern North Pacific to draw down atmospheric CO_2, as described above, global warming may have already begun to weaken the biological pump there. In the Bering Sea, which is called the "Sea of Silica" (Tsunogai *et al*., 1979), a coccolith bloom (*Emiliani huxeleyi*) has

been observed in the last 3 years on the eastern Bering Sea shelf (Hunt *et al*., 1999). The coccolith bloom affects the carbonate chemistry in the Bering Sea. Murata and Takizawa (2002) observed that the pCO_2 of surface water in the coccolith bloom area increased to 450 ppm in September 2000, although this area is usually undersaturated for atmospheric pCO_2 (approximately 360 ppm) in that season. Emerson *et al*. (2001) detected an increase in apparent oxygen utilization (AOU) in the intermediate water in the middle part of the Eastern Pacific. They suggested two possible causes for this phenomenon: a decrease in the formation of intermediate water due to strong stratification caused by global warming, or an increase in the decomposition of settling particles caused by increasing biological pump activity. Ono *et al*. (2002) compiled historical nutrients data (phosphate concentration) for the Oyashio region off Hokkaido and Sanriku. According to their statistical analysis, the NCP in the mixed layer has been decreasing, from approximately 180 mg-C $m^{-2}day^{-1}$ in 1970 to approximately 140 mg-C $m^{-2}day^{-1}$ in 1993. Watanabe *et al*. (2002) found an increase in the depth at which the concentration of chl *a* is undetectable from approximately 60 m in the early 1970s to approximately 70 m in the early 1990s. This suggests that phytoplankton has migrated deeper because the intensified stratification has increased the depth at which sufficient nutrients for the growth of phytoplankton are supplied. Although it is not clear whether these changes were caused by global warming or by natural decadal variability, we should pay close attention to and monitor changes in biogeochemistry brought about by global warming as well as verify the basic mechanism of the carbon cycle in the ocean.

9. Concluding Remarks

Recent studies have clarified the biological pump in the northwestern North Pacific as being characterized by a high export flux, export ratio, and C_{org}/C_{inorg} ratio (summarized in Fig. 1). The time-series observational experiment at station KNOT, conducted for approximately three years, was the first comprehensive observational study and clarified many aspects of the biological pump in the northwestern North Pacific. However, our knowledge of the biological pump is still inadequate because some controversial points have not yet been clarified; such as the role of DOC in the export flux, the seasonal change in the grazing pressure, the relation between primary production and the export flux/ratio, and the biogeochemical cycle in the twilight zone. Decadal time-series observations in the WSG, such as the long-term process studies at stations HOT, BAT, and OSP, are strongly recommended for the accurate quantification of the biological pump.

Acknowledgements

I thank Dr. Shizuo Tsunogai, professor emeritus at Hokkaido University, for his enthusiastic scientific lead. His hypothesis and theory on the biological pump in the northern North Pacific stimulated my scientific interest and motivated writing this paper. I am also appreciative of Dr. Hodaka Kawahata of the Geological Survey of Japan and an anonymous reviewer for reviewing the manuscript and their constructive comments.

References

Andreev, A., M. Kusakabe, M. C. Honda, A. Murata and C. Saito (2002): Vertical fluxes of nutrients and carbon through the halocline in the western subarctic gyre calculated by mass balance. *Deep-Sea Res. II*, **49**, 5577–5594.

Antia, A. N., W. Koeve, G. Fischer, T. Blanz, D. Sculz-Bull, J. Scholten, S. Neuer, K. Kremling, J. Kuss, R. Peinert, D. Hebbeln, U. Bathmann, M. Conte, U. Fehner and N. Zeitzschel (2001): Basin-wide particulate carbon flux in the Atlantic Ocean: Regional export patterns and potential for atmospheric CO_2 sequestration. *Global Biogeochem. Cycles*, **15**(4), 845–862.

Antoine, S., J. M. Andre and A. Morel (1996): Oceanic primary production 2. Estimation at global scale from satellite (coastal zone color scanner) chlorophyll. *Global Biogeochem. Cycles*, **10**(1), 57–69.

Aono, T., I. Kudo, K. Imai, Y. Nojiri and A. Tsuda (2002): The thorium flux during the Subarctic Pacific Iron Enrichment and Ecosystem Dynamics Study (SEEDS). In *The Extended Abstract of Oceanographic Society of Japan 2002 Spring Meeting*, p. 248 (in Japanese).

Balkanski, Y., P. Monfray, M. Battle and M. Heimann (1999): Ocean primary production derived from satellite data: an evaluation with atmospheric oxygen measurements. *Global Biogeochem. Cycles*, **13**(2), 257–271.

Behrenfeld, M. J. and P. G. Falkowski (1997): Photosynthetic rates derived from satellite-based chlorophyll concentration. *Limnol. Oceanogr*., **42**(1), 1–20.

Berelson, W. M. (2001): The flux of particulate organic carbon into the ocean interior: a comparison of four U.S. JGOFS Regional studies. *Oceanography*, **14**(4), 59–67.

Berger, W. H., K. Fisher, C. Lai and G. Wu (1987): Ocean carbon flux: global maps of primary production and export production. In *Biogeochemical Cycling and Fluxes between the Deep Euphotic Zone and Other Oceanic Realms*, ed. by C. Agegian, NOAA Symposium Series for Under Sea Research Program, **3**(2); Preprint in SIO ref. 87-30.

Betzer, P. R., W. L. Shower, E. A. Laws, C. D. Winn, B. R. Ditullio and P. M. Kroopnick (1984): Primary productivity and particle fluxes on a transect of the equator at 153W in the Pacific Ocean. *Deep-Sea Res*., **31**, 1–11.

Bory, A., C. Jeandel, N. Leblond, A. Vangriesheim, A. Khripounohh, L. Beaufort, C. Rabouille, E. Nicolas, K. Tachikawa, H. Etcheber and P. Buat-Menard (2001): Downward particle fluxes within different productivity regimes off the Mauritanian upwelling zone (EUMELI program). *Deep-Sea Res*., **48**, 2251–2282.

Broecker, W. S. and T.-H. Peng (1982): *Tracers in the Sea*. Eldigio Press, Columbia Univ., New York, 690 pp.

Buesselar, K. (1998): The decoupling of production and particulate export in the surface ocean. *Global Biogeochem. Cycles*, **12**(2), 297–310.

Bychkov, A. and T. Saino (1998): JGOFS NPTT meets to review plans for studies in North Pacific. *U.S. JGOFS News Lett.*, **9**, 11–12.

Codispoti, L. A., A. J. Docimead and K. Nasu (1986): Variability in the inorganic carbon system over the southeastern Bering Sea shelf during spring 1980 and spring-summer 1981. *Cont. Shelf Res.*, **5**, 133–160.

Deuser, W. G., T. D. Jickells, P. King and J. A. Commeau (1995): Decadal and annual changes in biogenic opal and carbonate fluxes to the deep Sargasso Sea. *Deep-Sea Res.*, **42**, 11/12, 1923–1932.

Doval, M. and D. A. Hansell (2000): Organic carbon and apparent oxygen utilization in the western South Pacific and central Indian Oceans. *Mar. Chem.*, **68**, 249–264.

Dugdale, R. C. and J. J. Goering (1967): Uptale of new and regenerated forms of nitrogen in primary productivity. *Limnol. Oceanogr.*, **12**, 196–206.

Emerson, S., S. Mecking and J. Abell (2001): The biological pump in the subtropical North Pacific Ocean: Nutrient sources, Redfield ratios, and recent changes. *Global Biogeochem. Cycles*, **15**(3), 535–554.

Eppley, R. W. and B. J. Peterson (1979): Particulate organic matter flux and planktonic new production in the deep ocean. *Nature*, **282**, 677–680.

Falkowski, P. G., R. T. Barber and V. Smetacek (1998): Biogeochemical controls and feedbacks on ocean primary production. *Science*, **281**, 200–206.

Fasham, M. J. R., J. L. Sarmiento, R. D. Slater, H. J. M. Ducklow and R. Williams (1993): Ecosystem behavior at Bermuda Station S and ocean weather station 'India': a general circulation model and observational analysis. *Global Biogeochem. Cycles*, **7**, 379–415.

Field, C. B., M. J. Behrenfeld, J. T. Randerson and P. Falkowski (1998): Primary production of the biosphere: integrating terrestrial and oceanic components. *Science*, **281**, 237–240.

Francois, R., S. Honjo, R. Krishfield and S. J. Manganini (2002a): Running the gauntlet in the twilight zone: The effect of midwater processes on the biological pump. *U.S. JGOFS News Lett.*, **11**(4), 4–6.

Francois, R., S. Honjo, R. Krishfield and S. J. Manganini (2002b): Factors controlling the flux of organic carbon to the bathypelagic zone of the ocean. *Global Biogeochem. Cycles*, **16**(4), 10.1029/2001GB001722.

Goes, J. I., T. Saino, H. Oaku, J. Ishizaka, C.-S. Wong and Y. Nojiri (2000): Basin scale estimates of sea surface nitrate and new production from remotely sensed surface temperature and chlorophyll. *Geophys. Res. Lett.*, **27**(9), 1263–1266.

Hama, T., T. Miyazaki, Y. Oguri, T. Iwakuma, M. Takahashi, A. Otsuki and S. Ichimura (1983): Measurement of photosynthetic production of a marine phytoplankton population using a stable ^{13}C isotopes. *Mar. Biol.*, **73**, 31–36.

Hansell, D. A. and C. A. Carlson (2001): Marine dissolved organic matter and the carbon cycle. *Oceanography*, **14**(4), 41–49.

Harada, K., H. Narita and Y. Shibamoto (2001): The export carbon flux estimated by ^{234}Th in the KNOT project. In *Extended Abstract of Oceanographic Society of Japan 2001 Spring Meeting*, p. 356 (in Japanese).

Harrison, P. L. (2002): Station Papa time series: insights into ecosystem dynamics. *J. Oceanogr.*, **58**, 259–264.

Honda, M. C. (2001): The study of carbon cycle in the western North Pacific by measurement of radiocarbon and sediment trap experiment. Ph.D. Thesis, Hokkaido University, 193 pp. (in Japanese).

Honda, M. C., M. Kusakabe, S. Nakabayashi, S. J. Manganini and S. Honjo (1997): Change in pCO_2 through biological activity in the marginal seas of the Western North Pacific: The efficiency of the biological pump estimated by a sediment trap experiment. *J. Oceanogr.*, **53**, 645–662.

Honda, M. C., K. Imai, Y. Nojiri, F. Hoshi, T. Sugawara and M. Kusakabe (2002): The biological pump in the northwestern North Pacific based on fluxes and major component of particulate matter obtained by sediment trap experiments (1997–2000). *Deep-Sea Res. II*, **49**, 5595–5626.

Honjo, S. (1996): Fluxes of particles to the interior of the open ocean. p. 91–154. In *Particle Flux in the Ocean*, ed. by V. Ittekkot, P. Schafer, S. Honjo and P. J. Depetris, SCOPE 57, John Wiley & Sons, New York.

Honjo, S. and S. J. Manganini (1993): Annual biogenic particle fluxes to the interior of the North Atlantic Ocean: Studied at 34°N21°W and 48°N21°W. *Deep-Sea Res.*, **40**, 587–607.

Honjo, S., J. Dymond, R. Collier and S. J. Manganini (1995): Export production of particles to the interior of the equatorial Pacific Ocean during the 1992 EqPac experiment. *Deep-Sea Res.*, **42**, 831–870.

Hunt, G. L., Jr., C. L. Baduini, R. D. Brodeur, K. O. Coyle, N. B. Kachel, S. A. Salo, J. D. Shumacher, P. J. Stabeno, D. A. Stockwell, T. E. Whitledge and S. I. Zeeman (1999): The Bering Sea in 1998: The second consecutive year of extreme weather-forced anomalies. *EOS*, **80**, #47, 561–566.

Imai, K., Y. Nojiri, N. Tsurushima and T. Saino (2002): Time-series of seasonal variation of primary productivity of station KNOT (44°N, 155°E) in the sub-arctic western North Pacific. *Deep-Sea Res. II*, **49**, 5395–5408.

IPCC (1995): Climate change 1994. *Radiative Forcing of Climate Change and an Evaluation of the IPCC IS92 Emission Scenarios*, Cambridge University Press, 339 pp.

Jickells, T. D., P. P. Newton, P. King, R. S. Lampitt and C. Boutle (1996): A comparison of sediment trap records of particle fluxes from 19 to 48°N in the north east Atlantic and their relation to surface water productivity. *Deep-Sea Res.*, **43**, 971–986.

Kameda, T. and J. Ishizaka (1999): The application of algorithm for the estimation of the primary production with satellite data to the ocean around Japan. In *Extended Abstract of Oceanographic Society of Japan 1999 Fall Meeting*, p. 252 (in Japanese).

Kameda, T. and J. Ishizaka (2000): The application of algorithm for the estimation of the primary production with satellite data to the ocean around Japan. In *Extended Abstract of Oceanographic Society of Japan 2000 Spring Meeting*, p. 346 (in Japanese).

Kano, K. (1990): Relation between increase of coral and at-

mospheric carbon dioxide concentration. *Umi to Sora*, **65**, 259–265 (in Japanese).

Karl, D. M., J. R. Christian, J. E. Dore, D. V. Hebel, R. M. Letelier, L. M. Tupas and C. D. Einn (1996): Seasonal and interannual variability in primary production and particle flux at station ALOHA. *Deep-Sea Res.*, **43**, 539–568.

Karl, D. M., J. E. Dore, R. Lukas, A. Michaels, N. R. Bates and A. Knap (2001): Building the long-term picture: The U.S. JGOFS time-series programs. *Oceanography*, **14**(4), 6–17.

Kawahata, H., M. Yamamuro and H. Ohta (1998): Sinking particles between the equatorial and subarctic regions (0°N–46°N) in the Central Pacific. *Geochem. J.*, **32**, 125–133.

Kawahata, H., A. Suzuki and H. Ohta (2000): Export fluxes in the western Pacific warm pool. *Deep-Sea Res. I*, **47**, 2061–2091.

Kemp, A. E. S., J. Pike, R. B. Pearce and C. B. Lange (2000): The "Fall dump"—a new perspective on the role of a "shade flora" in the annual cycle of diatom production and export flux. *Deep-Sea Res. II*, **47**, 2129–2154.

Knox, F. and M. McElroy (1984): Changes in atmospheric CO_2 content in the last 120,000 years: The phosphate extraction model. *J. Geophys. Res.*, **89**, 6027–6038.

Koblents-Mishke, O. I., V. V. Volkovinsky and Yu. G. Kabanova (1970): Plankton primary production of the world ocean. p. 183–193. In *Scientific Exploration of the South Pacific*, ed. by W. Wooster, National Academy of Sciences, Washington, D.C.

Lampitt, R. S. and A. N. Antia (1997): Particle flux in deep seas: regional characteristics and temporal variability. *Deep-Sea Res.*, **44**, 1377–1403.

Launchi, F. and R. G. Najjar (2000): A global monthly climatology of phosphate, nitrate, and silicate in the upper ocean: Spring-summer export production and shallow remineralization. *Global Biogeochem. Cycles*, **14**, 957–977.

Laws, E. A., P. G. Falkowski, W. O. Smith, Jr., H. Ducklow and J. J. McCarthy (2000): Temperature effects on export production in the open ocean. *Global Biogeochem. Cycles*, **14**(4), 1231–1246.

Lee, C., D. W. Murray, R. T. Barber, K. O. Buesseler, J. Dymond, J. I. Hedges, S. Honjo, S. J. Manganini, J. Marra, C. Moser, M. L. Peterson, W. L. Prell and S. G. Wekeham (1998): Particulate organic carbon fluxes: compilation of results from the 1995 US JGOFS Arabian Sea Process Study. *Deep-Sea Res.*, **45**, 2489–2501.

Lohrenz, S. E., G. A. Knauer, D. M. Karl and W. W. Broenkow (1987): VERTEX: carbon cycling in the northwestern Sargasso Sea: U.S. JGOFS Bermuda Atlantic Time-series Study. *Deep-Sea Res.*, **39**, 1373–1391.

Lohrenz, S. E., G. A. Knauer, V. L. Asper, M. Tuel, A. F. Michaels and A. H. Knap (1992): Seasonal variability in primary production and particle flux in the northwestern Sargasso Sea: U.S. JGOFS Bermuda Atlantic Time-series Study. *Deep-Sea Res.*, **39**, 1373–1391.

Longhurst, A., S. Sathyendranath, T. Platt and C. Caverhill (1995): An estimate of global primary production in the ocean satellite radiometer data. *J. Plankton Res.*, **17**(6), 1245–1271.

Lutz, M., R. Dunber and K. Caldeira (2002): Regional variability in the vertical flux of particulate organic carbon in the ocean interior. *Global Biogeochem. Cycles*, **16**(3), 10.1029/2000GB001383.

Maita, Y. and T. Odate (1988): Seasonal changes in size fractionated primary production and nutrient concentrations in the temperate neritic water of Funka Bay, Japan. *J. Oceanogr. Soc. Japan*, **44**, 268–279.

Martin, J. H., G. A. Knauer, D. M. Karl and W. W. Broenkow (1987): VERTEX: carbon cycling in the northeastern Pacific. *Deep-Sea Res.*, **34**, 267–285.

Michaels, A. F., A. H. Knap, R. L. Dow, K. Gundersen, R. J. Johnson, J. Sorensen, A. Close, G. A. Knauer, S. E. Lohrents, V. A. Asper, M. Tuel and R. Bidigare (1994): Seasonal patterns of ocean biogeochemistry at the U.S. JGOFS Bermuda Atlantic Time-Series Study Site. *Deep-Sea Res.*, **41**, 1013–1038.

Midorikawa, T., T. Umeda, N. Hiraishi, K. Ogawa, K. Nemoto, N. Kudo and M. Ishii (2002): Estimation of seasonal net community production and air-sea CO_2 flux based on the carbon budget above the temperature minimum layer in the western subarctic North Pacific. *Deep-Sea Res. I*, **49**, 339–362.

Minas, H. J., M. Minas and T. T. Packard (1986): Production in upwelling areas deduced from hydrographic and chemical fields. *Limnol. Oceanogr.*, **31**, 1182–1206.

Morel, A. (1991): Light and marine photosynthesis: A spectral model with geochemical and climatological implications. *Prog. Oceanogr.*, **26**, 263–306.

Muller-Karger, F., R. Varela, R. Thunell, M. Scranton, R. Bohrer, G. Taylor, J. Capelo, Y. Astor, E. Tappa, T.-Y. Ho and J. J. Walsh (2001): Annual cycle of primary production in the Cariaco Basin: Response to upwelling and implications for vertical export. *J. Geophys. Res.*, **106**, 4527–4542.

Murata, A. and T. Takizawa (2002): Impact of a coccolithophorid bloom on the CO_2 system in surface waters of the eastern Bering Sea Shelf. *Geophys. Res. Lett.*, **29**, 10.1029/2001GL013906.

Najjar, R. G., J. L. Sarmiento and J. R. Toggweiler (1992): Downwards transport and fate of organic matter in the ocean: simulations with a general circulation model. *Global Biogeochem. Cycles*, **6**, 45–76.

Noriki, S. and S. Tsunogai (1986): Particulate fluxes and major components of settling particles from sediment trap experiments in the Pacific Ocean. *Deep-Sea Res.*, **33**, 603–912.

Ono, T., K. Tadokoro, T. Midorikawa, J. Nishioka and T. Saino (2002): Multi-decadal decrease of net community production in western subarctic North Pacific. *Geophys. Res. Lett.*, **29**, 10.10291/2001GL014332.

Ostermann, D. (2001): Iceland Sea Carbonate flux increases dramatically. *Woods Hole Oceanographic Institution 2001 Annual Report*, 17–18.

Pace, M. L. G., A. Knauer, D. M. Karl and J. H. Martin (1987): Primary production and vertical flux in the eastern Pacific Ocean. *Nature*, **325**, 803–804.

Palmer, J. R. and I. J. Totterdell (2001): Production and export in a global ocean ecosystem model. *Deep-Sea Res.*, **48**, 1169–1198.

Parsons, T. R. and C. M. Lalli (1988): Comparative oceanic ecology of plankton communities of the subarctic Atlantic and Pacific Ocean. *Oceanogr. Mar. Biol. Ann. Rev.*, **26**, 317–

359.
Pilskaln, C. H., J. B. Paduan, F. P. Chavez, R. Y. Anderson and R. Y. Berelson (1996): Carbon export and regeneration in the coastal upwelling system of Monterey Bay, central California. *J. Mar. Res*., **54**, 1149–1178.
Platt, T., C. Caverhill and S. Sathyendranath (1991): Basin-scale estimates of oceanic primary production by remote sensing: The North Atlantic. *J. Geophys. Res*., **96**, 15147–15159.
Sambrotto, R. N. and C. J. Lorenzen (1987): Phytoplankton and primary production. p. 249–282. In *The Gulf of Alaska: Physical Environment and Biological Resources*, ed. by D. W. Hood and S. T. Zimmerman, Ocean Assessments Division, Alaska Office, NOAA, US Minerals Management Service, OCS study, MMS86B0095.
Sarmiento, J. L. and J. R. Toggweiler (1984): A new model for the oceans in determining atmospheric pCO_2. *Nature*, **308**, 621–624.
Sarmiento, J. L., J. Dunne, A. Gnanadesikan, R. M. Key, K. Matsumoto and R. Slater (2002): A new estimate of the $CaCO_3$ to organic carbon export ratio. *Global Biogeochem. Cycles*. **16**, 10.1029/2002GB001919.
Sasaoka, K., S. Saitoh, I. Asanuma, K. Imai, M. C. Honda, Y. Nojiri and T. Saino (2002): Temporal and spatial variability of chlorophyll *a* in the western sub-arctic Pacific determined from satellite and ship observations during 1997–1999. *Deep-Sea Res. II*, **49**, 5557–5576.
Schlitzer, R. (2002): Export and sequestration of particulate organic carbon in the North Pacific from inverse modeling. *Abstract of Workshop on Synthesis of JGOFS North Pacific Process Study in SCOR/JOS International Symposium: Our Oceanography toward World Oceanography; Sessions B1 and B2*, p. 21.
Schluter, M., E. J. Sauter, A. Schafer and W. Ritzrau (2000): Spatial budget of organic carbon flux to the seafloor of the northern North Atlantic (60°N–80°N). *Global Biogeochem. Cycles*, **14**(1), 329–340.
Shiomoto, A. (2000a): Efficiency of water-column light utilization in the subarctic north western Pacific. *Limnol. Oceanogr*., **45**(4), 982–987.
Shiomoto, A. (2000b): Chlorophyll-a and primary production during spring in the oceanic region of the Oyashio water, the north-western Pacific. *J. Mar. Biol. Assoc. U.K*., **80**, 343–354.
Shiomoto, A., Y. Ishida, M. Tamaki and Y. Yamanaka (1998): Primary production and chlorophyll-a in the northwestern Pacific Ocean in summer. *J. Geophys. Res*., **103**, 24651–24661.
Siegenthaler, U. and T. Wenk (1984): Rapid atmospheric CO_2 variations and ocean circulation. *Nature*, **308**, 624–626.
Six, K. D. and E. Maier-Reimer (1996): Effects of plankton dynamics on seasonal carbon fluxes in an ocean general circulation model. *Global Biogeochem. Cycles*, **10**, 559–583.
Smetacek, V. (2000): The giant diatom dump. *Nature*, **406**, 574–575.
Suess, E. (1980): Particle organic carbon flux in the oceans-surface productivity and oxygen utilization. *Nature*, **288**, 260–263.
Sundquist, E. T. (1985): Geological perspectives on carbon dioxide and the carbon cycle. p. 5–59. In *The Carbon Cycle and Atmospheric CO_2: Natural Variations Archean to Present*, ed. by E. T. Sundquist and W. S. Broecker, AGU Geophysical Monograph 32, Washington, D.C.
Taguchi, K., H. Takenakajima, A. Tanimura and T. Masuzawa (2002): The vertical profile in ^{234}Th at the station in the Shikoku Basin. In *The Extended Abstract of Oceanographic Society of Japan 2002 Spring Meeting*, p. 231 (in Japanese).
Takahashi, T., R. H. Wanninkof, R. A. Feely, R. F. Weiss, D. W. Chipman, N. Bates, J. Olafsson, C. Sabine and S. C. Sutherland (1999): Net sea-air CO_2 flux over global oceans: An improved estimate based on the sea-air pCO_2 difference. *Proceeding of the 2nd International Symposium on CO_2 in the Oceans*, 9–15.
Takahashi, T., S. C. Sutherland, C. Sweeney, A. Poisson, N. Metzl, B. Tilbrook, N. Bates, R. Wanninkhof, R. A. Feely, C. Sabine, J. Olafsson and Y. Nojiri (2002): Global sea-air CO_2 flux based on climatological surface ocean pCO_2, and seasonal biological and temperature effects. *Deep-Sea Res. II*, **49**, 1601–1622.
Taniguchi, A. (1999): Differences in the structure of the lower trophic levels of pelagic ecosystems in the eastern and western subarctic Pacific. *Prog. Oceanogr*., **43**, 289–315.
Taniguchi, A. and T. Kawamura (1972): Primary production in the Oyashio region with special reference to the subsurface chlorophyll maximum layer and phytoplankton-zooplankton relationship. p. 231–243. In *Biological Oceanography of the Northern North Pacific Ocean*, ed. by A. Y. Takenouchi, Idemitsu shoten, Tokyo.
Thingstad, T. F., A. Hagsrom and F. Rassoulzadegan (1997): Accumulation of degradable DOC in surface waters: Is it caused by a malfunctioning microbial loop? *Limnol. Oceanogr*., **42**, 398–404.
Thunell, R. C. (1998): Particle fluxes in a coastal upwelling zone: sediment trap results from Santa Barbara Basin. *Deep-Sea Res*., **45**, 1863–1884.
Thunell, R. C., R. Varela, M. Llano, J. Collister, F. Muller-Karger and R. Bohrer (2000): Organic carbon fluxes, degradation, and accumulation in an anoxic basin: Sediment trap results from Cariaco Basin. *Limnol. Oceanogr*., **45**(2), 300–308.
Treguer, P. and R. F. Anderson (2002): SOSG Workshop reviews progress toward synthesis of southern ocean results. *U.S. JGOFS News Lett*., **11**(4), 13–14.
Tsuda, A. and S. Takeda (2002): Subarctic Pacific iron experiment for ecosystem dynamics study (SEEDS) in the western North Pacific, summer 2001. *Pices Press*, **10**(1), 12–13.
Tsuda, A., H. Kasai and H. Saito (2002): Seasonal variability of nutrients, chrolophyll and new production in the Oyashio time-series observation. In *Extended Abstract of Oceanographic Society of Japan 2002 Spring Meeting*, p. 350 (in Japanese).
Tsunogai, S. and S. Noriki (1987): Organic matter fluxes and the sites of oxygen consumption in deep water. *Deep-Sea Res*., **34**(5/6), 755–767.
Tsunogai, S. and S. Noriki (1991): Particulate fluxes of carbonate and organic carbon in the ocean. Is the marine biological activity working as a sink of the atmospheric car-

bon? *Tellus*, **43B**, 256–266.

Tsunogai, S., M. Kusakabe, H. Isumi, I. Koike and A. Hattori (1979): Hydrographic features of the deep water of the Bering Sea-The Sea of Silica. *Deep-Sea Res*., **26**, 641–659.

Tsunogai, S., S. Noriki, K. Harada and K. Tate (1990): Vertical change index for the particulate transport of chemical and isotopic components in the ocean. *Geochem. J*., **24**, 229–244.

U.S. GOFS Working Group (1989): Sediment trap technology and sampling. U.S. GOFS Planning Report (10), 94 pp.

Watanabe, Y. W., H. Ishida, T. Ono, T. Nakano, N. Nagai and F. Nishibori (2002): The possibility of decrease of formation of water mass in the North Pacific by using chemical data. In *Extended Abstract of Oceanographic Society of Japan 2002 Spring Meeting*, p. 347 (in Japanese).

Welschmeyer, N. A., S. Storm, R. Goericke, G. Ditullio, M. Belvin and W. Peterson (1993): Primary production in the subarctic Pacific Ocean: Project SUPER. *Prog. Oceanogr*., **32**, 101–135.

Williams, P. J. L. (1995): Evidence for the seasonal accumulation of carbon-rich dissolved organic material, its scale in comparison with changes in particulate material and the consequential effect on net C/N assimilation rates. *Mar. Chem*., **51**, 17–29.

Wong, C. S., F. A. Whitney, D. W. Crawford, K. Iseki, R. J. Matear, W. K. Johnson, J. S. Page and D. Timothy (1999): Seasonal and interannual variability in particle fluxes of carbon, nitrogen and silicon from time series of sediment traps at Ocean station P, 1982–1993: relationship to changes in subarctic primary productivity. *Deep-Sea Res*., **46**, 2735–2760.

Wong, C. S., N. A. D. Waser, Y. Nojiri, W. K. Johnson, F. A. Whitney, J. S. C. Page and J. Zeng (2002): Seasonal and Interannual variability in the Distribution of surface nutrients and dissolved inorganic carbon in the Northern North Pacific: Influence of El Niño. *J. Oceanogr*., **58**, 227–243.

Yamanaka, Y. and E. Tajika (1996): The role of the vertical fluxes of particulate organic matter and calcite in the oceanic carbon cycle: studies using an ocean biogeochemical general circulation model. *Global Biogeochem. Cycles*, **10**, 361–382.

GEOPHYSICAL RESEARCH LETTERS, VOL. 33, L16603, doi:10.1029/2006GL026466, 2006

Click Here for Full Article

Quick transport of primary produced organic carbon to the ocean interior

M. C. Honda,[1] H. Kawakami,[1] K. Sasaoka,[2] S. Watanabe,[1] and T. Dickey[3]

Received 31 March 2006; revised 15 June 2006; accepted 27 June 2006; published 17 August 2006.

[1] Time-series observations of optical fields in the euphotic layer and particle fluxes at 150 m were made in the western North Pacific for half year of 2005. The ratio of surface photosynthetically available radiation (surface PAR) to in situ quantum irradiance at *ca.* 40 m (in situ QI), as an index of turbidity, began to increase in the middle of April, peaking between the end of June and the middle of July. Seasonal variability in the ratio of spectral irradiance at a wavelength of 555 nm to that at 443 nm ($Ed_{(555)}/Ed_{(443)}$) at 40 m, as an index of chlorophyll abundance, synchronized well with the surface PAR/in situ QI ratio. Organic carbon flux also increased between the end of June and the middle of July and correlated well with optical variability. This result suggests that primary produced carbon in the euphotic layer was quickly transported to the ocean interior. Using the $Ed_{(555)}/Ed_{(443)}$ and an empirical equation from shipboard observations, primary productivity was estimated to be *ca.* 300 mgC m^{-2} day^{-1} on average. Assuming that trapping efficiency was only 20% and organic carbon flux decreased drastically between 100 m and 150m, the export ratio at 100 m was estimated to be *ca.* 30 ± 10%, which is significantly higher than that in other oceans. **Citation:** Honda, M. C., H. Kawakami, K. Sasaoka, S. Watanabe, and T. Dickey (2006), Quick transport of primary produced organic carbon to the ocean interior, *Geophys. Res. Lett.*, *33*, L16603, doi:10.1029/2006GL026466.

1. Introduction

[2] To better understand the oceans' ability to uptake atmospheric CO_2, the downward transport of carbon via the "biological pump" mechanism needs to be quantified [e.g., *Volk and Hoffert*, 1985]. Time-series data collected using sediment trap has been effectively used for this purpose [e.g., *Honjo et al.*, 1999]. However, sediment traps have usually been deployed in the deep sea (>1000 m). Therefore, concern has been expressed about how well deep sediment trap data represents the biological activity in the upper layer. Interestingly, progress in satellite oceanography has enabled us to learn about spatial and temporal variation of biological activity [e.g., *Banse and English*, 1999]. Unfortunately, ocean color data provides only near surface information and the existence of clouds often hampers acquisition of satellite color data, especially for the coastal and high latitude region. Thus, we chose to simultaneously observe and quantify biological activity in the euphotic layer using in situ optical sensors and particle fluxes just below the winter mixed layer with a sediment trap. These concurrent observations have enabled the establishment of linkages and correlations between upper and deeper ocean biological and biogeochemical processes.

2. Experimental Procedure and Methods

[3] A bottom tethered mooring system was deployed at station K2 (47°N, 160°E, water depth 5280 m) in the Western Subarctic Gyre (WSG). The WSG has large seasonal variability in physical, chemical and biological parameters [*Harrison et al.*, 2004]. Seasonal surface water temperature and mixed layer range from *ca.* 1°C and *ca.* 100 m in winter to >10°C and *ca.* 30 m in summer, respectively. In late spring, primary productivity increases with temperature, light intensity and water stratification. Seasonal drawdown of nutrients from late winter to early autumn is larger than that in other oceans. The euphotic layer is relatively constant (*ca.* 50 m) and diatom numerically predominates the phytoplankton assemblage year round. A time-series sediment trap (McLane Mark7G) with 21 collecting cups was installed at 150 m that is *ca.* 50 m below the late winter mixed layer at station K2 (M. C. Honda, unpublished data, 2005). Sampling of settling particles began on 20 March 2005 and ceased on 11 September 2005. The particle collecting interval was 14 days for the first 4 cups and 7 days for the remaining 17 collecting cups. Collected samples were preserved with seawater based buffered 5% formalin. After pretreatment of samples, the concentrations of organic carbon were measured with an elemental analyzer and concentrations of Si, Ca and Al were measured with ICP-AES, and converted to organic materials, opal, $CaCO_3$ and lithogenic materials, respectively following *Honda et al.* [2002]. In order to estimate trapping efficiency, ^{230}Th and ^{232}Th was measured using the α counting method [*Anderson and Fleer*, 1982]. The Bio-optical Long-term Optical Ocean Measuring System (BLOOMS [*Dickey et al.*, 2003]) which consists of a Satlantic Inc. spectral radiometer [OCR-504-ICWS] with data acquisition/storage systems was installed for measurement of downwelling spectral irradiance (Ed) at 4 wavelengths (412, 443, 490, and 555 nm). The depth of BLOOMS measured with a depth sensor (RIGO DP1158) was stable during the experimental period (37.5 ± 2.0 m on average). The optical system was kept free of biofouling by copper shutters [*Manov et al.*, 2004]. The values of Ed at 4 wavelengths were measured every hour during the local daytime period (19:00–7:00 UTC)

[1]Mutsu Institute for Oceanography, Japan Agency for Marine-Earth Science and Technology, Yokosuka, Japan.
[2]Frontier Research Center for Global Change, Japan Agency for Marine-Earth Science and Technology, Yokohama, Japan.
[3]Ocean Physics Laboratory, University of California, Santa Barbara, Goleta, California, USA.

Copyright 2006 by the American Geophysical Union.
0094-8276/06/2006GL026466$05.00

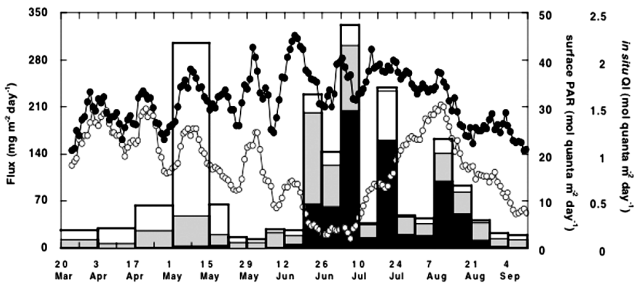

Figure 1. Sinking particles fluxes (bar graphs), and 7 days running mean of surface PAR (closed circles) based on optical data from SeaWiFS and in situ quantum irradiance spectra (QI: open circles). White, stripe, gray and black bars are fluxes of carbonate, lithogenic materials, organic materials, and biogenic opal, respectively.

from 20 March 2005 to 20 September 2005. The daily in situ quantum irradiance spectra (in situ QI) (mol quanta cm^{-2} sec^{-1}) between 412 and 555 nm were calculated from the Ed at 4 wavelengths following *Sorensen and Siegel* [2001].

3. Results

3.1. Fluxes of Settling Particles at 150 m

[4] The first increase of total mass flux (TMF) was observed in early May (Figure 1). The concentration of $CaCO_3$ for particles collected by mid-May was >50%. The main contributor to $CaCO_3$ flux was foraminiferal shell. After late June, TMF increased again with maximum values in early July. Compared to chemical compositions of the early settling particles, biogenic opal (mainly diatom testa) was predominant. Mean TMF was 96 mg m^{-2} day^{-1}. This value seemed too small compared to average TMF observed in the deep sea for the WSG (*ca.* 100 mg m^{-2} day^{-1} at 1000 m [*Honda et al.*, 2002]). Average flux of ^{230}Th was 0.0021 dpm m^{-2} day^{-1} or 0.76 dpm m^{-2} yr^{-1}. Assuming steady state and no effect of laterally transported ^{230}Th, ^{230}Th flux after subtracting authigenic ^{230}Th flux based on ^{232}Th was only 20 ± 7% of the expected ^{230}Th flux at 150 m estimated with ^{234}U concentrations and its decay constant in the upper water column (3.79 dpm m^{-2} yr^{-1}) [*Yu et al.*, 2001]. Although ^{230}Th method for trapping efficiency is usually applied to annual data [*Yu et al.*, 2001] and the above assumption is not always appropriate, it is likely that the trapping efficiency of the 150 m sediment trap was significantly low.

3.2. Relative Intensity of in situ QI

[5] Surface photosynthetically available radiation (PAR) obtained from SeaWiFS optical data generally increased from late March and reached maximum values in June (Figure 1). Surface PAR then tended to decrease. In situ QI at *ca.* 40 m was generally synchronized with surface PAR in April. However in situ QI decreased thereafter as opposed to increases of surface PAR and reached its minimum in late-June to early-July. In situ QI then increased again, peaking in mid-August. The relative decrease of in situ QI between late-April and early-August indicates increase of light attenuation or increase of turbidity in the water column above BLOOMS.

4. Discussion

4.1. Comparison of Optical Signals and Organic Carbon Fluxes

[6] It has been verified that Ed at *ca.* 440 nm is preferentially absorbed by pigments (chlorophyll) of principal phytoplankton as opposed to Ed at *ca.* 550 nm [*Kirk*, 1994]. Thus the ratio of Ed at 555 nm to that at 443 nm ($Ed_{(555)}/Ed_{(443)}$) serves as a good index of Chl-*a* [e.g., *Loisel and Morel*, 1998]. Using BLOOMS data, seasonal variability in the $Ed_{(555)}/Ed_{(443)}$ as proxies for Chl-*a* was evident (Figure 2). The $Ed_{(555)}/Ed_{(443)}$ began to increase in late-April and the maximum values were observed in late-June to early-July. This seasonal pattern correlated well with that of the surface PAR/in situ QI ratio (R = 0.94) and, moreover, that of the SeaWiFS-derived surface Chl-*a* in the vicinity of station K2 (R = 0.78, P < 0.001). This suggests that the increase of turbidity between the late-April and mid-August with maximum in July is likely attributable to increases of phytoplankton. As shown in Figure 2, seasonal variability in organic carbon flux (OCF) follows the same pattern as optical variability: OCF began to increase in late-April and increased more largely between the late-June and August. The correlation coefficient between OCF and the $Ed_{(555)}/Ed_{(443)}$ was found to be statistically significant (R = 0.62, P < 0.005). Based on good synchronization between seasonal patterns of OCF and optical signals, it is concluded that primary produced organic carbon in the euphotic layer was likely quickly transported to the ocean interior with time lag <1 week.

4.2. Estimation of Primary Productivity and Export Ratio

[7] Based on previous observations in the northern North Pacific (Figure 3), integrated Chl- *a* abundance (Chl-$a_{(int)}$) upper 40 m (mg m^{-2}) can be expressed as logarithmic function of the $Ed_{(555)}/Ed_{(443)}$ at 40 m:

$$\text{Chl-}a_{(\text{int})} = 29.89 + 33.375 \times \log\left(\text{Ed}_{(555)}/\text{Ed}_{(443)}\text{ratio}\right) \quad (1)$$

Using the following empirical equation, depth-integrated production in the upper 40 m (PP) can then be determined using equation 1 and daily surface PAR.

$$\text{PP} = \text{Chl-}a_{(\text{int})} \times \text{surface PAR} \times \Psi \quad (2)$$

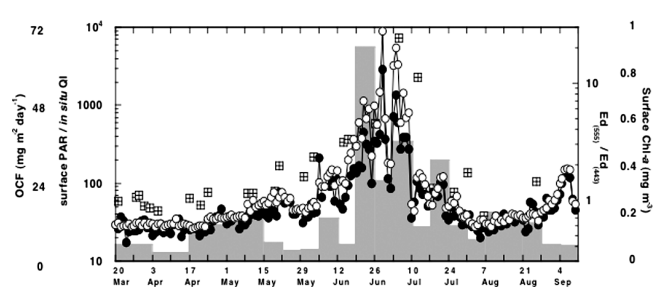

Figure 2. The $Ed_{(555)}/Ed_{(443)}$ (open circles), surface PAR/in situ QI ratios (closed circles), and Organic Carbon Flux (OCF) at 150 m (bar graphs). Squares are SeaWiFS derived surface Chl-*a*.

where Ψ is water column light utilization index [e.g., *Platt et al.*, 1988]. In this study, a constant value of Ψ (0.3 ± 0.1) reported by *Imai et al.* [2002] for the WSG was applied.

[8] Seasonal variability in estimated PP also shows similar pattern of the $Ed_{(555)}/Ed_{(443)}$ and Chl-$a_{(int)}$, resulting good synchronization of OCF (Figure 4). Minimum and maximum of PP were estimated to be *ca.* 50 mgC m^{-2} day^{-1} in late-March and *ca.* 1200 mgC m^{-2} day^{-1} in July, respectively. Mean PP was estimated to be 297 ± 99 mgC m^{-2} day^{-1}. This value was comparable to that observed in the WSG for the corresponding season (270 mgC m^{-2} day^{-1} [*Imai et al.*, 2002]). Figure 4 also shows PP estimated with satellite data and algorithm proposed by *Kameda and Ishizaka* [2005] ($PP_{(KI)}$) based on VGPM algorithm [*Behrenfeld and Falkowski*, 1997]. Though PP estimated in this study tends to be lower than $PP_{(KI)}$ after late-July and other factor such as temperature might be considered in equation 2, both estimates generally coincided well. Thus, the mean export ratio (ratio of mean OCF at 150 m, 13 mgC m^{-2} day^{-1}, to PP) was estimated to be 4 ± 1%. This export ratio was considerably smaller than the annual average of export ratio (*ca.* 45%) estimated using the seasonal amplitude of nutrients (new production) and the observed PP for the WSG [*Honda*, 2003]. However if trapping efficiency of our sediment trap was *ca.* 20% as described before, actual OCF at 150 m should be 5 times larger than the observed OCF, resulting in an export ratio of 22 ± 7%. Further, the export ratio of 45% by *Honda* [2003] was an estimate at 100 m. It has been reported that OCF decreases with depth [*Martin et al.*, 1987]. If decrease of OCF with depth can be formulated as a power function as proposed by them, OCF at 100 m becomes 1.4 times larger than OCF at 150 m. If this is the case, the OCF at 100 m is estimated to be *ca.* 90 mgC m^{-2} day^{-1} and becomes comparable to seasonal new production for the WSG (*ca.* 90 mgC m^{-2} day^{-1} [*Midorikawa et al.*, 2002]). Consequently, the export ratio is estimated to be *ca.* 31 ± 10%. This export ratio is significantly higher than that reported for other oceans (<10% [*Buesseler*, 1998]). Although many uncertainties remain, high export flux and ratio values in the WSG are supported by previous reports: export fluxes and ratios are high in the productive and diatom-dominant areas [*Buesseler*, 1998].

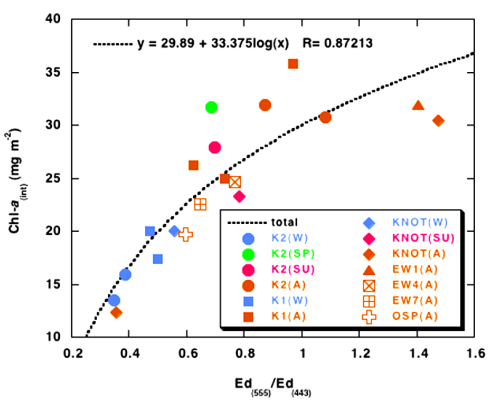

Figure 3. Relation between $Ed_{(555)}/Ed_{(443)}$ at 40 m and integrated Chl-*a* abundances upper 40 m (Chl-$a_{(int)}$). The $Ed_{(555)}/Ed_{(443)}$ were measured at 40 m with underwater optical sensor (Satlantic SeaWiFS Multichannel Radiometer), and Chl-*a* of discrete seawater samples upper 40 m were measured using Turner designs fluorometer aboard ship at various stations and seasons in the northern North Pacific during previous *R/V MIRAI* cruises [*Honda*, unpublished data]. Stations K2, K1, KNOT, EW1, EW4, EW7 and OSP are located at 47°N/160°E, 51°N/165°E, 44°N/155°E, 47°N/169°E, 46°N/175°W, 49–30°N/160°W and 50°N/145°W, respectively. W, SP, SU, and A in parenthesis indicate observation seasons of winter, spring, summer and autumn, respectively. Despite data collected at different locations and seasons, good correlation between $Ed_{(555)}/Ed_{(444)}$ and Chl-$a_{(int)}$ can be seen.

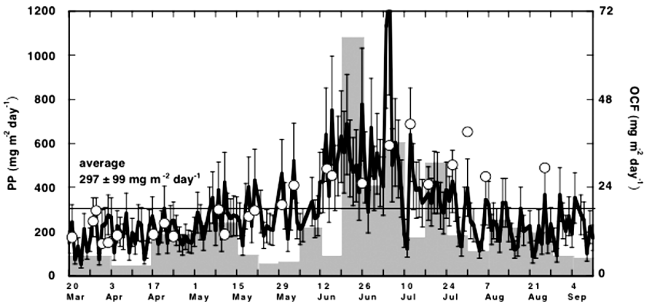

Figure 4. Seasonal variability in primary productivity estimated with the $Ed_{(555)}/Ed_{(443)}$ ratio and empirical equation (see text). Open circles are PP estimated with satellite data and algorithm [*Kameda and Ishizaka*, 2005]. Bar graphs are OCF at 150 m.

5. Concluding Remarks

[9] It was verified that measurement of optical fields in the water column was useful for the estimation of PP as a substitute for satellite data, and there is good evidence of quick transport of organic carbon assimilated in the euphotic layer to the ocean interior (at least to 150 m). For improved quantification, more data need to be accumulated; in particular, at least for one year's worth of data are needed especially for estimation of trapping efficiency. In addition, more precise values of Ψ are needed.

[10] **Acknowledgments.** We thank Susumu Honjo of Woods Hole Oceanographic Institution for promotion of our time-series observations. Derek Manov and Frank Spada of UCSB OPL provided technical support of the optical systems. We acknowledge Hiroaki Sakoh, Kazuhiro Hayashi, Toru Idai of Marine Works Japan and ship crews of *R/V MIRAI* for their efforts on maintenance of instruments, mooring system and mooring work. We appreciate anonymous reviewers for their constructive comments. Financial support for the development of the UCSB OPL optical instrumentation was provided in part by the U.S. National Science Foundation and the U.S. National Ocean Partnership Program.

References

Anderson, R. F., and A. P. Fleer (1982), Determination of natural actinides and plutonium in marine particulate material, *Anal. Chem.*, *54*, 1142–1147.

Banse, K., and D. C. English (1999), Comparing phytoplankton seasonality in the eastern and western Subarctic Pacific and the western Bering Sea, *Prog. Oceanogr.*, *43*, 235–288.

Behrenfeld, M. J., and P. G. Falkowski (1997), Photosynthetic rates derived from satellite-based chlorophyll concentration, *Limnol. Oceanogr.*, *42*(1), 1–20.

Buesseler, K. O. (1998), The decoupling of production and particulate export in the surface ocean, *Global Biogeochem. Cycles*, *12*(2), 297–310.

Dickey, T. D., et al. (2003), New sensors monitor bio-optical/biogeochemical ocean changes, *Sea Technol.*, *44*, 17–24.

Harrison, P. J., et al. (2004), Nutrient and plankton dynamics in the NE and NW gyres of the Subarctic Pacific ocean, *J. Oceanogr.*, *60*, 93–117.

Honda, M. C. (2003), Biological pump in northwestern North Pacific, *J. Oceanogr.*, *59*(5), 671–684.

Honda, M. C., et al. (2002), The biological pump in the northwestern North pacific based on fluxes and major component of particulate matter obtained by sediment trap experiments (1997–2000), *Deep Sea Res., Part II*, *49*, 5595–5625.

Honjo, S., et al. (1999), Monsoon-controlled export fluxes to the interior of the Arabian Sea: U.S. JGOFS 1994–1995 experiment, *Deep Sea Res., Part II*, *46*(8–9), 1859–1902.

Imai, K., et al. (2002), Time series of seasonal variation of primary productivity at station KNOT (44°N, 155°E) in the sub-arctic western North Pacific, *Deep Sea Res., Part II*, *49*, 5395–5408.

Kameda, T., and J. Ishizaka (2005), Size-fractionated primary production estimated by a two-phytoplankton community model applicable to ocean color remote sensing, *J. Oceanogr.*, *61*, 663–672.

Kirk, J. T. O. (1994), *Light and Photosynthesis in Aquatic Ecosystem*, 2nd ed., pp. 305–313, Cambridge Univ. Press, New York.

Loisel, H., and A. Morel (1998), Light scattering and chlorophyll concentration in case 1 water: A reexamination, *Limnol. Oceanogr.*, *43*, 847–858.

Manov, D., et al. (2004), Methods for reducing biofouling on moored optical sensors, *J. Atmos. Oceanic Technol.*, 957–967.

Martin, J. H., et al. (1987), VERTEX: Carbon cycling in the northeast Pacific, *Deep Sea Res., Part A*, *34*, 267–285.

Midorikawa, T., et al. (2002), Estimation of seasonal net community production and air-sea CO_2 flux based on the carbon budget above the temperature minimum layer in the western subarctic North Pacific, *Deep Sea Res., Part I*, *49*, 339–362.

Platt, T., et al. (1988), Ocean primary productivity and available light: Further algorisms for remote sensing, *Deep Sea Res., Part II*, *35*, 855–879.

Sorensen, J. C., and D. A. Siegel (2001), Variability of the effective quantum yield for carbon assimilation in the Sargasso Sea, *Deep-Sea Res., Part II*, *48*, 2005–2035.

Volk, T., and M. I. Hoffert (1985), Ocean carbon pumps: Analysis of relative strengths and efficiencies in ocean-driven atmospheric CO_2 changes, in *The Carbon Cycle and Atmospheric CO_2: Natural Variations Archean to Present*, *Geophys. Monogr. Ser.*, vol. 32, edited by E. Sundquist and W. S. Broecker, pp. 99–110, AGU, Washington, D. C.

Yu, E. F., et al. (2001), Trapping efficiency of bottom tethered sediment traps estimated from the intercepted fluxes of ^{230}Th and ^{231}Pa, *Deep Sea Res., Part I*, *48*, 865–889.

T. Dickey, Ocean Physics Laboratory, University of California, Santa Barbara, 6487 Calle Real, Unit A, Goleta, CA 93117, USA.

M. C. Honda, H. Kawakami, and S. Watanabe, Mutsu Institute for Oceanography, Japan Agency for Marine-Earth Science and Technology, 2-15, Natsushima, Yokosuka, Kanagawa 237-0061, Japan. (hondam@jamstec.go.jp)

K. Sasaoka, Frontier Research Center for Global Change, Japan Agency for Marine-Earth Science and Technology, 3173-25, Showa, Kanazawa, Yokohama 236-0001, Japan.

Accepted to Journal of Oceanography

Draft Version 20061120

Utility of an automatic water sampler to observe seasonal variability in nutrients and DIC in the northwestern North Pacific

By

Makio C. Honda[1] and Shuichi Watanabe[1]

[1]Japan Agency for Marine-Earth Science and Technology

Key words: Time-series observation, mooring system, automatic water sampling, nutrients, biological pump,

Abstract

Concentrations of nutrients (NO_3, NO_2, $Si(OH)_4$, PO_4) and dissolved inorganic carbon (DIC) were measured in time-series seawater samples collected by automatic water sampler (Remote Access Sampler, RAS) in the Northwestern North Pacific for approximately 15 months in 2005 and 2006. Seasonal variability and concentrations of NO_3 + NO_2 (NO_x) and $Si(OH)_4$ were comparable to previous shipboard observations although there were small errors associated with measurements of PO_4 and DIC. Concentrations of these nutrients began to decrease in late April. After the end of June, NO_x and $Si(OH)_4$ decreased rapidly, with large fluctuations. After October, these nutrients increased again until late spring 2006. The ratio of the decrease of $Si(OH)_4$ to that of NO_x suggested that numbers of biogenic opal-producing creatures such as diatoms increased after the end of June. This conclusion was supported by a rapid increase in biogenic opal flux recorded in a sediment trap at 150 m. The relationship between NO_x concentrations at the RAS depth of 35 m and NO_x integrated over the upper 100 m was determined using previous shipboard hydrocast data. This relationship was used to estimate integrated mixed layer NO_x from RAS data. Estimated new production based on seasonal drawdown of integrated NO_x averaged approximately 156 mg-C m^{-2} day^{-1} annually and agreed with previous estimates. Thus, an automatic seawater sampler that documents annual maximum and minimum nutrient concentrations and episodic events such as storms and spring blooms, which might be missed by ordinary research vessel, will contribute to time-series observations of nutrients and, by extension, biological pump activity.

1. Introduction

Biological activity in the ocean plays an important role in the uptake of atmospheric CO_2, which is being increased by anthropogenic activity. The processes of assimilation (primary production), calcification, and transport of carbon to the ocean interior are referred to as the biological pump (Volk and Hoffert, 1985; Sarmiento and LeQuere, 1996; Falkowski *et al*., 1998; Sigman and Boyle, 2000). This mechanism is influenced by ambient physical, chemical, and biological conditions. Recently, changes in the biological pump from global warming and its positive or negative feedback to global warming have been of great concern (e.g., Heinze, 2004; Orr *et al*., 2005). However, these changes can be detected only by long-term observations. Therefore it is apparent that time-series observations are necessary and much effort has been expended to conduct time-series observations in the world ocean, for example, in the subtropical Pacific (Station ALOHA; Karl *et al*., 1996; 2001), the middle Atlantic (Station BATS; Dickey *et al*., 2001) and the Eastern North Pacific (Station OSP; Harrison *et al*., 1999; 2004).

Based on these time-series studies, frequent observations (at least monthly) are required for a

better understanding of its role in the uptake of atmospheric CO_2. However, conducting high frequency observations, especially during the winter season in high latitudes, is difficult with ordinary research vessels. Observations using automatic samplers or automatic sensors on mooring systems have allowed time-series observations for seasonal variability in the biogeochemistry with high sampling frequency (*e.g.*, Dickey *et al.*, 1998). As a result, episodic events such as sudden increases of biological pump activity caused by meteorological disturbances and the spring bloom have been observed.

The time-series sediment trap has been one of the more effective samplers for the time-series study of the biological pump (e.g., Honjo, 1996; Conte *et al.,* 2001; 2003). However, sediment traps have usually been deployed in the deep ocean (below 1000 m) to avoid biological and hydrodynamic disturbances, and there is concern about how well deep sediment trap data reflect biological activity in the upper ocean layer and the behavior of sinking particles in the mesopelagic layer or "twilight zone." Recently, remote sensing technology for oceanography (satellite oceanography) has advanced and large-scale time-series observation has become possible (Banse and English, 1999; Campbell *et al.,* 2002; Behrenfeld *et al.,* 2005; Dickey *et al.,* 2006). However, remote sensing provides data primarily about physical conditions and biological activity near the sea surface. In addition, the existence of clouds often hampers acquisition of satellite ocean color data, especially for coastal and high-latitude regions. To clarify how much carbon is assimilated in the upper ocean and transported to the ocean interior, time-series observations in the surface euphotic zone or mixed layer are required.

Since 2001, we have been conducting time-series observations in the Western North Pacific using a mooring system (Fig. 1a). This mooring system consists of automatic samplers such as sediment traps (between the subsurface layer and the deep ocean), phytoplankton and zooplankton samplers and an optical sensor (in the euphotic layer; <50 m). An automatic water sampler called a Remote Access Sampler (RAS) has also been installed on the mooring system to collect seawater samples for measurements of nutrients and dissolved inorganic carbon (DIC), which are good indicators of biological pump. Although automatic water sampling systems have been developed before (*e.g.*, Bell *et al.*, 2002), there have been few reports that document time-series observations of nutrients and DIC in the pelagic ocean. In this study, preliminary results of seasonal variability in nutrients and DIC observed by our automatic water sampler are presented and the potential of the automatic sampler for the study of the biological pump is introduced.

2. Materials and Methods

2.1 Description of the study area

A bottom-tethered mooring system was deployed at station K2 (47°N, 160°E, water depth 5280 m). Its position was selected after the geographic bottom survey with a multi channel narrow beam echo sounding system (SeaBeam 2112.004) for discovery of flat sea floor within a few miles radius and an altimeter (Datasonics PSA900D) attached below a multiple water sampling system with CTD for determination of precise water depth. Details about geographic survey and mooring work were described elsewhere (Idai et al., 2005; Honda 2005)

Station K2 was located in the North Pacific Western Subarctic Gyre (WSG). The WSG has large seasonal variability in physical, chemical, and biological parameters (reviewed by Harrison *et al.*, 2004). Surface water temperatures range from approximately 1°C in winter to over 10°C in summer and mixed-layer depth (MLD) ranges from a maximum of 150 m in winter to approximately 20 m in summer. In late spring, primary productivity increases with temperature, light intensity, and water stratification. Seasonal drawdown of nutrients and DIC from late winter to early autumn is greater than in other oceans

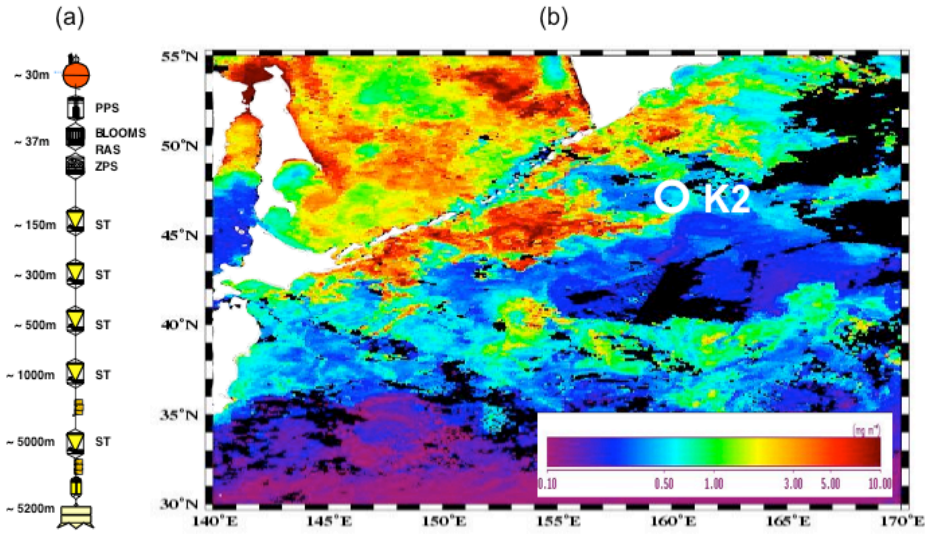

Figure 1 (a) Mooring system. PPS, phytoplankton sampler; BLOOMS, Bio-optical Long-term Optical Ocean Measuring System; RAS, automatic water sampler; ZPS, zooplankton sampler; ST, sediment trap. Data from BLOOMS, PPS, ZPS and ST are not presented in this paper. (b) Location of station K2. Color image shows SeaWiFS Chlorophyll-*a* monthly composite in June 2005 (courtesy of K. Sasaoka, JAMSTEC).

(Tsurushima *et al*., 2002). However nutrients are not depleted even in late summer or early autumn. The euphotic layer is relatively constant, extending to approximately 50 m depth (Imai *et al*., 2002) and diatoms numerically predominate in the phytoplankton assemblage throughout the year (Mochizuki *et al*., 2002).

High biological pump activity is suspected based on large seasonal changes in nutrient concentrations (Launchi and Najjar, 2000) and pCO_2 (Takahashi *et al*., 2002). Station KNOT is a well-known time-series station in the WSG (see special issue of Deep-Sea Research II 49, Nos. 24-25). Between 1998 and 2001, a comprehensive study was conducted at station KNOT (44°N, 155°E) and some unique characteristics were reported, such as large seasonal variability in nutrients and carbonate species (Tsurushima *et al*., 2002) and a high transfer efficiency of organic carbon (Honda *et al*., 2002). However data did not always represent oceanographic conditions in the WSG since station KNOT is located at the southeastern boundary of the WSG and is sometimes influenced by subtropical and coastal water. We set station K2 for succeeding station KNOT. At station K2, time-series observations by both our moored system and by the R/V MIRAI have been conducted since 2001. In addition, a scientific cruise that focused on comparison of the biological pump at station K2 with that at station ALOHA was conducted in 2005 by the VERtical Transport In the Global Ocean (VERTIGO) project group (Buesseler *et al*., 2006; http://cafethorium.whoi.edu/).

2.2 Description of automatic water sampler

We automatically collected time-series water samples using a Remote Access Sampler (RAS; McLane RAS 3-48-500). The RAS uses a pump to draws water out of an acrylic sample container in which a collapsed sample bag is mounted (Fig. 2). This creates a pressure gradient that pushes ambient seawater through the intake and into the inflating sample bag. The 500 ml capacity sample bags are made of 3 laminated layers: a thin exterior Mylar® film for protection, a vacuum-coated aluminum-foil

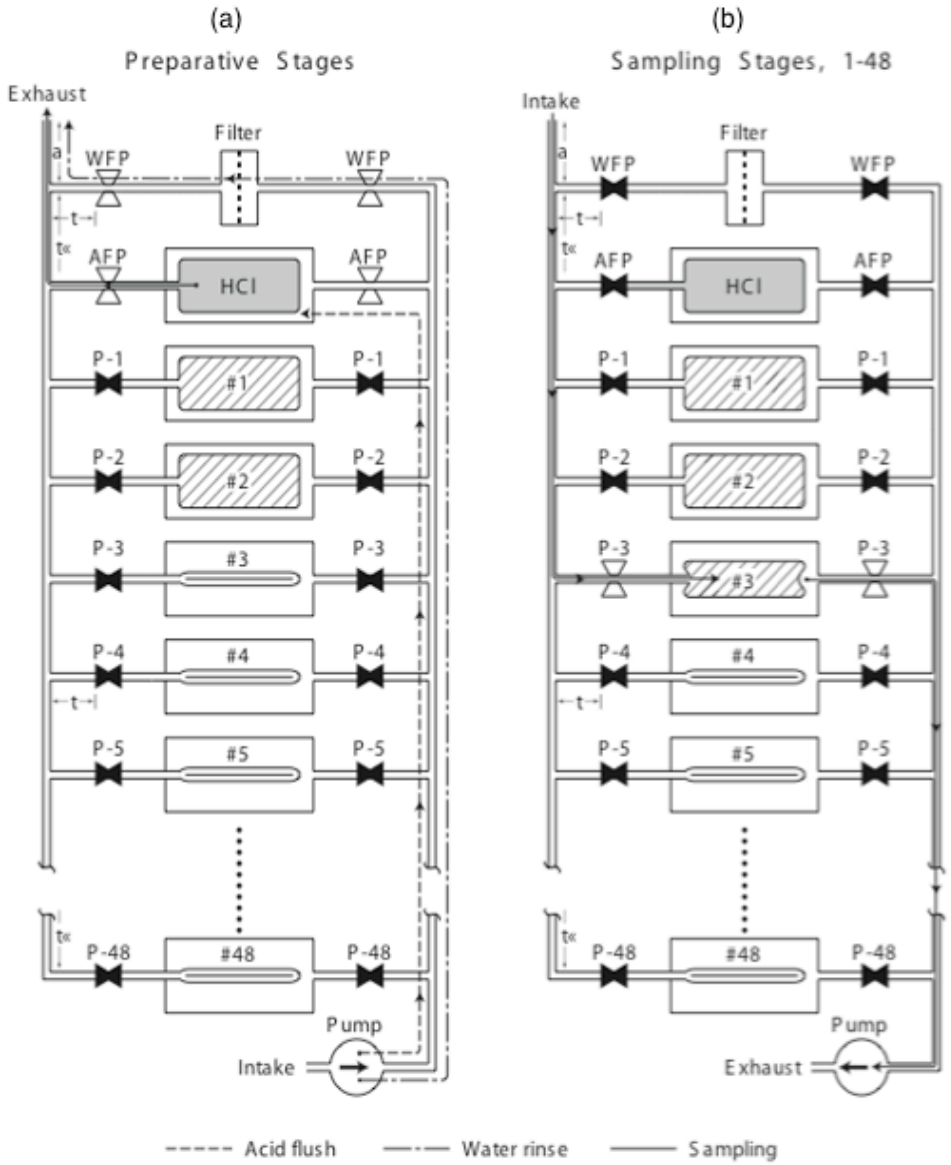

Figure 2. Function diagram of the Remote Access Sampler (RAS) (courtesy of S. Honjo). During the preparative stage ((a) left panel) the RAS executes two functions in order to avoid contamination from biofouling along the intake path "**a**" (upper-left corner). First, through the acid flush path, a pair of AFP (Acid Flush Path) valves opens and a pump applies pressure to a sample bag containing HCl that flushes the intake manifold "**a**" and then closes the AFP valves to isolate the HCl bag. Second, WFP (Water Flush Path) valves open in the water rinse path and filtered *in situ* seawater is pumped to rinse out any remaining HCl from "**a**". WFP valves then close. The RAS is then ready for water sampling through the sampling path ((b) right panel). Microprocessor commands open twin valves of the next empty bag, pre-loaded with a preservative (bag P-3, for example). The pump runs in reverse to generate a lower pressure in the sheath holding the sample bag resulting in the drawing in of *in situ* seawater of programmed volume. The bag is then isolated for preservation by closing valves P-3 until the next programmed cycle that starts with HCl flushing. In an actual RAS, all valves are arranged along two circumferences and virtual manifold "**t**" and "**t<<**" do not exist.

layer for blocking solar radiation and minimizing gas diffusion, and an inner Teflon® film for reinforcement and insulation of sample water from the aluminum-foil layer. Each bag was pre-loaded with an $HgCl_2$ preservative solution (see section 2.3), connected to a distribution valve and placed within a rigid acrylic 600 ml sample bag container, or sheath. Before deployment, the space surrounding the sample bag within each sheath was filled with filtered surface seawater with salinity adjusted to approximately 40 by the addition of NaCl. We employed saline water with higher density rather than pure water with lower density than ambient seawater because there was possibility that exhausted pure water during seawater sampling ascend from the outlet at lower part of RAS (Exhaust in Fig.2 (b)) and contaminate seawater sampled from the inlet at upper part of RAS (Intake in Fig.2 (b)). Each RAS held 49 identical bag assemblages. Of these, 48 were used to sample seawater in a scheduled sequence at programmed event times. The remaining bag was filled with 6 M HCl that was used to flush the seawater intake path before each water sampling event to prevent biofouling. After flushing with HCl, the intake path was flushed with ambient seawater and then seawater samples of approximately 500 ml were collected. Execution records documenting sample timing, estimated sample volume, flushing periods, and electricity consumption were logged by the RAS instruments and retrieved from the memory after recovery.

The mooring system with RAS was deployed and recovered twice during this study; the first deployment from March 2005 to September 2005 (phase I) and the second deployment from October 2005 to May 2006 (phase II). The RAS was initialized to collect *in situ* seawater samples at 4-day intervals from 20 March 2005 to 29 May 2006 (436 days), except between 20 December 2005 and 11 April 2006, when the sampling interval was 8 days. This produced 94 seawater samplings, although several samplings failed because of accidental disconnection of the suction tube or loss of the acrylic sheath with the sample bag.

2.3 Preservation of samples

We used a mercuric chloride ($HgCl_2$) solution as a preservative. Before deployment, 2 ml $HgCl_2$ solution (36,000 ppm; 3.6 g $HgCl_2$ in 100 ml distilled water) was pre-loaded in each sample bag. In a seawater sample of approximately 500 ml, the final concentration of $HgCl_2$ was approximately 140 ppm. This $HgCl_2$ concentration is comparable to that used for long-term preservation of seawater samples for measurements of nutrients (105 ppm; Kattner, 1999) and approximately 15 times higher than that used in the measurement of carbonate species (approximately 10 ppm; DOE, 1994).

During the R/V *MIRAI* cruise MR05-01 in March 2005, we collected seawater samples by RAS and tested the effectiveness of the preservation method for nutrient and DIC samples. We added $HgCl_2$ solution to 500 ml seawater samples, as described above, and measured concentrations of nutrients and DIC when seawater samples were first collected (March 2005), after 6 months (September 2005) and after 15 months (June 2006). Samples were stored in a refrigerator at 4°C between analyses. We found good agreement between all three sets of measurements: within 2% for nutrients and 0.2% for DIC (Table 1). Thus we determined that the chosen concentration of preservative was appropriate for these observations.

2.4 Sampling depth, temperature, and salinity

Depth of the RAS was measured every 120 min during the mooring deployment with a depth sensor (RIGO RMD-500). Water temperature at the RAS depth was deduced by a thermister inside of the RAS electronics pressure housing. This thermister recorded the temperature inside of the RAS housing when seawater sampling started and stopped for each sample. The initial temperature reading should have represented the environmental temperature since at least 4 days would have passed since the

Table 1. Results from test of preservation method for nutrients and DIC in RAS samples. For comparison, ordinal hydrocast data are also shown. All data are normalized to salinity of 33.

		Hydrocast	RAS sampling		
Sampling Date		04-Mar-05	07-Mar-05	07-Mar-05	07-Mar-05
Analysis Date		04-Mar-05	18-Mar-05	04-Oct-05	23-Jun-06
Sample number		2	6	2	2
N-DIC	(μmol kg^{-1})	2120.93 ± 4.88	2129.46 ± 4.89	2120.07 ± 4.89	2123.53 ± 7.15
N-NO_3	(μmol kg^{-1})	23.03 ± 0.12	23.82 ± 0.12	23.72 ± 0.12	23.26 ± 0.10
N-NO_x	(μmol kg^{-1})	23.16 ± 0.12	23.97 ± 0.12	23.89 ± 0.12	23.50 ± 0.10
$Si(OH)_4$	(μmol kg^{-1})	40.86 ± 0.20	41.08 ± 0.20	41.74 ± 0.20	41.13 ± 0.49
PO_4	(μmol kg^{-1})	1.89 ± 0.01	1.90 ± 0.01	1.92 ± 0.01	1.90 ± 0.00

previous sampling, although its accuracy is ± 0.5°C, it cannot detect low temperatures (<2°C) and the temperature usually increased by up to 2–3°C by the end of sampling.

The salinities of RAS samples were measured onboard by an inductively coupled salinometer (AutoLab®: YEO-KAL) after recovery. Based on replicate analysis, measurement error was 0.02 on average.

2.5 Nutrients and DIC

After recovery, each RAS water sample was sub-divided into four aliquots for onboard analysis of DIC, nutrients, salinity, and other biogeochemical constituents (not included in this article).

Nutrient concentrations [(NO_x (NO_2 + NO_3), $Si(OH)_4$ and PO_4] were measured with an onboard continuous flow analytical system (BRAN+LUEBEB TRAACS® 800) following the procedures of Aoyama (2005). The efficiency of the copperized-cadmium reductor (Cu-Cd column) used in nitrate analysis was checked frequently because of accelerated loss of efficiency resulting from $HgCl_2$ in samples.

PO_4 concentrations could not be determined in approximately 20% of the samples (18 out of 89) because of color-dulling of phosphomolybdous acid produced in the molybdenum blue method (Murphy and Riley, 1961).

For DIC analysis, sample water was introduced directly from the sampling bag assemblage into a DIC extraction module with a CO_2 coulometer (Ishii *et al.*, 1998) by applying a gentle N_2-gas pressure to the sheath cavity.

The variabilities (deviations from the mean) in analyses from six replicate RAS samples collected at 6 hour intervals were 0.40, 0.33, 0.002, and 2.9 μmol kg^{-1} for NO_x, $Si(OH)_4$, PO_4, and DIC, respectively. Analytical errors, based on replicate analyses of reference materials were less than 0.09, 0.19, 0.004, and 1.1 μmol kg^{-1} for NO_x, $Si(OH)_4$, PO_4^{3-} (n=10), and DIC (n=27), respectively.

3. Results

The results obtained from RAS samples in this study were validated through comparison with two other sets of data (Figs. 3 and 4). Hydrocast data were collected at 35 m depth at station K2 during the cruises that deployed and recovered the mooring system and RAS. Climatological data from other cruises conducting hydrocasts at station K2 from 2001 to 2006 were also used for comparison (http://www.jamstec.go.jp/mirai/). In addition, the VERTIGO cruise (R/V Roger Revelle) took place during mooring deployment (30 July to 15 August 2005) near station K2 (between 46.1°N and 47.9°N and 158.67°E and 161.32°E) and

Table 2. Depths, *in situ* temperatures, salinities, nutrients and DIC for RAS samples during phase I and phase II. S/N is sample number. Experimental day numbers start with first RAS sampling on 20 March 2005, which was also Julian day (JD) 80. 1 January 2006 is expressed as JD 367 in this study. N.S. and N.D. indicate no sample and no data, respectively.

(Phase I) Deployment date: 17-Mar-05 Recovery date: 22-Sep-05 Position: 47-01N, 159-57E Water depth: 5206m

S/N	Sampling date	Experimental days	Julian Days	RAS depth (m)	Water temp (deg-C)	Salinity	NO_3 (μmol kg^{-1})	NO_2 (μmol kg^{-1})	$Si(OH)_4$ (μmol kg^{-1})	PO_4 (μmol kg^{-1})	DIC (μmol kg^{-1})
1	20-Mar-05	1	80	35.8	2	32.918	24.01	24.20	42.68	1.94	2106.8
2	24-Mar-05	5	84	36.0	2	32.901	23.80	23.99	42.67	1.94	2104.8
3	28-Mar-05	9	88	35.8	2	33.049	24.10	24.29	43.13	1.94	2116.4
4	01-Apr-05	13	92	35.9	2	32.912	24.01	24.21	43.08	1.96	2097.5
5	05-Apr-05	17	96	35.3	2	32.932	24.29	24.49	43.79	1.96	2010.6
6	09-Apr-05	21	100	36.8	2	32.951	24.57	24.78	44.85	2.00	2123.7
7	13-Apr-05	25	104	37.1	2	32.950	24.81	25.01	45.34	2.03	2097.9
8	17-Apr-05	29	108	35.0	2	32.962	24.89	25.11	45.79	2.01	2117.4
9	21-Apr-05	33	112	35.7	2	32.907	24.54	24.79	45.16	2.03	2113.0
10	25-Apr-05	37	116	35.4	2	32.910	23.51	23.77	43.70	1.93	2090.2
11	29-Apr-05	41	120	35.3	2	32.894	23.43	23.71	43.56	1.92	2069.2
12	03-May-05	45	124	35.1	2	32.896	23.12	23.42	43.18	2.00	2070.6
13	07-May-05	49	128	35.5	2	32.900	22.79	23.05	42.55	1.90	2107.3
14	11-May-05	53	132	36.7	3	32.922	22.88	23.15	43.39	1.89	2085.7
15	15-May-05	57	136	35.3	2	32.903	22.91	23.18	43.13	1.91	2062.4
16	19-May-05	61	140	35.1	3	32.927	22.42	22.71	42.29	1.77	2073.1
17	23-May-05	65	144	36.7	3	32.925	21.75	22.02	41.74	1.84	2105.8
18	27-May-05	69	148	35.4	3	32.963	23.23	23.47	45.66	1.93	1935.6
19	31-May-05	73	152	34.6	3	32.905	22.78	23.04	44.38	1.88	2073.7
20	04-Jun-05	77	156	36.1	4	32.887	22.47	22.74	43.93	1.91	2084.4
21	08-Jun-05	81	160	35.7	4	32.893	21.69	21.98	43.05	1.84	2080.5
22	12-Jun-05	85	164	34.8	4	32.880	21.71	21.99	42.88	1.83	2080.5
23	16-Jun-05	89	168	35.3	4	32.878	22.11	22.36	43.93	1.85	2087.9
24	20-Jun-05	93	172	35.3	4	32.915	22.21	22.44	45.09	1.88	2081.3
25	24-Jun-05	97	176	35.6	4	32.921	22.64	22.89	45.58	1.93	2095.7
26	28-Jun-05	101	180	35.7	4	32.896	21.60	21.85	44.48	1.86	2095.0
27	02-Jul-05	105	184	35.2	6	32.883	19.35	19.62	38.41	1.71	2069.1
28	06-Jul-05	109	188	35.8	6	32.860	17.63	17.89	30.33	1.69	2047.5
29	10-Jul-05	113	192	36.1	6	32.863	18.87	19.10	37.95	1.77	2061.2
30	14-Jul-05	117	196	34.6	6	32.859	18.92	19.15	39.50	1.75	2071.2
31	18-Jul-05	121	200	35.4	5	32.853	19.18	19.42	37.58	N.D.	1959.0
32	22-Jul-05	125	204	35.6	6	32.879	19.22	19.54	37.04	N.D.	2065.7
33	26-Jul-05	129	208	35.1	5	32.937	21.66	21.92	42.36	1.97	2081.5
34	30-Jul-05	133	212	34.9	6	32.849	17.06	17.32	30.30	1.77	2052.2
35	03-Aug-05	137	216	34.9	7	32.841	16.26	16.52	26.72	1.66	2057.4
36	07-Aug-05	141	220	35.7	5	N.S.	N.S.	N.S.	N.S.	N.S.	N.S.
37	11-Aug-05	145	224	34.6	4	32.982	19.57	19.85	37.25	1.76	2035.5
38	15-Aug-05	149	228	35.0	5	32.955	19.26	19.50	37.13	N.D.	2049.9
39	19-Aug-05	153	232	35.0	7	32.910	17.37	17.62	28.93	N.D.	2024.3
40	23-Aug-05	157	236	34.6	5	32.965	19.04	19.30	36.36	1.77	2056.7
41	27-Aug-05	161	240	34.8	6	32.849	15.52	15.74	23.13	1.32	1976.7
42	31-Aug-05	165	244	34.8	7	32.887	18.16	18.42	32.12	N.D.	2007.2
43	04-Sep-05	169	248	34.6	7	32.853	16.81	17.07	24.60	1.71	2058.1
44	08-Sep-05	173	252	35.7	8	32.805	14.42	14.67	17.61	1.54	2038.6
45	12-Sep-05	177	256	34.2	11	32.777	13.05	13.25	15.65	N.D.	1967.1
46	16-Sep-05	181	260	34.9	10	N.S.	N.S.	N.S.	N.S.	N.S.	N.S.
47	20-Sep-05	185	264	36.1	10	32.955	12.69	12.91	21.54	1.28	1987.1

Table 2. Continued

(Phase II) Deployment date: 25-Sep-05 Recovery date: 31-May-06 Position: 47-00N, 159-58E Water depth: 5206m

S/N	Sampling date	Experimental days	Julian Days	RAS depth (m)	Water temp (deg-C)	Salinity	NO_3 (μmol kg^{-1})	NO_2 (μmol kg^{-1})	$Si(OH)_4$ (μmol kg^{-1})	PO_4 (μmol kg^{-1})	DIC (μmol kg^{-1})
48	01-Oct-05	196	275	38.70	11	32.855	12.86	13.06	18.30	1.27	2035.7
49	05-Oct-05	200	279	38.45	11	32.772	12.78	12.96	16.45	1.28	2032.2
50	09-Oct-05	204	283	48.80	10	32.707	13.41	13.63	14.23	1.31	2029.9
51	13-Oct-05	208	287	38.35	10	N.S.	N.S.	N.S.	N.S.	N.S.	N.S.
52	17-Oct-05	212	291	41.70	10	32.614	11.90	12.12	14.66	1.22	2025.2
53	21-Oct-05	216	295	37.55	9	32.552	11.21	11.42	14.42	1.17	2020.1
54	25-Oct-05	220	299	41.50	9	32.567	12.25	12.50	16.38	1.25	2029.0
55	29-Oct-05	224	303	44.60	8	32.506	12.47	12.80	17.62	1.27	2028.1
56	02-Nov-05	228	307	43.45	8	32.512	12.65	13.01	17.98	1.33	2026.0
57	06-Nov-05	232	311	39.65	8	32.531	12.89	13.24	18.44	1.31	2028.5
58	10-Nov-05	236	315	38.75	8	32.554	13.19	13.51	17.98	1.32	2028.9
59	14-Nov-05	240	319	52.60	9	32.707	13.90	14.20	18.59	1.37	2037.9
60	18-Nov-05	244	323	38.40	9	32.740	14.25	14.59	18.51	1.38	2040.3
61	22-Nov-05	248	327	45.20	9	32.725	13.96	14.29	18.17	1.36	2031.7
62	26-Nov-05	252	331	49.90	8	32.682	13.84	14.17	18.37	1.37	2034.6
63	30-Nov-05	256	335	42.20	7	N.S.	N.S.	N.S.	N.S.	N.S.	N.S.
64	04-Dec-05	260	339	45.25	6	32.556	14.18	14.46	19.80	N.D.	2023.2
65	08-Dec-05	264	343	41.95	6	32.609	14.84	15.11	20.09	N.D.	2022.9
66	12-Dec-05	268	347	50.05	5	32.625	15.80	16.06	22.91	N.D.	2029.5
67	16-Dec-05	272	351	49.95	6	32.671	15.81	16.08	23.27	1.42	2037.3
68	20-Dec-05	276	355	50.50	5	32.675	16.46	16.71	24.54	1.43	2035.0
69	28-Dec-05	284	363	37.90	4	32.693	17.93	18.14	27.24	1.57	2041.0
70	05-Jan-06	292	371	40.05	4	32.765	19.28	19.47	29.91	1.66	2053.3
71	13-Jan-06	300	379	37.30	3	32.821	20.34	20.53	31.99	1.59	2063.4
72	21-Jan-06	308	387	36.35	3	32.810	19.95	20.12	31.48	1.69	2057.5
73	29-Jan-06	316	395	39.50	3	32.789	21.55	21.75	33.89	N.D.	2053.7
74	06-Feb-06	324	403	35.90	2	32.895	22.14	22.32	36.38	1.80	2078.6
75	14-Feb-06	332	411	36.25	2	32.910	22.47	22.65	37.11	1.84	2075.1
76	22-Feb-06	340	419	35.65	2	32.930	22.97	23.15	38.33	N.D.	2081.6
77	02-Mar-06	348	427	36.60	2	32.919	23.00	23.20	38.63	1.84	2083.9
78	10-Mar-06	356	435	37.80	2	32.923	23.17	23.38	38.18	N.D.	2083.0
79	18-Mar-06	364	443	53.50	2	32.952	24.00	24.22	39.47	N.D.	2088.6
80	26-Mar-06	372	451	38.90	2	32.958	24.24	24.46	40.65	N.D.	2087.5
81	03-Apr-06	380	459	40.25	2	32.944	23.89	24.11	40.80	N.D.	2083.7
82	11-Apr-06	388	467	37.45	2	32.923	24.03	24.23	37.70	N.D.	2072.9
83	15-Apr-06	392	471	38.70	2	32.930	24.13	24.33	36.61	N.D.	2074.1
84	19-Apr-06	396	475	38.00	2	N.S.	N.S.	N.S.	N.S.	N.S.	N.S.
85	23-Apr-06	400	479	36.40	2	32.929	24.17	24.39	40.96	N.D.	2082.5
86	27-Apr-06	404	483	37.05	2	32.921	23.94	24.18	42.10	1.96	2092.2
87	01-May-06	408	487	38.00	2	32.917	23.71	23.96	40.98	1.98	2096.5
88	05-May-06	412	491	35.30	2	32.913	23.67	23.91	41.95	1.95	2088.4
89	09-May-06	416	495	36.10	2	32.934	23.59	23.82	42.19	1.96	2053.9
90	13-May-06	420	499	36.15	3	32.913	23.66	23.91	40.81	N.D.	2072.3
91	17-May-06	424	503	35.60	3	32.908	23.18	23.44	39.81	1.92	2079.8
92	21-May-06	428	507	38.00	3	32.903	23.50	23.74	40.45	N.D.	2068.5
93	25-May-06	432	511	35.30	3	32.874	23.26	23.50	40.76	1.87	2071.9
94	29-May-06	436	515	38.55	3	33.100	22.86	23.10	40.92	1.92	2087.3

were used for comparison (courtesy of K. Buesseler and P. Henderson, Woods Hole Oceanographic Institution).

3.1 Water depth, temperature, and salinity

3.1.1 Water depth

The RAS sampling depth increased slightly from March to September 2005 (Fig. 3a). This might be attributed to a decrease of current velocity resulting in less tilt of the mooring system or more stretching of the mooring wire ropes during deployment. However, the RAS sampling depths were very stable during phase I, with an average of 35.4 ± 0.6 m (mean ± 1σ) and a range from 34.2 to 37.1 m (Table 2). During phase II, RAS depths showed greater variation and ranged from 35.3 to 53.5 m with an average of 40.5 ± 5.0 m (mean ± 1σ). The surface mixed-layer depths (MLD) shown in Fig. 3a were defined with 0.125 criteria, that is a depth with density (sigma theta) of 0.125 higher than that at surface, based on hydrocast and climatological data. The maximum MLD was in March (approximately 140 m) and the minimum was in July (approximately 20 m). Based on seasonal changes in the MLD, we believe that the RAS was located in the mixed layer throughout the year except for the period between mid-June 2005 to late September 2005.

3.1.2 Water temperature

Water temperature at RAS depth (*i.e., in situ* water temperature) was approximately 2°C by early May 2005 (Julian day (JD) 128; Table 2, Fig. 3b). Thereafter, *in situ* water temperatures increased with some fluctuation to the annual maximum of approximately 11°C in September and October 2005. Temperatures then decreased until February 2006 and increased again beginning in May 2006. The seasonal variability of *in situ* temperature observed in this study coincided well with hydrocast and climatological temperature data. Compared to sea surface temperature (SST) around station K2, as observed by the Advanced Very High Resolution Radiometer (AVHRR) sensor aboard satellite NOAA, *in situ* temperature was substantially lower than SST between early June 2005 and late September 2005, while *in situ* temperature generally agreed with SST during other periods. This evidence supports the conclusion that the RAS was located in the surface mixed layer throughout the year except for the period between early June and late September 2005.

3.1.3 Salinity

Salinity values had large fluctuations, but generally tended to be higher during winter and lower in autumn, with trends similar to those evident in hydrocast and climatological salinity data (Fig. 3c). RAS salinities were approximately 0.2 lower than hydrocast and climatological values. This resulted from the dilution of RAS samples by preservative (2 ml $HgCl_2$ solution), and the actual dilution factor depended on the seawater sample volume. If the RAS seawater sample volumes were exactly 500 ml, RAS samples were diluted by 0.4 %. Taking this dilution into account, observed RAS salinity data were corrected (closed circles in Fig. 3c). Corrected salinity generally coincided with hydrocast, climatological, and VERTIGO salinity data, ranging from approximately 32.6 to 33.1. As VERTIGO salinity data with large fluctuation show, salinity is expected to be variable at 35 m at station K2 in summer.

3.2 Nutrients and DIC

The following nutrient and DIC data were normalized to a constant salinity of 33 to correct for the dilution of the RAS seawater sample by the addition of 2 ml preservative, and to eliminate the effects of natural evaporation and precipitation. For comparison, hydrocast, climatological, and VERTIGO data were also normalized to a salinity of 33.

3.2.1 NO_x

We observed maximum NO_x (NO_3 + NO_2) concentrations, normalized to a salinity of 33 (N-NO_x), in the middle of April 2005 (JD 108;

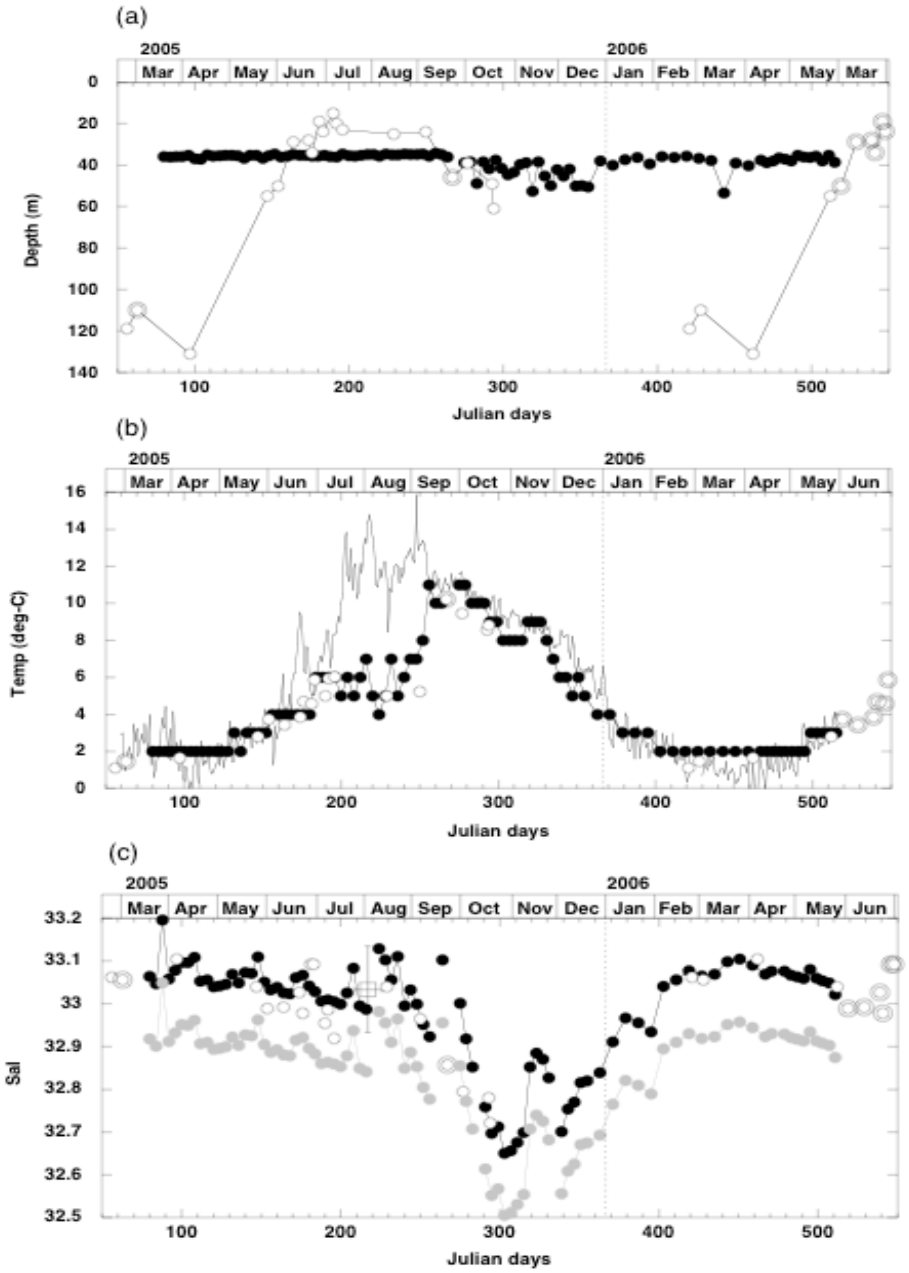

Figure 3. (a) Seasonal variability in RAS sampling depths (closed circles), and the mixed layer depths (MLD) based on hydrocast data (double circles) and climatological data (open circles) (see text). RAS sampling depths are depths when respective seawater samplings were conducted. Horizontal axis is Julian days (JD). JD 1 and JD 367 are 1 January 2005 and 1 January 2006, respectively. (b) Seasonal variability in *in situ* temperature observed by RAS thermister (closed circles), and water temperature at 35 m based on hydrocast data (double circles) and climatological data (open circles) (see text). Solid line indicates Sea Surface Temperature (SST) obtained by satellite (courtesy of K. Sasaoka, JAMSTEC). (c) Seasonal variability in salinity of RAS samples. Gray circles are observed salinities and closed circles are salinities corrected for dilution of RAS sample by mainly preservative. Double circles and open circles show hydrocast and climatological data, respectively. A square with cross is a mean VERTIGO salinity data (see text). Vertical error bar is standard deviation (1s) of VERTIGO salinity data (n = 26) and horizontal error bar is period when VERTIGO data were obtained.

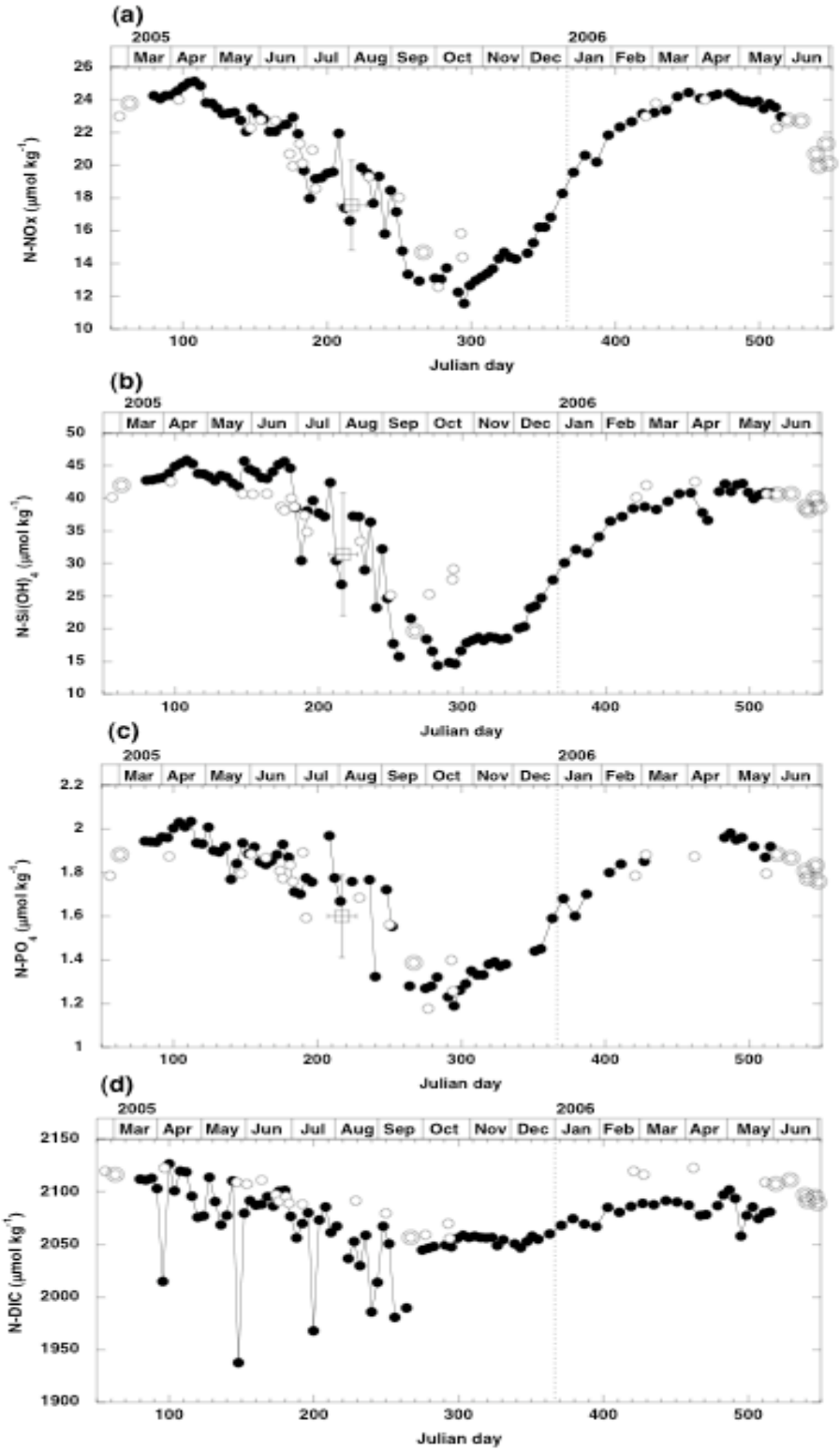

Figure 4. Seasonal variability in (a) NO_x, (b) $Si(OH)_4$, (c) PO_4^{3-}, and (d) DIC. Closed circles, open circles and double circles show observed data from RAS, climatological data and hydrocast data, respectively. A square with cross is VERTIGO data with standard deviation. All data are normalized to a salinity of 33.

Table 2 and Fig. 4a). After that, N-NO_x concentrations decreased. The decrease after the end of June (JD 180) was particularly large and accompanied by large fluctuations. These fluctuations might have occurred because the RAS was located just below the mixed layer where a steep vertical gradient in N-NO_x concentrations resulted in variable RAS nutrient data. The annual minimum N-NO_x was observed in late October 2005 (JD 295). Based on climatological N-NO_x data and previous reports (Wong *et al.*, 2002a, b), this minimum value of approximately 11 μmol kg^{-1} was comparable to the annual minimum value observed in surface water, although the surface water minimum generally appears in summer. Thus, the RAS could have observed the surface nutrient minimum, although the RAS depth was slightly below the mixed layer during July and September. N-NO_x concentrations increased again toward the middle of April 2006 (JD 478). Seasonal variability in N-NO_x was comparable to that of hydrocast and climatological data. In addition, our data from July and August 2005 were comparable to those from the VERTIGO research group in July and August 2005, which also showed large fluctuations in N-NO_x concentrations near station K2 at 35 m depth.

3.2.2 $Si(OH)_4$

Concentrations of normalized $Si(OH)_4$ [N-$Si(OH)_4$] also increased by middle April 2005 and then decreased (Fig. 4b). However, unlike N-NO_x, N-$Si(OH)_4$ maintained high concentrations through the end of June (JD 180) and the annual maximum concentration was observed during this period. After that, N-$Si(OH)_4$ concentrations decreased substantially until the middle of October 2005 (approximate JD 280) with fluctuations similar to N-NO_x. After mid-October 2005, N-$Si(OH)_4$ increased again toward April 2006 (JD 478). Seasonal variability in N-$Si(OH)_4$ coincided with that of hydrocast and climatological data. In addition, N-$Si(OH)_4$ in RAS samples coincided well with VERTIGO N-$Si(OH)_4$ data within its variability.

3.2.3 PO_4

Concentrations of PO_4 could not be determined for approximately 20% of the total samples as described in section 2.5 (see also Discussion section 4.1), but normalized PO_4 (N-PO_4) concentrations from the remaining samples showed the same seasonal patterns as N-NO_x; a decrease from April 2005 to October 2005 with fluctuations and an increase again to April of 2006 (Fig. 4c). Seasonal variability agreed with hydrocast, climatological, and VERTIGO data. The ratio of changes in N-NO_x and N-PO_4^{3-} concentrations ($\Delta N/\Delta P$) was approximately 16, a ratio consistent with the phytoplankton N/P uptake ratio reported previously (Redfield *et al.*, 1963; Anderson and Sarmiento, 1994).

The correlation between salinity and nutrient concentrations was better during phase II than phase I. Correlation coefficients (r) during phase II were 0.90 for NO_x, 0.88 for $Si(OH)_4$, and 0.84 for PO_4. During phase I the coefficients were 0.55 for NO_x, 0.55 for $Si(OH)_4$, and 0.37 for PO_4. These are attributed to that nutrients behaved with non-conservative property unlike salinity during phase I while nutrients behaved with conservative property like salinity during phase II. The decrease in nutrient concentrations from late spring to late summer can be explained by biological activity in the mixed layer, and the nutrient increases from late autumn to late winter resulted from physical processes; *i.e.* the expansion of the mixed layer supplied nutrients from deeper water (>100 m).

3.2.4 DIC

N-DIC also shows a seasonal decrease from April to September 2005 and an increase from October 2005 to April 2006 (Fig. 4d). N-DIC in RAS samples collected in the early parts of phase I (March and April 2005) and phase II (October and November 2006) agreed with hydrocast N-DIC data. However the variation in N-DIC was large during phase I and low N-DIC concentrations (less than 2030 μmol

kg^{-1}) were often observed. Based on climatological data, the annual minimum N-DIC concentration at station K2 is at least 2030 μmol kg^{-1}, and that is usually observed at the near surface in autumn. During phase II, concentrations of N-DIC from RAS samples were consistently lower than climatological data.

4. Discussion

4.1 Low DIC and PO_4 in RAS samples

Observed N-DIC values from RAS samples were substantially lower than climatological N-DIC values, with some exceptions, and in some RAS samples there were problems with measurement of PO_4. Sample storage was probably not the cause, since we had verified that preservation with $HgCl_2$ permitted measurements of nutrients and DIC after long periods of storage (see Section 2.3).

The low DIC values were not accompanied by decreases of N-NO_x and N-$Si(OH)_4$. In the ocean, the biogenic production of $CaCO_3$ and gas exchange with the atmosphere reduces DIC without a decrease in nutrient concentrations. However these are unlikely explanations for the variations observed because the biogenic production of $CaCO_3$ is not predominate in the WSG, and CO_2 exchange should not occur so quickly at the RAS depth (approximately 35 m) as is evident in the sudden decreases of N-DIC (Fig. 4d). In addition, these mechanisms cannot explain the systematic reduction of N-DIC during phase II. Authigenic $CaCO_3$ production in the RAS sampling bag is another possibility, however the degree of supersaturation in seawater is estimated to be at most 2.5 for calcite and 1.5 for aragonite, which is too low for authigenic $CaCO_3$ production.

We attribute the unexpected low N-DIC concentrations to depletion of DIC by CO_2 degassing from the RAS seawater sample, possibly caused by a decrease in pH from the HCl solution used for pre-washing the sampling inlet. Although this HCl solution was subsequently rinsed with ambient seawater before sampling, and sampling started 5 minutes after the HCl flush, some HCl might have remained in the sampling line, or sampled seawater might have been affected by HCl. Another possibility is that degassing occurred after recovery, especially for seawater samples collected during phase II. RAS samples from phase II were kept onboard at room temperature (approximately 15°C) for one month until onboard chemical analysis. Degassing during storage might have taken place although RAS samples were sealed with plastic caps to prevent interaction with the atmosphere. Degassing could have also resulted from reduced pressure after sampling. The RAS system collected seawater samples using a pressure gradient caused by withdrawing water from the acrylic container holding the sample bag. However, if intake rate of seawater sample was slower than exhaust rate of high saline seawater in an acrylic container, the pressure in the sample bag would be higher than that of the surrounding high saline water after valves (e.g. P3 valve at both side in Fig.2 (b)) closed and pump stopped, resulting in degassing within the sample bag until pressure was equalized

Thus, the usefulness of the RAS for collecting seawater samples for DIC measurements is questionable at this time. To improve usefulness in the future, the use of a copper barrier for effective anti-biofouling (Dickey *et al.,* 2003; Manov *et al*., 2004; Honda *et al*., 2006) might be more appropriate than HCl, and DIC measurements should be conducted as soon as possible after sample recovery.

Problems with PO_4 measurements could have been caused by incomplete reduction of phosphomolybdic acid to phosphomolybdous acid (*i.e.* molybdenum blue), by the reducing agent ascorbic acid. Possible interfering substances were $HgCl_2$ and HCl. Eberlein and Kattner (1987) reported that $HgCl_2$ and HCl would cause interference in the total phosphorus measurements because ascorbic acid reacts with free chlorine and is thereby unable to reduce the phosphomolybdic acid. $HgCl_2$ can probably be eliminated as the cause of the problem because

all RAS samples were preserved with $HgCl_2$, but only about 20% had problems with PO_4 analysis, and Kattner (1999), as well as our test of sample preservation, demonstrated that use of $HgCl_2$ is not problematic for PO_4 measurement. Contamination of RAS samples by HCl might affect measurements of PO_4 by changing the pH of the seawater sample. However HCl contamination would also cause lowered DIC measurements, which were not always evident in the problematic samples. Other possible causes, such as the effect of suspended particles or colloidal substances in RAS samples, should be investigated to improve measurements of PO_4 concentrations.

4.2 Application of RAS data to oceanography

4.2.1 The ratio of changes in $Si(OH)_4$ and NO_x

Data comparing N-$Si(OH)_4$ with N-NO_x were divided into three groups–data from before and after the end of June 2005 during phase I, and data from phase II (Fig. 5). Before the end of June 2005, the ratio of changes of N-$Si(OH)_4$ to N-NO_x ($\Delta Si/\Delta N$) was approximately 0.4, without a statistically significant correlation. However, $\Delta Si/\Delta N$ between July and September 2005 was estimated to be 3.2 with good correlation (r^2 = 0.9). This increase in $\Delta Si/\Delta N$ could be caused by (1) predominance of diatoms after the end of July; (2) an increase in the diatom Si/N uptake ratio which occurs under any type of stress such as lower or higher temperature, light limitation, or iron limitation; or (3) preferential decomposition of particulate inorganic nitrogen (PIN) (reviewed by Saito *et al.*, 2002).

The first cause is the most likely based on the dramatic increase in biogenic opal flux observed in sediment trap samples at 150 m

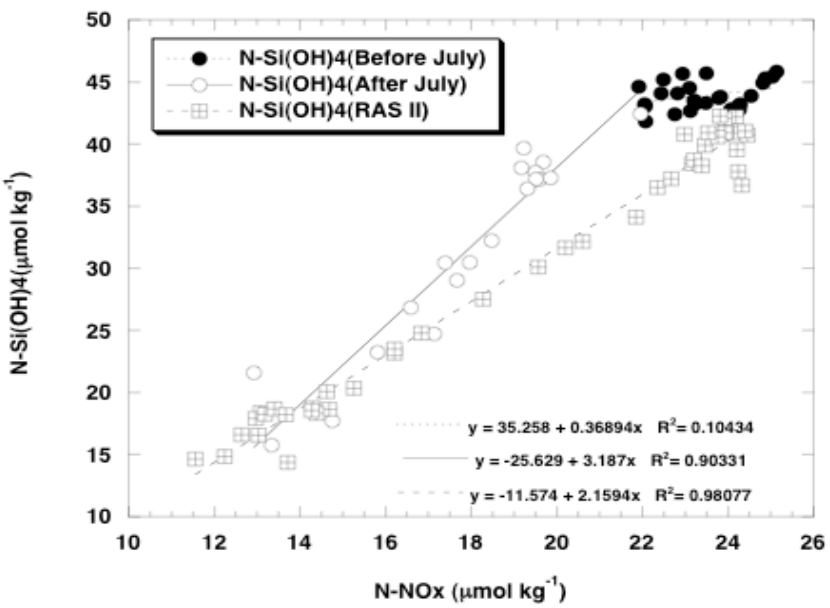

Figure 5. The relationship between normalized NO_x (N-NO_x) and $Si(OH)_4$ (N-$Si(OH)_4$). Data are divided into three groups: closed circles with dotted regression line, data from before the end of June 2005; open circles with solid regression line, from July through September 2005; squares with broken regression line, after October 2005 (phase II).

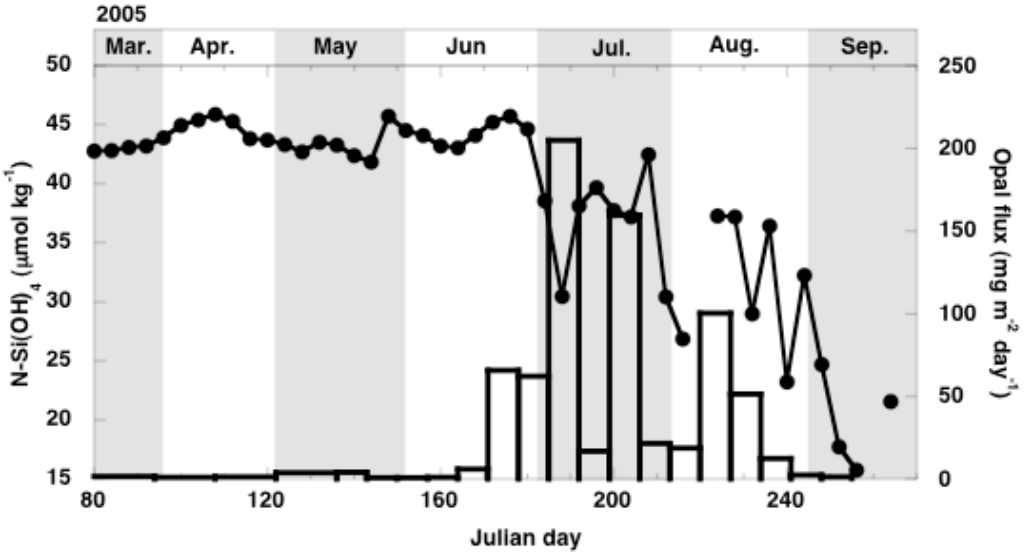

Figure 6. N-Si(OH)$_4$ concentrations between 20 March 2005 and 20 September 2005 (line graph) and biogenic opal flux at 150 m observed by sediment trap (bar graph, Honda *et al*., 2006).

after late June. Before this, opal flux had been very low (Fig. 6). The large decrease of dissolved Si(OH)$_4$ was accompanied by not only by the increase in opal flux, but also by an increase of phytoplankton abundance and primary productivity in the euphotic layer based on optical observation (Honda *et al*., 2006). This evidence indicates that nutrients and DIC assimilated by phytoplankton, primarily diatoms, in the euphotic layer were quickly transported vertically to at least 150 m in the ocean interior.

4.2.2 Estimation of Annual New Production

One method for assessing the level of activity of the biological pump is to determine of magnitude of the seasonal NO_x drawdown and to estimate annual new production (Eppley, 1989; Codispoti, 1989; Wong *et al*., 2002a, b; Lourey and Trull, 2001). Launchi and Najjar (2000) estimated annual global new production in the upper 100 m using the annual minimum NO_x data observed at the surface in the late August and data from 100 m in winter as the annual maximum. On the other hand, Wong *et al*. (2002b) estimated annual new production for the North Pacific using seasonal surface nutrient data observed by ships of opportunity and assuming that the surface mixed layer is 50 m thick.

Even though in this study the RAS collected seawater samples at one depth, this depth was generally located in or very close to the surface MLD (Fig. 3a). The RAS data provide annual maximum and minimum NO_x values in the mixed layer and therefore RAS data from this study can contribute to estimation of annual new production. The determination of new production requires an estimate of the seasonal drawdown of nutrients integrated over the upper 100 m of the water column, which is the depth of the permanent halocline or pycnocline in the WSG (Favorite *et al*., 1976) and of the chlorophyll-*a* depletion layer at station K2 (Kawakami, unpublished data). We estimated the seasonal drawdown of integrated nutrients (the nutrient inventory) in the upper 100 m using only data from 35.5 m, which was the approximate average RAS depth during phase I.

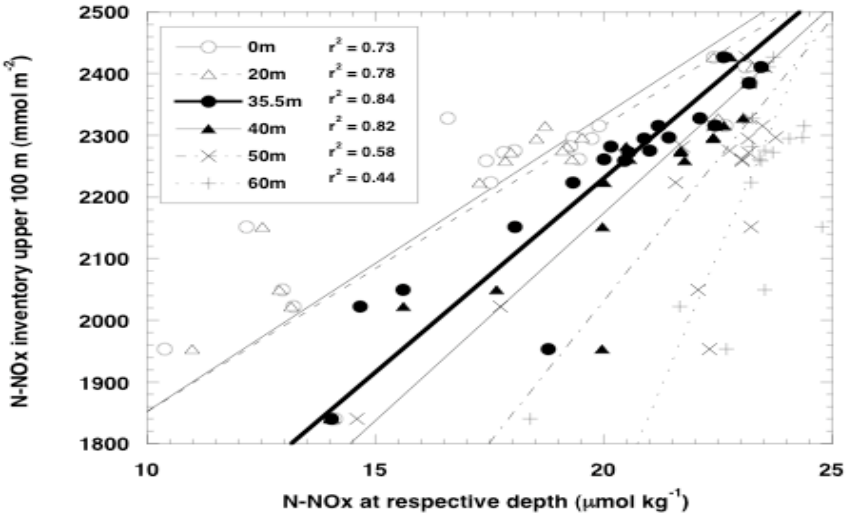

Figure 7. Relationship between N-NO_x at 35.5 m (RAS depth during phase I) and N-NO_x inventory (total N-NO_x) integrated over the upper 100 m based on climatological data (solid circles and heavy solid line). Correlation coefficient (r^2) is 0.84. Data also shown for depths of 0 m (open circles, $r^2 = 0.73$), 20 m (open triangles, $r^2 = 0.78$), 40 m (solid triangles, $r^2 = 0.82$), 50 m ('X' signs, $r^2 = 0.58$) and 60 m ('plus' signs, $r^2 = 0.44$).

We used previously observed climatological data to derive an empirical equation for estimating integrated nutrients in the upper 100 m using nutrient data from 35.5 m although at low N-NO_x values, there was a larger deviation from the derived regression line because these low values correspond to samples from below the mixed layer (Fig. 7). We applied this empirical equation to the maximum and minimum RAS nutrient values and assumed that biological drawdown of N-DIC follows the Redfield ratio ($\Delta C/\Delta N = 6.6$). We estimated the annual new production (the difference between maximum inventory estimated with maximum N-NO_x observed in April 2005 and minimum inventory with minimum N-NO_x observed in October 2005) at approximately 156 mg-C m^{-2} day^{-1} or 57 g-C m^{-2} yr^{-1}. This estimate is slightly higher than estimates by Midorikawa *et al.* (2002) (approximately 33 g-C m^{-2} yr^{-1}) and Andreev *et al.* (2002) (approximately 37 g-C m^{-2} yr^{-1}), and is comparable to those by Wong *et al.* (2002b) (57–88 g-C m^{-2} yr^{-1}; average, 67 g-C m^{-2} yr^{-1}) and Launchi and Najjar (2000) (40–60 g-C m^{-2} yr^{-1}).

We also investigated the relationship between the N-NO_x inventory in the upper 100 m and N-NO_x concentrations at various discreet depths (0–100 m) other than 35.5 m (Fig. 7) and verified that N-NO_x values at depths shallower than 40 m have good correlation with the N-NOx inventory in the upper 100 m ($r^2 > 0.7$) while N-NO_x values from depths greater than 60 m do not show good correlation ($r^2 < 0.5$). The N-NO_x inventory in the upper 100 m was more highly correlated with N-NO_x concentrations at 35.5 m and 40 m ($r^2 > 0.8$, $p < 0.0001$) than at the surface ($r^2 = 0.73$) (Fig.7). Therefore annual new production in the WSG can be estimated from RAS data obtained from one depth accurately as long as that depth is shallower than 40 m.

5. Concluding remarks

The determination of nutrient and DIC concentrations is essential for understanding biological pump processes and variability, especially in the northwestern North Pacific Ocean where seasonal changes in biological

activity are large. However, ordinary shipboard sampling limits the temporal resolution of time-series observations used for biogeochemical studies.

This study confirms the utility of automated water sampling systems for time-series observation of NO_x and $Si(OH)_4$. It remains difficult to moor instruments near the sea surface in the northwestern North Pacific because of rough seas, with waves exceeding 20 m in height, and the presence of ships with drafts greater than 10 m. However, combining satellite and sediment trap data with data from an RAS deployed at subsurface levels will contribute greatly to quantifying seasonal variability in nutrients and biological pump activity. Moreover, coupling RAS data with mathematical simulations will reveal more precisely the variability of the biological pump and CO_2 exchange between the atmosphere and ocean.

Acknowledgements

We express our appreciation to S. Honjo of the Woods Hole Oceanographic Institution (WHOI) for his efforts to promote time-series observations with mooring systems. We especially thank K. Hayashi of Marine Works Japan, Co. (MWJ) who maintained the RAS system and established procedures of chemical analysis of RAS sample. We are grateful to J. Kemp and his team of WHOI and T. Idai of MWJ for their mooring work and maintenance of the mooring system. We appreciate K. Doherty of McLane Research Laboratories, Inc. for design of the RAS. Masters M. Akamine and Y. Kita and the officers and crews of the *R/V MIRAI*, and the onboard analytical team from MWJ including J. Hamanaka, K. Sato, A. Takeuchi, M. Kamata, M. Moro and F. Shibata provided us with their expertise. K. Sasaoka, M. Wakita and Y. Nakano of Japan Agency for Marine-Earth Science and Technology (JAMSTEC) provided satellite data, approved climatological data and estimates of $CaCO_3$ supersaturation rates for RAS samples, respectively. We thank K. Buesseler of WHOI and the VERTIGO group for their permission to use unpublished data. Finally, we acknowledge reviewers, P. Brewer, Y. Nakaguchi and T. Gamo, for their constructive and suggestive comments.

Appendix

Spell-out of abbreviation in text and captions are as follows:

AFP: Acid Flush Path
AVHRR: Advanced Very High Resolution Radiometer
DIC: Dissolved Inorganic Carbon
MLD: Mixed Layer Depth
RAS: Remotely Access Sampler
SST: Sea Surface Temperature
VERTIGO: VERtical Transport In the Global Ocean
WFP: Water Flush Path
WSG: Western Subarctic Gyre

References

Anderson, L. A., and J. L. Sarmiento (1994): Redfield ratios of remineralization determined by nutrient data analysis. *Global Biogeochem. Cycles*, **8**, 65-80.

Andreev, A., M. Kusakabe, M. Honda, A. Murata, and C. Saito (2002): Vertical fluxes of nutrients and carbon through the halocline in the western subarctic Gyre calculated by mass balance. *Deep-Sea Res. II*, **49**, 5577–5593.

Aoyama, M. (2005): 3.4 Nutrients, p. 128. in *WHP P6, A10, I3/I4 revisit data book: Blue Earth Global Expedition 2003 (BEAGLE2003) vol.2,* ed. by H. Uchida and M. Fukasawa, Aiwa printing, Tokyo.

Banse, K., and D. C. English (1999): Comparing phytoplankton seasonality in the eastern and western Subarctic Pacific and the western Bering Sea. *Prog. Oceanogr*., **43**, 235-288.

Behrenfeld, M. J., E. Boss, D. A. Siegel and D. M. Shea (2005): Carbon-based ocean productivity and phytoplankton physiology from space. *Global Biogeochemical Cycles,* **19**, No. 1, GB100610.1029/2004GB002299

Bell, J., J. Betts and E. Boyle (2002): MITESS: a moored in situ trace element serial sampler for deep-sea moorings. *Deep-Sea Res. I,* **49**, 2103-2118.

Buesseler, K. O., J. Bishop, P. Boyd, K. Casciotti, F. Dehairs, C. Lamborg, D. Siegel, M. W. Silver, D. Steinberg, S. Saitoh, T. Trull, J. R. Valdes and B. Van Mooy (2006): What we know from VERTIGO - OS22H-02. *Abstracts of 2006 AGU Ocean Sciences Meeting - Honolulu*.

Campbell, J. and 22 co-authors (2002): Comparisons of algorithms for estimating ocean primary production from surface chlorophyll, temperature, and irradiance, *Global Biogeochemical Cycles*, ***16(10)***, doi: 10.1029/2001GB001444, 2002.

Codispoti, L. A. (1989): Phosphorous vs. nitrogen limitation of new and export production. p. 377-394. In *Productivity of the Ocean: Present and Past*, ed. by W. H. Berger, V. S. Smetacek, and G. Wefer, Wiley, New York.

Conte, M. H., N. Ralph and E. Ross (2001): Seasonal and interannual variability in deep ocean particle fluxes at the Oceanic Flux Program/Bermuda Atlantic Time-series (BATS) site in the western Sargasso Sea near Bermuda, *Deep-Sea Res. II*, **48**, 1471-1505, 2001.

Conte, M. H., T. D. Dickey, J. C. Weber, R. J. Johnson and A. H. Knap (2003): Transient physical forcing of pulsed export of bioreactive organic material to the deep Sargasso Sea, *Deep-Sea Res. I*, **50**(10-11), 1157-1187.

Dickey, T., J. Marra, R. Weller, D. Sigurdson, C. Langdon, and C. Kinkade (1998): Time-series of bio-optical and physical properties in the Arabian Sea: October 1994 - October 1995, *Deep-Sea Res. II*, **45**, 2001-2025, 1998.

Dickey, T., S. Zedler, D. Frye, H. Jannasch, D. Manov, D. Sigurdson, J. D. McNeil, L. Dobeck, X. Yu, T. Gilboy, C. Bravo, S. C. Doney, D. A. Siegel, and N. Nelson (2001): Physical and biogeochemical variability from hours to years at the Bermuda Testbed Mooring site: June 1994 - March 1998, *Deep-Sea Res. II*, **48**, 2105-2131.

Dickey, T., Moore, C., O-SCOPE Group (2003): New sensors monitor bio-optical / biogeochemical ocean changes, *Sea Tech.,* 44, 17-24.

Dickey, T., M. Lewis, and G. Chang (2006): Optical oceanography: recent advances and future directions using global remote sensing and in situ observations, *Rev. Geophys.,* in press.

DOE (1994): *Handbook of methods for the analysis of the various parameters of the carbon dioxide system in seawater.* Dickson, A. G., Goyet, C. (Eds) Version 2,

Carbon Dioxide Information Center, Report ORNL/CDIAC-74, Oak Ridge National Laboratory, Oak Ridge, TN, USA.

Eberlein, K. and G. Kattner (1987): Automatic method for the determination of ortho-phosphate and total dissolved phosphorus in the marine environment. Fresenius 'Z. Anal. Chem., **326**, 354-357.

Eppley, R. W. (1989): New production: history, methods, and problem. p. 85-97. In, *Productivity of the Ocean: Present and Past,* ed. by W. H. Berger, V. S. Smetacek, and G. Wefer, Wiley, New York.

Falkowski, P. G., R. T. Barber, and V. Smetacek (1998): Biogeochemical controls and feedbacks on ocean primary production, *Science*, **281**, 200-206.

Favorite, F., A. J. Dodimead and K. Nasu (1976): Oceanography of the Subarctic pacific Region, 1960-71. *Bull. Int. North Pacific Fishery Commission*, **33**, 1-187.

Harrison, P. J., P. W. Boyd, D. E. Varela, S. Takeda, A. Shiomoto, and T. Odate (1999): Comparison of factors controlling phytoplankton productivity in the NE and NW Subarctic Pacific gyres, *Prog. Oceanogr.* ***43***, 205-234, 1999.

Harrison, P. J., F. A. Whitney, A. Tsuda, H. Saito and K. Tadokoro (2004): Nutrient and plankton dynamics in the NE and NW gyres of the Subarctic Pacific ocean, *J. Oceanogr.* ***60,*** 93-117, 2004.

Heinze, C (2004): Simulating oceanic CaCO3 export production in the greenhouse. *Geophys. Res. Let.* **31**, L16308, doi:10.1029/2004 GL020613.

Honda, M. C., K. Imai, Y. Nojiri, F. Hoshi, T. Sugawara and M. Kusakabe (2002): The biological pump in the northwestern North Pacific based on fluxes and major component of particulate matter obtained by sediment trap experiments (1997-2000). *Deep-Sea Res. II,* **49**, 5595-5626.

Honda, M. C. (2005): Time-series observation for study of CO_2 cycle in the North Pacific with mooring systems, Navigation, **163**, 67-77 (in Japanese).

Honda, M. C., H. Kawakami, K. Sasaoka, S. Watanabe, and T. Dickey (2006): Quick transport of primary produced organic carbon to the ocean interior, Geophys. Res. Lett., 33, L16603, doi:10.1029/2006GL026466.

Honjo, S. (1996): Fluxes of particles to the interior of the open ocean. p. 91-154. In *Particle Flux in the ocean*, *SCOPE 57* ed. by V. Ittekkot, P. Schafer, S. Honjo, and P. J. Depetris, John Wiley and Sons, New York.

Idai, T., M. Honda, S. Honjo, and J. Kemp (2006): Mooring systems for time-series observation for biogeochemistry in the northwestern North Pacific, JAMSTEC Rep. Res. Dev., **1**, 73-91.

Imai, K., Y. Nojiri, N. Tsurushima, and T. Saino (2002): Time series of seasonal variation of primary productivity at station KNOT (44°N, 155°E) in the sub-arctic western North Pacific. *Deep-Sea Res. II*, **49**, 5395–5408.

Ishii, M., H. Y. Inoue, H. Matsueda and E. Tanoue (1998): Close coupling between seasonal biological production and dynamics of dissolved inorganic carbon in the Indian Ocean section and the western Pacific ocean sector of the Antarctic ocean. *Deep-Sea Res. I*, **45**, 1187-1209.

Karl, D. M., J. R. Christian, J. E. Dore, D. V. Hebel, R. M. Letelier, L. M. Tupas and C. D. Winn (1996): Seasonal and interannual variability in primary production and particle flux at station ALOHA. *Deep-Sea Res*., **43**, 539-568.

Karl, D. M., J. E. Dore, R. Lukas, A. Michaels, N. R. Bates and A. Knap (2001): Building the long-term picture: The U.S.JGOFS Time-series programs. *Oceanogr.,* **14** (4), 6-17.

Kattner, G. (1999): Storage of dissolved inorganic nutrients in seawater: poisoning

with mercuric chloride. *Mar. Chem.,* **67**, 61-66.

Launchi, F. and R. G. Najjar (2000): A global monthly climatology of phosphate, nitrate, and silicate in the upper ocean: Spring-summer export production and shallow remineralization. *Global Biogeochem. Cycles,* **14**, 957-977.

Lourey, M. and T. W. Trull (2001): Seasonal nutrient depletion and carbon export in the Subantarctic and Polar Frontal Zones of the Southern Ocean south of Australia. *J. Geophys. Res.*, **106** (c12), 31463-31487.

Manov, D., G. Chang and T, Dickey (2004): Methods for reducing biofouling on moored optical sensors. *J. Atoms. Ocean Tech.*, 957-967.

Midorikawa, T., T. Umeda, N. Hiraishi, K. Ogawa, K. Nemoto, N. Kudo and M. Ishii (2002): Estimation of seasonal net community production and air-sea CO_2 flux based on the carbon budget above the temperature minimum layer in the western subarctic North Pacific. *Deep-Sea Res. I*, **49**, 339–362

Mochizuki, M., N. Shiga, M. Saito, K. Imai and Y. Nojiri (2002): Seasonal changes in nutrients, chlorophyll *a* and the phytoplankton assemblage of the western subarctic gyre in the Pacific Ocean. *Deep-Sea Res. II*, **49**, 5421–5439.

Murphy, J. and J. P. Riley (1961): Modified single solution method for the determination of phosphate in natural water. *Anal. Chem. Acta.*, **27**, 31-36.

Orr, J. C., V. J. Fabry, O. Aumont, L. Bopp, S. C. Doney, R. A. Feely, A. Gnanadesikan, N. Gruber, A. Ishida, F. Joos, R. M. Key, K. Lindsay, E. Maier-Reimer, R. Matear, P. Monfray, A. Mouchet, R. G. Najjar, G-K. Plattner, K. B. Rodgers, C. L. Sabine, J. L. Sarmiento, R. Schlitzer, R. D. Slater, I. J. Totterdell, M-F. Weirig, Y. Yamanaka and A. Yool (2005): Anthropogenic ocean acidification over the twenty-first century and its impact on calcifying organisms. *Nature*, **437**, 681-686.

Redfield, A. C., B. H. Ketchum and F. A. Richards (1963): The influences of organisms on the composition of seawater. P. 26-77. In *The Sea*, ed. by M. H. Hill, Wiley-Interscience, New York.

Saito, H., A. Tsuda and H. Kasai (2002): Nutrient and plankton dynamics in the Oyashio region of the western subarctic Pacific Ocean. *Deep-Sea Res. II*, **49**, 5463-5486.

Sarmiento, J. L., and C. LeQuere (1996): Oceanic carbon dioxide uptake in a model of century-scale global warming, *Science*, **274**, 1346-1350.

Sigman, D. M., and E. A. Boyle (2000): Glacial/Interglacial variations in atmospheric carbon dioxide. *Nature*, **407**, 859-869.

Takahashi, T., S. C. Sutherland, C. Sweeny, A. Poisson, N. Metzl, B. Tilbrook, N. Bates, R. Wanninkhof, R. A. Feely, C. Sabine, J. Olafsson and Y. Nojiri (2002): Global sea-air CO_2 flux based on climatological surface ocean pCO_2, and seasonal biological and temperature effects. *Deep-Sea Res. II*, **49**, 1601–1622.

Tsurushima, N., Y. Nojiri, K. Imai and S. Watanabe (2002): Seasonal variations of carbon dioxide system and nutrients in the surface mixed layer at station KNOT (44°N, 155°E) in the subarctic western North Pacific. *Deep-Sea Res. II*, **49**, 5377–5394.

Volk, T., and M. I. Hoffert (1985): Ocean carbon pumps: Analysis of relative strengths and efficiencies in ocean-driven atmospheric CO_2 changes. P. 99-110. In *The Carbon Cycle and Atmospheric CO_2: In Natural Variations Archean to Present*, ed. by E. Sundquist, and W.S. Broecker, AGU, Washington, D. C..

Wong, C. S., N. A. D. Waser, Y. Nojiri, F. A. Whitney, J. S. Page, J. Zeng (2002a): Seasonal cycles of nutrients and dissolved inorganic carbon at high and mid latitudes

in the North Pacific Ocean during the *skaugran* cruises: determination of new production and nutrient uptake ratios. *Deep-Sea Res. II*, **49**, 5317–5338.

Wong, C. C., N. A. D. Waser, Y. Nojiri, Wm. K. Johnson, F. A. Whitney, J. S. C. Page and J. Zeng (2002b): Seasonal and Interannual Variability in the Distribution of Surface Nutrients and Dissolved Inorganic Carbon in the Northern North Pacific: Influence of El Niño. *J. Oceanogr*. **58**, 227-243.

Mooring systems for time-series observation for biogeochemistry in the northwestern North Pacific: design, preparation and mooring work

Toru Idai*, Makio Honda*, Susumu Honjo** and John Kemp**

Abstract For the better understanding of carbon cycle in the northwestern North Pacific where rough sea condition frequently refuses oceanographic observation by research vessel, time-series observation for the biogeochemistry with mooring system has been requested strongly. Mutsu Institute for Oceanography (MIO) challenged to deploy the mooring system that is anchored on the sea floor at > 5,000 m depth and its top with automatic instruments is located in the euphotic layer, upper 30 – 50 m. In order to enable this deployment, behaviors of mooring system such as tilt and depth for instruments during deployment and observation were simulated, and precise lengths of wire and nylon ropes used for mooring systems were measured under the mooring tension on land. Based on these procedures, two types mooring systems were deployed at stations K-1 (51°N, 165°E) and K-3 (39°N, 160°E) in October 2002 and recovered in November 2003. Mooring systems were successfully deployed within 300 m from a "target" points and depths of top of mooring systems could be located between 40 – 60 m for K-1 mooring and 50 – 70 m for K-3 mooring as we designed except high current period.

Keywords: pre-stretch, BGC mooring, PO Mooring, time-series, northwestern North Pacific

1. Introduction

The Northwestern North Pacific is the terminal zone of the deep-sea water circulation, resulting the high productivity. As diatom species without carbonate test are pre-dominant, the biological activity in this area plays an important role in absorbing atmospheric CO_2.

In September 2000, Mutsu Institute for Oceanography (MIO) initiated a project named "HIgh LAtitude Time-Series observational study (HILATS)" with using two types mooring systems: One is for biogeochemistry and consists of automatic sampler collecting such as seawater, zoo and phytoplankton and sinking particles (BGC mooring systems: Fig. 1 (a)). The other is for physical oceanography and consists of CTD / ACM profiler (PO mooring systems: Fig. 1 (b)). This project has been conducted with cooperation of Woods Hole Oceanographic Institution (WHOI).

This report introduces the above mooring system focusing on its concept, design, preparation and mooring works.

2. Design of mooring system

2.1 Principal points

The most important point of these mooring systems is how precisely automatic samplers just below a top buoy of mooring systems are located within the euphotic layer (upper 50 m). On the other hand, these instruments should be never installed upper 30 m because of rough seas with waves exceeding 20 m in height and presence of ships with drafts >10 m. Therefore the following points on materials and design were considered.

(1) A top buoy of mooring system should be located around 30 m below sea surface precisely. In order to keep mooring system straight against the external force (wave and current), a 64" syntactic form buoy was selected. " is the inch of length unit. Its buoyancy was adjusted to be approximately 1.3 ton and two times larger than that used for Acoustic Doppler Current Profiler (ADCP) mooring system (Ito et al., 1995)[1)] in the project "Tropical Ocean Climate Study (TOCS)" (http://www.jamstec.go.jp/tocs/E/).

(2) In order to avoid significant elongation by high tension and partition by "fish bite", 1/4" or 5/16" torque-balanced wire rope with polyethylene jacket (Wire Rope Corporation of America, Inc.) were selected as a main mooring rope. Unlike an ordinary wire rope, this wire rope has a fewer torsion resulting a smaller elongati and a fewer occurrence of kink. We use wire ropes of 5/16" for "BGC" mooring systems of upper 1,000 m and 1/4" for below 1,000 m in order to reduce weight and hydrodynamic resistance, while 1/4" wire ropes was used mainly for "PO" mooring systems with MMP.

(3) In order to recover mooring system certainly, tandem-releaser system (Edgtech:Model 8242XS) was selected.

* Mutsu Institution for Oceanography, Japan Agency for Marine-Earth Science and Technology
** Woods Hole Oceanographic Institution

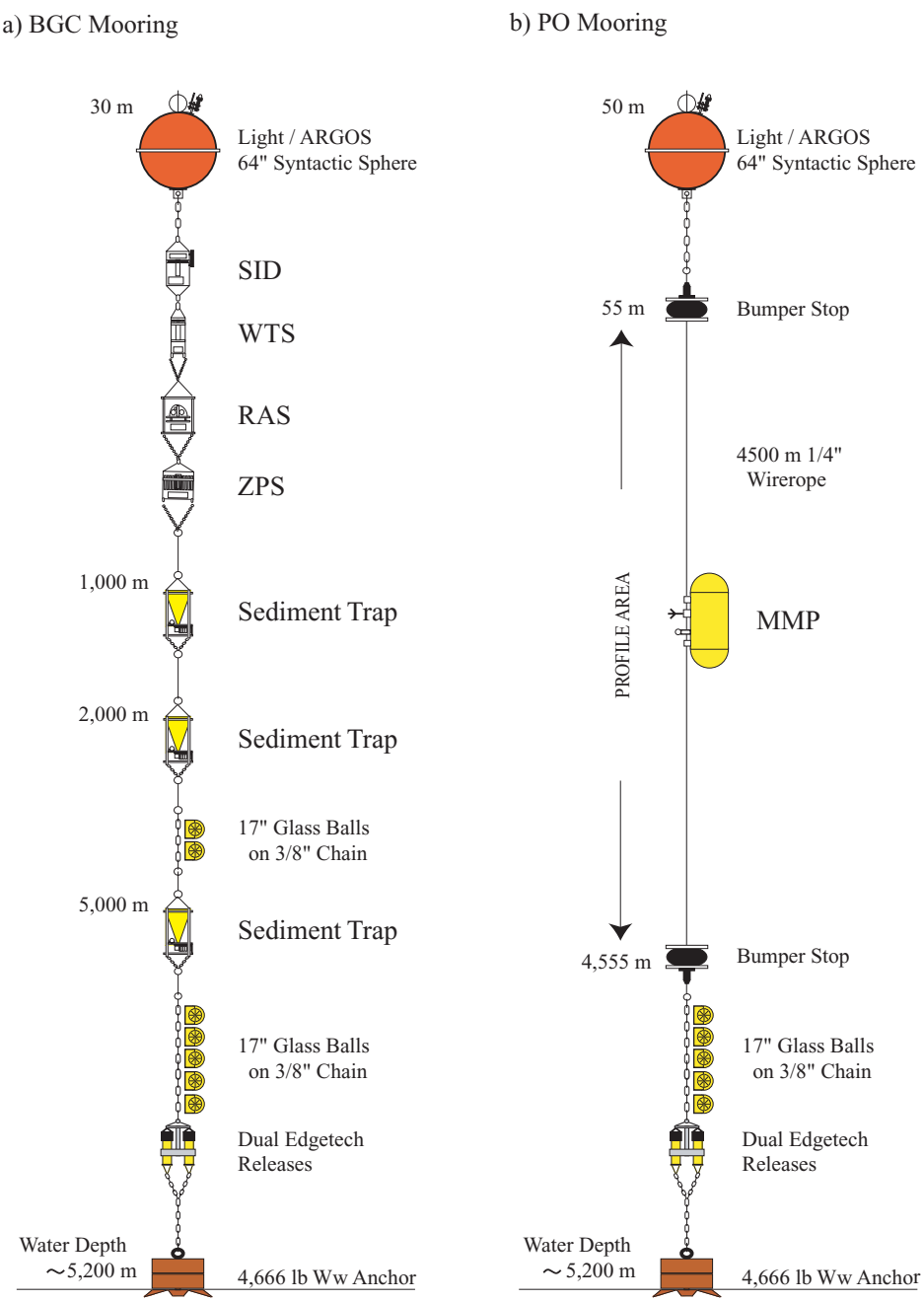

Figure 1: Schematic diagram of Mooring System for Time-Series Observational Study

(4) An impact load occurs when anchor is dropped into the sea surface and lands on the sea floor. As a shock absorber, flotation systems of glass balls were installed just above a releaser system and nylon rope of 1” was inserted between an anchor and a releaser system. This floatation system has enough buoyancy to held whole mooring system even if top buoy of 64” syntactic foam buoy is lost.

(5) Imawaki reported that the weight of anchor should be heavier than high tension of 1.25 times and more (1976)[2]. In order to keep mooring system straight with high tension (1.3 ton) and increase friction resistance, heavy anchor of approximately 2 ton with a “mace plate”, which was like a spike to grip seafloor, is prepared.

(6) A positioning system (Seimac ARGOS compact mooring locator: CML) is installed on respective top buoys. When a top buoy appears on the sea surface intentionally or accidentally, ARGOS CML starts to transmit signal of its position to land. Therefore it enables us to know its position easily.

Table 1: BGC Mooring Design Tention

	K-1 BGC Mooring Description	Joint	Item Length (m)	Total (kg)	Mooring Length (m)	Mooring Weight (kg)	Above Bottom (m)	Mooring Depth (m)	Safety Rate
1	64" Syntatic Sphere		2.270	-1360.8		-1360.8	5106.6	29.8	
	Hardware	L	0.280	3.6	2.6	-1357.1	5104.3	32.1	
2	3/4" Proof Coil Chain		5.000	40.0	7.6	-1317.1	5104.0	32.4	3.64
	Hardware	F	0.255	2.4	7.8	-1314.7	5099.0	37.4	
3	Instrument - "SID" - (OOS)		1.694	59.0	9.5	-1255.7	5098.8	37.6	4.44
	Hardware	H	0.235	1.9	9.7	-1253.8	5097.1	39.3	
4	Instrument - "WTS"		2.855	56.7	12.6	-1197.1	5096.9	39.5	4.57
	Hardware	H	0.235	1.9	12.8	-1195.2	5094.0	42.4	
5	Instrument - "RAS"		2.285	35.0	15.1	-1160.2	5093.8	42.6	4.79
	Hardware	H	0.235	1.9	15.3	-1158.2	5091.5	44.9	
6	Instrument - "ZPS"		3.355	26.0	18.7	-1132.2	5091.2	45.2	4.90
	Hardware	H	0.235	1.9	18.9	-1130.3	5087.9	48.5	
7	3-TON Miller Swivel		0.161	3.2	19.1	-1127.1	5087.7	48.7	2.66
	Hardware	H	0.235	1.9	19.3	-1125.2	5087.5	48.9	
8	500M 5/16" Wire - (Z)		499.329	106.5	518.7	-1018.8	5087.3	49.1	3.44
	Hardware	H	0.235	1.9	518.9	-1016.8	4587.9	548.5	
9	403 Meters 5/16" Wire - (AA)		402.258	85.8	921.2	-931.1	4587.7	548.7	3.76
	Hardware	H	0.235	2.2	921.4	-928.9	4185.4	951.0	
10	50 Meters 5/16" Wire - (AO)		49.919	10.6	971.3	-918.2	4185.2	951.2	3.81
	Hardware	I	0.215	2.2	971.5	-916.1	4135.3	1001.1	
11, 12, 13	Sediment Trap	O	3.571	35.0	975.1	-881.1	4135.1	1001.3	6.32
	Hardware	J	0.046	0.4	975.1	-880.6	4131.5	1004.9	
14	5 Meters 3/8" Trawler Chain		5.000	10.1	980.1	-870.5	4131.5	1004.9	3.45
	Hardware	A	0.210	1.3	980.3	-869.2	4126.5	1009.9	
15	500 Meters 1/4" Wire - (O)		499.585	70.2	1479.9	-798.9	4126.2	1010.2	2.88
	Hardware	A	0.210	1.3	1480.1	-797.6	3626.7	1509.7	
16	440.1 Meters 1/4" Wire - (R)		439.560	61.8	1919.7	-735.8	3626.4	1510.0	3.13
	Hardware	A	0.210	1.3	1919.9	-734.4	3186.9	1949.5	
17	50 Meters 1/4" Wire - (AL)		50.103	7.0	1970.0	-727.4	3186.7	1949.7	3.16
	Hardware	K	0.200	1.4	1970.2	-726.0	3136.6	1999.8	
18, 19, 20	Sediment Trap	O	3.571	35.0	1973.8	-691.0	3136.4	2000.0	6.04
	Hardware	J	0.046	0.4	1973.8	-690.6	3132.8	2003.6	
21	2 Meters 3/8" Trawler Chain		2.700	5.5	1976.5	-685.1	3132.8	2003.6	4.38
	Hardware	A	0.210	1.3	1976.7	-683.8	3130.1	2006.3	
22	500 Meters 1/4" Wire - (#A)		501.054	70.5	2477.8	-613.3	3129.8	2006.6	3.75
	Hardware	A	0.210	1.3	2478.0	-612.0	2628.8	2507.6	
23	500 Meters 1/4" Wire - (#B)		500.932	70.4	2978.9	-541.5	2628.6	2507.8	4.25
	Hardware	A	0.210	1.3	2979.1	-540.2	2127.7	3008.7	
24	20 Meters 1/4" Wire - (#5/20)		20.153	2.8	2999.3	-537.4	2127.4	3009.0	4.28
	Hardware	A	0.210	1.3	2999.5	-536.1	2107.3	3029.1	
25	20 Meters 1/4" Wire - (#6/20)		20.153	2.8	3019.7	-533.2	2107.1	3029.3	4.31
	Hardware	A	0.210	1.3	3019.9	-531.9	2086.9	3049.5	
26	4-17" Glassballs on 3/8" Trawler		4.000	-99.6	3023.9	-631.5	2086.7	3049.7	4.75
	Hardware	A	0.210	1.3	3024.1	-630.2	2082.7	3053.7	
27	4-17" Glassballs on 3/8" Trawler		4.000	-99.6	3028.1	-729.8	2082.5	3053.9	4.11
	Hardware	A	0.210	1.3	3028.3	-728.5	2078.5	3057.9	
28	500 Meters 1/4" Wire - (#C)		501.065	70.5	3529.4	-658.1	2078.3	3058.1	3.50
	Hardware	A	0.210	1.3	3529.6	-656.7	1577.2	3559.2	
29	500 Meters 1/4" Wire - (#D)		500.708	70.4	4030.3	-586.3	1577.0	3559.4	3.92
	Hardware	A	0.210	1.3	4030.5	-585.0	1076.3	4060.1	
30	500 Meters 1/4" Wire - (#E)		501.020	70.5	4531.5	-514.5	1076.1	4060.3	4.47
	Hardware	A	0.210	1.3	4531.7	-513.2	575.1	4561.3	
31	4-17" Glassballs on 3/8" Trawler		4.000	-99.6	4535.7	-612.9	574.9	4561.5	4.90
	Hardware	A	0.210	1.3	4535.9	-611.5	570.9	4565.5	
32	200 Meters 1/4" Wire - (FF)		199.878	28.1	4735.8	-583.4	570.7	4565.7	3.94
	Hardware	A	0.210	1.3	4736.0	-582.1	370.8	4765.6	
33	50 Meters 1/4" Wire - (#FF)		50.232	7.1	4786.2	-575.0	370.6	4765.8	4.00
	Hardware	K	0.195	2.2	4786.4	-572.8	320.3	4816.1	
34, 35, 36	Sediment Trap	O	3.571	35.0	4790.0	-537.8	320.1	4816.3	11.62
	Hardware	J	0.046	0.4	4790.1	-537.4	316.6	4819.8	
37	3 Meters 3/8" Trawler Chain		2.000	4.1	4792.1	-533.4	316.5	4819.9	5.62
	Hardware	A	0.210	1.3	4792.3	-532.0	314.5	4821.9	
38	100 Meters 1/4" Wire - (UU)		100.009	14.1	4892.3	-518.0	314.3	4822.1	4.44
	Hardware	A	0.210	1.3	4892.5	-516.6	214.3	4922.1	

Table 1: (continued).

	K-1 BGC Mooring Description	Joint	Item Length (m)	Total (kg)	Mooring Length (m)	Mooring Weight (kg)	Above Bottom (m)	Mooring Depth (m)	Safety Rate
39	50 Meters 1/4" Wire - (YY)		49.993	7.0	4942.5	-509.6	214.1	4922.3	4.51
	Hardware	A	0.210	1.3	4942.7	-508.3	164.1	4972.3	
40	25 Meters 1/4" Wire - (#2/25)		25.108	3.5	4967.8	-504.7	163.9	4972.5	4.56
	Hardware	A	0.210	1.3	4968.0	-503.4	138.8	4997.6	
42	25 Meters 1/4" Wire- (#3/25)		25.147	3.5	4993.2	-499.9	138.6	4997.8	4.60
	Hardware	A	0.210	1.3	4993.4	-498.6	113.4	5023.0	
	20 Meters Adj 1/4" Wirerope		20.000	2.8	5013.4	-495.7	113.2	5023.2	4.64
	Hardware	A	0.210	1.3	5013.6	-494.4	93.2	5043.2	
43	5M 1/4" Jac. Wirerope		5.109	0.7	5018.7	-493.7	93.0	5043.4	4.66
	Hardware	A	0.210	1.3	5018.9	-492.4	87.9	5048.5	
44	5 Meters 3/8" Trawler Chain		5.000	10.1	5023.9	-482.2	87.7	5048.7	6.22
	Hardware	A	0.210	1.3	5024.1	-480.9	82.7	5053.7	
45	4-17" Glassballs on 3/8" Trawler		4.000	-99.6	5028.1	-580.5	82.5	5053.9	5.17
	Hardware	A	0.210	1.3	5028.3	-579.2	78.5	5057.9	
46	4-17" Glassballs on 3/8" Trawler		4.000	-99.6	5032.3	-678.8	78.3	5058.1	4.42
	Hardware	A	0.210	1.3	5032.5	-677.5	74.3	5062.1	
47	4-17" Glassballs on 3/8" Trawler		4.000	-99.6	5036.5	-777.2	74.1	5062.3	3.86
	Hardware	A	0.210	1.3	5036.7	-775.8	70.1	5066.3	
48	4-17" Glassballs on 3/8" Trawler		4.000	-99.6	5040.7	-875.5	69.9	5066.5	3.43
	Hardware	A	0.210	1.3	5040.9	-874.1	65.9	5070.5	
49	4-17" Glassballs on 3/8" Trawler		4.000	-99.6	5044.9	-973.8	65.6	5070.8	3.08
	Hardware	A	0.210	0.4	5045.2	-973.4	61.6	5074.8	
50	4-17" Glassballs on 3/8" Trawler		4.000	-99.6	5049.2	-1073.0	61.4	5075.0	2.80
	Hardware	A	0.210	0.4	5049.4	-1072.6	57.4	5079.0	
51	4-17" Glassballs on 3/8" Trawler		4.000	-99.6	5053.4	-1172.2	57.2	5079.2	2.56
	Hardware	A	0.210	0.4	5053.6	-1171.8	53.2	5083.2	
52	4-17" Glassballs on 3/8" Trawler		4.000	-99.6	5057.6	-1271.5	53.0	5083.4	2.36
	Hardware	A	0.210	0.4	5057.8	-1271.0	49.0	5087.4	
53	4-17" Glassballs on 3/8" Trawler		4.000	-99.6	5061.8	-1370.7	48.8	5087.6	2.19
	Hardware	A	0.210	0.4	5062.0	-1370.3	44.8	5091.6	
54	5 Meters 3/8" Trawler Chain		5.000	10.1	5067.0	-1360.1	44.6	5091.8	2.21
	Hardware	C	0.235	2.1	5067.2	-1358.0	39.6	5096.8	
55,56	Dual EGG Acoustic Releases	M	1.945	66.0	5069.2	-1292.0	39.4	5097.0	4.94
	Hardware	D	0.245	2.7	5069.4	-1289.3	37.4	5099.0	
57	5 Meters 3/8" Trawler Chain		5.000	10.1	5074.4	-1279.1	37.2	5099.2	2.35
	Hardware	C	0.235	2.1	5074.7	-1277.0	32.2	5104.2	
58	20 Meters 1" Nylon		21.794	0.3	5096.5	-1276.7	31.9	5104.5	3.96
	Hardware	C	0.235	2.1	5096.7	-1274.6	10.1	5126.3	
59	5 Meters 3/8" Trawler Chain		5.000	10.1	5101.7	-1264.4	9.9	5126.5	2.37
	Hardware	D	0.245	2.7	5101.9	-1261.7	4.9	5131.5	
	4000 Lb Ww Anchor		0.662	2268.0	5102.6	1006.2	4.7	5131.7	
	OVERALL MOORING LENGTH		**5102.592**		Depth		4.0	5132.4	

2.2 Tension and strength of mooring system

(1) Designed tension and safety rate

Tables 1 and 2 show designed tension (load) and safety rate (the ratio of designed tension to official working load limit) on respective parts for BGC mooring and PO mooring, respectively. It can be seen that the largest tension is loaded on a releaser and 3/8” chain with glass balls just above a releaser (1.4tf). However, safety rate of even these parts are higher than two (2.19 for BGC Mooring system and 2.16 for PO mooring system).

(2) Tilt and variation of tension of mooring system under static load

In order to design mooring systems, tilt and variation of tension of mooring system under static load was computed with software “MOORDSGN” developed by Dr. Clark Darnall, senior engineer of Polar Science Center, Applied Physics Laboratory, University of Washington. With data of cross section area of mooring system (mooring ropes and instruments) and data of current velocity at any 6 layers, tilt, variation of tension and depths for principal parts respective instruments can be calculated. After input the length and material from Tables 1 and 2, cross section area, drag coefficient and so on are given automatically.

Assuming that various current velocities from 0 cm sec^{-1} to 50 cm sec^{-1} at 0 m decrease with increasing depth monotonically to 1000 m, where velocity is 0 cm sec^{-1}, tilt of mooring systems were simulated (Fig. 2, a for BGC mooring system and Fig. 2, b for PO mooring systems). Tables 3 and 4 summarize horizontal distances

Table 2: PO Mooring Design Tention

	K-1 PO Mooring Description	Joint	Item Length (m)	Item Weight (kg)	Mooring Length (m)	Mooring Weight (kg)	Above Bottom (m)	Below Surface (m)	Safety Rate
1	64" Syntatic Sphere		2.27	-1360.8	2.3	-1360.8	5068.0	50.0	
	Hardware	L	0.28	3.6	2.6	-1357.2	5065.8	52.2	
2	5 Meters 3/4" Proof Coil Chain		5.00	40.0	7.6	-1317.2	5065.5	52.5	3.64
	Hardware	F	0.26	2.4	7.8	-1314.7	5060.5	57.5	
3	3-TON Miller Swivel		0.16	3.2	8.0	-1311.5	5060.2	57.8	2.29
	Hardware	B	0.23	1.6	8.2	-1309.9	5060.1	57.9	
4	4500 Meters 1/4" Wire (C)		4500.15	632.8	4508.3	-677.2	5059.8	58.1	3.40
	Hardware	B	0.23	1.6	4508.6	-675.6	559.7	4558.3	
5	3-TON Miller Swivel		0.16	3.2	4508.7	-672.4	559.5	4558.5	4.46
	Hardware	B	0.23	1.6	4509.0	-670.8	559.3	4558.7	
6	20 Meters 1/4" Wire - (#1/20)		20.13	2.8	4529.1	-667.9	559.1	4558.9	3.44
	Hardware	A	0.21	1.3	4529.3	-666.6	539.0	4579.0	
7	4-17" Glassballs on 3/8" Trawler		4.00	-99.6	4533.3	-766.3	538.7	4579.2	3.92
	Hardware	A	0.21	1.3	4533.5	-765.0	534.7	4583.2	
8	2-17" Glassballs on 3/8" Trawler		2.00	-24.9	4535.5	-789.9	534.5	4583.5	3.80
	Hardware	A	0.21	1.3	4535.7	-788.6	532.5	4585.5	
9	430 Meters 1/4" Wire - (#O)		430.66	60.6	4966.4	-728.0	532.3	4585.7	3.16
	Hardware	A	0.21	1.3	4966.6	-726.7	101.7	5016.3	
10	25 Meters 1/4" Wire - (#1/25)		25.11	3.5	4991.7	-723.2	101.5	5016.5	3.18
	Hardware	A	0.21	1.3	4991.9	-721.9	76.3	5041.7	
11	15 Meters 1/4" Wire - (#1/25)		15.00	2.1	5006.9	-719.8	85.4	5041.9	3.20
	Hardware	A	0.21	1.3	5007.1	-718.5	70.4	5056.9	
12	5.7 Meters 3/8" Trawler Chain		5.70	11.6	4997.6	-710.3	76.1	5057.1	4.22
	Hardware	A	0.21	1.3	4997.8	-709.0	70.4	5062.8	
13	4-17" Glassballs on 3/8" Trawler		4.00	-99.6	5001.8	-808.7	70.2	5063.0	3.71
	Hardware	A	0.21	1.3	5002.0	-807.4	66.2	5067.0	
14	4-17" Glassballs on 3/8" Trawler		4.00	-99.6	5006.0	-907.0	66.0	5067.2	3.31
	Hardware	A	0.21	1.3	5006.2	-905.7	62.0	5071.2	
15	4-17" Glassballs on 3/8" Trawler		4.00	-99.6	5010.2	-1005.4	61.8	5071.4	2.98
	Hardware	A	0.21	1.3	5010.4	-1004.1	57.8	5075.4	
16	4-17" Glassballs on 3/8" Trawler		4.00	-99.6	5014.4	-1103.7	57.6	5075.6	2.72
	Hardware	A	0.21	1.3	5014.7	-1102.4	53.6	5079.6	
17	4-17" Glassballs on 3/8" Trawler		4.00	-99.6	5018.7	-1202.1	53.4	5079.8	2.50
	Hardware	A	0.21	1.3	5018.9	-1200.8	49.4	5083.8	
18	4-17" Glassballs on 3/8" Trawler		4.00	-99.6	5022.9	-1300.4	49.2	5084.0	2.31
	Hardware	A	0.21	1.3	5023.1	-1299.1	45.2	5088.0	
19	4-17" Glassballs on 3/8" Trawler		4.00	-99.6	5027.1	-1398.8	45.0	5088.2	2.14
	Hardware	A	0.21	1.3	5027.3	-1397.5	41.0	5092.2	
20	5 Meters 3/8" Trawler Chain		5.00	10.1	5032.3	-1387.3	40.8	5092.5	2.16
	Hardware	C	0.24	2.1	5032.5	-1385.2	35.8	5097.5	
21	Dual EGG Acoustic Releases	M	1.95	66.0	5034.5	-1319.2	35.5	5097.7	4.40
	Hardware	D	0.25	2.7	5034.7	-1316.5	33.6	5099.6	
22	5 Meters 3/8" Trawler Chain		5.00	10.1	5039.7	-1306.3	33.3	5099.9	2.30
	Hardware	C	0.24	2.1	5039.9	-1304.2	28.3	5104.9	
23	20 Meters 1" Nylon (#2)		21.95	0.3	5061.9	-1303.9	28.1	5105.1	3.83
	Hardware	C	0.24	2.1	5062.1	-1301.8	6.1	5127.1	
24	5 Meters 3/8" Trawler Chain		5.00	10.1	5067.1	-1291.7	5.9	5127.3	2.32
	Hardware	D	0.25	2.7	5067.4	-1289.0	0.9	5132.3	
25	4000 Lb Ww Anchor		0.66	2268.0	5068.0	979.0	0.7	5132.5	
	OVERALL MOORING LENGTH		5083.24				0.0	5133.2	

of instruments from a anchored point and depths of time-series instruments and principal parts under static load.

Based on previous observation data, current velocity near sea surface in the northwestern North Pacific is expected to be at most 30 cm sec^{-1}. In this case, subsurface instruments except sediment traps are located between 60 and 70 m, which is still within the euphotic zone of this area. Therefore our mooring design is appropriate for this area. On the other hand, a top of PO mooring system was expected to be deepened to approximately 170 m under high current velocity of 30 cm sec^{-1}.

It is noted that the inclination of PO mooring is larger than that of BGC mooring although horizontal cross sectional area of PO mooring is smaller than that of BGC mooring. It might be attributed to a problem in segment numbers for PO mooring. If we simulate the inclination of PO mooring line with segment numbers of 9 (500 m × 9) instead of 1 (4,500 m × 1), the inclination

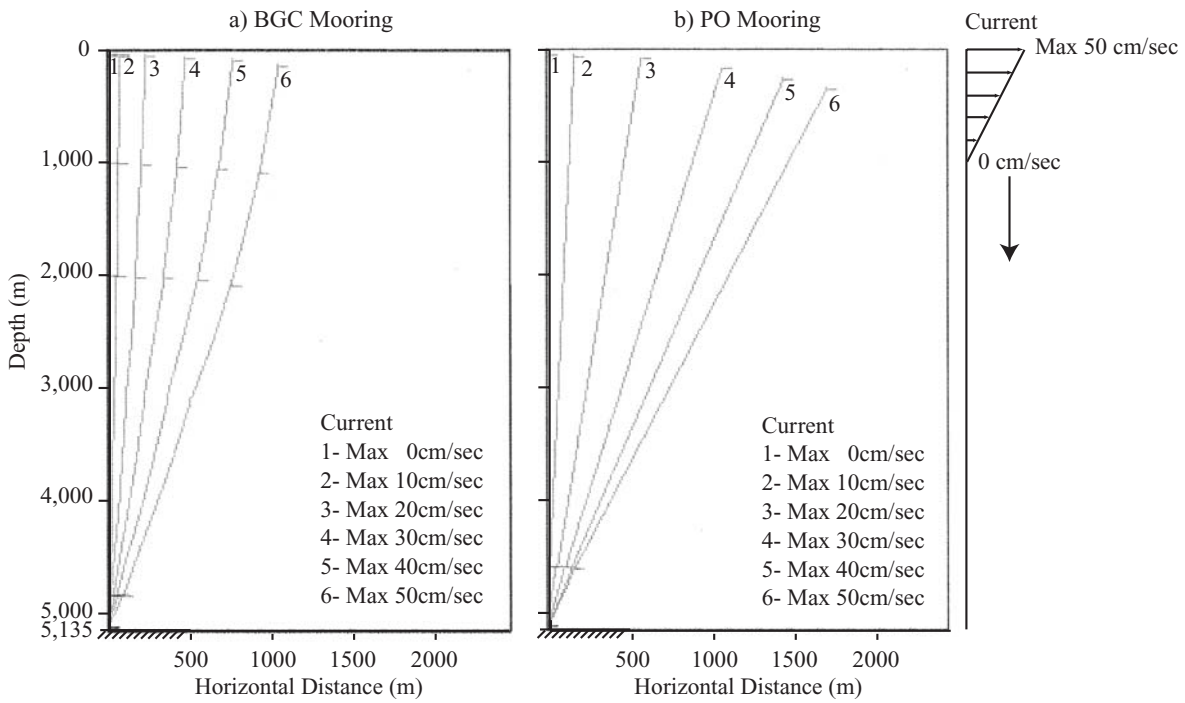

Figure 2: Result of Static Calculation

Table 3: Result of Static Calculation for BGC Mooring

	Current	Top Buoy	Horizontal Distance	SID	WTS	RAS	ZPS	Sediment Trap 1,000m	Sediment Trap 2,000m	Sediment Trap 4,818m	Releaser
1.	0cm/sec	30m	0m	37.9m	39.8m	42.9m	45.4m	1,001m	2,001m	4,819m	5,100m
2.	10cm/sec	31m	72m	38.5m	40.4m	43.5m	46.0m	1,002m	2,002m	4,819m	5,100m
3.	20cm/sec	35m	223m	43.2m	45.1m	48.2m	50.7m	1,006m	2,005m	4,820m	5,100m
4.	30cm/sec	53m	469m	61.0m	62.9m	66.0m	68.5m	1,023m	2,020m	4,821m	5,100m
5.	40cm/sec	90m	754m	97.9m	99.8m	102.9m	105.4m	1,057m	2,050m	4,825m	5,100m
6.	50cm/sec	142m	1,023m	149.5m	151.4m	154.5m	157.0m	1,106m	2,092m	4,830m	5,101m

Table 4: Result of Static Calculation for PO Mooring

	Current	Top Buoy	Horizontal Distance	4,500m Wire Top	4,500m Wire Bottom	Releaser
1.	0cm/sec	50m	0m	58.1m	4,575m	5,097m
2.	10cm/sec	53m	160m	60.6m	4,576m	5,097m
3.	20cm/sec	83m	574m	90.8m	4,578m	5,097m
4.	30cm/sec	161m	1,055m	169.5m	4,585m	5,097m
5.	40cm/sec	258m	1,436m	266.2m	4,595m	5,098m
6.	50cm/sec	346m	1,704m	354.0m	4,600m	5,098m

of PO mooring is smaller than that of BGC mooring. Taking into account for the characteristics of wire rope, suitable segments number should be determined for exact simulation in future.

(3) Behavior analysis of mooring systems during deployment

Behavior of mooring system during deployment was analyzed with software "behavior analysis program for Ocean Acoustic Tomography mooring system" developed by JAMSTEC and Japan Airplane, Inc." (Shinke et al., 1994)[3] in 1981 based on "lumped-mass method" by Kawadate et al.(1987, 1988)[4) 5)].

Tables 5 and 6 show respective parameters for simulation. Mooring system is divided each 500 m. Assuming the external forces such as wave and current velocity are negligible, behavior of mooring system during deployment was simulated (Figs. 3, 4).

After an anchor is dropped into sea surface at "anchor point", anchor descends being pulled toward a top buoy. This motion is called as "Horizontal Return Distance

Table 5: Simulating Parameter of BGC Mooring at K-1

a) Particle	Weight in Air (kg)	Weight in Water (kg)	Cross Section Area (m^2)	Hight (m^2)	Drag coefficient Cd	Added inertia coefficient Tangental	Nomal
Top Buoy	2558	-1360	2.97	1.8	0.5	0.1	0.1
Instruments	392	197	5.91	9.2	1.3	0.1	0.1
Sediment	81	40	3.25	3.5	1.3	0.1	0.1
Sediment	83	42	3.25	3.5	1.3	0.1	0.1
Glass Float	209	-175	10.04	8	0.5	0.1	0.1
Glass Float	102	-89	5.02	4	0.5	0.1	0.1
Sediment	86	45	3.25	3.5	1.3	0.1	0.1
Glass Float	180	-810	35.14	28	0.5	0.1	0.1
Releaser	72	68	0.78	1.9	0.7	0.1	0.1
Anchor	2310	2145	1.04	1.3	1.2	0.4	0.4

b) Line	Length (m)	Size (m)	Mass in Air (kg/m)	Mass in Water (kg/m)	Drag coefficient Tangental	Nomal	Young's modules (kgf/m^2)	Damping ratio D	Segment Stp
ROPE	5	0.04	8.22	8	0.04	2.2	2.00E+04	0.04	1
ROPE	953	0.01	0.23	0.21	0.02	1.1	1.40E+04	0.04	2
ROPE	994	0.01	0.15	0.14	0.02	1.1	1.40E+04	0.04	2
ROPE	1044	0.01	0.15	0.14	0.02	1.1	1.40E+04	0.04	2
ROPE	1500	0.01	0.15	0.14	0.02	1.1	1.40E+04	0.04	3
ROPE	250	0.01	0.15	0.14	0.02	1.1	1.40E+04	0.04	1
ROPE	233	0.01	0.15	0.14	0.02	1.1	1.40E+04	0.04	1
ROPE	5	0.03	3.66	3.54	0.04	2.2	2.00E+04	0.04	1
ROPE	30	0.03	0.39	0.01	0.1	1.1	2.49E+01	0.04	1

Table 6: Simulating Parameter of PO Mooring at K-1

a) Particle	Weight in Air (kg)	Weight in Water (kg)	Cross Section Area (m^2)	Hight (m^2)	Drag coefficient Cd	Added inertia coefficient Tangental	Nomal
Top Buoy	2569	-1349	2.97	1.8	1	0.1	0.1
Glass Float	52	-143	7.53	0.4	1	0.1	0.1
Glass Float	102	-687	35.14	0.4	1	0.1	0.1
Releaser	72	68	0.78	0.4	0.7	0.1	0.1
Anchor	2310	2145	1.04	1.3	1.2	0.4	0.4

b) Line	Length (m)	Size (m)	Mass in Air (kg/m)	Mass in Water (kg/m)	Drag coefficient Tangental	Nomal	Young's modules (kgf/m^2)	Damping ratio D	Segment Stp
ROPE	4525	0.02	0.25	0.08	0.1	1.1	1.40E+04	0.04	9
ROPE	460	0.02	0.25	0.08	0.1	1.1	1.40E+04	0.04	1
ROPE	5	0.03	3.66	3.54	0.04	2.2	2.00E+04	0.04	1
ROPE	30	0.03	0.39	0.01	0.1	1.1	2.49E+01	0.04	1

(HRD)". HRD (between anchor dropped point and actual anchor landing position on the sea floor) were calculated to be 674.0 m and 771.3 m for K-1 and K-3 BGC mooring systems, respectively, and 591.8 m and 662.4 m for K-1 and K-3 PO mooring systems, respectively. The difference of HRD between BGC and PO mooring systems are likely attributed to the difference in hydrodynamic resistance caused by instruments. The longer HRD at station K-3 is likely attributed to a deeper water depth and longer mooring system. Although this computation assumes that mooring systems during deployment is kept straight and ignores the external force and ship speed of approximately 1 knot, it could be expected that HRD was approximately 12 – 14 % of lengths of mooring systems. Therefore we dropped an anchor at approximately distance of 10 % of mooring system length after we passed over a "target position".

3. Preparation

A water depth of mooring point is approximately 5,000 m. In order to locate a top buoy at 30 m, accuracy of the length of mooring system should be less than 0.1 % taking the extension under high tension into account. Efforts were made in lowering errors from an echosounder, mooring position and wire elongation as much as possible.

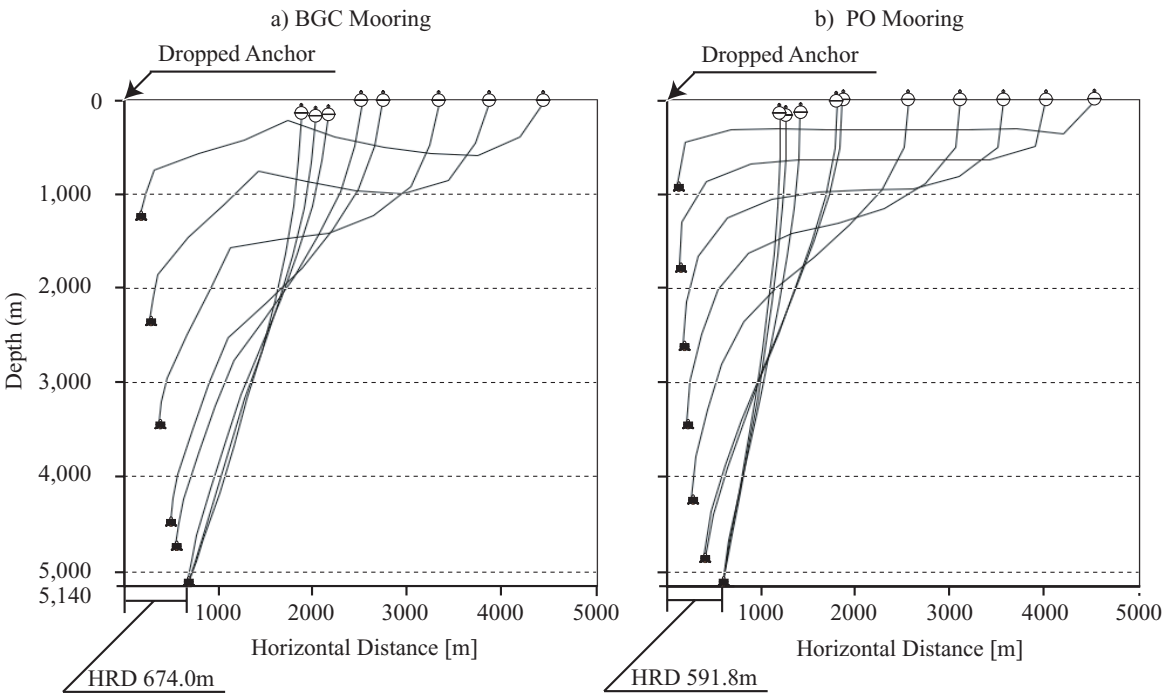

Figure 3: Result of Mooring Deployment simulation program at K-1

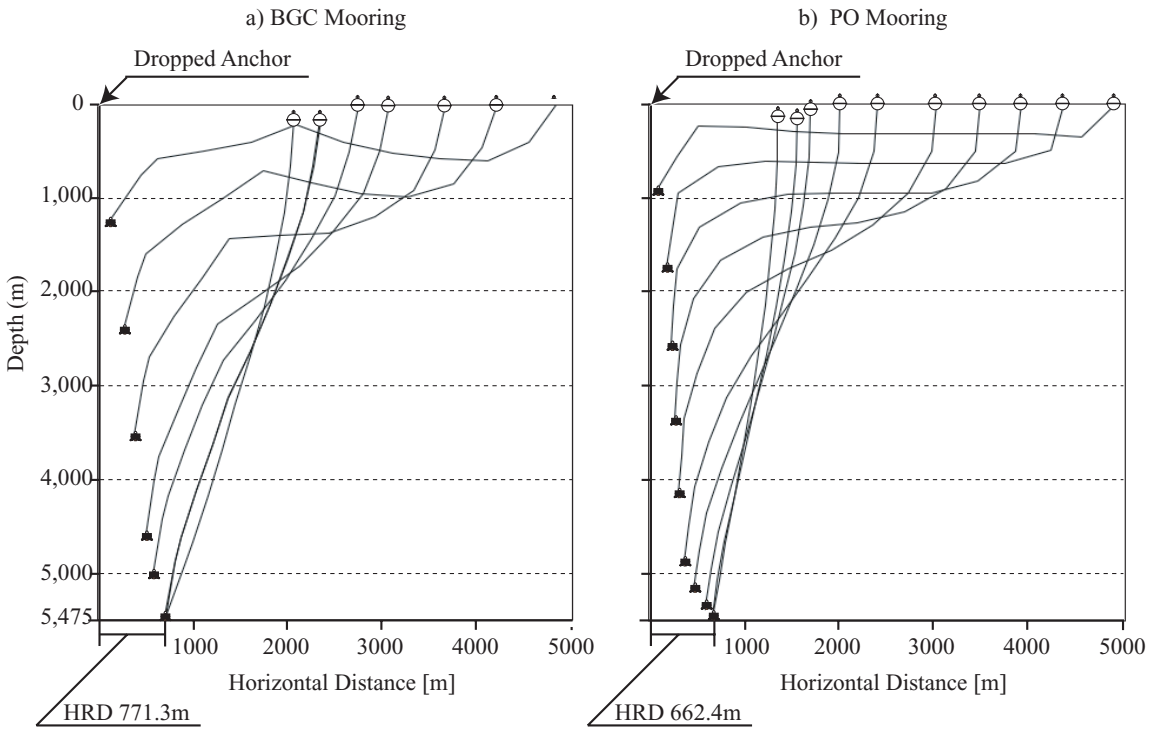

Figure 4: Result of Mooring Deployment simulation program at K-3

3.1 Press work of wire rope terminal

A wire rope terminal was self-made by using " a wire rope lock machine" (Photo 1). A wire rope terminal consists of a galvanized eyebolt and a flexible plastic cover called "boot" (Fig. 5). A "boot" plays a role in reducing bending stress on terminal (Photo 2). After a press work of wire terminal is completed (for certification of its safety), a wire terminal is stretched with 66 % of safe working load by using stretch machine (Fig. 6). This " wire rope lock machine" can work for different wire types (5/16" and 1/4") with using different "dices".

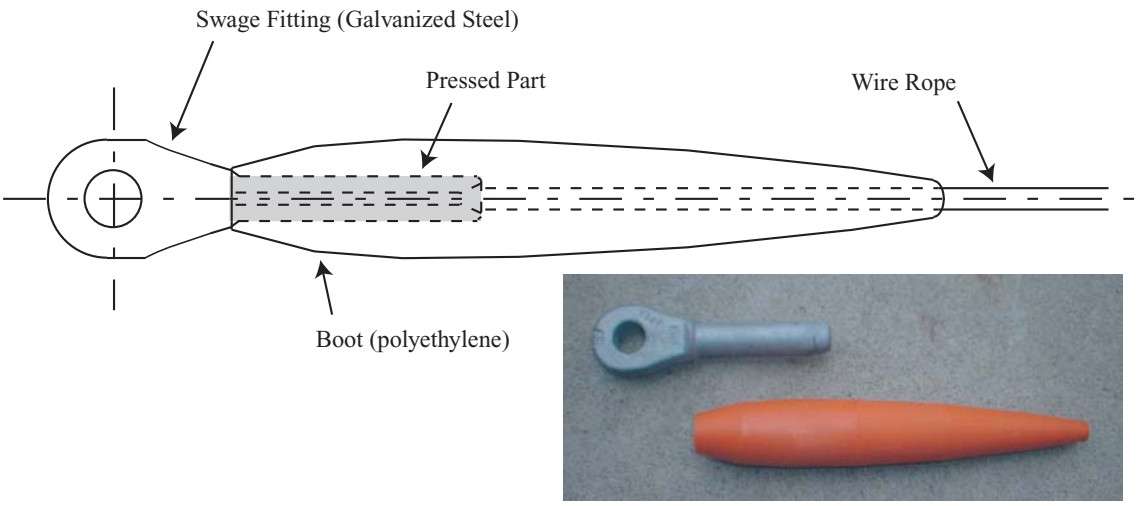

Figure 5: Wire Rope End

Photo 1: Wire Rope Lock Machine

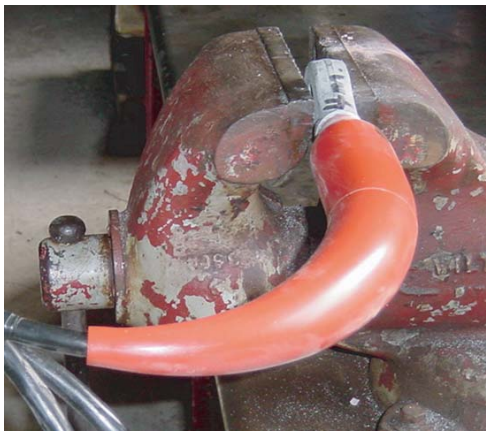

Photo 2: Wire Rope End

3.2 Pre-stretch work

Even if a wire rope is designed and produced based on its specification, some error occurs because of mechanical and human error. In addition, wire and nylon ropes are stretched under high tension. Therefore lengths of all wire and nylon ropes used for mooring system should be measured under high tension on land. This working process is called as “pre-stretch work”. At first, a wire rope is stretched with tension of approximately 1,300 kgf that is a load on mooring system when an anchor descend to the sea floor. Sequentially, tension of 800 kgf that is average load on wire ropes is loaded and its length was measured.

For pre-stretch work, following heavy equipments are needed (Fig. 7).

1) 20 ton semi-truck × 1
2) 10 ton truck × 1
3) Bulldozer × 1
4) Power shovel × 1
5) Power generator (three phase AC 220V) × 1
6) Tension meter (5 ton) × 1
7) Electronic distance meter × 1
8) Wire rope winding machine × 1

Pre-stretch work should be conducted at the place where a wire rope of 500 m is extended and trailer and power shovel can move around. In addition, this place should be sequestered from human habitation for safety. Moreover it should be nearby from Mutsu Institution for Oceanography to load and offload all equipment in the daylight. After investigation, a meadow located in Aomori prefecture (Fureai Grand Farm) was selected.

Pre-stretch working procedure is as follows:

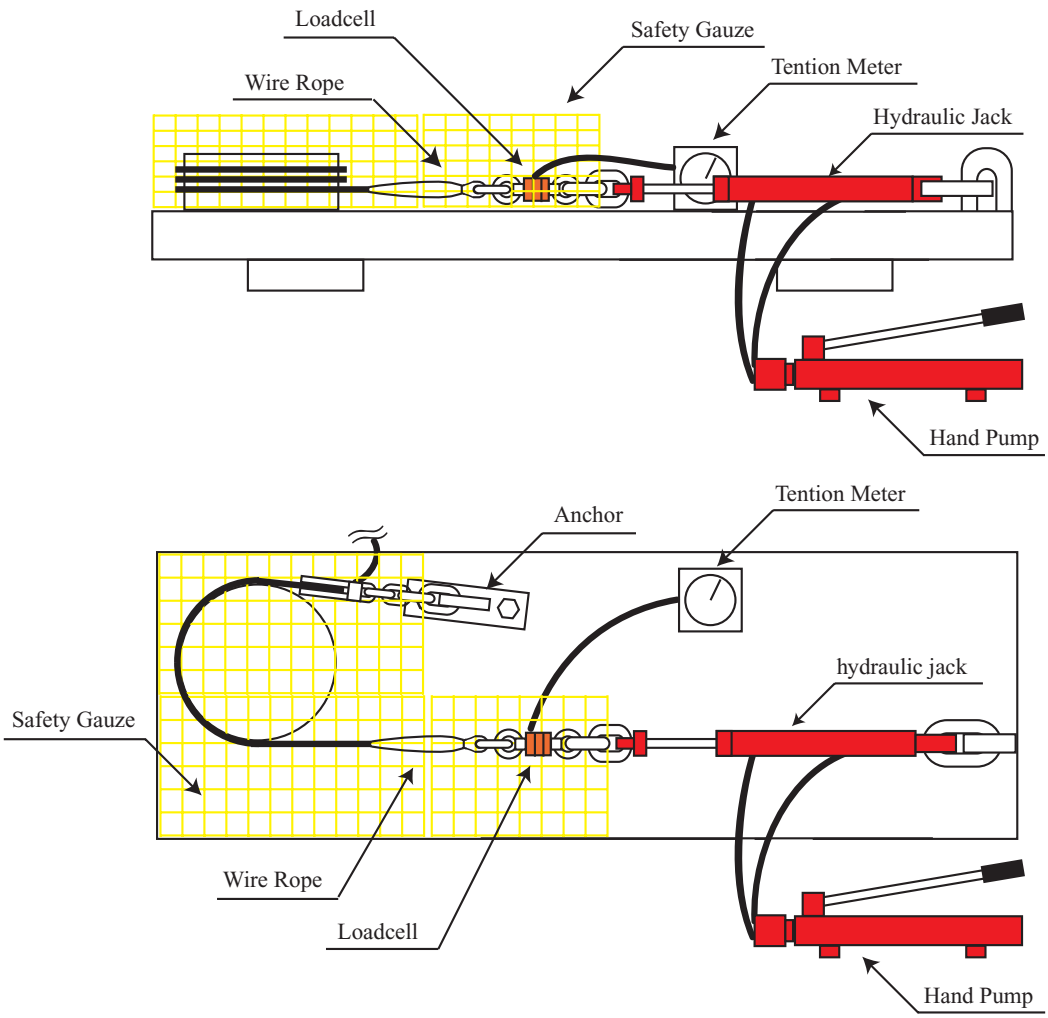

Figure 6: Wire Rope Test Stretch Machine

(1) A 20 ton semi-truck is fixed with handbrake and wheel stoppers.
(2) A top of wire rope is pull out from a winding real fixed on semi-truck by a bulldozer and introduced to a power shovel.
(3) Both ends of wire rope are fixed at a semi-truck and a power shovel.
(4) The power shovel car pulls a wire rope and tension of 90 kgf, 1,300 kgf and 800 kgf, in turn, is loaded on a wire rope.
(5) At tensions of 90 kgf and 800 kgf, lengths of wire ropes are measured by using an electronic distance meter. The former and later are regarded to as lengths of wire rope without and with mooring tension, respectively.
(6) After measurement, the extended wire rope is rewinded by power generator. Other winding real with wire rope is fixed on semi-truck and wire ropes of 4,500, 500, 200, 100 and 50 m are pre-stretched following the above procedure.

3.3 Result of pre-stretch

In this report, lengths of wire ropes under different situation are defined as follows:

Order length (OL): length of a wire rope that we order to a maker or we make initially.

Real length (RL): length of wire rope when wire rope is stretched with low tension of 90 kgf. This length is regarded as real wire length without tension.

Pre-stretch length (Pre): length of wire rope when wire rope is stretched with tension of 800 kgf which is average load on wire ropes (see Table 1 and 2). This length is regarded as wire length during mooring and the final mooring system is designed with Pre.

Table. 7 shows OL, average of RL, difference of RL and OL, average of Pre, difference of Pre and RL and standard deviations of differences. It is hard to estimate Pre-stretch length from only OL for difference of OL and RL is grand value. Even compare with RL and Pre, differences are 1.2 m ± 0.36 (SD) at 500 m which is used frequently and 8.3 m ± 1.4 (SD) at 4,500 m.

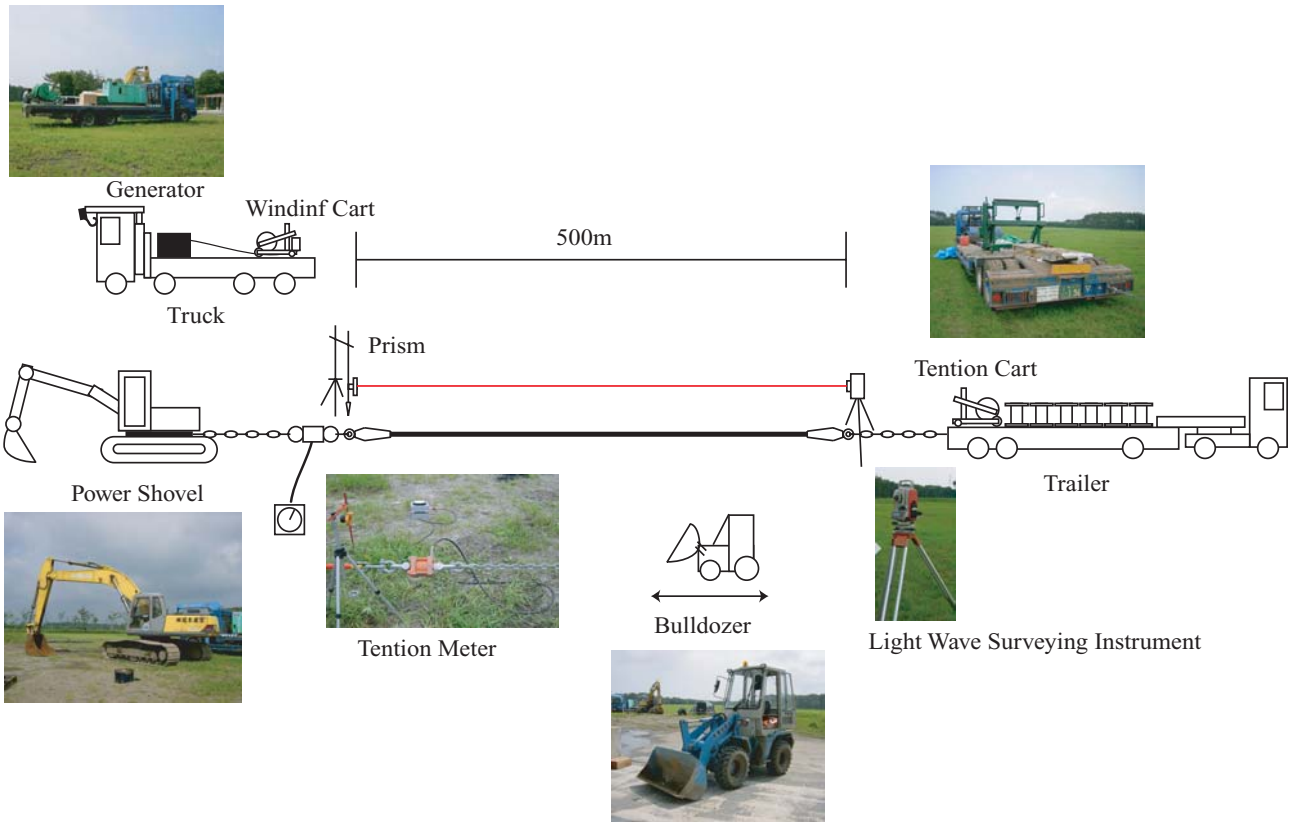

Figure 7: Wire Stretch Working Summary

Table 7: Order Length (OL), Average Real Length (RL), Average Pre-Stretch Length (Pre) and difference of RL-OL and Pre-RL in the Pre-Stretch Working

OL (m)	n	RL (m)	RL-OL (m)	±	Pre (m)	Pre-RL (m)	±
4500	2	4507.62	7.62	2.97	4515.92	8.30 (0.18%)	1.40
500	36	499.03	-0.97	1.08	500.24	1.21 (0.24%)	0.36
417	15	416.11	-0.79	1.29	416.95	0.84 (0.20%)	0.31
200	18	199.24	-0.76	0.32	199.72	0.48 (0.24%)	0.14
100	15	99.74	-0.26	0.07	100.06	0.32 (0.32%)	0.03
50	28	49.94	-0.06	0.16	50.08	0.14 (0.28%)	0.06

Therefore all wire ropes should be pre-stretched to improve the depth of instruments.

4. Deployment work of mooring system

4.1 Determination of target point

There is no point in that a precise length of mooring system is measured if water depth of target point is not measured accurately. In addition, it is impossible to install a mooring system on the target point decide previously and, therefore, a sea floor with flat area of approximately 1 mile radius should be found. Therefore the water depth and ambient bottom topography should be measured precisely. Bottom topography was measured by using a multi narrow beam echo sounding system (SeaBeam 2112.004) installed on R/V Mirai (Fig. 8 and 9). Official measurement error of SeaBeam was still ± 0.5 % even after correction of sound velocity with *in situ* temperature and salinity. It corresponded to 50 m at an area with 5,000 m water depth and is problematic for our mooring system. Instead of SeaBeam, precise water depth was measured with an altimeter (Datasonics PSA900D) installed on the multiple water sampling system with CTD (CTD / CMS). Taking into account for a ship motion, measurement of water depth by the altimeter was conducted several times at several points and final target position was decided. As long as time-series observation with mooring system was continued, we deploy mooring system aiming this target point.

4.2 Deployment procedure

(1) Start position

Essentially the deployment work of mooring system

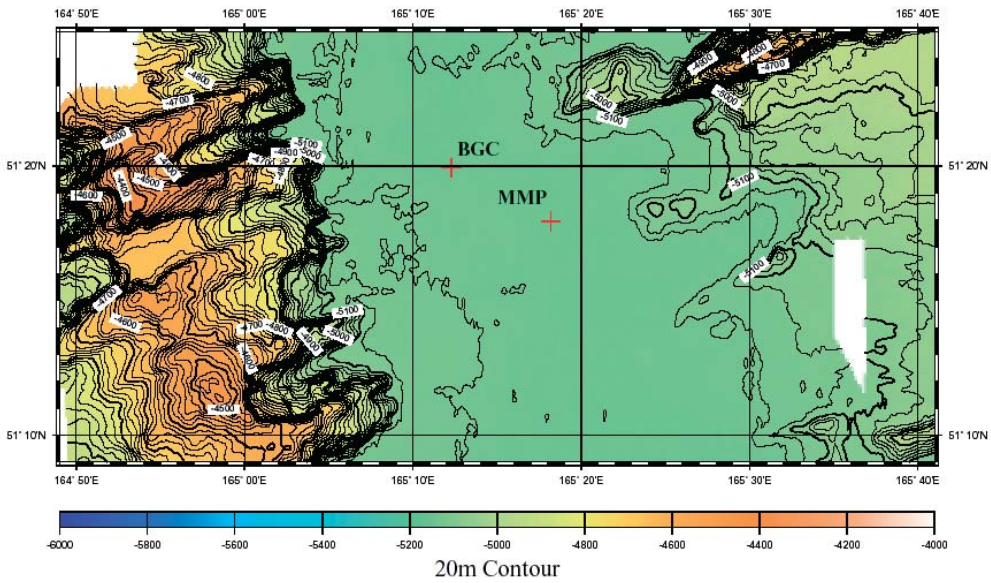

Figure 8: Sea-Beam at Station K-1 from MIRAI MR02-K05 Leg.2 Cruise Report

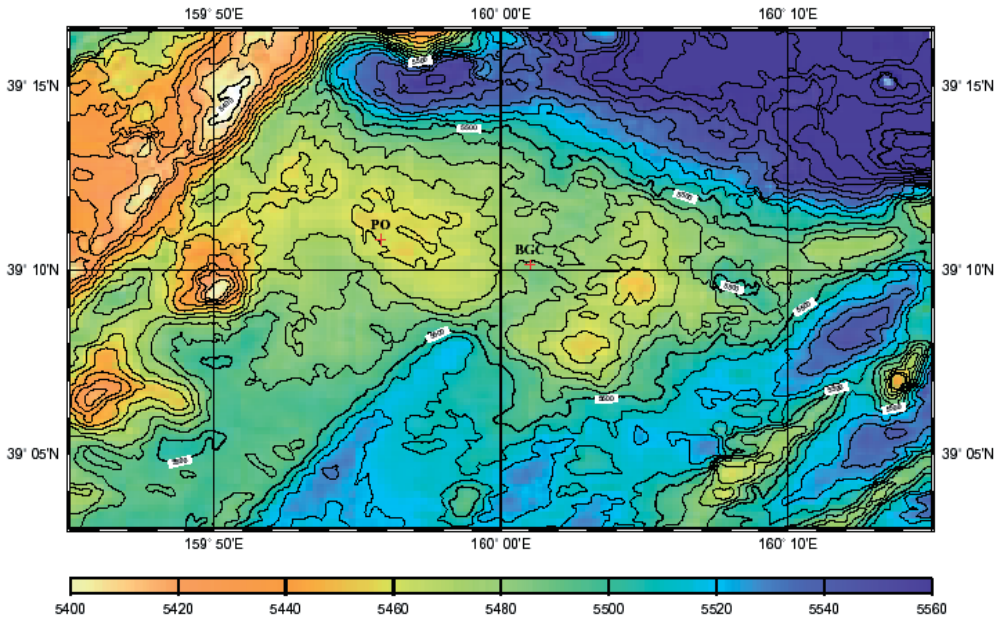

Figure 9: Sea-Beam at Station K-3 from MIRAI MR02-K05 Leg.2 Cruise Report

starts, in other words, a top buoy is dropped approximately 7 miles short of anchor drop point. After a group of grass balls just above a releaser system is dropped, mooring system is towed for approximately one hour in order to make mooring system straight.

(2) Ship speed during deployment

Ship speed relative to water is zero when a top buoy and a series of instruments (SID, RAS, WTS and ZPS) are deployed into the sea. After this step, ship speed is increased to 1 knot extending main wire rope for BGC mooring. Although too much tension on mooring system should be avoided, it is cautioned that slack of wire rope is never caught by ship screw. For PO mooring, ship speed during deployment is 1.5 knot after a top buoy is deployed. This speed is kept until anchor is dropped and, however, sometimes adjusted up to 2 knot depending on tension of mooring system and sea condition.

(3) Ship heading

Essentially ship heading is set to upwind during deployment. However ship heading is changed in order to keep mooring system straight.

(4) Extension of main wire and nylon ropes

Extension of main wires and nylon ropes should be watched carefully verifying its tension, and adjustment

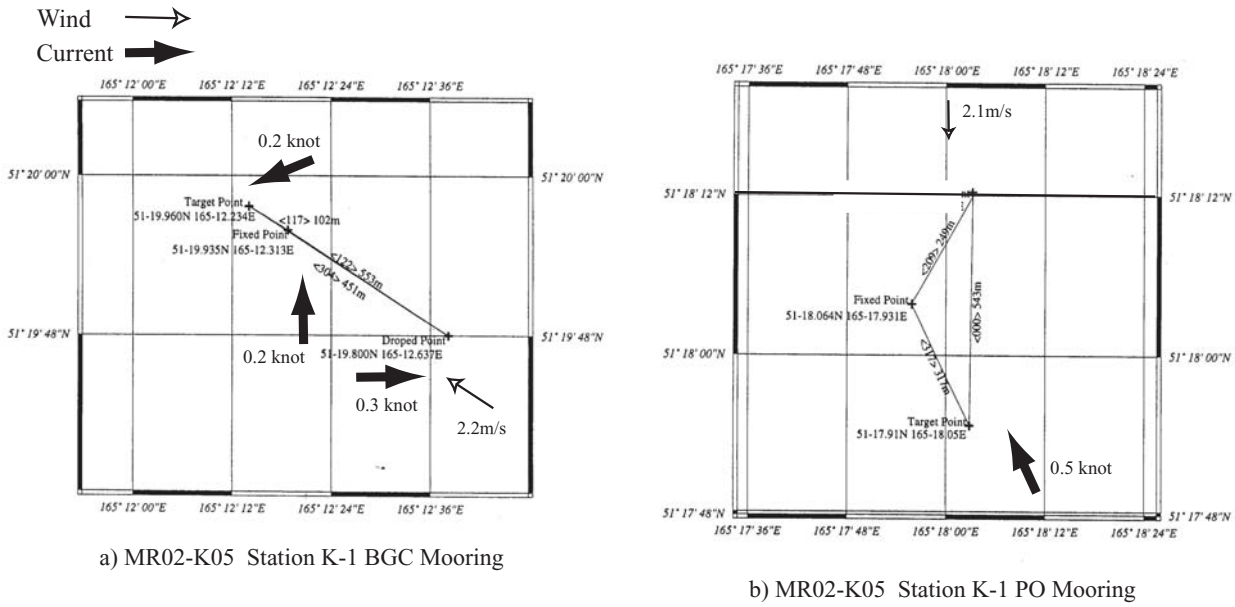

a) MR02-K05 Station K-1 BGC Mooring

b) MR02-K05 Station K-1 PO Mooring

Figure 10: Mooring Fixed Point and Dropped Anchor Point at K-1 from Akamine (2002)[6)]

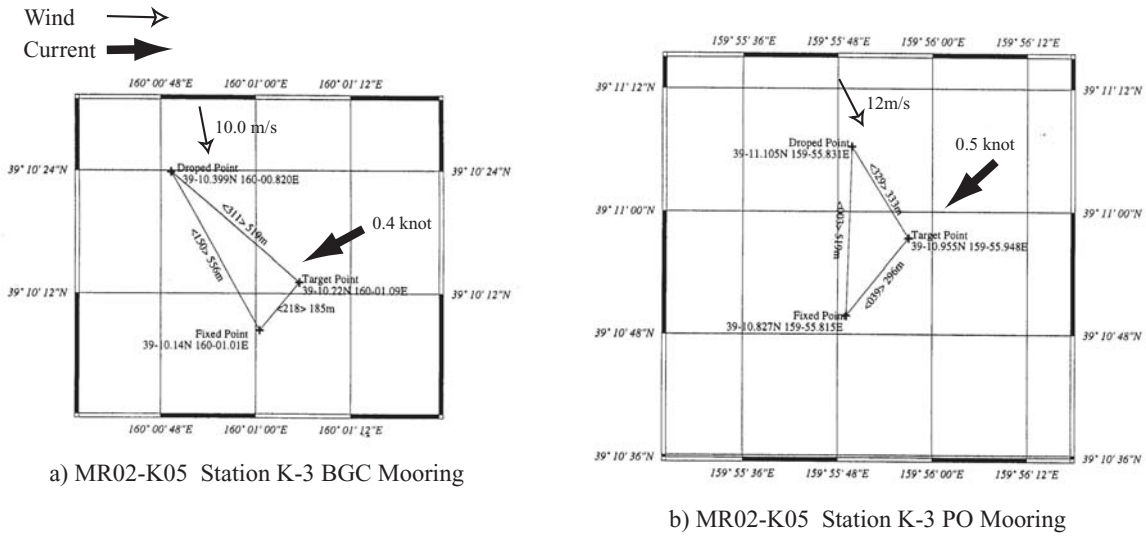

a) MR02-K05 Station K-3 BGC Mooring

b) MR02-K05 Station K-3 PO Mooring

Figure 11: Mooring Fixed Point and Dropped Anchor Point at K-3 from Akamine (2002)[6)]

of tension on mooring system is conducted by rotation speed of winch drum. When terminals of wire rope and nylon rope are connected with other ones, wire ropes is certainly anchored to a cleat on board and tension of mooring system is loaded on this. After a terminal is released from tension, connection is conducted. Groups of glass balls are deployed one by one with two safety ropes.

(5) Anchor drop

Based on results of simulation, an anchor is dropped approximately 10 % of length of mooring system after we passed through target position. An anchor is hung up 0.1 mile short of anchor dropped point and timing of anchor drop is counted down.

(6) Verification of a top buoy submersion under water

After anchor is dropped, we are back to a start point along a cruise truck and we certify that a top buoy disappears (sinks). Usually it takes approximately 1 hour for top buoy to disappear.

(7) Positioning

After a top buoy disappears, we determine a mooring point (fixed point). From 4 – 6 points on the circumference with a radius of 1 mile centering an expected fixed point, a transducer is hung down and slant range between a releaser and a transducer is measured.

(8) Record

In order to refer the next deployment or check deployment procedure, it is recommended that serial

Table 8: Loading Result of used Mooring Line

Material	Size (inch)	Official Working Load Limit (tf)	Official Minimum Braking Load (tf)	Braking Load (tf)	Existance ratio (%)	Braking Extention ratio (%)
Wire Rope	1/4	2.3	3.06	3.26	106.50	7.0
Wire Rope	1/4	2.3	3.06	3.38	110.50	4.0
Wire Rope	1/4	2.3	3.06	3.42	111.80	3.2
Wire Rope	1/4	2.3	3.06	3.38	110.50	4.4
Wire Rope	1/4	2.3	3.06	3.35	109.50	3.8
Wire Rope	1/4	2.3	3.06	3.37	110.10	4.4
Wire Rope	1/4	2.3	3.06	3.17	103.60	3.3
Wire Rope	1/4	2.3	3.06	3.18	103.90	4.2
Wire Rope	1/4	2.3	3.06	3.27	106.90	4.2
Wire Rope	5/16	3.5	3.06	5.56	119.10	4.2
Material	Size	Official Working Load Limit (tf)	Tested Load (tf)	Transform		
Chain	3/4	4.8	6.1	None	-	-
Chain	3/8	3.0	6.1	None	-	-
Chain	1/2	5.1	6.1	None	-	-
Ring	7/8	5.0	6.1	None	-	-
Ring	5/8	3.0	6.1	None	-	-
Shackle	1/2	3.0	6.1	None	-	-
Shackle	5/8	4.5	6.1	None	-	-
Shackle	3/4	6.5	6.1	None	-	-

Table 9: Result of Loading Test

Method	Detail	Maximum Load (tf)	Braking Load (tf)	Elastic Point (tf)	n	Transform
Nondestructive Testing	MT	-	-	-	25	None
	RT	-	-	-	10	None
Loading Test	Normal	-	7.1 ~ 11.7	6.0	16	None
	Repitation	-	11.3 ~ 11.5	6.0	4	None
	Wrest (Photo.3 a)	-	6.8 ~ 9.8	-	2	70% of Spec.
	Widen (Photo.3 b)	-	10.8 ~ 11.7	7.0	9	None
	Cut (Photo.3 c)	-	1.6 ~ 1.8	-	10	20% of Spec.
	Sideway (Photo.3 d)	-	12.3	-	1	None
	Tangle with Shackle (Photo.3 e)	-	11.4	-	1	None
	Shackle (Photo.3 f)	-	15.3 ~ 19.4	10.0	5	None
Construction Test of cross section area	Chain	-	-	-	4	None
	Shackle	-	-	-	2	None
Hardness Test of cross section area	Vickers Hardness	-	-	-	3	None
Tangle Test	with Shackle for 10days	1.6	-	-	2	None
	with Widen for 2weeks	2.7	-	-	1	None
Damege Test	Wrest	4.5	-	-	1	None
	Sideway	4.5	-	-	1	a Little
1/2inch Loading Test	Chain	-	2.4	-	1	10% of Spec.

numbers of instruments, time of respective work are recorded precisely.

5. Results

5.1 Deployment position

Fig. 10 and 11 show the physical relation between a target point (home base), a dropped point that an anchor was dropped from the ship and a fixed point that a mooring system was actually set (Akamine, 2002)[6]. Wind direction / velocity and current direction / velocity were observed by using an anemometer and Acoustic Doppler Current Profiler (ADCP) installed on R/V Mirai, respectively. Going upwind, we deployed a mooring system from a top buoy. On Fig. 10 and 11, current direction and velocity for respective cases are averages during deployment work while those are three representative current direction / velocity in the case of BGC mooring at station K-1. It can be seen that a fixed point was shifted depending on current direction and speed.

The distances between a target point and fixed point for BGC mooring system were 102 m and 185 m at stations K-1 (Fig. 10, a) and K-3 (Fig. 11, a), respectively.

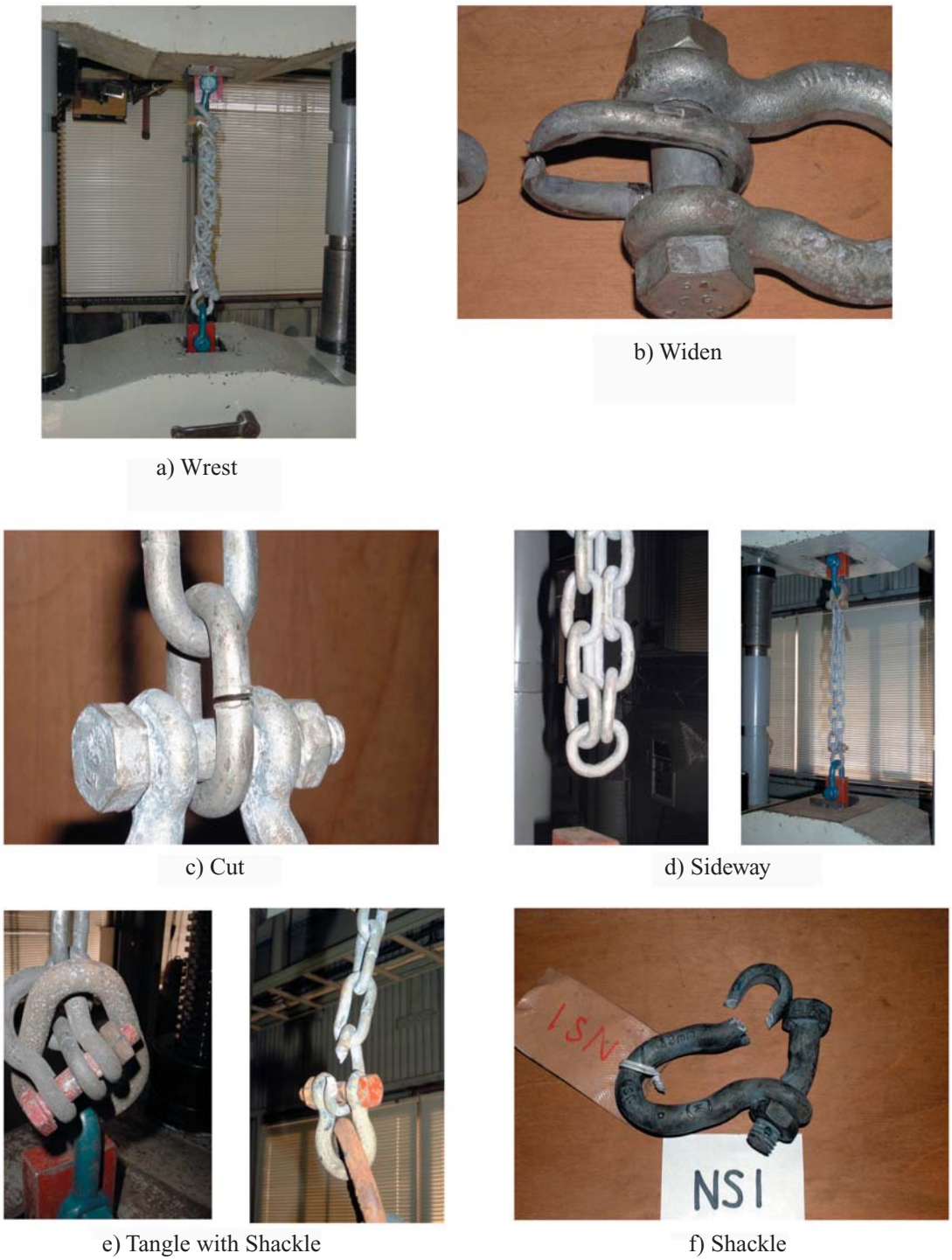

a) Wrest

b) Widen

c) Cut

d) Sideway

e) Tangle with Shackle

f) Shackle

Photo 3: Loading Test

Those distances for PO mooring system were 317 m and 296 m at station K-1 (Fig. 10, b) and K-3 (Fig. 11, b), respectively. These corresponded to approximately 2 % for total BGC mooring system and 6 % of total PO mooring system (*ca*. 5,000 m) and less than that simulated previously (10 %. see 2.2.(3)). In future deployment, drift of mooring system by a current had better be taken into account.

5.2 Strength of used wire rope

In order to verify whether wire ropes used can be reused or not, tensile and break test was conducted for several wire ropes with different diameters (1/4” and 5/16”) used for one year deployment during September 2001 and October 2002. Wire ropes selected at random were tested and measured its extension rate and breaking force (Table 8).

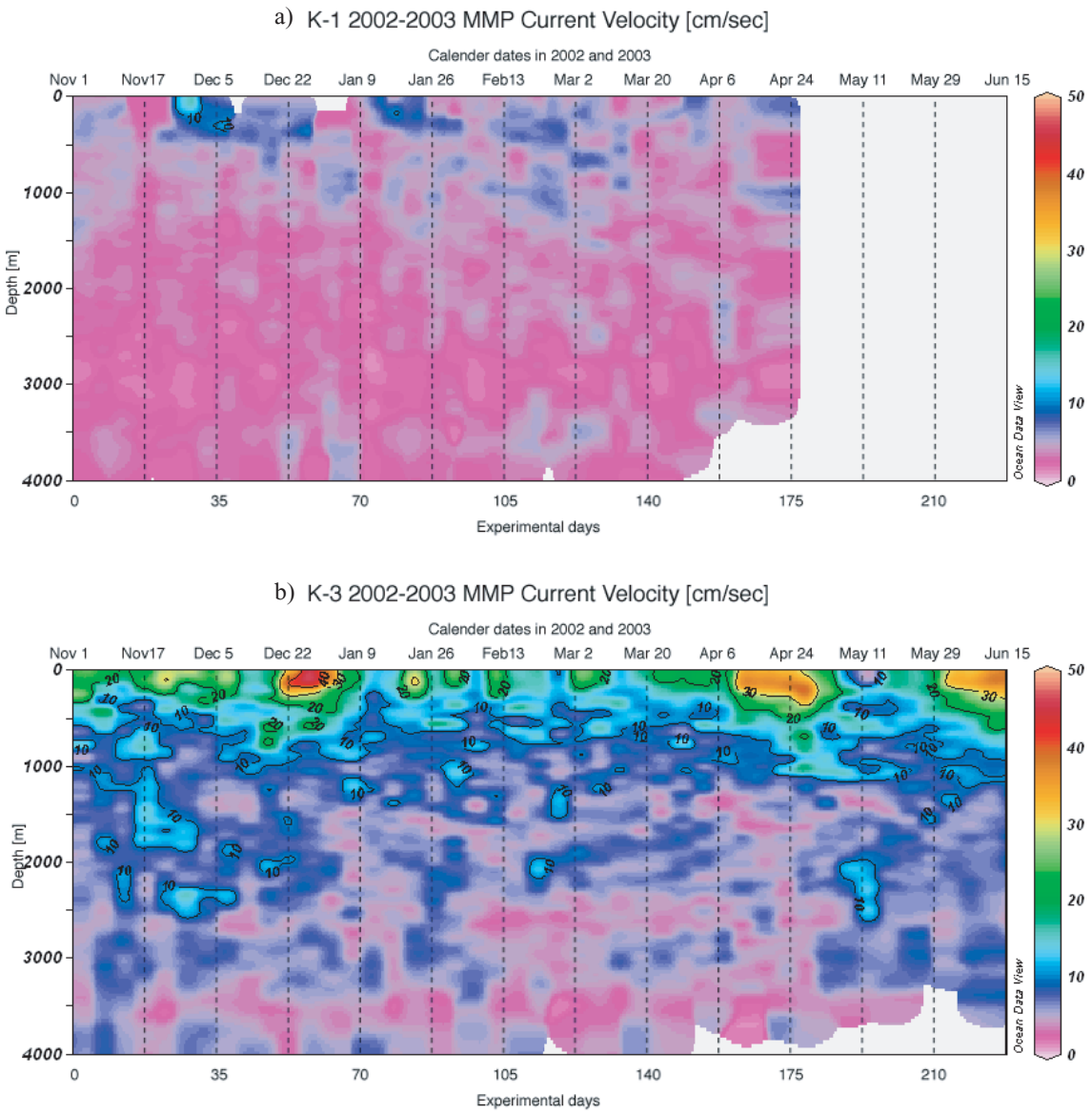

Figure 12: Current Velocity at K-1 and K-3 measured by MMP

As a result, it was verified that 10 wire ropes held initial capability. The break points of all wire ropes were their terminal connecter. Simultaneously chains, shackles and rings used for deployment were also tested and showed no critical skew and crack under safety working load. Even if surface of chains, shackles and rings are oxidized, its capability after one year deployment was still kept. Therefore it was concluded that the above items could be re-used after one year deployment. However it is noted that wire ropes are usually vinyl-coated. It is difficult to detect all damages of vinyl coating from a few thousand meter's wire ropes occurred during deployment and / or recovery work. In this case, a part of wire ropes might be oxidized by water invasion and its capability might be largely lowered. This point should be taken into account.

5.3 Strength test of chain and shackle

The above test for chain and shackle is for certification of their safe working load. In order to verify their breaking load and to observe their physical change under high tension, nondestructive and destructive tests were conducted for chains and shackles used from October 2002 and October 2003.

As a nondestructive test, the magnetic particle examination and the X-ray for chains and shackles were conducted in order to detect or certify cracks, pinhole and condition of welding. In destructive test, chains under various situations such as that chains are entangled, pulled to abnormal direction, force-enlarged, oxidized and loaded for long time. Cross sections of chains before and after loading were also observed microscopically. In addition, "Vickers hardness test" that is a

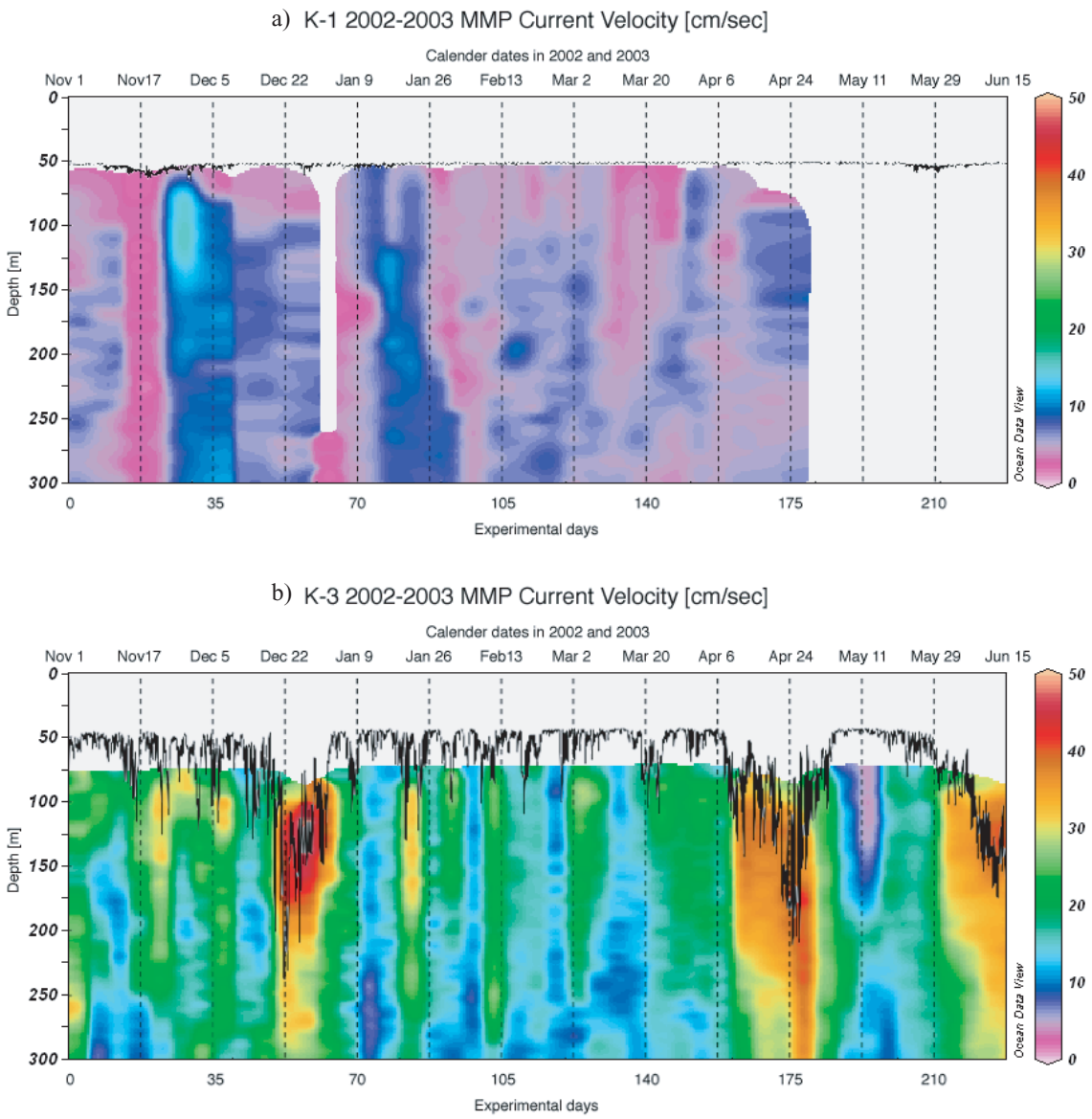

Figure 13: Comparison of Current Velocity and Depth Sensor at K-1 and K-3

measurement of crater size on chain made by press of quadrangular pyramid of diamond was carried out.

Photo 3 and Table 9 show results of nondestructive and destructive test. Based on nondestructive test, new and used chains and shackles did not show problematic damage such as abrasion, contortion and oxidation. Any problems in welding were not observed either. The yield point load of 3/8" chains was approximately 6 ton and chains were partitioned at approximately 10 – 11 ton. However yield point load of entangled chain was smaller than that of normal chain and entangled chain was partitioned at approximately 6 – 7 ton load.

5.4 Analysis of behavior of mooring system during observation

During deployment of 2002 – 2003, current direction / velocity and a water depth of WTS (phytoplankton sampler) were monitored by MMP and a depth sensor (RIGO DS5000), respectively.

Fig. 12 shows time-depth distribution of current velocity. At station K-1, maximum current velocity of 40 cm sec^{-1} was observed at around 100 m during November and December 2002. During this period, current velocity at around 1,000 m and below 1,000 m were 10 cm sec^{-1} and 5 cm sec^{-1}, respectively. At station K-3, between the late of December 2002 and the early January 2003, maximum velocity of 58 cm sec^{-1} was observed at around 100 – 150 m. Current velocity at around 1,000 m was 15 cm sec^{-1} and 10 cm sec^{-1} at even 2,000 m, In general, current velocity at station K-3 was larger than that at K-1.

Fig. 13 shows seasonal variability in depth of WTS

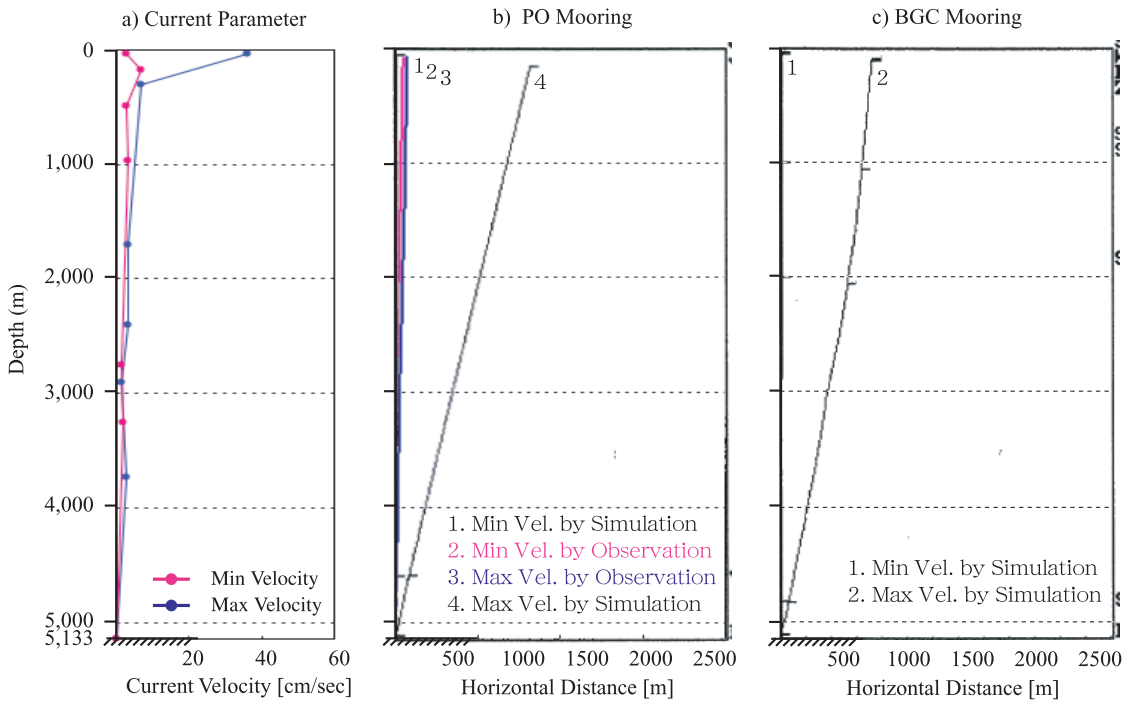

Figure 14: Comparison of MMP current velocity, statics calculation program, current velocity and Tilt at K-1

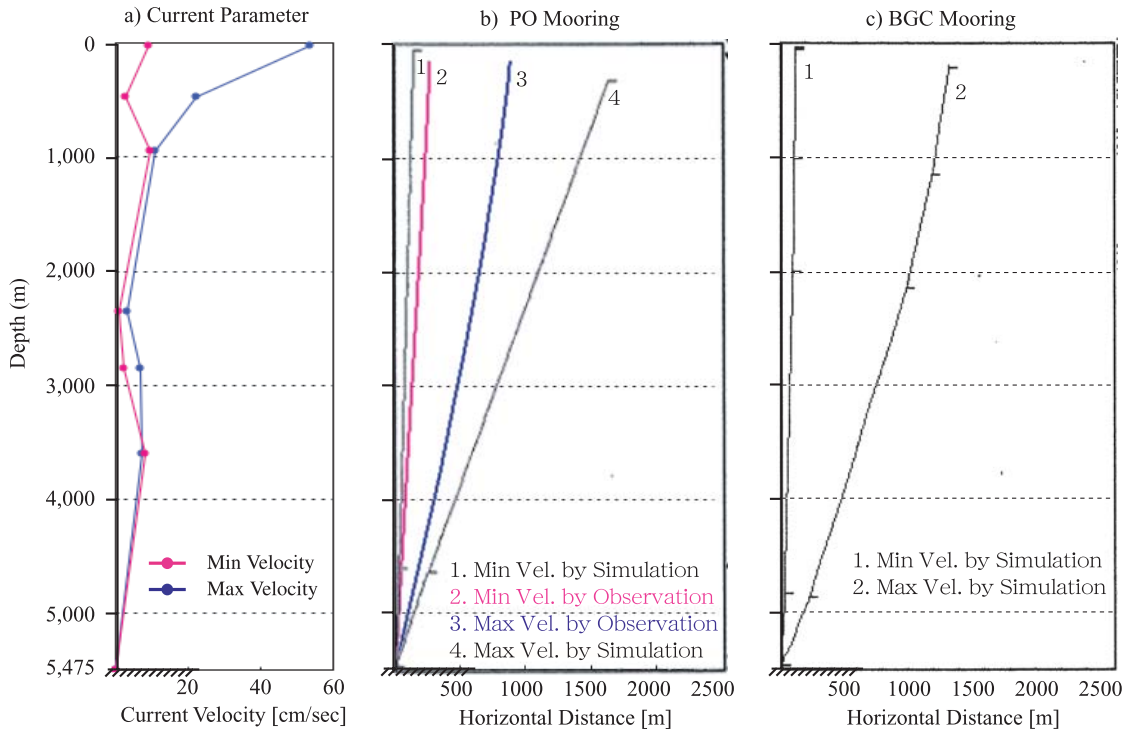

Figure 15: Comparison of MMP current velocity, statics calculation program, current velocity and Tilt at K-3

(solid line) with time-depth distribution of current velocity upper 300 m. Although PO mooring with MMP was a few km away from BGC mooring, a depth of WTS on BGC mooring was deepened when current velocity increased. Average depth of WTS at station K-1 was 60 – 70 m and relatively stable while WTS was sometimes deepened up to more than 200 m when current velocity increased by 50 cm sec^{-1}.

Fig. 14 (a) and Fig. 15 (a) show maximum and minimum current velocity at 6 depths for stations K-1 and K-3, respectively. Assuming that these current directions are identical and using software of behavior analy-

sis (see section 2.2 (2)), tilt, water depth and tension of principal parts were re-simulated (Figs. 14 (b) (c) for K-1 and Figs 15 (b) (c) for K-3). In Figs. 14(b) and 15(b), actual tilt (or shape) of mooring systems observed by MMP are also shown.

During deployment, even when the maximum current was given, maximum inclination by simulation program has never exceeded. Especially, BGC Moorings (Fig. 14 c and 15 c) were as the simulation from only depth of WTS by depth sensor could be compared though. As for calculation not suiting at PO mooring, a current direction is considered.

6. Concluding remarks

Two types of mooring systems (BGC and PO mooring systems) for time-series observation of biogeochemistry in the northwestern North Pacific were designed, constructed with various preparations and deployed / recovered. Two years deployment for approximately 10 mooring systems revealed that a main purpose that an upper part of mooring system with time-series instruments are located within upper euphotic zone were accomplished. It was also verified that quality of materials used for mooring system was kept after 1- year deployment.

However high current velocity deepened a top buoy of BGC mooring systems by 200 m several times a year. Although correction such as current direction is required, all moorings were prediction within the limits of a simulation program.

Acknowledgement

Although mooring masters from Woods Hole Oceanographic Institution conducted mooring work (deployment and recovery), mooring works was never conducted successfully without enthusiastic works of ship crew of R/V MIRAI and R/V KAIREI. We also thank administrative staff of Mustu Institute for Oceanography for their support on paper works.

References

1) Ito, A., Takao, K., Yoneyama, K., Ando, K., Kawano, T. and Kuroda, Y., "Design for Subsurface Mooring with an Acoustic Doppler Current Profiler and Its Motions in the Open Sea", Report of JAMSTEC, **32** p.27-38 (1995).
2) Imawaki, S., "Mooring Operations of the Woods Hole Oceanographic Institution", Journal of Oceanography, **8**, p.340-350 (1976).
3) Shinke, T., Nakamura, T. and Nakano, I. "Falling Motion Analysis of the Mooring System for Ocean Acoustic Tomography", Journal of the Japan Society for Marine Surveys and Technology, **6** (2) p.1-11 (1994).
4) Kawadate, K., Nagahama, T., Ishii, H., Shinozaki, T., Tashiro, A., "The two-dimension dynamic calculating method of line used all over the sea", the Kyushu University application power research report, **63**, p.179-188 (1987).
5) Kawadate, K., Hashimoto, Y., Nagahama, T., Ishii, H., Shinozaki, T., Tashiro, A., "The dynamic simple calculating method used for a mooring line construction problem", the Kyushu University application power research report, **66**, p.131-144 (1988).
6) Akamine, M., "Ship's Handling for Deployment MMP/BGC Moorings", MR02-K05 Leg.2 10.Oct.-6.Nov.2002 Preliminary Cruise Report, p.154-186, JAMSTEC (December 2002).

(Received December 14, 2004)

Geochemical Journal, Vol. 38, pp. 581 to 592, 2004

Particulate organic carbon fluxes estimated from ^{234}Th deficiency in winters and springs in the northwestern North Pacific

HAJIME KAWAKAMI,[1]* YOUNG-LIANG YANG,[2,3] MAKIO C. HONDA[4] and MASASHI KUSAKABE[2,5]

[1]Mutsu Institute for Oceanography, Japan Agency for Marine-Earth Science and Technology, 690 Aza-kitasekine, Oaza-sekine, Mutsu 035-0022, Japan
[2]Department of Ocean Research, Japan Agency for Marine-Earth Science and Technology, 2-15 Natsushima-cho, Yokosuka 237-0061, Japan
[3]Department of Environmental Science, Qingdao University, Qingdao, Shandong Province 266071, People's Republic of China
[4]Mutsu Institute for Oceanography, Japan Agency for Marine-Earth Science and Technology, 2-15 Natsushima-cho, Yokosuka 237-0061, Japan
[5]Nakaminato Laboratory, National Institute of Radiological Sciences, 3609 Isozaki-cho, Hitachinaka 311-1202, Japan

(Received November 4, 2003; Accepted June 2, 2004)

Activities of particulate and dissolved ^{234}Th and concentrations of particulate organic carbon (POC) were measured in the northwestern North Pacific in winters and springs. The export fluxes of POC from surface waters were estimated by using ^{234}Th as a tracer. The POC fluxes in winter showed a wide variation (20–190 mg-C $m^{-2}d^{-1}$) and were higher in the western region than in the eastern region. The influence of the Oyashio Current and the supply of substances from the continent to the study area also appeared to be higher in the western region. Therefore, the horizontal distribution of POC fluxes in winter was influenced by continental materials. In the spring bloom, the fluxes of POC were much higher (up to 520 mg-C $m^{-2}d^{-1}$), as were the e-ratios (up to 70%). In the northwestern North Pacific, the efficiencies of export of POC from the euphotic zone were higher than in other areas of the world ocean. The increase in POC fluxes in spring was considered to depend not only on the increased abundance of phytoplankton, but also on the transition of phytoplankton species, as evidenced by the relationship between ^{234}Th adsorption rates and the concentrations of POC.

Keywords: ^{234}Th, POC, PON, export production, northwestern North Pacific

INTRODUCTION

Global warming due to the increase of greenhouse gases, such as carbon dioxide, in the atmosphere is of great concern to the world community. Over the past few decades, the carbon cycle in the ocean has been studied to clarify the balance between carbon dioxide in the atmosphere and that in the ocean. In order to better understand the processes of carbon transport to the deep ocean, in particular, it is essential to estimate the efficiency of the biological CO_2 pump in the ocean surface.

The northern North Pacific Ocean, especially its western part, has been attracting the attention of biogeochemists because of its importance in global biogeochemical cycles of carbon and related substances. Characterized by intense winter cooling and supply of nutrients by upwelling, the northwestern North Pacific Ocean is thought to make a significant contribution to the global CO_2 sink in winter. It is well documented that the spring blooms, consisting mainly of diatoms, occur only in the western part of the subarctic Pacific (Saito *et al.*, 2002; Yamaguchi *et al.*, 2002). Owing to their relatively large size and thus high settling velocity, diatoms may play a key role in the area in transporting particulate organic carbon (POC) to the interior of the ocean (e.g., Tsunogai and Noriki, 1991; Kemp *et al.*, 2000; Smetacek, 2000).

Previous methods for measuring the export flux relied on sediment traps deployed at relatively shallow depths (*ca.* 200 m) or floating sediment traps. However, such shallow traps have many problems associated with hydrodynamics and the invasion of predatory zooplankton ("swimmers"). Buesseler and co-workers have reported the biases in the quantity and quality of material caught in floating traps (Buesseler, 1991, 1998; Buesseler *et al.*, 1994), and proved that the ^{234}Th method works best for estimating particle export from the euphotic zone (Buesseler *et al.*, 1998). ^{234}Th is a short-lived (half-life = 24.1 d) radionuclide that can serve as a valuable tracer for studying the rates of particle-associated scavenging processes and the subsequent export of particles from the euphotic zone (Bhat *et al.*, 1969; Matsumoto, 1975; Coale and Bruland, 1985, 1987; Bacon *et al.*, 1996; Murray *et*

*Corresponding author (e-mail: kawakami@jamstec.go.jp)

Copyright © 2004 by The Geochemical Society of Japan.

al., 1996; Buesseler *et al.*, 1998). This tracer is introduced into the water column as a dissolved species arising from the radioactive decay of the conservative ^{238}U in seawater, and it is redistributed between the dissolved and particulate phases depending on the reactivity of the particles and the availability of particle surfaces.

Global estimates of POC fluxes derived from ^{234}Th measurements have been carried out in the North Atlantic Bloom Experiment (NABE) (Buesseler *et al.*, 1992), the Equatorial Pacific Process Study (EqPac) (Buesseler *et al.*, 1995; Bacon *et al.*, 1996; Murray *et al.*, 1996), the Bermuda Atlantic Time-series Study (BATS) (Michaels *et al.*, 1994; Buesseler, 1998), the Arabian Sea Process Study (Buesseler *et al.*, 1998; Lee *et al.*, 1998), the Northeast Water Polynya off Greenland (Cochran *et al.*, 1995), the Antarctic Ocean (Rutgers van der Loeff *et al.*, 1997), and the northeastern North Pacific (Station Papa) (Charette *et al.*, 1999). The results of those studies indicate that the ratios of POC export to primary production (e-ratios) fall in the range of <5–10% in much of the ocean (Buesseler, 1998); these ratios are significantly higher at high latitudes and during episodic export pulses such as spring blooms. Several studies have revealed the importance of diatoms in association with POC export (Buesseler, 1998; Charette *et al.*, 1999; Amiel *et al.*, 2002). However, the estimates of export production in the northwestern North Pacific are poorly constrained. Information on the magnitude and rate of export production in bloom and non-bloom periods is important because it can reveal general information about the structure of the phytoplanktonic community and provide estimates of this region's contribution to global export production.

The purpose of this study was to evaluate the spatial variation of POC fluxes estimated by the ^{234}Th method in winter and in a spring bloom in the northwestern North Pacific. In this paper, we present profiles of ^{234}Th (in both dissolved and particulate form), POC, and particulate organic nitrogen (PON) in the northwestern North Pacific and the Okhotsk Sea. Sampling was conducted during the winter seasons of 1997, 1998, and 2000, and during a spring bloom in 1999 and 2000. We estimate the export fluxes of POC and PON out of the euphotic zone and discuss the effects of changes in planktonic species on the behavior of ^{234}Th in the euphotic zone during the spring bloom.

Sampling and Analysis

Water sampling

Samples were collected during the R/V *Mirai* cruises MR97-02 (Nov. 1997), MR98-K01 (Nov.–Dec. 1998), MR99-K02 (May 1999), MR00-K01 (Jan. 2000), and MR00-K03 (May–Jun. 2000) in the northwestern North Pacific and Okhotsk Sea. Sampling stations for the cruises

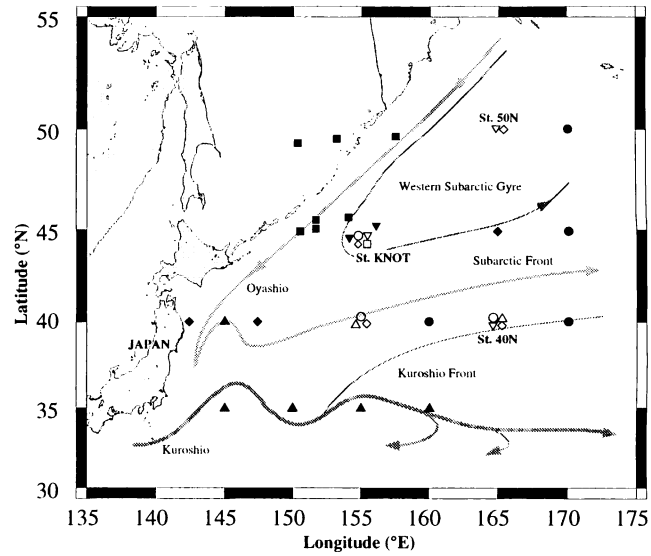

Fig. 1. Sampling locations in the northwestern North Pacific. ● Nov. 1997 (MR97-02); ▲ Nov.–Dec. 1998 (MR98-K01); ▼ May 1999 (MR99-K02); ◆ Jan. 2000 (MR00-K01); ■ May–Jun. 2000 (MR00-K03). The open symbols clustered together are at the same position. The lines with arrows show ocean currents.

are shown in Table 1 and Fig. 1. Hydrographic parameters were simultaneously measured at each station. During the MR97-02, MR98-K01, and MR00-K01 cruises, surveys were carried out to clarify the spatial variation of ^{234}Th in the northwestern North Pacific in winter. In the spring of 1999, we carried out an intensive survey of a spring bloom (MR99-K02). In 2000, we had the opportunity to survey the area along the Kuril Islands inside the Okhotsk Sea and the Pacific.

Sample analysis

Seawater samples, taken by 30-L Niskin bottle samplers from the upper 300 m (at some stations, 200 m) of the water column, were immediately filtered through precombusted (4 h at 450°C) Whatman GF/F glass fiber filters (0.7 μm nominal pore size) of 47-mm (for ^{234}Th) or 25-mm diameter (for POC, PON, and chlorophyll *a*). After filtration, water samples were acidified with HCl to pH 1, and ^{230}Th yield tracer (2–4 dpm) and 100 mg Fe (as $FeCl_3$) were added. Then ammonia was added to the water samples to induce precipitation. The particulate samples collected on the filters for the measurement of ^{234}Th were digested with a mixture of concentrated HCl and HNO_3 in the presence of ^{230}Th yield tracer. Subsequently, radiochemical separation and purification of the nuclides were achieved by procedures similar to those of Anderson and Fleer (1982) using an anion ion exchange technique. Column separation was carried out on board to remove

Table 1. Sampling locations and POC export fluxes from the euphotic zone in the northwestern North Pacific

Station	Location	Date	Euphotic zone# (m)	^{234}Th fluxes (dpm m^{-2}day^{-1})	POC/^{234}Th (μg-C dpm^{-1})	POC fluxes (mg-C m^{-2}day^{-1})	Remarks
(MR97-02)							
Stn. 1	40°N, 155°E	12 Nov., 97	100	2100	71	150	
Stn. KNOT	44°N, 155°E	16 Nov., 97	100	1200	100	120	
Stn. 3	40°N, 160°E	18 Nov., 97	100	1200	65	81	
Stn. 4	40°N, 165°E	19 Nov., 97	100	760	62	47	
Stn. 7	50°N, 170°E	24 Nov., 97	75	540	90	49	
Stn. 8	45°N, 170°E	26 Nov., 97	100	1100	72	81	
Stn. 9	40°N, 170°E	28 Nov., 97	100	730	67	49	
(MR98-K01)							
Stn. 8	40°N, 145°E	20 Nov., 98	100	2600	74	190	
Stn. 10	35°N, 145°E	25 Nov., 98	100	2100	80	170	
Stn. 11	35°N, 150°E	26 Nov., 98	100	1200	47	54	
Stn. 14	40°N, 155°E	30 Nov., 98	100	1300	51	66	
Stn. 16	35°N, 155°E	2 Dec., 98	100	1300	74	96	
Stn. 17	35°N, 160°E	3 Dec., 98	150	660	34	23	
Stn. 20	40°N, 165°E	8 Dec., 98	150	690	51	35	e-ratio = 15%
(MR99-K02)							
Stn. KNOTL	44°N, 154.5°E	12 May, 99	100	2200*	150	330	
Stn. 50N	50°N, 165°E	17 May, 99	100	460*	83	38	
Stn. 40N	40°N, 165°E	20 May, 99	100	1600*	87	140	
Stn. KNOT2	44°N, 155°E	25 May, 99	100	1700*	210	350	e-ratio = 70%
Stn. HP2	44.3°N, 156.2°E	27 May, 99	100	1600*	320	520	e-ratio = 70%
(MR00-K01)							
Stn. 1	40°N, 142.5°E	6 Jan., 00	150	2100	82	170	
Stn. 2	40°N, 147.5°E	13 Jan., 00	100	790	100	82	
Stn. KNOT	44°N, 155°E	17 Jan., 00	75	260	90	23	e-ratio = 45%
Stn. 14	40°N, 155°E	23 Jan., 00	150	750	89	67	
Stn. 6	50°N, 165°E	26 Jan., 00	100	390	78	30	
Stn. 7	45°N, 165°E	28 Jan., 00	100	370	87	32	
Stn. 8	40°N, 165°E	30 Jan., 00	150	1300	72	95	
(MR00-K03)							
Stn. KNOT	44°N, 155°E	11 May, 00	100	580	100	61	
Stn. 6	44.8°N, 150.8°E	15 May, 00	150	870	140	120	
Stn. 8	48.5°N, 150.5°E	17 May, 00	100	220	89	19	Okhotsk Sea
Stn. 11	45.5°N, 152.2°E	19 May, 00	75	95	120	12	an eddy
Stn. 12	45.2°N, 152.8°E	20 May, 00	100	140	100	15	an eddy
Stn. 17	49°N, 153.2°E	31 May, 00	60	280	100	30	Okhotsk Sea
Stn. 22	49.1°N, 157.9°E	1 Jun., 00	100	2100*	270	560	
Stn. 15	46°N, 154°E	4 Jun., 00	100	2600*	170	430	

**Non-steady-state model used to calculate ^{234}Th flux.*
#Thickness of euphotic zone used for flux calculations.

^{238}U from the dissolved samples. The rest of the sample purification for dissolved and particulate ^{234}Th was performed in the land-based laboratory at the Japan Marine Science and Technology Center (now the Japan Agency for Marine-Earth Science and Technology). Finally, alpha sources were prepared by using TTA extraction and plating onto stainless steel planchets.

The planchets were covered with aluminum foil (6.6 mg cm^{-2}) and first beta-counted using a low background (0.1–0.3 cpm), anticoincidence, gas-flow beta detector to determine their ^{234}Th activity, and then alpha-counted with silicon surface barrier detectors to determine the yield from the ^{230}Th activity. To check the accuracy and precision of the ^{234}Th determination, we analyzed two equilibrated deep-water samples with the techniques described above. The results were also used to determine the beta/alpha ratios of the detectors. Calibrations for instrument counting efficiencies (β/α ratio), ^{234}Th decay correction,

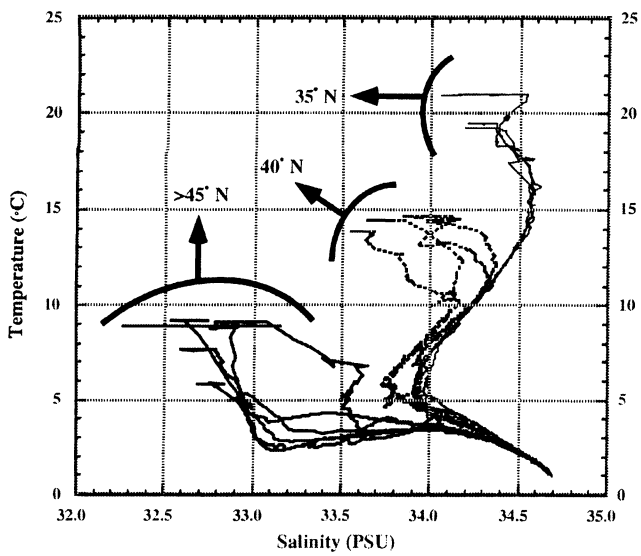

Fig. 2. T-S diagram for water masses in the western North Pacific in Nov. 1997.

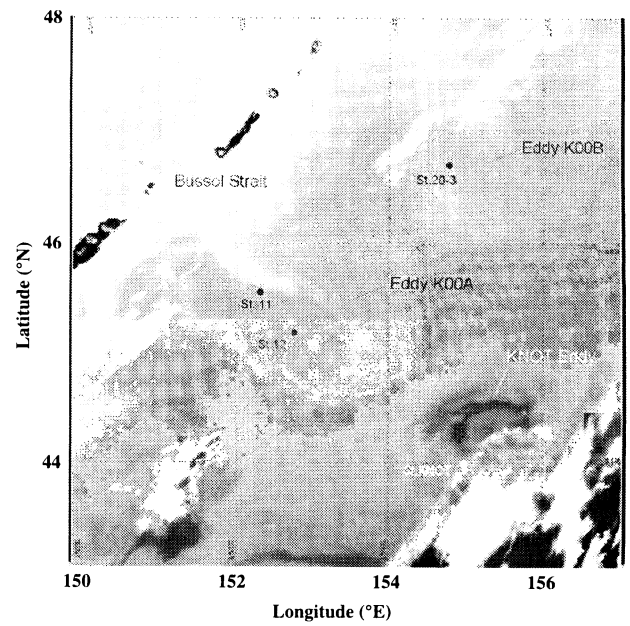

Fig. 3. Mesoscale eddies off the Kuril Islands as shown in an NOAA AVHRR infrared satellite image for 29 May 2000 (UTC). Light shades of gray correspond to cold water. The clouds are white and warm water is dark. Locations of some stations for the MR00-K03 cruise are shown.

and ^{234}Th ingrowth correction were also made. All reported errors are within 1 standard deviation based on the propagation of alpha- and beta-counting errors and the corresponding uncertainties in background, detector blanks, and efficiency as well as errors in spike calibrations.

The samples for POC and PON analyses were stored frozen until analysis. POC and PON were measured with a CHN analyzer (Grasshoff *et al.*, 1999). Before the measurements, the particle samples were treated with the vapor of concentrated HCl for 24 h to remove calcium carbonate, and dried under vacuum at 40°C for 3 h.

Oceanographic Setting of the Study Area

General oceanographic setting

In the study area, two western boundary currents, the Kuroshio and the Oyashio, are associated with subtropical anticyclonic and subarctic cyclonic gyres, respectively (Fig. 1). These currents interact with each other, resulting in a system of a complex frontal structure and mixing of water masses, known as the Kuroshio–Oyashio confluence region (Kawai, 1972). To the north of this region, the Oyashio carries waters originating in the Western Subarctic Gyre and the Okhotsk Sea to the southeast coast of Hokkaido. This Oyashio Water is cold and nutrient-rich, leading to high abundance of phytoplankton and high trophic levels, and is one of the most productive waters of the world ocean (Saito *et al.*, 2002; Yamaguchi *et al.*, 2002). In contrast, the region that comprises the Subtropical Water, south of the Kuroshio Current, is made up of warm, highly saline water. In general, the upper water column of the Subtropical Water is well stratified, severely constraining the vertical mixing of nutrient-rich water essential for phytoplankton growth.

Water masses in the surface can be classified into three groups (Fig. 2). The first group is characterized by high temperature and high salinity influenced by the Kuroshio water and is located around 35°N. The second group has low temperature and low salinity, indicative of the Subarctic Gyre Water, and is located in the regions of >45°N. The third group has characteristics of a mixture of the above two water masses, and is located in the Subarctic Front (40°N).

In addition, mesoscale anticyclonic eddies off the Kuril Islands make the water structure in the area even more complex (Fig. 3). Kusakabe *et al.* (2002) have shown that the boundaries of the eddies are composed of highly productive coastal Oyashio water, and encompass low-temperature Okhotsk Sea water.

Hydrographic properties during the spring bloom

The waters in the region have significant seasonal variations. The biogeochemical cycle of carbon in this region reflects these variations in physical parameters and biological activity. Surveys of a spring phytoplankton bloom were carried out over two separate periods during the MR99-K02 cruise. A variety of measurements were

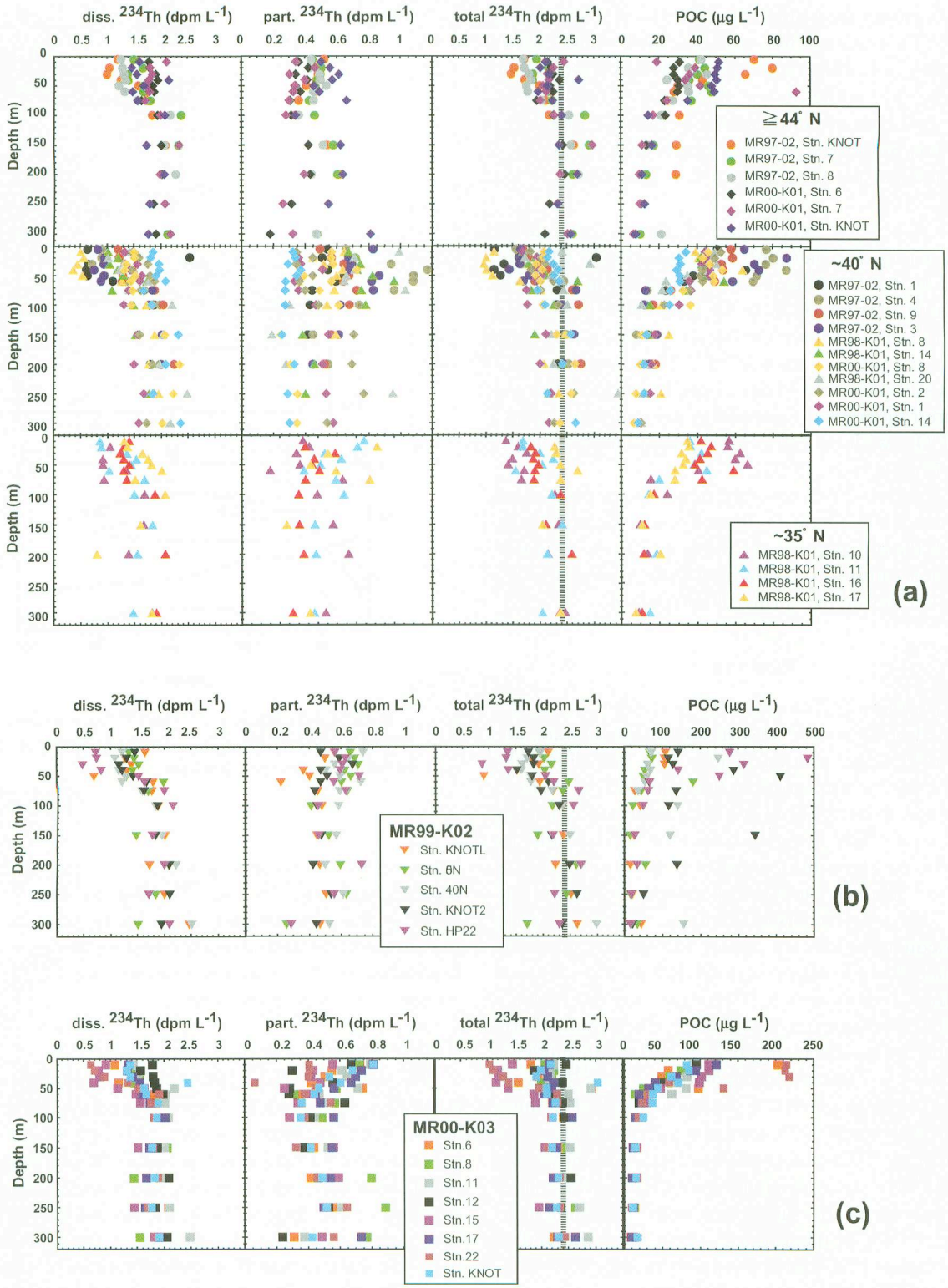

Fig. 4. Vertical distributions of dissolved ^{234}Th, particulate ^{234}Th, total ^{234}Th, and POC. (a) Data obtained during cruises MR97-02, MR98-K01, and MR00-K01; (b) data obtained during cruise MR99-K02; and (c) data obtained during cruise MR00-K03. Shapes of marks used in the plots are the same as those in Fig. 1. Vertical lines in the plots of total ^{234}Th indicate ^{238}U concentration equal to the radioactive equilibrium activity of ^{234}Th (ca. 2.4 dpm L^{-1}). The upper panel of (a) shows the data at or north of 44°N, the middle panel shows data at and around 40°N, and the bottom panel shows data at and around 35°N. Note that the horizontal axes of POC for each plot are different.

made, including measurements of carbonate species. At Stn. 50N, fluorescence was high (*ca.* 10.0 mg m^{-3}) in the upper 20 m, indicating that a spring phytoplankton bloom was occurring, while at Stn. 40N, it was low (1.0 mg m^{-3}) in the upper ocean (Sasaoka, personal communication). Thus Stns. 50N and 40N can be judged to reflect bloom and pre-bloom conditions, respectively, at that time.

During the first survey period, the study area had patches acting as a net sink for atmospheric CO_2 surrounded by areas acting as a net source for atmospheric CO_2 (Murata *et al.*, 2002). In the area under bloom conditions, the CO_2 influx to the ocean reached a maximum of approximately 12 mmol $m^{-2}d^{-1}$. The downward CO_2 flux was still dominant 14 days later. In contrast, the area under pre-bloom conditions was a net source of atmospheric CO_2, with an efflux of approximately 3 mmol $m^{-2}d^{-1}$ (Murata *et al.*, 2002).

Murata *et al.* (2002) reported that diatoms play an important role in the total CO_2 drawdown in the northwestern North Pacific, because the ratios of SiO_2 to total CO_2 and nitrates + nitrites consumption ($\Delta Si/\Delta C$ and $\Delta Si/\Delta N$) were higher during the spring bloom period.

Results

Vertical profiles of ^{234}Th and POC in winter

Vertical profiles of ^{234}Th (dissolved, particulate, and total) and POC are plotted in Fig. 4(a). For simplicity errors are not shown; errors in the data are, on average, 7.6% for dissolved ^{234}Th, 11.9% for particulate ^{234}Th, and 6.6% for total ^{234}Th. In general, the total ^{234}Th results for all the cruises show the commonly observed depletion relative to ^{238}U throughout the upper approximately 100-m layer. This deficiency is attributed to ^{234}Th scavenging and subsequent downward export *via* settling particles. Below that, down to approximately 300 m, there was occasionally a zone in which ^{234}Th exceeded the radioactive equilibrium value (*ca.* 2.4 dpm L^{-1}; Chen *et al.*, 1986), presumably by release from particles sinking through the upper zone. The concentrations of particulate ^{234}Th generally did not show a vertical change as marked as those of dissolved and total ^{234}Th, except at some stations where the particulate ^{234}Th concentrations tended to mirror the dissolved ^{234}Th, showing a maximum in the surface layer and a minimum in the subsurface layer. Enrichment of particulate ^{234}Th in the surface seems most marked in waters of higher POC content. Approximately 15%–35% of the total ^{234}Th was in particulate form.

Spatial variability of the vertical profiles, especially those of particulate ^{234}Th, was largest along the 40°N line (Fig. 4(a)), reflecting the variable features of the water structures such as the coastal water, Oyashio Water, and Kuroshio Front, and their respective biogeochemistries.

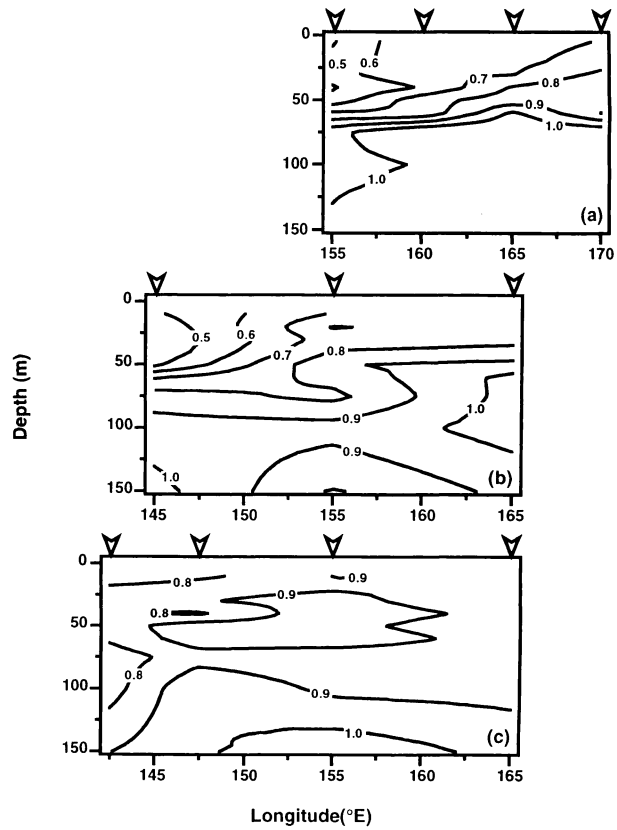

Fig. 5. Vertical distributions of $^{234}Th/^{238}U$ ratios along the 40°N line in Nov. 1997 (a), Nov.–Dec. 1998 (b), and Jan. 2000 (c). Arrows indicate sampling stations.

The east-west horizontal gradient is more obvious from the ratios of total ^{234}Th to ^{238}U (Fig. 5). The $^{234}Th/^{238}U$ ratios in the western part of the study area are smaller than those in the eastern part; therefore, because the concentration of ^{238}U is almost constant, the ^{234}Th concentrations are lower in the west.

^{234}Th distributions in the spring bloom

The data on ^{234}Th and POC obtained in spring are plotted in Figs. 4(b) and (c). General vertical profiles in spring are the same as those in winter, although the geographical area covered for sampling was different. Noteworthy differences between the spring and winter data are POC concentrations, especially in the spring of 1999; POC concentrations in the blooming area are approximately five times greater than POC concentrations in winter samples (Fig. 4(b)). The concentration of total ^{234}Th in the high production area (Stn. HP2) was the lowest in this study, possibly because of the vigorous removal of ^{234}Th. In the spring of 2000, despite the relatively small sampling area, there was a wide variation in the distribution of ^{234}Th and POC data (Fig. 4(c)). The Okhotsk Water

and the Pacific Subarctic Water influenced by the Okhotsk Water (Stns. 8, 11, 12, and 17) had a higher total ^{234}Th activity, probably because the spring bloom was yet to occur in those waters.

Discussion

^{234}Th export fluxes

The ^{234}Th method for estimating the export flux is based on the disequilibrium between ^{234}Th and ^{238}U that exists in the euphotic zone. The actual measurement used here is the activity of total ^{234}Th. The activity balance of total ^{234}Th in seawater can be described by the following equation:

$$\partial^{234}\mathrm{Th}_T/\partial t = (^{238}\mathrm{U} - {}^{234}\mathrm{Th}_T)\lambda - P + V \qquad (1)$$

where ^{238}U is the uranium activity calculated from salinity, $^{234}\mathrm{Th}_T$ is the measured activity of total ^{234}Th, λ is the decay constant for ^{234}Th (0.0288 d^{-1}), P is the rate of removal of ^{234}Th on settling particles, and V is the sum of the advective and diffusive ^{234}Th fluxes.

We assume that the horizontal gradient of ^{234}Th in this region is negligible. Although a meridional gradient most likely exists, the mean flow of the currents is zonal, from west to east, making V in the meridional direction small. Advection terms generally have very little effect on the value, with the exception of near the equator and upwelling areas (Dunne *et al.*, 2000). V can be considered negligible because it is much lower than the removal rate (P) (Buesseler, 1998). Calculations from the North Atlantic Bloom Experiment and the Southern Ocean show that vertical advection comprised only 1%–10% of the ^{234}Th flux (Buesseler *et al.*, 1992, 2001). Based on evidence from sediment trap experiments (Honda *et al.*, 2002), temporal variation of particulate fluxes in winter in the northern North Pacific is relatively small. Therefore, we assume a steady-state condition when calculating the winter results. For the ^{234}Th balance calculation during the spring blooms, a non-steady-state condition is assumed (see below for details).

The export fluxes of ^{234}Th can be determined from the ^{234}Th deficit relative to ^{238}U. The total ^{234}Th activity profile is integrated from the sea surface down to the euphotic depth. Here we use chlorophyll *a* distribution as a measure to set the bottom of the euphotic layer; i.e., the chlorophyll *a* concentration reaches a minimum at the bottom of the layer. The euphotic depth ranged mostly from 75 m to 150 m (Table 1).

POC/^{234}Th ratios

POC/^{234}Th ratios show wide variations in various regions and with different filtration systems (Buesseler, 1998). In order to use POC/^{234}Th and PON/^{234}Th ratios to convert the rate of removal of particulate ^{234}Th to POC and PON export fluxes out of the euphotic zone, it is important to understand the extent to which POC/^{234}Th ratios vary between various sampling techniques.

In this study, the concentrations of POC and particulate ^{234}Th were determined by filtering approximately 40 L of seawater through a 0.7-μm GF/F filter. The ratios of integrated POC to ^{234}Th in the euphotic layer did not vary very much, with an average and standard deviation of 73 ± 17 μg-C dpm^{-1} in winter (MR97-02, MR98-K01, and MR00-K01) (Table 1). Harada *et al.* (2001) deployed floating sediment traps at Stn. KNOT in Nov. and Dec. of 1998. The POC/^{234}Th ratios obtained at 100 m depth by the traps were 73 and 62 μg-C dpm^{-1}. Although our depths of interest were not strictly the same as Harada *et al.*'s and the sampling locations were not exactly the same, these numbers are comparable to ours, implying that measuring POC/^{234}Th in particles collected on a 0.7-μm GF/F filter can be regarded as representative of POC/^{234}Th ratios in winter. However, in the spring of 1999, POC/^{234}Th ratios showed larger values and wide variation (80–320 μg-C dpm^{-1}) (Table 1). The POC/^{234}Th ratios in this study fell within the range of 10–560 μg-C dpm^{-1} compiled by Buesseler *et al.* (1998) for spring. However, the POC/^{234}Th ratios of material caught in floating sediment traps at Stn. KNOT in spring were lower (74 μg-C dpm^{-1}) than the ratios in the particles we collected on 0.7-μm GF/F filters (Harada *et al.*, 2001), though it is the only data available for comparison.

On the basis on evidence from a compilation of POC/^{234}Th ratios in particles of different types, Moran *et al.* (1997) suggested that as suspended particles are packaged into large, rapidly sinking aggregates, carbon is preferentially remineralized over ^{234}Th. The sinking particles are thus depleted in organic carbon relative to ^{234}Th, leading to lower POC/^{234}Th ratios. Buesseler *et al.* (1995) also pointed out that the POC to ^{234}Th ratio is higher in suspended particles than in sinking particles; that is, the suspended particles were fresher than sinking particles. Therefore, we would expect that our estimated POC fluxes should give upper limits. However, as discussed below, during the spring bloom period when a transition of phytoplankton species occurred, the larger diatoms would have a higher POC/^{234}Th ratio than the smaller phytoplankton, as suggested by Charette and Moran (1999).

POC and PON fluxes in winter

The vertical flux of POC (F_{POC}) was calculated from ^{234}Th by using the ratios of POC to particulate ^{234}Th as follows:

$$F_{POC} = \left(\mathrm{POC}/^{234}\mathrm{Th}_p\right) \times \lambda \int_0^{z_0} \left(^{238}\mathrm{U} - {}^{234}\mathrm{Th}_T\right) dz \qquad (2)$$

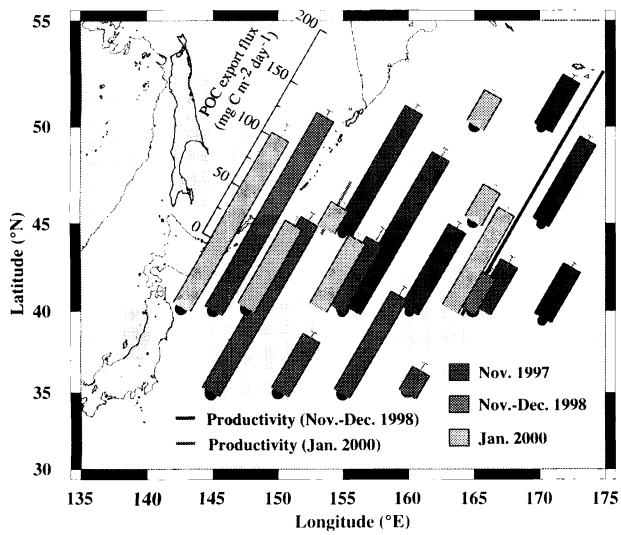

Fig. 6. Horizontal distributions of POC fluxes and productivity in Nov. 1997, Nov.–Dec. 1998, and Jan. 2000. Productivity data are quoted from Imai et al. (2002).

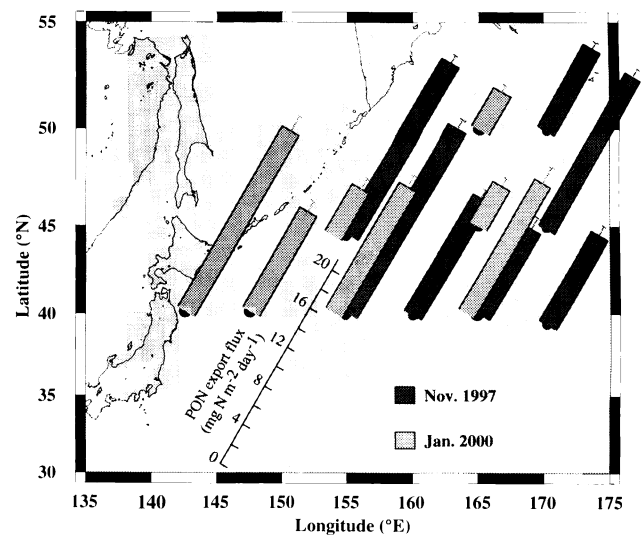

Fig. 7. Horizontal distributions of PON fluxes in Nov. 1997 and Jan. 2000.

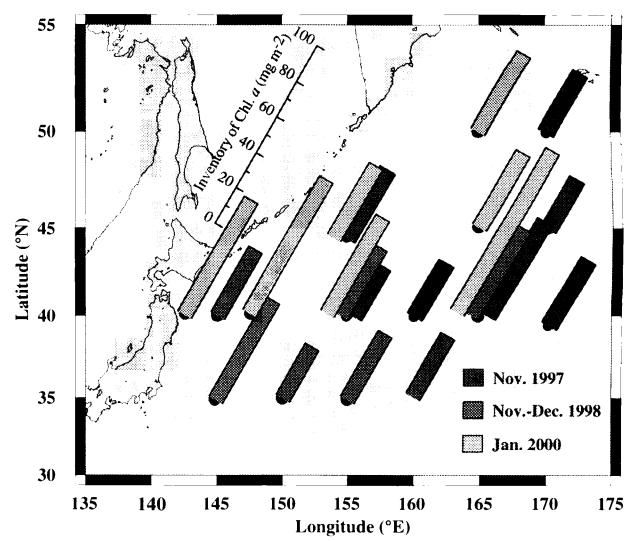

Fig. 8. Horizontal distributions of chlorophyll a in Nov. 1997, Nov.–Dec. 1998, and Jan. 2000. (Data courtesy of Dr. Sasaoka.)

where z_0 is the depth at the base of euphotic zone and $^{234}Th_p$ is the measured activity of particulate ^{234}Th. The ratios POC/$^{234}Th_p$ were determined from inventories of POC and particulate ^{234}Th above depth z_0. In this calculation, POC/$^{234}Th_p$ ratios of particles on the 0.7-μm GF/F filter were presumed to be equal to the ratios of settling particles, as discussed in the section above. Similar terminology is appropriate to the nitrogen cycle, and the fluxes of PON (F_{PON}) were calculated similarly to POC fluxes.

The horizontal distributions of POC fluxes in winter are shown in Fig. 6. The variations of POC fluxes were wide (20–190 mg-C $m^{-2}d^{-1}$). Andreev *et al.* (2002) calculated the average annual POC flux at about 100 m depth in the western Subarctic Gyre (Fig. 1) to be approximately 100 mg-C $m^{-2}d^{-1}$. In addition, Midorikawa *et al.* (2002) estimated the annual average of new production (which should be equivalent to the export flux at a steady state) at 48°N 165°E to be 95 ± 7 mg-C $m^{-2}d^{-1}$. Considering the temporal and spatial variations of the fluxes, these values agree reasonably well with each other. The fluxes of POC appeared higher in the western part of the study area than in the eastern part. The distribution of PON fluxes in winter (Fig. 7) also shows, to a lesser extent, a trend similar to that of POC. The nutrient-rich Oyashio Current, which leads to a high abundance of phytoplankton in the western region, is possibly responsible for the difference. Sediment trap experiments also showed fluxes of aluminum to be higher in the western region (44°N 155°E) than in the eastern region (40°N 165°E and 50°N 165°E) (Honda *et al.*, 2002). The continental materials were thought to also affect the profiles of ^{234}Th and POC fluxes. However, these factors alone cannot explain the east-west difference of POC fluxes, because the inventories of chlorophyll *a* do not show a clear difference between the western and the eastern regions (Fig. 8) and, therefore, the biomasses of phytoplankton in the euphotic zone are apparently equivalent between the western and the eastern regions. Sediment trap experiments also showed fluxes of opal to be higher in the western region (44°N 155°E) than in the eastern region (40°N 165°E and 50°N 165°E) (Honda *et al.*, 2002). The efficiency of materials sinking out of the

Table 2. PON export fluxes and rates of N (NO_2 + NO_3) decrease in spring

Date	Site	PON/^{234}Th (μg-N/dpm)	PON fluxes (mg-N m^{-2}day^{-1})	N decrease rates (mg-N m^{-2}day^{-1})	E ratio (%)
(MR99-K02)					
12 May, 99	44°N, 154.5°E	32	69	150	46
25 May, 99	44°N, 155°E (KNOT)	36	60	150	40
27 May, 99	44.3°N, 156.2°E	55	91	200	46
(MR00-K03)					
1 Jun., 00	49.1°N, 157.9°E	55	120	180	64
4 Jun., 00	46°N, 154°E	42	110	110	100

euphotic zone is reportedly related to the presence of diatoms (Smetacek, 1985; Sancetta *et al.*, 1991; Buesseler, 1998). The difference in standing stocks of diatoms is likely associated with the difference in POC flux between the west and the east.

POC fluxes in the bloom period

During the spring bloom, the fluxes of POC changed suddenly because the standing stocks of phytoplankton increased dramatically. The concentrations of ^{234}Th also decreased, possibly because of enhanced scavenging at that time. Therefore, a steady-state model cannot be used to calculate ^{234}Th flux in the bloom. Using a linear approximation, Eq. (1) gives a rate of removal (P) of ^{234}Th from the euphotic zone as follows:

$$P = [(^{238}U_1 + {}^{238}U_2)/2 - (^{234}Th_1 + {}^{234}Th_2)/2]\lambda - [(^{234}Th_2 - {}^{234}Th_1)/(t_2 - t_1)], \quad (3)$$

where t_1 and t_2 represent the beginning and the end of the time interval, and $^{238}U_n$ and $^{234}Th_n$ are measured activities in the euphotic zone at t_n.

On the basis of sediment trap data (Honda *et al.*, 2002) and satellite data (Murata *et al.*, 2002), April 23 was regarded as immediately before the spring bloom; we therefore set t_1 to be April 23 (1999 and 2000). We assumed the vertical distributions of ^{238}U and ^{234}Th on April 23 to be the same as those in winter; we therefore used the winter data (Jan. 2000) for $^{238}U_1$ and $^{234}Th_1$. The other calculations for the fluxes of POC and PON are similar to those of the winter studies.

In the spring bloom, the deficiencies of ^{234}Th relative to ^{238}U were higher than in winter. The fluxes of POC in the bloom in 1999 were several times higher than in winter; the maximum value was 520 mg-C m^{-2}d^{-1} (Table 1). In spring 2000, high fluxes of POC close to those in 1999 were also observed at two stations (Stns. 15 and 22), but most of the POC fluxes were not as high as in the spring of 1999 (Table 1). In particular, the POC fluxes near the eddy and in the Okhotsk Sea were lower than at the rest of the stations, and are the lowest values observed in this study (10–20 mg-C m^{-2}d^{-1}).

In the spring bloom period, the fluxes of POC and the e-ratios were notably higher than in winter, with the highest e-ratio being 70% (Table 1). Tsurushima *et al.* (2002) estimated the net community productivity from May to June in 1999 at Stn. KNOT to be 600 mg-C m^{-2}d^{-1}, which is almost the same as the primary productivity that they measured. This almost 100% e-ratio is concordant with the high e-ratio shown by our measurements. We think these high POC fluxes and e-ratios are related to the increased abundance of phytoplankton (diatoms) in the spring bloom. We assume that the low POC fluxes in spring 2000 were related to the eddy and that these sampling regions were still in "winter mode".

The rates of nitrogen decrease in the euphotic zone (ΔNO_x; NO_x = nitrates + nitrites) were calculated by the following equation:

$$\Delta NO_x = (N_1 - N_2)/(t_2 - t_1), \quad (4)$$

where t_1 and t_2 represent the beginning and the end of the time interval, respectively, and N_1 and N_2 are the measured concentrations of nitrates + nitrites (NO_x) at t_1 and t_2, respectively.

We assumed that t_1 was April 23, and that N_1 was the "winter mode data", similar to the calculation of ^{234}Th fluxes. The "winter mode data" were used at a station where the nutrients were at an almost constant concentration throughout the surface layer (44.8°N 156°E in early spring 1999) (Murata *et al.*, 2002). The differences in the NO_x concentrations were calculated from the differences between the vertical distribution of the winter mode data and the spring vertical distribution data.

If the rates of NO_x decrease are assumed to be new productivity, then the e-ratios of nitrogen were high in spring, ranging from 40% to 100% (Table 2). Therefore, the sinking efficiencies of nitrogen in the northwestern North Pacific were also much higher in spring.

The e-ratios in much of the world ocean were estimated to be <5%–10% (Buesseler, 1998). In this study, the stations at which primary productivity was measured

Table 3. Summary of POC export studies based upon the ^{234}Th approach

Site	Term	POC flux (mg-C m^{-2}day^{-1})	E ratio (%)	Reference
North Atlantic (NABE sites)	Apr. 25–May 30, 1989	80–920	8–79	Buesseler (1998)
North Atlantic (BATS sites)	Mar.–Oct., 1993–1995	10–70	1–56	Buesseler (1998)
Equatorial Pacific (EqPac sites)	Feb. 23–Oct. 21, 1992	20–110	2–10	Buesseler (1998)
Polynya, Greenland	Spring, 1992–1993	160–840	41–88	Buesseler (1998)
Antarctic	Spring (bloom), 1992	50–350	16–100	Buesseler (1998)
Arabian Sea	Jan.–Sep., 1995	10–310	1–27	Buesseler (1998)
Subtropical and equatorial Atlantic	May–Jun., 1996	40–510	—	Charette and Moran (1999)
Western and central Equatorial Pacific	Oct., 1994	50–160	—	Dunne *et al.* (2000)
	Apr.–May, 1996	40–150	—	Dunne *et al.* (2000)
Northeastern North Pacific	May, 1996	30–150	8	Charette *et al.* (1999)
	Aug., 1996	30–140	13	Charette *et al.* (1999)
	Feb., 1996, 97	10–70	6	Charette *et al.* (1999)
Northwestern North Pacific	Nov.–Dec., 1997	50–150	—	This study
winter	Nov.–Dec., 1998	20–190	15[a]	This study
	Jan.–Feb., 2000	20–170	45[b]	This study
spring	May, 1999	40–520	70[b]	This study
	May–Jun., 2000	10–560	—	This study

[a]*St. 40N.*
[b]*St. KNOT.*

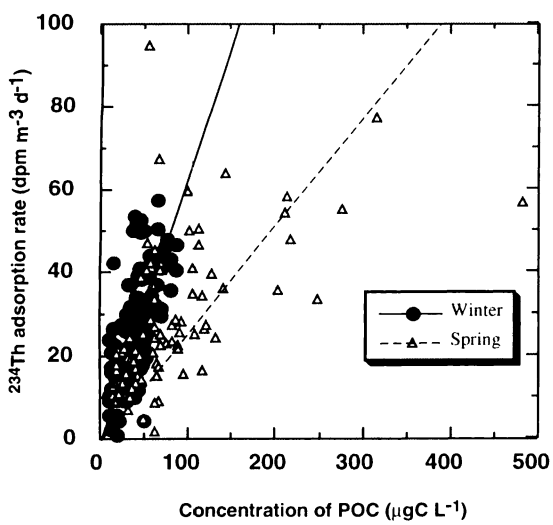

Fig. 9. Relationship between ^{234}Th adsorption rate and POC concentration. The solid and dotted lines are linear regressions for winter data and spring data, respectively.

(Imai *et al.*, 2002) were Stn. 40N in 1998 and Stn. KNOT in 1999 and 2000. The calculated e-ratios in the northwestern North Pacific were 15%–45% in winters and 70% in the spring bloom (Table 1). The e-ratios and POC fluxes in this region were much higher than in much of the world ocean (Table 3), with POC fluxes in the northwestern North Pacific being about three times higher than those in the northeastern North Pacific in spring.

Seasonal variation in the composition of particulate matter

With the negligible advection and diffusion, ^{234}Th adsorption rates were calculated from the following:

$$\partial A^{d}_{Th}/\partial t = A_U\lambda - A^{d}_{Th}\lambda - J, \quad (5)$$

where A_U is the activity of ^{238}U, λ is the decay constant of ^{234}Th, and A^{d}_{Th} is the activity of dissolved ^{234}Th. J is the rate of net adsorption of dissolved ^{234}Th onto particles. The adsorption rates calculated for the spring bloom were based on the non-steady-state model, and those for the other seasons were based on a steady-state condition.

The relationship between ^{234}Th adsorption rate and POC concentration in this study was linear in winter, but showed poor linearity in spring (Fig. 9). The regression line for the winter data is steeper than that of spring. Because ^{234}Th adsorption rates are regarded as proportional to the surface area of POC, they would be proportional to the concentrations of POC if the sizes of POC did not change with time. Thus, the change in the slope in Fig. 9 implies that the size of POC changes in spring, most likely through the appearance of larger phytoplankton. Charette *et al.* (1999) observed in the subarctic Northeast Pacific Ocean that the POC/^{234}Th ratios were two times higher on the large particles collected by the sediment trap when compared with >1-μm particles collected by *in situ* filtration. A similar trend of POC/^{234}Th ratios being higher on large particles than on small particles was found in the South and Equatorial Atlantic Ocean (Charette and

Moran, 1999); they attributed this to the presence of large diatoms that would have a higher POC/^{234}Th ratio relative to smaller phytoplankton.

The dominance of large diatoms in spring is well documented (Imai *et al.*, 2002; Liu *et al.*, 2002; Mochizuki *et al.*, 2002); the dominant species in this region have been estimated to be centric diatoms all the year round, but pennate diatoms increased during the spring bloom. The trends toward higher POC/^{234}Th ratios in spring (Table 1) can thus be attributed to the transition of phytoplankton structure to larger diatoms in spring. These results showed that the increase in POC fluxes in spring was due not only to the increased abundance of phytoplankton, but also to the transition of phytoplankton species.

Conclusion

The ^{234}Th/^{238}U disequilibrium in the euphotic zone was used to derive the export fluxes of ^{234}Th and particulate organic carbon and nitrogen in the northwestern North Pacific Ocean. The estimated export fluxes of particulate ^{234}Th were higher, in general, over the regions characterized by higher rates of water column productivity. The ^{234}Th data were used to derive the fluxes of particulate organic carbon and nitrogen out of the euphotic zone.

POC fluxes in winter showed wide variation (20–190 mg-C $m^{-2}d^{-1}$) in the northwestern North Pacific, and tended to be higher in the western region than in the eastern region. The influence of the Oyashio Current and the supply of substances from the continent to the study area appeared to be higher in the western region than in the eastern region. This tendency seemed to influence the primary productivity and biomass in this area. Thus, the horizontal distribution of POC fluxes in winter was influenced by the continental materials. The fluxes of POC and e-ratios in the spring bloom were much higher (up to 520 mg-C $m^{-2}d^{-1}$ and 70%, respectively). Therefore, in the northwestern North Pacific, the export efficiencies of POC from the euphotic zone were higher than in other areas in the world ocean. The increase in POC fluxes in spring depended not only on the increased abundance of phytoplankton, but also on the transition of species of phytoplankton.

Acknowledgments—We thank the captains, officers, and crews of R/V *Mirai* for their helpful support during these cruises. We also thank the marine technicians of Marine Works Japan Ltd. and Global Ocean Development Inc. for their on-board work on the observations. We are grateful to Dr. K. Sasaoka, Hokkaido University, for allowing us to use his unpublished data. We would like to acknowledge the helpful comments of Dr. C.-A. Huh, Institute of Earth Sciences, Taipei, Taiwan, Dr. K. Taguchi, Mie University, and Dr. H. Obata, University of Tokyo.

References

Amiel, D., Cochran, J. K. and Hirschberg, D. J. (2002) ^{234}Th/^{238}U disequilibrium as an indicator of the seasonal export of particulate organic carbon in the North Water. *Deep-Sea Res. II* **49**, 5191–5209.

Anderson, R. F. and Fleer, A. P. (1982) Determination of natural actinides and plutonium in marine particulate material. *Anal. Chem.* **54**, 1142–1147.

Andreev, A., Kusakabe, M., Honda, M., Murata, A. and Saito, C. (2002) Vertical fluxes of nutrients and carbon through the halocline in the western subarctic gyre calculated by mass balance. *Deep-Sea Res. II* **49**, 5577–5593.

Bacon, M. P., Cochran, J. K., Hirschberg, D., Hammar, T. R. and Fleer, A. P. (1996) Export flux of carbon at the equator during the EqPac time-series cruises estimated from ^{234}Th measurements. *Deep-Sea Res. II* **43**, 1133–1154.

Bhat, S. G., Krishnaswamy, S. K., Lal, D., Rama, D. and Moore, W. S. (1969) ^{234}Th/^{238}U ratios in the ocean. *Earth Planet. Sci. Lett.* **5**, 483–491.

Buesseler, K. O. (1991) Do upper-ocean sediment traps provide an accurate record of particle flux? *Nature* **353**, 420–423.

Buesseler, K. O. (1998) The decoupling of production and particulate export in the surface ocean. *Global Biogeochem. Cycles* **12**, 297–310.

Buesseler, K. O., Bacon, M. P., Cochran, J. K. and Livingston, H. D. (1992) Carbon and nitrogen export during the JGOFS North Atlantic Bloom Experiment estimated from ^{234}Th:^{238}U disequilibria. *Deep-Sea Res. I* **39**, 1115–1137.

Buesseler, K. O., Michaels, A. F., Siegel, D. A. and Knap, A. H. (1994) A three-dimensional time-dependent approach to calibrating sediment trap fluxes. *Global Biogeochem. Cycles* **8**(2), 179–193.

Buesseler, K. O., Andrews, J. A., Hartman, M. C., Belastock, R. and Chai, F. (1995) Regional estimates of the export flux of particulate organic carbon derived from thorium-234 during the JGOFS EqPac program. *Deep-Sea Res. II* **42**, 777–804.

Buesseler, K. O., Ball, L., Andrews, J., Benitez-Nelson, C., Belastock, R., Chai, F. and Chao, Y. (1998) Upper ocean export of particulate organic carbon in the Arabian Sea derived from thorium-234. *Deep-Sea Res. II* **45**, 2461–2487.

Buesseler, K. O., Benitez-Nelson, C., Rutgers van der Loeff, M., Andrews, J., Ball, L., Crossin, G. and Charette, M. A. (2001) An intercomparison of small- and large-volume techniques for thorium-234 in seawater. *Mar. Chem.* **74**, 15–28.

Charette, M. A. and Moran, S. B. (1999) Rates of particulate scavenging and particulate organic carbon export estimated using ^{234}Th as a tracer in the subtropical and equatorial Atlantic Ocean. *Deep-Sea Res. II* **46**, 885–906.

Charette, M. A., Moran, S. B. and Bishop, J. K. B. (1999) ^{234}Th as a tracer of particulate organic carbon export in the subarctic northeast Pacific Ocean. *Deep-Sea Res. II* **46**, 2833–2861.

Chen, J. H., Edwards, R. L. and Wasserburg, G. J. (1986) ^{238}U, ^{234}U and ^{232}Th in seawater. *Earth Planet. Sci. Lett.* **80**, 241–251.

Coale, K. H. and Bruland, K. W. (1985) ^{234}Th:^{238}U disequi-

libria within the California Current. *Limnol. Oceanogr.* **30**, 22–33.

Coale, K. H. and Bruland, K. W. (1987) Oceanic stratified euphotic zone as elucidated by ^{234}Th:^{238}U disequilibria. *Limnol. Oceanogr.* **32**, 189–200.

Cochran, J. K., Barnes, C., Achman, D. and Hirschberg, D. J. (1995) Thorium-234/Uranium-238 disequilibrium as an indicator of scavenging rates and particulate organic carbon fluxes in the northeast water polynya, Greenland. *J. Geophys. Res.* **100**, 4399–4410.

Dunne, J. P., Murray, J. W., Rodier, M. and Hansell, D. A. (2000) Export flux in the western and central equatorial Pacific: Zonal and temporal variability. *Deep-Sea Res. I* **47**, 901–936.

Grasshoff, K., Kremling, K. and Ehrhardt, M. (1999) *Methods of Seawater Analysis*. Third, Completely Revised and Extended Edition, WILEY-VCH.

Harada, K., Shibata, Y. and Narita, H. (2001) Export fluxes of carbon by ^{234}Th at Stn. KNOT. *Proc. Japan Oceanographic Society Spring Meeting, 2001*, 356 (in Japanese).

Honda, M., Imai, K., Nojiri, Y., Hoshi, F., Sugawara, T. and Kusakabe, M. (2002) The biological pump in the northwestern North Pacific based on fluxes and major components of particulate matter obtained by sediment-trap experiment (1997–2000). *Deep-Sea Res. II* **49**, 5595–5625.

Imai, K., Nojiri, Y., Tsurushima, N. and Saino, T. (2002) Time series of seasonal variation of primary productivity at station KNOT (44°N, 155°E) in the sub-arctic western North Pacific. *Deep-Sea Res. II* **49**, 5395–5408.

Kawai, H. (1972) Hydrography of the Kuroshio Extension. *Kuroshio: Physical Aspects of the Japan Current* (Stommel, H. and Yoshida, K., eds.), 235–352, University of Washington Press, Seattle, WA.

Kemp, A. E. S., Pike, J., Pearce, R. B. and Lange, C. B. (2000) The "Fall dump"—a new perspective on the role of a "shade flora" in the annual cycle of diatom production and export flux. *Deep-Sea Res. II* **47**, 2129–2154.

Kusakabe, M., Andreev, A., Lobanov, V., Zhabin, I., Kumamoto, Y. and Murata, A. (2002) Effect of the anticyclonic eddies on water masses, chemical parameters and chlorophyll distributions in the Oyashio Current region. *J. Oceanogr.* **58**, 691–701.

Lee, C., Murray, D. W., Barber, R. T., Buesseler, K. O., Dymond, J., Hedges, J. I., Honjo, S., Manganini, S. J., Marra, J., Moser, C., Peterson, M. L., Prell, W. L. and Wakeham, S. G. (1998) Particulate organic carbon fluxes: compilation of results from the 1995 US JGOFS Arabian Sea Process Study—By the Arabian Sea Carbon Flux Group. *Deep-Sea Res. II* **45**, 2489–2501.

Liu, H., Imai, K., Suzuki, K., Nojiri, Y., Tsurushima, N. and Saino, T. (2002) Seasonal variability of picophytoplankton and bacteria in the western subarctic Pacific Ocean at station KNOT. *Deep-Sea Res. II* **49**, 5409–5420.

Matsumoto, E. (1975) Radioactive disequilibrium in the surface layer of the ocean. *Geochim. Cosmochim. Acta* **39**, 205–212.

Michaels, A. F., Bates, N. R., Buesseler, K. O., Carlson, C. A. and Knap, A. H. (1994) Carbon-cycle imbalances in the Sargasso Sea. *Nature* **372**, 537–540.

Midorikawa, T., Umeda, T., Hiraishi, N., Ogawa, K., Nemoto, K., Kudo, N. and Ishii, M. (2002) Estimation of seasonal net community production and air–sea CO_2 flux based on the carbon budget above the temperature minimum layer in the western subarctic North Pacific. *Deep-Sea Res. I* **49**, 339–362.

Mochizuki, M., Shiga, N., Saito, M., Imai, K. and Nojiri, Y. (2002) Seasonal changes in nutrients, chlorophyll *a* and the phytoplankton assemblage of the western subarctic gyre in the Pacific Ocean. *Deep-Sea Res. II* **49**, 5421–5439.

Moran, S. B., Elles, K. M. and Smith, J. N. (1997) ^{234}Th/^{238}U disequilibrium in the central Arctic Ocean: Implications for particulate organic carbon export. *Deep-Sea Res. II* **44**, 1593–1606.

Murata, A., Kumamoto, Y., Saito, C., Kawakami, H., Asanuma, I., Kusakabe, M. and Inoue, H. Y. (2002) Impact of a spring phytoplankton bloom on the CO_2 system in the mixed layer of the northwestern North Pacific. *Deep-Sea Res. II* **49**, 5531–5555.

Murray, J. W., Young, J., Newton, J., Dunne, J., Chapin, T. and Paul, B. (1996) Export flux of particulate organic carbon from the central equatorial Pacific determined using a combined drifting trap–^{234}Th. *Deep-Sea Res. II* **43**, 1095–1132.

Rutgers van der Loeff, M. M., Friedrich, J. and Bathmann, U. V. (1997) Carbon export during the spring bloom at the southern polar front, determined with the natural tracer ^{234}Th. *Deep-Sea Res. II* **44**, 457–478.

Saito, H., Tsuda, A. and Kasai, H. (2002) Nutrient and plankton dynamics in the Oyashio region of the western subarctic Pacific Ocean. *Deep-Sea Res. II* **49**, 5463–5486.

Sancetta, C., Villareal, T. and Falkowski, P. (1991) Massive fluxes of rhizosolenid diatoms: A common occurrence. *Limnol. Oceanogr.* **36**, 1452–1457.

Smetacek, V. S. (1985) The role of sinking diatom life-history cycles: Ecological, evolutionary and geological significance. *Mar. Biol.* **84**, 239–251.

Smetacek, V. S. (2000) The giant diatom dump. *Nature* **406**, 574–575.

Tsunogai, S. and Noriki, S. (1991) Particulate fluxes of carbonate and organic carbon in the ocean. Is the marine biological activity working as a sink of the atmospheric carbon? *Tellus* **43B**, 256–266.

Tsurushima, N., Nojiri, Y., Imai, K. and Watanabe, S. (2002) Seasonal variations of carbon dioxide system and nutrients in the surface mixed layer at station KNOT (44°N, 155°E) in the subarctic western North Pacific. *Deep-Sea Res. II* **49**, 5377–5394.

Yamaguchi, A., Watanabe, Y., Ishida, H., Harimoto, T., Furusawa, K., Suzuki, S., Ishizaka, J., Ikeda, T. and Takahashi, M. M. (2002) Structure and size distribution of plankton communities down to the greater depths in the western North Pacific Ocean. *Deep-Sea Res. II* **49**, 5513–5530.

Journal of Oceanography, Vol. 61, pp. 129 to 139, 2005

Temporal Change of Dissolved Inorganic Carbon in the Subsurface Water at Station KNOT (44°N, 155°E) in the Western North Pacific Subpolar Region

MASAHIDE WAKITA[1,2]*, SHUICHI WATANABE[1,2], YUTAKA W. WATANABE[1], TSUNEO ONO[4], NOBUO TSURUSHIMA[3] and SHIZUO TSUNOGAI[1]

[1]*Graduate School of Environmental Earth Science, Hokkaido University, Sapporo 060-0810, Japan*
[2]*Japan Agency for Marine-Earth Science and Technology, Yokosuka 237-0061, Japan*
[3]*National Institute for Advanced Industrial Science and Technology, Tsukuba 305-8569, Japan*
[4]*Hokkaido National Fisheries Research Institute, Kushiro 085-0802, Japan*

(Received 3 December 2003; in revised form 11 May 2004; accepted 16 May 2004)

The dissolved inorganic carbon (DIC) and related chemical species have been measured from 1992 to 2001 at Station KNOT (44°N, 155°E) in the western North Pacific subpolar region. DIC (1.3~2.3 μmol/kg/yr) and apparent oxygen utilization (AOU, 0.7~1.8 μmol/kg/yr) have increased while total alkalinity remained constant in the intermediate water (26.9~27.3σ_θ). The increases of DIC in the upper intermediate water (26.9~27.1σ_θ) were higher than those in the lower one (27.2~27.3σ_θ). The temporal change of DIC would be controlled by the increase of anthropogenic CO_2, the decomposition of organic matter and the non-anthropogenic CO_2 absorbed at the region of intermediate water formation. We estimated the increase of anthropogenic CO_2 to be only 0.5~0.7 μmol/kg/yr under equilibrium with the atmospheric CO_2 content. The effect of decomposition was estimated to be 0.8 ± 0.7 μmol/kg/yr from AOU increase. The remainder of non-anthropogenic CO_2 had increased by 0.6 ± 1.1 μmol/kg/yr. We suggest that the non-anthropogenic CO_2 increase is controlled by the accumulation of CO_2 liberated back to atmosphere at the region of intermediate water formation due to the decrease of difference between DIC in the winter mixed layer and DIC under equilibrium with the atmospheric CO_2 content, and the reduction of diapycnal vertical water exchange between mixed layer and pycnocline waters. In future, more accurate and longer time series data will be required to confirm our results.

Keywords:
· Dissolved inorganic carbon,
· temporal change,
· anthropogenic CO_2,
· western North Pacific subpolar region.

1. Introduction

The increase of atmospheric CO_2 concentration (e.g., Keeling and Whorf, 2002) has recently generated considerable interest in global carbon cycles. The oceans have taken up anthropogenic CO_2 of 1.6~2.0 Pg C/yr in the 1990s (e.g., McNeil *et al*., 2003). High latitudinal oceans are especially important as a sink for anthropogenic CO_2 since they are the source of the intermediate and deep water masses, and a direct pathway for the transport of anthropogenic CO_2 into the ocean interior.

The uptake rate of anthropogenic CO_2 in the North Pacific was estimated in the 1990s to be 0.55 ± 0.09 Pg C/yr, which is about 32% of the total for the global ocean (Watanabe *et al*., 2000). Its subpolar region is the only area forming southward North Pacific Intermediate Water (NPIW), characterized by a salinity minimum centered at 26.8σ_θ (e.g., Reid, 1965; Talley, 1991). The subpolar region is therefore an important area for transporting anthropogenic CO_2 into the ocean interior over the North Pacific (e.g., Tsunogai *et al*., 1993).

The rate of increase of anthropogenic CO_2 and the dissolved inorganic carbon (DIC) inventory in the North Pacific has been estimated in several recent studies. Watanabe *et al*. (2000) indirectly estimated the rate of increase of anthropogenic CO_2 inventory with a tracer dating technique in the North Pacific. In the temperate North Pacific, Tsunogai *et al*. (1993), Slansky *et al*. (1997) and Ono *et al*. (1998) directly estimated the rate of increase of DIC inventory between the 1970s and the 1990s. Watanabe *et al*. (1996) and Takahashi *et al*. (1999) also

* Corresponding author. E-mail: mwakita@jamstec.go.jp

Copyright © The Oceanographic Society of Japan.

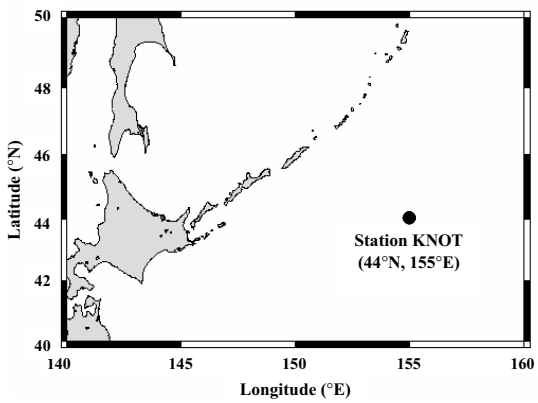

Fig. 1. Location of Station KNOT in the western North Pacific subpolar region.

found a significant increase of DIC inventory between 1973 and 1992 in the subpolar North Pacific. However, these analyses were based substantially on a single pair dataset, and included the potential uncertainty in the rate of DIC increase due to the choice of data sets (Ono *et al.*, 2000). Thus, the most fundamental and reliable approach to the direct estimation of the oceanic rate of anthropogenic CO_2 increase is to collect more accurate, longer time series observations of the oceanic CO_2 species.

We have observed the oceanic CO_2 species and its related hydrographic components (dissolved O_2, DO) from 1992 to 2001 at a station, 44°N, 155°E, in the western North Pacific subpolar region (Fig. 1). This station is named KNOT and has been a Japanese JGOFS time series station since 1998 (e.g. Tsurushima *et al.*, 2002). The purpose of this study is to estimate directly the oceanic rate of anthropogenic CO_2 increase at Station KNOT by using our decadal data of the oceanic CO_2 species in 1992~2001. Moreover, we examined the factors controlling the rate of increase of DIC in the intermediate water (26.9~27.3σ_θ) during the same period.

2. Methods

2.1 Sampling and shipboard measurements of chemical parameters

Station KNOT is located in the western subpolar gyre and just north of the Subpolar Front during the period from 1982 to 1995 (Isoda *et al.*, 2002). At Station KNOT, the seasonal amplitude of DIC in surface mixed layer was 107 μmol/kg in the 1999~2000 time series, which was larger than those at other pelagic ocean time series sites (Tsurushima *et al.*, 2002). This large variation is mainly due to biological production in spring to fall and strong vertical mixing in winter (Tsurushima *et al.*, 2002; Imai *et al.*, 2002).

On the T/S *Hokusei Maru*, Hokkaido University, CTD observations and water samplings were carried out at Station KNOT from 1993 to 2001 (Fig. 1 and Table 1). Seawater samples were collected from 13~16 layers from the surface to 1500 db in 1992~1997 and 25 layers from the surface to 3000 db in 1998~2001. We obtained samples by using 1.2-l Niskin bottles for the 1992~1997 observations and 10-l Niskin bottles for the 1998~2001 series, mounted on a CTD system. We measured temperature, salinity, DO, DIC and total alkalinity (TA). Temperature and salinity were measured with a Neil Brown (MARK IIIB) CTD system in 1992~1997 and a Seabird CTD system in 1998~2001. DO, DIC and TA were analyzed on board within 24 hours of sampling. Sampling, measurement and standardization of DO measurement in the seawater were carried out according to JGOFS protocols (Knap *et al.*, 1996). We analyzed DO with a piston burette (Metrohm Ltd.) in 1992~1997 and potentiometric titration with an autoburette (751 GPD Titrino, Metrohm Ltd.) in 1998~2001. The precision of DO analysis was estimated as < 0.7 μmol/kg, obtained from duplicate determinations. We calculated Apparent Oxygen Utilization (AOU) as the difference between observed concentration and equilibrium concentration with atmosphere (Weiss, 1970).

2.2 Measurements of DIC and TA

The methods by which DIC and TA were measured in this study are listed in detail in Table 1. A modified coulometric method of Johnson *et al.* (1985) was used for the determination of DIC. In 1992 and 1995, the sampling, measurement and standardization for DIC were carried out according to the method of Tsunogai *et al.* (1993). This method uses a calcium carbonate reagent of JIS K8617 special grade (purity 98.90%) as our reference material as well as a running substandard seawater sample. The coefficient of variation in DIC was ±0.2%. In 1997, 2000 (00/7) and 2001, the DIC contents were determined by the method described in Ono *et al.* (1998). We prepared and used a working standard of DIC on board the vessel according to the method described by Dickson *et al.* (2003). This working DIC standard was calibrated against sodium carbonate (Asahi Glass Co., Ltd., purity 99.97%) at least every half-year according to a DOE (1994). Since 2000, we calibrated our working standard once a year against a US certified reference material of DIC distributed by A. G. Dickson of Scripps Institution of Oceanography (SIO-CRM). The DIC content determined by our working standard agreed with that of SIO-CRM within about 2 μmol/kg (±0.1%) in 2000 (00/7) and 2001. The precision of DIC analysis was estimated as ±0.1% from duplicate determinations in 1997, 2000 (00/7) and 2001.

Table 1. Observations carried out from 1992 to 2001 at Station KNOT and methods of DO, DIC and TA analyses.

Code name[a]	Cruise name	Sampling date year/month/day	Depth[b] (m)	Layer[c]	Temp. Salinity	DO	DIC	TA
92/6	HO92-2	1992/06/23	1500	16	Neil Brown	piston burette	Tsunogai *et al.* (1993)	×
95/6	HO95-2	1995/06/23	1500	13	Neil Brown	piston burette	Tsunogai *et al.* (1993)	×
97/7	HO97-3	1997/07/13	1500	13	Neil Brown	piston burette	Ono *et al.* (1998)	×
98/6-1	HO98-1	1998/06/04	3000	25	Seabird	autoburrette	Tsurushima *et al.* (2002)[e]	Tsurushima *et al.* (2002)[f]
98/6-2	HO98-2	1998/06/26	3000	25	Seabird	autoburrette	Tsurushima *et al.* (2002)[e]	Tsurushima *et al.* (2002)[f]
98/7	HO98-3-1	1998/07/21	3000	25	Seabird	autoburrette	Tsurushima *et al.* (2002)[e]	Tsurushima *et al.* (2002)[f]
98/8	HO98-3-2	1998/08/13	3000	25	Seabird	autoburrette	Tsurushima *et al.* (2002)[e]	Tsurushima *et al.* (2002)[f]
99/6-1	HO99-1	1999/06/05	3000	25	Seabird	autoburrette	Tsurushima *et al.* (2002)[e]	Tsurushima *et al.* (2002)[f]
99/6-2	HO99-2	1999/06/27	3000	25	Seabird	autoburrette	Tsurushima *et al.* (2002)[e]	Tsurushima *et al.* (2002)[f]
99/7	HO99-3-1	1999/07/22	3000	25	Seabird	autoburrette	Tsurushima *et al.* (2002)[e]	Tsurushima *et al.* (2002)[f]
99/8	HO99-3-2	1999/08/14	3000	25	Seabird	autoburrette	Tsurushima *et al.* (2002)[e]	Tsurushima *et al.* (2002)[f]
00/6-1	HO00-1	2000/06/09	3000	25	Seabird	autoburrette	Tsurushima *et al.* (2002)[e]	Tsurushima *et al.* (2002)[f]
00/6-2	HO00-2	2000/06/25	3000	25	Seabird	autoburrette	Tsurushima *et al.* (2002)[e]	Tsurushima *et al.* (2002)[f]
00/7	HO00-3B	2000/07/31	3000	25	Seabird	autoburrette	Ono *et al.* (1998)[d]	Ono *et al.* (1998)
01/6	HO01-1	2001/06/04	3000	25	Seabird	autoburrette	Ono *et al.* (1998)[d]	Ono *et al.* (1998)
01/7	HO01-3A	2001/07/12	3000	25	Seabird	autoburrette	Ono *et al.* (1998)[d]	Ono *et al.* (1998)

[a]Sampling year and month are given in the code name.
[b]Maximum water depth of sampling.
[c]Number of sampling layers.
[d]DIC content determined by our working standard agreed well with that certified manometrically at SIO-CRM within 2 μmol/kg (±0.1%) in 2000 and 2001.
[e]DIC content of SIO-CRM we determined and that certified in SIO differed by 6.3 μmol/kg in 1999, and showed good agreement within about 2 μmol/kg in 2000.
[f]TA contents in our working standards showed no significant difference from that of the SIO-CRM.

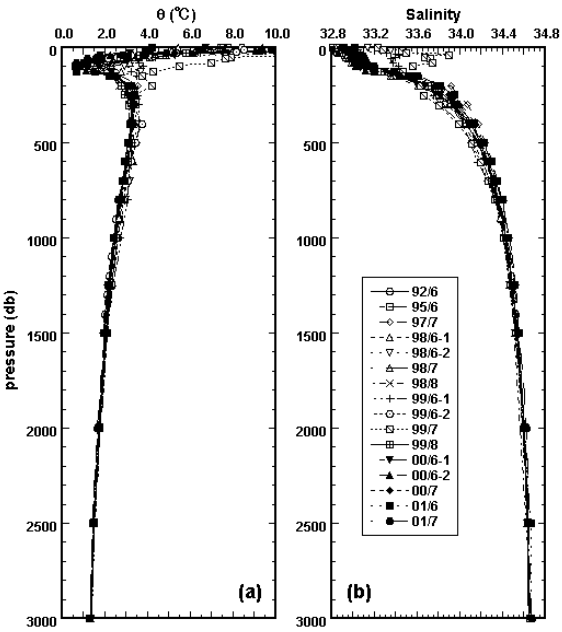

Fig. 2. Vertical profiles of (a) potential temperature (θ) and (b) salinity at Station KNOT from 1992 to 2001.

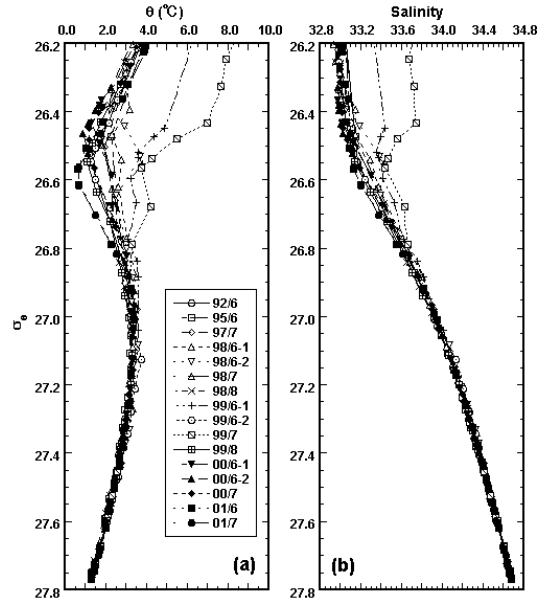

Fig. 3. Profiles of (a) potential temperature (θ) and (b) salinity against density (σ_θ) at Station KNOT from 1992 to 2001.

In 1998, 1999 and 2000 (00/6-1, 00/6-2), the sampling, measurement and standardization for DIC and TA were carried out according to the method described by Tsurushima *et al.* (2002). The working standards of DIC and TA were examined at the PICES (North Pacific Marine Science Organization) international intercalibration exercises in 1999 and 2000. The difference between DIC content of SIO-CRM we determined and that certified in SIO was 6.3 μmol/kg in 1999, and showed good agreement, less than about 2 μmol/kg (±0.1%) in 2000. At the PICES intercalibration in 2000, our TA contents showed no significant difference from the SIO-CRM. The precisions of DIC and TA analyses were estimated as ±0.1% from duplicate determinations in 1998, 1999 and 2000 (00/6-1, 00/6-2).

In 2000 (00/7) and 2001, TA was determined by the improved single point titration method described by Culberson *et al.* (1970). We measured TA using a glass electrode standardized against Tris buffer (DOE, 1994), 2-aminopyridine buffer (DOE, 1994). Drift was corrected using a 0.03 M phthalic acid buffer of a seawater base. The precision of TA was determined as ±0.2% from duplicate determinations in 2000 (00/7) and 2001.

2.3 Correction of systematic errors among datasets

We eliminated the systematic errors of DO and DIC among each dataset, because the methods used for these determinations were slightly different from cruise to cruise. We corrected the DIC concentrations during the period from 98/6-1 to 01/7 to the certified SIO-CRM value, because we calibrated the working standard against SIO-CRM once a year from 1998 to 2001.

For the preceding periods, we corrected the systematic errors assuming that oceanic properties in the water mass deeper than 27.4σ_θ (820 m) had been constant for the period from 1992 to 2001, because the water mass deeper than 27.4σ_θ has not changed for the last ten years within the variations of potential temperature (θ) (±0.01 ~ ±0.02°C) and salinity (±0.001 ~ ±0.002) (Figs. 2 and 3), and because AOU and CFC-11 deeper than 27.4σ_θ in 1985 agreed with those in 1999 at Station KNOT (Watanabe *et al.*, 2001). We corrected the contents of DO and DIC in 92/6, 95/6 and 97/7 at the isopycnal surfaces of 27.4σ_θ, 27.5σ_θ and 27.6σ_θ to fit the mean observed value from 1998 to 2001 at the same isopycnal surfaces (Table 2). The values of DO and DIC at each isopycnal surface were obtained by linear interpolation. For contents of DO in 97/7, –10 μmol/kg was added to original data. We added the DIC contents to 19 μmol/kg in 92/6, 10 μmol/kg in 95/6 and 10 μmol/kg in 97/7. These systematic errors probably derive from the standardization because of the absence of a common reference material (SIO-CRM). The above corrections of DIC and DO are listed in Table 3. After the corrections, the standard errors of DO (±0.8 ~ ±1.2 μmol/kg) and DIC (±1 μmol/kg) on 27.4σ_θ, 27.5σ_θ and 27.6σ_θ during last ten years agree

Table 2. Average concentrations of DO and DIC with their standard errors at each isopycnal surface at Station KNOT from 1998 to 2001.

σ_θ	Depth (ave.) (m)	DO (μmol/kg)	DIC (μmol/kg)
27.40	816	30.5 ± 1.4	2372 ± 1
27.50	1091	37.9 ± 0.6	2377 ± 1
27.60	1511	57.6 ± 1.2	2377 ± 1
27.70	2216	97.1 ± 1.1	2362 ± 1
27.73	2478	110.8 ± 1.1	2354 ± 1
27.75	2798	124.3 ± 1.2	2345 ± 1

Table 3. Values of the corrections of DO and DIC from 1992 to 2001 at Station KNOT.

Code name	DO (μmol/kg)	DIC (μmol/kg)
92/6	—	19
95/6	—	10
97/7	–10	10
98/6-1	—	6.3
98/6-2	—	6.3
98/7	—	6.3
98/8	—	6.3
99/6-1	—	6.3
99/6-2	—	6.3
99/7	—	6.3
99/8	—	6.3
00/6-1	—	—
00/6-2	—	—
00/7	—	2
01/6	—	2
01/7	—	2

with those in each isopycnal surface of 27.7σ_θ, 27.73σ_θ and 27.75σ_θ from 1998 to 2001 (Table 2), which suggests that these corrections are appropriate.

3. Results and Discussion

3.1 Decadal change of the structure of water mass

The vertical distributions of θ and salinity from 1992 to 2001 are shown in Figs. 2 and 3. The layer of minimum temperature that was the remnant of the winter mixed layer water usually existed at about 26.6σ_θ (about 100 m) and the maximum temperature was observed between 27.0σ_θ (about 300 m) and 27.1σ_θ (about 390 m) in the last ten years. These observations indicate that Station KNOT was located in the western subpolar gyre from 1992 to 2001, according to Favorite *et al.* (1976) and Ueno and Yasuda (2000).

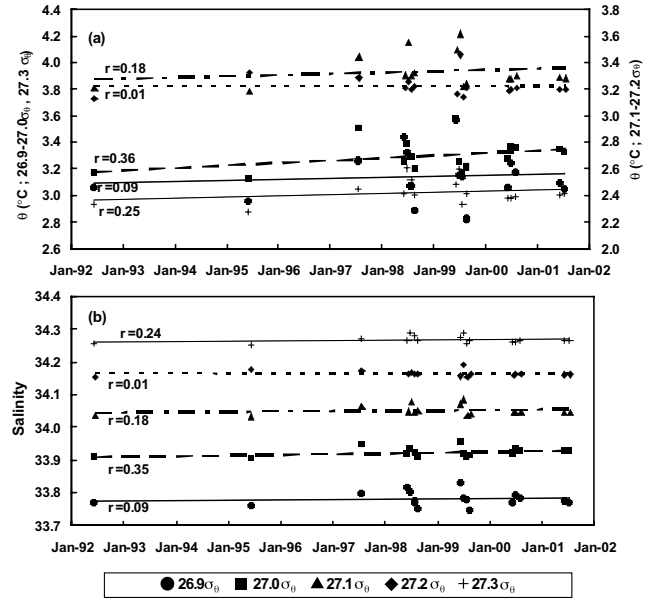

Fig. 4. (a) Potential temperature (θ) and (b) salinity on the isopycnal surface of 26.9σ_θ (solid circles), 27.0σ_θ (solid squares), 27.1σ_θ (solid triangles), 27.2σ_θ (solid diamonds), 27.3σ_θ (plus) and 27.2σ_θ (cross) surfaces at Station KNOT during the period from 1992 to 2001. We show the linear regression lines on 26.9σ_θ (solid line), 27.0σ_θ (dashed line), 27.1σ_θ (dashed-dotted line), 27.2σ_θ (dotted line) and 27.3σ_θ (thin line). In addition, we also show the correlation coefficient (r) and the probability value (p) for the linear regression lines of θ and salinity on each isopycnal surface.

In the water mass shallower than 26.8σ_θ (about 180 m), the recorded values of θ and salinity in 01/6 and 01/7 were the minimum in our dataset, while the values in 98/6-1, 98/6-2, 99/6-1, and 99/7 were the maximum values recorded (Figs. 2 and 3). The higher values of θ and salinity in 98/6-1, 98/6-2, 99/6-1 and 99/7 might be due to the migration of subtropical water from the south (Tsurushima *et al.*, 2002), because Station KNOT is located just north of the Subpolar Front (Kono, 1997; Isoda *et al.*, 2002).

The values of θ and salinity deeper than 26.9σ_θ (about 230 m) were not greatly different from year to year during the last ten years (Figs. 2 and 3). We could not detect decadal changes of the θ and salinity from 26.9σ_θ to 27.3σ_θ (about 630 m). Their standard errors from 26.9σ_θ to 27.3σ_θ were ±0.02 ~ ±0.05°C and ±0.002 ~ ±0.006, respectively, during last ten years, which is comparable to values deeper than 27.4σ_θ (±0.01 ~ ±0.02°C (θ) and ±0.001 ~ ±0.002 (salinity)) (Fig. 4). We thus assumed that the structure of intermediate water from 26.9σ_θ to 27.3σ_θ did not change during the period from 1992 to 2001.

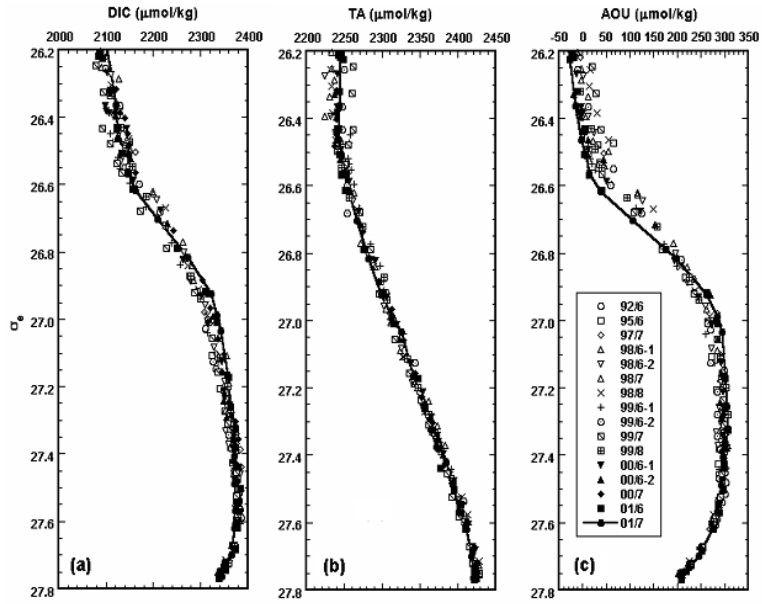

Fig. 5. Profiles of (a) DIC, (b) TA and (c) AOU against density (σ_θ) at Station KNOT from 1992 to 2001. We show the vertical profiles of DIC, AOU and TA in the most recent observation (01/7) as a solid line to clarify these temporal changes.

Table 4. Increase rate of DIC and other properties on the 26.9–27.3σ_θ surfaces at Station KNOT. Error shows the standard error of the slope of linear regression.

Isopycnal surface	Depth (ave.)[(a)] (m)	$d\mathrm{DIC}_{obs}/dt$ (μmol/kg/yr)	$d_{anth}\mathrm{DIC}_{air\text{-}sea}/dt$ (μmol/kg/yr)	$d\mathrm{DIC}_{org}/dt$[(b)] (μmol/kg/yr)	$d\mathrm{AOU}_{obs}/dt$ (μmol/kg/yr)	$d_{non\text{-}anth}\mathrm{DIC}_{air\text{-}sea}/dt$[(c)] ($\mu$mol/kg/yr)
26.9σ_θ	230 ± 37	2.3 ± 1.0	0.6 ± 0.2	0.8 ± 0.8	1.1 ± 1.1	0.9 ± 1.3
27.0σ_θ	293 ± 41	2.6 ± 0.9	0.5 ± 0.1	1.2 ± 0.8	1.8 ± 1.2	0.9 ± 1.2
27.1σ_θ	379 ± 43	2.5 ± 0.9	0.6 ± 0.1	0.8 ± 0.7	1.2 ± 1.0	1.1 ± 1.1
27.2σ_θ	487 ± 48	1.3 ± 0.6	0.7 ± 0.1	0.6 ± 0.5	0.8 ± 0.7	0.0 ± 0.8
27.3σ_θ	626 ± 47	1.3 ± 0.6	0.6 ± 0.1	0.5 ± 0.6	0.7 ± 0.8	0.2 ± 0.9

[(a)]Averages and standard deviations at the isopycnal surfaces.
[(b)]$d\mathrm{DIC}_{org}/dt = 0.69d(\mathrm{AOU})/dt$: $0.69 = \mathrm{C}_{org}/-\mathrm{O}_2$ (Anderson and Sarmiento, 1994).
[(c)]$d(_{non\text{-}anth}\mathrm{DIC}_{air\text{-}sea})/dt = d(\mathrm{DIC}_{obs})/dt - d(\mathrm{DIC}_{org})/dt - d(_{anth}\mathrm{DIC}_{air\text{-}sea})/dt$.

3.2 *Decadal variations in the vertical profile in DIC, TA and AOU*

The vertical profile of DIC was similar to that of AOU due to decomposition of organic matter (Figs. 5(a) and (b)). DIC and AOU were at their minima in the surface water due to photosynthesis and gas exchange of CO_2 and O_2 across the air-sea interface. Both properties increased with density, and decreased slightly below 27.6σ_θ. On the other hand, TA increased with density and had a strong correlation with salinity (TA = 106.9 salinity – 1296, r = 0.98) (Figs. 3(b) and 5(c)).

Comparing the vertical profiles of DIC, TA and AOU in the most recent observation (01/7) with the other data obtained in the last ten years, we found that the temporal changes in DIC and AOU below 26.9σ_θ decreased with increasing density (Fig. 5). AOU in 01/7 above 26.8σ_θ was smaller than that in the other data, while the temporal change of DIC above 26.8σ_θ had a large variation. These changes of AOU and DIC in the mixed layer (above 26.8σ_θ) may be caused by the large variation of water mass structure. It is thus difficult to detect decadal changes above 26.8σ_θ. In the next section we focus on the decadal changes in AOU, TA and DIC on 26.9~27.3σ_θ for the period from 1992 to 2001, since NPIW is generally seen from 26.8σ_θ to 27.4σ_θ.

3.3 *Rate of increase of DIC in the intermediate water (26.9~27.3σ_θ)*

We found that DIC between 26.9σ_θ and 27.3σ_θ increased at rates of 1.3~2.3 (ave. 2.0 ±0.8) μmol/kg/yr, based on linear regression (Fig. 6 and Table 4). The values of DIC on each isopycnal surface were obtained by linear interpolation. The rates in the upper intermediate water (26.9~27.1σ_θ) were higher than these in the lower water (27.2~27.3σ_θ) (Table 4).

If oceanic physical and biological conditions are in a steady state, the rate of DIC increase on any isopycnal surface is the rate of anthropogenic CO_2 increase absorbed in seawater. In the steady state, the average rate of increase of anthropogenic CO_2 was estimated to be 2.0 ± 0.8 μmol/kg/yr on 26.9~27.3σ_θ at Station KNOT. However, Watanabe *et al*. (2000) reported that the rate of anthropogenic CO_2 increase was estimated to be 0.3~0.6 μmol/kg/yr in the 1990s on 26.9~27.3σ_θ in the western North Pacific subpolar region, on the assumption of oceanic conditions steady-state, based on the thermodynamic method using temperature, salinity, the TA and the rate of increase of atmospheric CO_2. Our estimate is three times higher than theirs. It is thus difficult to explain the rate of increase of DIC on 26.9~27.3σ_θ at Station KNOT only in terms of the rate of increase of anthropogenic CO_2, based on the assumption of steady-state oceanic physical and biological conditions during the observation period.

3.4 *Rate of increase of TA in the intermediate water (26.9~27.3σ_θ)*

The values of TA on 26.9~27.3σ_θ were statistically insignificant during the period from 1992 to 2001 (Fig. 6(b)). The values of TA on each isopycnal surface were obtained by linear interpolation. The standard deviation of TA on 26.9~27.3σ_θ was 2~4 μmol/kg, which is close to the analytical error of TA. This suggests that the rate of dissolution of particulate carbonate has not changed over these isopycnal surfaces during the period from 1992 to 2001 at Station KNOT. Bates (2001) and Winn *et al*. (1998) also reported that the temporal change of TA in the mixed layer is insignificant at the subtropical stations BATS (31°50′ N, 64°10′ W) and HOT (22°45′ N, 158°00′ W). This is consistent with the observational results that the saturation depths of calcite and aragonite are about 750 m and 500 m, respectively, in North Pacific (Millero, 1996) and the depth of 26.9~27.3σ_θ surface at Station KNOT (about 200~600 m) is almost shallower than these saturation depths. Thus these isopycnal surfaces are not sensitive to the effect of dissolution of particulate carbonate.

3.5 *Rate of increase of AOU in the intermediate water (26.9~27.3σ_θ)*

The rate of AOU increase on 26.9~27.3σ_θ was the range 0.7~1.8 (ave. 1.1 ± 1.0) μmol/kg/yr and decreased with increasing density (Fig. 6(c) and Table 4). The trend of AOU increase on 27.0~27.1σ_θ was significant at the 80% confidence level, while the other isopycnal surfaces (26.9σ_θ, 27.2σ_θ and 27.3σ_θ) show no trend of AOU increase. Ono *et al*. (2001) reported that AOU has increased in the range from 0.6 to 1.3 μmol/kg/yr between 26.7σ_θ and 27.2σ_θ from 1968 to 1998 in the western North Pacific subpolar region (near the area east of Japan). The rates of increase of AOU in our study agreed well with their results.

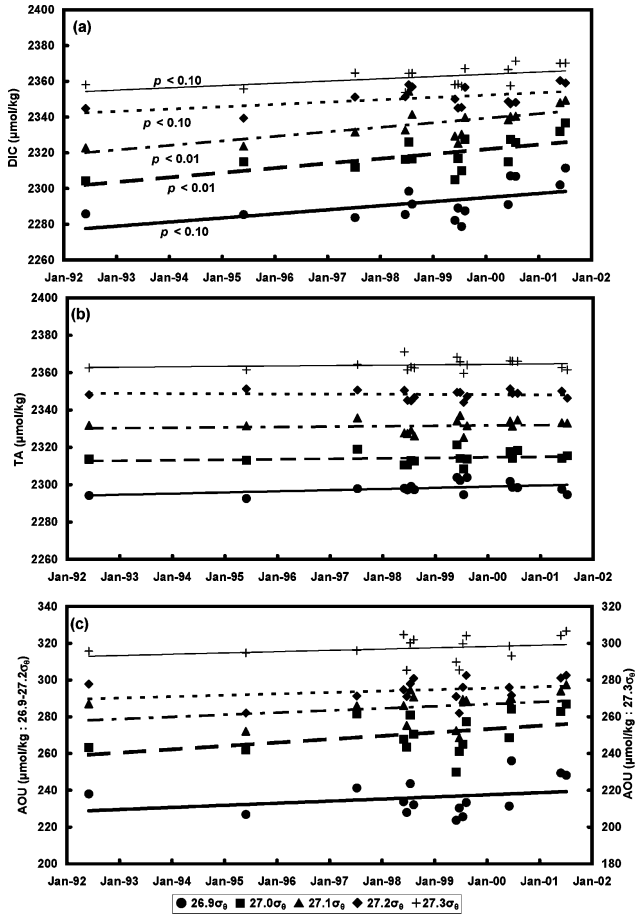

Fig. 6. Temporal changes in (a) DIC, (b) TA and (c) AOU on the isopycnal surface of 26.9σ_θ (solid circles), 27.0σ_θ (solid squares), 27.1σ_θ (solid triangles), 27.2σ_θ (solid diamonds) and 27.3σ_θ (plus) surfaces at Station KNOT from 1992 to 2001. We show the linear regression lines on 26.9σ_θ (solid line), 27.0σ_θ (dashed line), 27.1σ_θ (dashed-dotted line), 27.2σ_θ (dotted line) and 27.3σ_θ (thin line). In addition, we also show the probability value (p) for the linear regression lines of DIC on each isopycnal surface. The values of TA from 1992 to 1997 were computed using the strong correlation between TA and salinity on 26.9~27.3σ_θ from 1998 to 2001 (TA/μmol/kg = 140.4 salinity – 2447, r = 0.99).

The increase of AOU could be caused by the change in the physical and biological conditions of the ocean. To clarify whether or not oceanic biological activity changed at Station KNOT in the period from 1992 to 2001, we examined the change in primary production due to biological activity and the export flux of carbon from the surface to the ocean interior. According to Honda *et al.* (2002), the equations of vertical change in particulate organic carbon (POC) flux based on observed data are as follows at Station KNOT,

$$\mathrm{POC} = 1120.9Z^{-0.63} \text{ (Nov.–Dec. 1998)} \quad (1)$$

$$\mathrm{POC} = 1691.5Z^{-0.63} \text{ (May–June 1999)} \quad (2)$$

where Z is water depth. Using the above equations, we can estimate the flux of decomposition of POC from 230 m ($26.9\sigma_\theta$) to 626 m ($27.3\sigma_\theta$) to be 6~9 gC/m^2/yr in the intermediate water ($26.9\sim27.3\sigma_\theta$). On the other hand, the rate of increase of AOU in this study was an average of 1.1 μmol/kg/yr between this intermediate water at Station KNOT (Fig. 6(c) and Table 4). The temporal increase in the flux of decomposition of POC is calculated to be about 4 g C/m^2/yr, using our rate of increase of AOU (1.1 μmol/kg/yr) and the stoichiometric ratios for carbon to oxygen ($C_{org}/-O_2 = 0.69$: Anderson and Sarmiento, 1994). The temporal increase of flux of decomposition (4 g C/m^2/yr) is comparable to 44~67% of flux of decomposition (6~9 gC/m^2/yr) from $26.9\sigma_\theta$ to $27.3\sigma_\theta$, which is not reasonable. The flux of POC observed at 1000 m at Station KNOT during the period from 1989/June to 1990/January (average 11 gC/m^2/day) agreed with values found during the period from 2000/June to 2001/January (Noriki, personal communication). Ono *et al.* (2002) also reported that the net rate of biological phosphate consumption from February to August decreased linearly at 0.40 mmol P/m^2/yr (0.51 g C/m^2/yr) in the surface of the western North Pacific subpolar region during the last three decades. Thus the increase of primary production and the export flux due to biological activity may not have caused the rate of increase of AOU in the intermediate water at Station KNOT in the past decade.

In addition, Watanabe *et al.* (2001) suggested that the formation rate of the intermediate water in the North Pacific has reduced at least during past fifteen years. Watanabe *et al.* (2003) showed that both the linear trends and the oscillations of DO, phosphate and temperature in the North Pacific Intermediate Water in the last four decades showed a strong correlation with the North Pacific Index, an anomaly of sea surface level pressure in the wintertime in the North Pacific (Minobe, 1999). They suggested that atmospheric oscillations and/or artificial greenhouse warming effects simultaneously caused the reduction of the formation rate of the subsurface water in the ocean. Thus, the rate of increase of AOU on $26.9\sim27.3\sigma_\theta$ may be due to the increase of residence time of intermediate water.

3.6 *Factors controlling the rate of increase of DIC in the intermediate water ($26.9\sim27.3\sigma_\theta$)*

In general, observed DIC ($\mathrm{DIC_{obs}}$) along an isopycnal surface is the sum of the changes of DIC due to the gas exchange of CO_2 at the air-sea interface ($\mathrm{DIC_{air\text{-}sea}}$), the decomposition of organic matter ($\mathrm{DIC_{org}}$) and the dissolution of calcium carbonate ($\mathrm{DIC_{CaCO3}}$). To clarify the factors controlling the rate of increase of DIC, we can express Eqs. (3)~(5), as follows (e.g., Brewer, 1978; Chen and Millero, 1979),

$$d(\mathrm{DIC_{obs}})/dt = d(\mathrm{DIC_{air\text{-}sea}})/dt + d(\mathrm{DIC_{org}})/dt + d(\mathrm{DIC_{CaCO3}})/dt \quad (3)$$

$$d(\mathrm{DIC_{air\text{-}sea}})/dt = d(\mathrm{DIC_{obs}})/dt - (C_{org}/-O_2)d(\mathrm{AOU_{obs}})/dt - 0.5d(\mathrm{TA_{obs}})/dt \quad (4)$$

$$= d({}_{\mathrm{anth}}\mathrm{DIC_{air\text{-}sea}})/dt + d({}_{\mathrm{non\text{-}anth}}\mathrm{DIC_{air\text{-}sea}})/dt \quad (5)$$

where $d(\mathrm{DIC_{obs}})/dt$, $d(\mathrm{AOU_{obs}})/dt$ and $d(\mathrm{TA_{obs}})/dt$ are the rates of increase of DIC, AOU and TA observed on any isopycnal surfaces. $C_{org}/-O_2$ is the stoichiometric ratio of carbon to oxygen at the organic matter decomposition (Redfield *et al.*, 1963; Anderson and Sarmiento, 1994). The term $d({}_{\mathrm{anth}}\mathrm{DIC_{air\text{-}sea}})/dt$ is the rate of increase of DIC due to the gas exchange of the anthropogenic CO_2 at the air-sea interface and is defined that the near-surface water in the region of the formation of this intermediate water has followed the atmospheric perturbation and therefore has taken up anthropogenic CO_2 in equilibrium with the atmospheric CO_2 increase. The term $d({}_{\mathrm{non\text{-}anth}}\mathrm{DIC_{air\text{-}sea}})/dt$ is defined as the rate of increase of DIC due to the uptake of non-anthropogenic CO_2 through gas exchange at the air-sea interface in the region of the intermediate water formation, because ${}_{\mathrm{non\text{-}anth}}\mathrm{DIC_{air\text{-}sea}}$ fluxes estimated by Gloor *et al.* (2003) showed a large influx in the North Pacific, acting as a CO_2 sink. The term $d(\mathrm{TA_{obs}})/dt$ can be eliminated, because TA has not changed over the isopycnal surfaces ($26.9\sim27.3\sigma_\theta$) during the period from 1992 to 2001 at Station KNOT. Thus, in the intermediate water ($26.9\sim27.3\sigma_\theta$) at Station KNOT from 1992 to 2001, the factors causing the rate of increase of DIC were the rate of increase of AOU, ${}_{\mathrm{anth}}\mathrm{DIC_{air\text{-}sea}}$ and ${}_{\mathrm{non\text{-}anth}}\mathrm{DIC_{air\text{-}sea}}$, and we can express these factors with Eqs. (3)~(5) and $(C_{org}/-O_2) = 0.69$ (Anderson and Sarmiento, 1994), as following,

$$d({}_{\mathrm{non\text{-}anth}}\mathrm{DIC_{air\text{-}sea}})/dt = d(\mathrm{DIC_{obs}})/dt - 0.69d(\mathrm{AOU_{obs}})/dt - d({}_{\mathrm{anth}}\mathrm{DIC_{air\text{-}sea}})/dt. \quad (6)$$

We calculated the rate of increase of ${}_{anth}DIC_{air\text{-}sea}$ using observed temperature, salinity and the average values of TA on each isopycnal surface (26.9~27.3σ_θ) and the rate of increase of atmospheric CO_2 between 1992 and 2001 (1.7 ppm/yr, Keeling and Whorf, 2002). In this calculation we have used the dissociation constants of carbonic acid originally given by Mehrbach *et al.* (1973) and refitted by Dickson and Millero (1987). This yields the increase rate of ${}_{anth}DIC_{air\text{-}sea}$ at 0.5~0.7 μmol/kg/yr (Table 4), which agrees with values estimated by Watanabe *et al.* (2000). On the basis of Eq. (6), the remainder of $d({}_{non\text{-}anth}DIC_{air\text{-}sea})/dt$ was estimated to be 0.9~1.1 μmol/kg/yr in the upper intermediate water (26.9~27.1σ_θ) (Table 4). Thus, the rate of increase of DIC on 26.9~27.3σ_θ (ave. 2.0 ± 0.8 μmol/kg/yr) has been controlled by the increase of anthropogenic CO_2 (ave. 0.6 ± 0.1 μmol/kg/yr), the decomposition of organic matter due to AOU increase (ave. 0.8 ± 0.7 μmol/kg/yr) and the uptake of non-anthropogenic CO_2 through gas exchange at the region of intermediate water formation (ave. 0.6 ± 1.1 μmol/kg/yr).

Since the increase of non-anthropogenic CO_2 must have resulted from the recent changes due to the artificial greenhouse warming effect and/or the natural climate change at the region of the upper intermediate water formation, we can suggest the following possibilities for the factors controlling the increase of non-anthropogenic CO_2: the accumulation of non-anthropogenic CO_2 liberated back to atmosphere at this region due to 1) the decrease of difference between DIC in the winter mixed layer and DIC under equilibrium with the atmospheric CO_2 increase (Tsunogai, 2000) and 2) the reduction of diapycnal vertical water exchange between mixed layer and pycnocline waters.

The intermediate water (26.9~27.1σ_θ) at KNOT existed in the layer of maximum temperature. This water mass was transported from the area east of Japan to the Gulf of Alaska (Ueno and Yasuda, 2000), which indicates that the region of the upper intermediate water formation at KNOT is derived from the area east of Japan. Midorikawa *et al.* (2003) reported that the partial pressure of oceanic CO_2 in winter ($pCO_2{}^{sea}{}_{win}$) was higher than 400 μatm from 1998 to 2001 in the area east of Japan, which was a source of atmospheric CO_2. However, because of the increase of atmospheric CO_2 concentration, the temporal difference between $pCO_2{}^{sea}{}_{win}$ and atmospheric CO_2 must has decreased in the area east of Japan, which indicates that non-anthropogenic CO_2 liberated back to atmosphere has accumulated in the winter mixed layer. To examine this possibility, we calculated DIC in winter at the area east of Japan (DIC_{win}) and DIC in equilibrium with the atmospheric CO_2 increase (${}_{anth}DIC_{air\text{-}sea}$), and estimated the difference between DIC_{win} and ${}_{anth}DIC_{air\text{-}sea}$. In this test calculation, because the values of θ, salinity and TA in the intermediate water at KNOT had not changed for the period from 1992 to 2001, and we cannot estimated the elapsed time from the area east of Japan to KNOT, we calculated DIC_{win} and ${}_{anth}DIC_{air\text{-}sea}$ for convenience by using $pCO_2{}^{sea}{}_{win}$ in the area east of Japan and the atmospheric CO_2 concentrations from 1998 to 2001 and observed temperature, salinity and the average values of TA on 26.9σ_θ at KNOT. As a result, the difference between DIC_{win} (2110~2120 μmol/kg normalized to a salinity of 33) and ${}_{anth}DIC_{air\text{-}sea}$ (2100~2110 μmol/kg normalized to a salinity of 33) from 1998 to 2001 could have decreased by about 2.0 μmol/kg/yr, which almost agrees with $d({}_{non\text{-}anth}DIC_{air\text{-}sea})/dt$ (0.9~1.1 μmol/kg/yr) in the upper intermediate water (26.9~27.1σ_θ) at KNOT. Thus, possibility 1) has some possibility to explain the increase of non-anthropogenic CO_2 in the upper intermediate water (26.9~27.1σ_θ) at KNOT.

We now examine possibility 2). Ono *et al.* (2001) suggested that the linear increase of AOU, phosphate and salinity between 26.7σ_θ and 27.2σ_θ from 1968 to 1998 was caused by the reduction of diapycnal vertical water exchange between mixed layer and pycnocline waters in the western North Pacific subpolar region (near the area east of Japan), based on the linear decrease of salinity and density in the winter mixed layer. This suggestion agrees with the surface stratification in winter induced by the linear decrease of phosphate in the winter mixed layer of the same region from 1968 to 1998 (Ono *et al.*, 2002). The reduction of diapycnal vertical water exchange between mixed layer and pycnocline waters could affect the upper intermediate water at KNOT, because the region of the upper intermediate water formation at KNOT is similar to that obtained by Ono *et al.* (2001) and Ono *et al.* (2002). If the temporal change of $pCO_2{}^{sea}{}_{win}$ near the area east of Japan could be controlled basically by the depth of the winter mixed layer, the temporal trend of $pCO_2{}^{sea}{}_{win}$ would have decreased due to the linear decrease of the depth of winter mixed layer (Ono *et al.*, 2001). This would lead us to expect a decrease of DIC in the winter mixed layer and an increase of DIC in the upper intermediate water. We suggest that the increase of DIC in the upper intermediate water over time near the area east of Japan is responsible for the accumulation of non-anthropogenic CO_2 liberated back to the atmosphere. Thus, possibility 2) also has some possibility to explain the increase of non-anthropogenic CO_2 in the upper intermediate water (26.9~27.1σ_θ) at KNOT.

The greater DIC of the winter mixed layer would have decreased due to the shoaling of the depth of the layer (Ono *et al.*, 2001), the more the difference between $pCO_2{}^{sea}{}_{win}$ and atmospheric CO_2 would have decreased, according to the possibility 1), which would facilitate the accumulation of non-anthropogenic CO_2 in the upper in-

termediate water. However, the temporal change of $pCO_2^{sea}{}_{win}$ was insignificant during the period form 1998 to 2001 (Midorikawa *et al.*, 2003). An additional time series dataset is required to understand the linkage of the accumulation of non-anthropogenic CO_2 between the area east of Japan and KNOT, and clarify which of the possibilities 1) or 2) affects the factors controlling the increase of non-anthropogenic CO_2.

This paper first showed the decadal linear increase of DIC in the intermediate water (26.7~27.2σ_θ) at KNOT in the western North Pacific subpolar region. Since Ono *et al.* (2000) reported that the linear increase of AOU and phosphate superimposed on bidecadal oscillation from 26.7σ_θ to 27.2σ_θ of the western North Pacific subpolar region (near the area east of Japan), the increase of DIC from 26.9σ_θ to 27.3σ_θ at Station KNOT also possibly has a bidecadal oscillation. Thus the rate of increase of DIC in the intermediate water at Station KNOT may be an overestimate according to the ten years' time series data during the period from 1992 to 2001. In future, more accurate and longer time series data will be required to confirm our results. Similarly, by using a decadal dataset of DIC in the subtropical mode water of the North Atlantic Ocean, Bates *et al.* (2002) suggested that the rate of increase of DIC in this region is caused by the increase of anthropogenic CO_2 and the increase in the accumulation of non-anthropogenic CO_2 due to the reduction of vertical water exchange. We suggest that this phenomenon might have happened in the ocean of the North Hemisphere and is likely to contribute substantially to the interannual variability in oceanic CO_2 uptake.

Acknowledgements

We would like to thank the captain, officers, crew of the T/S *Hokusei Maru*, Hokkaido University for their help, and scientists for the kind cooperation in sampling and on board measurements. We are grateful to Prof. S. Noriki, Dr. H. Narita and members of the Laboratory of Marine and Atmospheric Geochemistry, Graduate School of Environmental Earth Science, Hokkaido University for valuable discussions, comments and encouragement. This study was partly funded by the Japan Science and Technology Corporation as a CREST (Core Research for Evolutional Science and Technology) program and the Sasakawa Scientific Research Grant from The Japan Science Society. Finally, we also express our deep thanks to two anonymous reviewers who gave us many useful comments.

Reference

Anderson, L. A. and J. L. Sarmiento (1994): Redfield ratios of remineralization determined by nutrient data analysis. *Global Biogeochem. Cycles*, **8**, 65–80.

Bates, N. R. (2001): Interannual variability of oceanic CO_2 and biogeochemical properties in the Western North Atlantic subtropical gyre. *Deep-Sea Res., Parts II*, **48**, 1507–1528.

Bates, N. R., A. C. Pequignet, R. J. Johnson and N. Gruber (2002): A short-term sink for atmospheric CO_2 in subtropical mode water of the North Atlantic. *Nature*, **420**, 489–493.

Brewer, P. G. (1978): Direct observation of the oceanic CO_2 increase. *Geophys. Res. Lett.*, **5**, 997–1000.

Chen, C. T. A. and F. J. Millero (1979): Gradual increase of oceanic carbon dioxide. *Nature*, **227**, 205–206.

Culberson, C., R. M. Pytkowitcz and J. E. Hawley (1970): Seawater alkalinity determination by the pH method. *J. Mar. Res.*, **28**, 15–21.

Dickson, A. G. and F. J. Millero (1987): A comparison of the equilibrium constants for the dissociation of carbonic acid in seawater media. *Deep-Sea Res.*, **40**, 107–118.

Dickson, A. G., G. C. Anderson and J. D. Afghan (2003): Reference materials for oceanic CO_2 analysis: 1. Preparation, distribution and use. *Mar. Chem.* (submitted).

DOE (1994): *Handbook of Methods for the Analysis of the Various Parameters of the Carbon Dioxide in Sea Water; Ver. 2*, ed. by A. G. Dickson and C. Goyet.

Favorite, F., A. J. Dodimead and K. Nasu (1976): Oceanography of the subarctic Pacific region, 1960–1971. *INPFC*, **33**, 1–187, Vancouver.

Gloor, M., N. Gruber, J. Sarmiento, C. L. Sabine, R. A. Feely and C. Rodenbeck (2003): A first estimate of present and preindustrial air-sea CO_2 flux patterns based on oceanic interior carbon measurements and models. *Geophys. Res. Lett.*, **30**, 1010, doi:10.1029/2002GL015594.

Honda, M. C., K. Imai, Y. Nojiri, F. Hoshi, T. Sugawara and M. Kusakabe (2002): The biological pump in the northwestern North Pacific based on fluxes and major components of particulate matter obtained by sediment-trap experiments (1997–2000). *Deep-Sea Res. II*, **49**, 5595–5625.

Imai, K., Y. Nojiri, N. Tsurushima and T. Saino (2002): Time series of seasonal variation of primary productivity at station KNOT (44°N, 155°E) in the sub-arctic western North Pacific. *Deep-Sea Res. II*, **49**, 5395–5408.

Isoda, Y., S. Shimizu, T. Izawa and T. Azumaya (2002): Interannual variations of North Pacific Intermediate Water across 155E and 180E sections in the subarctic North Pacific. *Umi to Sora*, **77**, 143–151.

Johnson, K., A. E. King and J. M. Sieburth (1985): Coulometric TCO_2 analyses for marine studies: An introduction. *Mar. Chem.*, **16**, 61–81.

Keeling, C. D. and T. P. Whorf (2002): Atmospheric CO_2 records from sites in the SIO air sampling network. In *Trends*, A Compendium of Data on Global Change, Carbon Dioxide Information Analysis Center, Oak Ridge National Laboratory, U.S. Department of Energy, Oak Ridge, Tenn., U.S.A.

Knap, A., A. Michaels, A. Close, H. Ducklow and A. Dickson (eds.) (1996): Protocols for the Joint Global Ocean Flux Study (JGOFS) core measurements. JGOFS Report No. 19, vi + 170 pp. Reprint of the IOC manuals and guides No. 29, UNESCO.

Kono, T. (1997): Modification of the Oyashio Water in the Hokkaido and Tohoku areas. *Deep-Sea Res. I*, **44**, 669–688.

McNeil, B. I., R. J. Matear, R. M. Key, J. L. Bullister and J. L. Sarmiento (2003): Anthropogenic CO_2 uptake by the ocean

based on the global chlorofluorocarbon data set. *Science*, **299**, 235–239.

Mehrbach, C., C. H. Culberson, J. E. Hawley and R. M. Pytkowicz (1973): Measurement of the apparent dissociation constants of carbonic acid in the seawater at atmospheric pressure. *Limnol. Oceanogr.*, **18**, 897–907.

Midorikawa, T., S. Sonoki, K. Saito, H. Takano, H. Kamiya, M. Ishii and H. I. Inoue (2003): Seasonal changes in oceanic pCO_2 in the Oyashio region from winter to spring. *J. Oceanogr.*, **59**, 871–882.

Millero, F. J. (1996): *Chemical Oceanography*. CRC Press, Boca Raton, Florida, 272 pp.

Minobe, S. (1999): Resonance in bidecadal and pentadecadal climate oscillations over the North Pacific: role in climate regime shifts. *Geophys. Res. Lett.*, **26**, 855–858.

Ono, T., S. Watanabe, K. Okuda and M. Fukasawa (1998): Distribution of total carbonate and related properties in the North Pacific along 30°N. *J. Geophys. Res.*, **103**, 30873–30883.

Ono, T., Y. W. Watanabe and S. Watanabe (2000): Recent increase of DIC in the western North Pacific. *Mar. Chem.*, **72**, 317–328.

Ono, T., T. Midorikawa, Y. W. Watanabe, K. Tadokoro and T. Saito (2001): Temporal increases of phosphate and apparent oxygen utilization in the subsurface waters of western subarctic Pacific from 1968 to 1998. *Geophys. Res. Lett.*, **28**, 3285–3288.

Ono, T., K. Tadokoro, T. Midorikawa, J. Nishioka and T. Saino (2002): Multi-decadal decrease of net community production in western subarctic North Pacific. *Geophys. Res. Lett.*, **29**, 10.1029/2001GL014332.

Redfield, A. C., B. H. Ketchum and F. A. Richards (1963): The influence of organisms on the composition of seawater. p. 26–77. In *The Sea*, ed. by M. H. Hill, Wiley-Interscience, New York.

Reid, J. L. (1965): Intermediate waters of the Pacific Ocean. *The John Hopkins Oceanographic Study*, **2**, Baltimore, p. 85.

Slansky, C. M., R. A. Feely and R. H. Wanninkhof (1997): The stepwise linear regression method for calculating anthropogenic CO_2 invasion into the North Pacific Ocean. *Proceeding of International Marine Science Symposium on Biogeochemical Processes in the North Pacific*, 70–79, Japan.

Takahashi, Y., E. Matsumoto and Y. Watanabe (1999): Improved method for calculating anthropogenic CO_2 in the upper layer of the North Pacific subtropical gyre along 175°E. *J. Oceanogr.*, **55**, 717–730.

Talley, L. D. (1991): An Okhotsk Sea anomaly: implications for ventilation in the North Pacific. *Deep-Sea Res. A*, **38**, Suppl., S171–S190.

Tsunogai, S. (2000): North Pacific water's larger potential sink capacity for absorbing anthropogenic CO_2 and the processes recovering it. p. 533–560. In *Dynamics and Characterization of Marine Organic Matter*, ed. by N. Handa, E. Tanoue and T. Hama, TERRAPUB, Tokyo.

Tsunogai, S., T. Ono and S. Watanabe (1993): Increase in the total carbonate in the western North Pacific water and a hypothesis on the missing sink of anthropogenic carbon. *J. Oceanogr.*, **49**, 305–315.

Tsurushima, N., Y. Nogiri, K. Imai and S. Wanatabe (2002): Seasonal variations of carbon dioxide system and nutrients in the surface mixed layer at Station KNOT (44°N, 155°E) in the subarctic North Pacific. *Deep-Sea Res. II*, **49**, 5377–5394.

Ueno, H. and I. Yasuda (2000): Distribution and formation of the mesothermal structure (temperature inversions) in the North Pacific subarctic region. *J. Geophys. Res.*, **105**, 16885–16898.

Watanabe, Y. W., Y. Takahashi, T. Kitao and K. Harada (1996): Total amount of oceanic excess CO_2 taken from the North Pacific Subpolar Region. *J. Oceanogr.*, **52**, 301–312.

Watanabe, Y. W., T. Ono and A. Shimamoto (2000): Increase in the uptake rate of oceanic anthropogenic carbon in the North Pacific determined by CFC ages. *Mar. Chem.*, **72**, 297–315.

Wanatabe, Y. W., T. Ono, A. Shimamoto, T. Sugimoto, M. Wakita and S. Watanabe (2001): Probability of a reduction in the formation rate of the subsurface water in the North Pacific during the 1980s and 1990s. *Geophys. Res. Lett.*, **28**, 3289–3292.

Wanatabe, Y. W., T. Ono, M. Wakita, N. Maeda and T. Gamo (2003): Synchronous bidecadal periodic changes of oxygen, phosphate and temperature between the Japan Sea deep water and the North Pacific intermediate water. *Geophys. Res. Lett.*, **30**, 10.1029/2003GL018338.

Weiss, R. F. (1970): The solubility of nitrogen, oxygen and argon in water and seawater. *Deep-Sea Res.*, **17**, 721–735.

Winn, C. D., Y. H. Lee, F. T. Mackenzie and D. M. Karl (1998): Rising surface ocean dissolved inorganic carbon at the Hawaii Ocean Time-series site. *Mar. Chem.*, **60**, 33–47.